A Study of the Effect of Tunnel Aspect Ratio on Control of Smoke Flow in Tunnel Fires

A thesis submitted to the University of Sheffield
in fulfilment of the requirements for the
degree of Doctor of Philosophy

By

M. Z. Abu Bakar

Department of Chemical and Process Engineering
University of Sheffield
November 1999

Contents

Abstract

In the event of a tunnel fire, the emergency ventilation system is often brought in action to create a safe route upstream clear of smoke for evacuation and fire fighting. The "critical ventilation velocity" is used to represent the value of the ventilation velocity which is just able to force the smoke moving in one direction. This value has become one of the important criteria for the design of the tunnel ventilation systems.

This study reviewed current knowledge on the critical ventilation velocity and studies of tunnel fires. The literature review showed that the critical ventilation data are limited in number. The influence of fire power on the critical ventilation velocity remains uncertain and in addition, the most important issue which is the effect of tunnel geometry on the critical ventilation velocity has not been studied yet.

To establish better model prediction of the critical ventilation velocity, the present work systematically investigated the effect of tunnel geometries on the critical ventilation velocity on five small scale model tunnels which have approximately the same height but different widths. Three dimensional Computer Fluid Dynamics (CFD) simulations were also carried out to investigate the flow behaviour and compare the modelling results with the experimental results.

The present work found that cross-sectional geometry did affect the critical ventilation velocity. The critical ventilation velocity has been related to the distribution of the fire plume inside the tunnel at critical ventilation conditions. The present work also explored the new dimensionless of the critical ventilation velocity and the heat release rate and suggests that the mean hydraulic tunnel height $\left(\overline{H}\right)$ should be used as the characteristic length for the buoyant forces in the dimensionless analysis instead of tunnel height (H). A simple one dimensional relationship has been derived based on the new dimensionless analysis for predicting the critical ventilation velocity for large scale tunnels in any cross-sectional geometry.

Finally, the scaling problem was resolved by comparing the present results with the large scale results obtained in the literature review, expressed in the new dimensionless analysis. The results showed that the present results agreed with most of the large scale experimental results. This suggests that the present results can be used with high degree of confidence to predict the critical ventilation velocity for larger scale tunnels in any cross-sectional geometry.

Acknowledgements

List of Figures

List of Tables

Nomenclature

A	Preexponential factor, $(kg\ m^{-2}\ s^{-1}\ atm^{-1})$
A_p	cross-sectional area of the pipe (m^2)
A_T	cross-sectional area of the tunnel (m^2)
C	constant (dimensionless) (Equation 2.11, 2.12)
C_d	discharged coefficient (Equation 5.1)
C_p	specific heat capacity, $(kJ\ kg^{-1}\ K^{-1})$
d_o	diameter of the orifice throat (m) (Equation 5.1)
d	depth of smoke layer (m) Equation 2.2)
D_p	Diameter of the ventilation pipe (m)
E	velocity approach factor (Equation 5.1)
Fr	Froude number (dimensionless)
Fr_m	modified Froude number (dimensionless)
$Fr_{m(a)}$	modified Froude number (Equation 2.7)
g	gravitational force, $(m\ s^{-2})$
H	Tunnel height, (m)
$\overline{H}$	mean hydraulic tunnel height defined as the ratio of 4 times the tunnel cross-sectional area to the tunnel perimeter (m).
k	constant (Equation 2.9, 2.13)
K'	constant (Equation 2.10)
K	constant (Equation 2.11)
K_g	grade correction factor (Equation 2.3)
M	smoke production rate $(kg\ s^{-1})$
P	perimeter of the fire, (m) (Equation 2.1)
q_m	mass flow rate $(kg\ s^{-1})$ (Equation 5.1)
R_i	Richardson number (dimensionless)
Q	fire convective heat release rate (kW)
Q'	fire convective heat release rate per tunnel unit width $(kW\ m^{-1})$
$Q*$	normalised heat release rate (Equation 3.17), based on H
Q''	normalised heat release rate, (based on hydraulic tunnel height)
R_e	Reynolds number (dimensionless)

T	temperature of the hot layer (°C)
T_o	ambient temperature (°C)
U	ventilation velocity, (m s⁻¹) (Equation 2.1)
U_c	critical ventilation velocity, (m s⁻¹) (Equation 2.2)
U_v	ventilation velocity immediately upstream from fire (m s⁻¹) (Equation 2.6)
V_s	Smoke velocity (m s⁻¹)
V_p	average velocity in pipe, (m s⁻¹)
V*	dimensionless critical velocity (based on H, tunnel height)
V″	dimensionless critical velocity (based on hydraulic tunnel height)
W	tunnel width, (m)
w′	characteristic vertical velocity (m s⁻¹) (Equation 2.8)
ρ_o	ambient air density, (kg m⁻³)
ρ	average air density, (kg m⁻³)
ρ_f	air density at the fire site, (kg m⁻³)
ρ_s	smoke density, (kg m⁻³)
$\Delta\rho$	density difference, (kg m⁻³)
ΔT	the temperature rise above ambient (°C)
Δp	differential pressure (Pa)
ε	expansion factor (Equation 5.1)
ν	kinematics viscosity (kg N⁻¹ s⁻¹ m⁻¹)
θ	tunnel slope (percentage)
l	characteristic vertical length (m)

Chapter 1

Introduction

Tunnel fire can be considered as a rare event, however the experience of the most recent incidents, Mont Blanc in France (1999) where 34 people were killed, Alpine Tunnel in Austria (1999) where 4 people were killed, 67 people injured and other incidents such as Channel Tunnel fire (1996) and the Nihonzaka tunnel fire in Japan (1979) has shown us that such fires could be devastating and deadly.

The probability of vehicle fires, considered among the most dangerous of all hazards in tunnel is about one fire per 10^7 vehicle kilometres (Touvinen et al, 1996). One fire/10^7 is reported for the Elbe tunnel in Germany and $1.3/10^7$ for cars and $4.5/10^7$ for trucks are reported on the entire English road network (Heselden, 1978).

In the last 30 years there has been a great improvement in the understanding of tunnel fires and the knowledge of the methods to control them. The main objectives of fire and smoke control in road tunnels were to protect the users and make fire-fighting operations possible. However, the objectives had to be complemented by a number of work hypotheses and clarified for each case depending on tunnel length, traffic, ventilation system, environment and others.

The evolution of the tunnel fire research started from the real tests to the most recent technology, Computational Fluid Dynamics. The real phenomenon of tunnel fires can only be achieved by performing the fires in the full scale tunnel such as Ofnegg tunnel (Haerter, 1965), Zwenberg tunnel (Feizlmayr, 1976), Memorial tunnel (Kennedy, 1997). However, there are several drawbacks such as the operating cost is enormous and the test can only be performed in one tunnel shape. In addition, it is difficult to control since the geometry is large. As a consequence, in recent years, more tests on tunnel fires were performed in small scale experiments (Hwang et al, 1976; Chaiken et al, 1979; Lee et al,

1979; Vantelon et al, 1991; Oka & Atkinson, 1995; Hwang & Wargo, 1986; Atkinson & Wu, 1996; Xue et al, 1993; Kwack et al, 1990; Apte et al, 1991; Bettis, 1993, 1994).

The most recent technique is the use of Computer Fluid Dynamics to study and understand the behaviour of tunnel fires. There are several computer codes which have been used such as the CFX written by AEA Technology, JASMINE code from Fire Research Station and multi purpose FLUENT code from FLUENT Europe Ltd. The capability of CFD to predict the qualitative features of tunnel fires has been examined by several workers (Fletcher, 1994; Lea, 1995; Woodburn & Britter, 1996). However, further research is required especially obtaining the quantitative values for example the prediction of the critical ventilation velocity as well as the validation of the experimental results.

One of the major research areas is the utility of ventilation system to control the smoke flow. Extensive research results have been obtained world-wide in the case of road tunnels ventilation in case of fires. However new knowledge is still needed. A few uncertainties such as the effects of various parameters (tunnel slopes, fire locations and tunnel geometry) on the ventilation velocity and scaling procedures from small scale to large scale require further investigation to be organised into a consistent methodology to be efficiently implemented by designers and operators.

Figure 1.1 illustrates the movement of the smoke during a tunnel fire under natural ventilation where the smoke will travel at both upstream and downstream from the fire seat. Once a fire takes place a plume of hot smoke will rise to the ceiling of the tunnel, entraining air as it rises, thus increasing the volume of smoke but reducing its temperature. The smoke spreads out underneath the tunnel roof, and as more smoke is produced air convection currents are created. The stratified smoke layer may become fully mixed and would then act as an obstacle. This presents a major problem for the victims to escape and makes difficult for rescue and fire fighting.

In the event of tunnel fire, the emergency ventilation system is often brought in action to create a safe route for evacuation and fire fighting. In practice, there are three type of ventilation systems; longitudinal, transverse and semi-transverse.

"Longitudinal ventilation" is characterised by an airflow at the same speed over the whole tunnel length, or over successive sections separated by extraction and/ or injection devices. An example of longitudinal ventilation fan is shown in Figure 1.2.

"Transverse ventilation" describes a cross-ventilation system in which air flows across the tunnel section, with both inflow and outflow at either the tunnel bed, sides or ceiling.

"Semi-transverse ventilation" is a hybrid of the above two types in which inflow is typically spaced at intervals along the tunnel and outflow is longitudinal, with flow direction often being reversed in the event of fire.

The main interest of the present study is the use of longitudinal ventilation to control the smoke flow during tunnel fires. With the utility of longitudinal ventilation system, the smoke and the combustion products will be forced to move in the direction of the air flow. i.e. 'downstream', hence keeping the 'upstream' from the fire seat clear. However, at low ventilation velocity, the hot products can still travel in the 'upstream' direction against the direction of the air. This flow of the products is defined as 'backlayering' as described in Figure 1.3. The minimum ventilation velocity which can just prevent the movement of the 'backlayering' is defined as the 'critical ventilation velocity', shown in Figure 1.4. This value has become one of the prime criteria for the design of the tunnel ventilation system. The desired value of the critical velocity is necessary to make sure that all the combustion products have been driven downstream and also to avoid over-estimation of the ventilation velocity.

Current methods to predict the critical ventilation velocity for tunnel emergency ventilation systems are based on the sets of equations derived by applying Froude number preservation combining with some experimental data based on the works of Heselden (1978) and Danziger & Kennedy (1982) which were incorporated in the US Department of Transport Subway Environment Simulation Program. These models suggested that the critical velocity for the horizontal tunnel varies with the one third power of the heat release rate (HRR) from the fire.

Recent results from the Gallery tunnel tests in Buxton (Bettis et al, 1993,1994) also suggested that the critical velocity does vary as the one third power of the HRR, but only at lower HRRs. However, at higher HRR, the critical velocity was nearly independent of heat output over a wide range of fire sizes. Their conclusions were supported by Lea (1995) in his CFD work on the same Gallery tunnel and by Oka and Atkinson (1995) who performed experiment on 1/10 scale model of the Gallery tunnel. The new findings had led some uncertainties on the existing models mainly the capability of the existing empirical models to predict the desired critical ventilation velocity, particularly at higher HRRs. The mechanisms for this phenomenon need to be addressed.

This thesis describes the research work conducted to investigate the effect of tunnel geometry or aspect ratio on the critical ventilation velocity. Five reduced scale model tunnels which have the same height and different cross - sectional geometries were used in order to systematically measure the critical ventilation velocity. In addition to the experimental works, three dimensional modellings were performed to predict the critical ventilation velocity for the model tunnels and examine the flow behaviour inside the tunnels.

The next chapter discusses the review of the literature of various aspects of tunnel fires, giving particular emphasises to the critical ventilation velocity. Chapter 3 discusses the scaling issues. Chapter 4 describes the objectives and approaches in the present study. Chapter 5 discusses experimental investigation, followed by Chapter 6, the experimental results. Then Chapter 7 gives the discussion of the experimental results. After that Chapter 8 discusses the three dimensional modellings using FLUENT package which is available in the University of Sheffield together with the comprehensive comparisons of the experimental and CFD results. Chapter 9 proposes dimensional analysis to the critical ventilation velocity and HRR and finally Chapter 10 gives the overall conclusions and suggestions for future works.

Upstream   Downstream
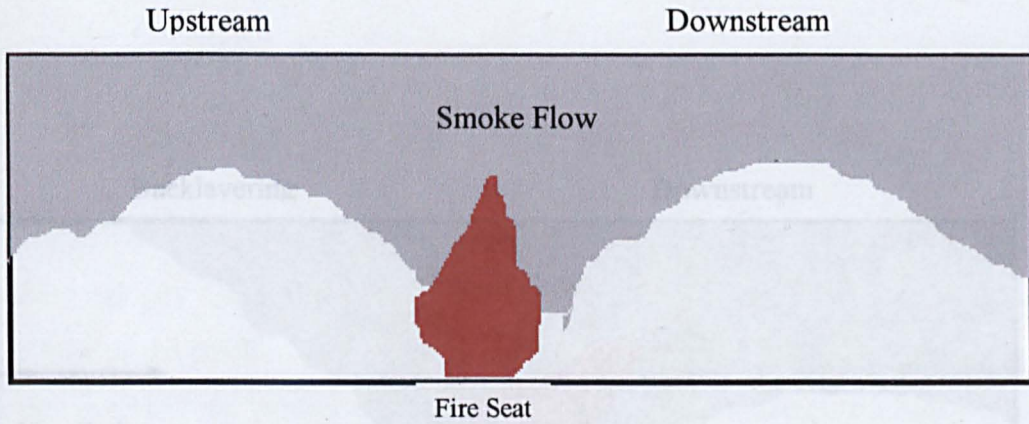
Figure 1.1: Illustration of a tunnel fire under natural ventilation
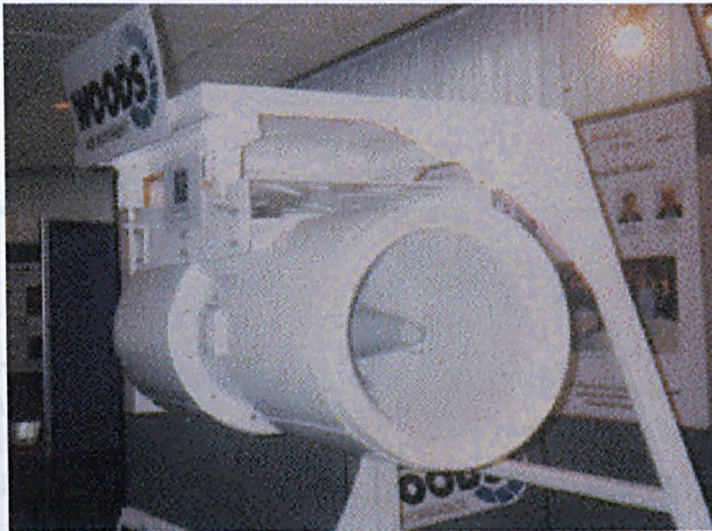
Figure 1.2: Longitudinal ventilation fan [Woods Technology, Display in 9th International
Symposium on Aerodynamic of Vehicle and Tunnel Ventilation, Italy, 1997)

Backlayering   Downstream

Smoke Flow

Ventilation
Flow

Fire Seat

Figure 1.3: Illustration of a tunnel fire underventilated causing backlayering

Downstream

Smoke Flow

Ventilation
Flow at Uc
Critical Ventilation Rate

Fire Seat
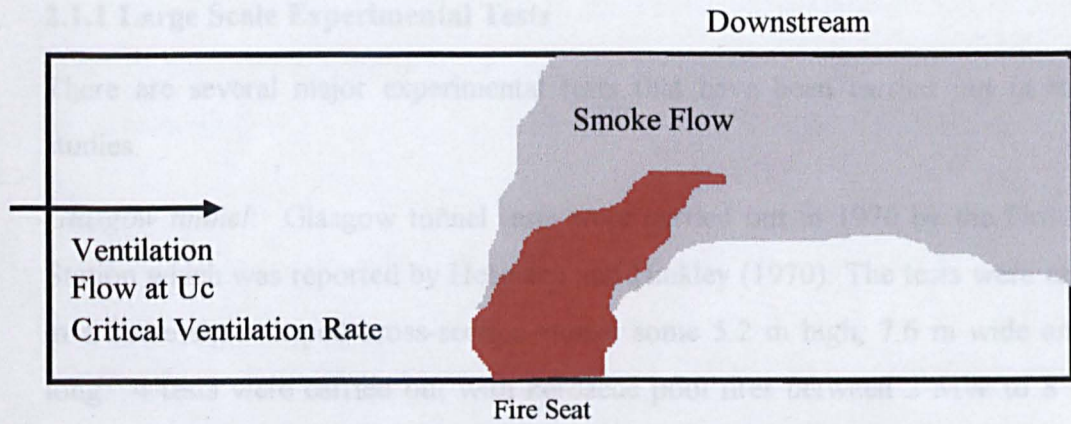
Figure 1.4: Illustration of a tunnel fire sufficiently ventilated to prevent

backlayering

Chapter 2

Literature Review

The motivation to study tunnel fires began in the early 1970s, initiated from the coal mining industry. Since then, more works have been done especially the ways to control the flow of the smoke. Earlier works focused on the experimental and theoretical fields which involved the studies on the general aspects of the combustion in fire, based on both reduced and large scales. Several comprehensive measurements were made such as the depth of the smoke layer in the tunnel; the rate of the flow of smoke and air; the velocities and temperatures distributions of the smoke across the tunnel and finally the critical ventilation velocities to prevent the smoke backlayering.

2.1 Experimental Study of Tunnel Fires

2.1.1 Large Scale Experimental Tests

There are several major experimental tests that have been carried out in tunnel fire studies.

Glasgow tunnel: Glasgow tunnel tests were carried out in 1970 by the Fire Research Station which was reported by Heselden and Hinkley (1970). The tests were carried out in a horse shoe shaped cross-section tunnel some 5.2 m high, 7.6 m wide and 600 m long. 4 tests were carried out with kerosene pool fires between 2 MW to 8 MW and using only natural ventilation. The pool fire was placed in an increasing number of 1.2 m square trays. The progress of the smoke was observed and the average velocity was taken. Some of the uncertainties from this experiment were that the heat output rate was slightly inaccurate since the fires were 'spread' and no account were taken on the reduced temperatures involved. The other problem was that the duration of the fire was short, as a result it was unclear if a steady state heat output was achieved.

Ofnegg tunnel: Ofnegg tunnel tests were done in 1965 and was reviewed by Haerter (1965). The tunnel has a horse shoe shaped cross-section with dimensions of 6 m high, 4 m wide and 190 m long. Altogether, 11 tests were carried out with three petrol pool fire sizes (100 litre , 6.6 m^2; 500 litre, 47.5 m^2; 1000 litre , 95 m^2). Unfortunately, the fire sizes were not measured. Again, the burning times were reported to be short. The ventilation rates were in the range of 2-3 m/s. The objectives of the tests were to investigate factors such as visibility, temperature distribution, gas concentrations and critical zones for survival.

Zwenberg tunnel : Zwenberg tunnel tests were carried out in Austria and was reported by Feizlmayr (1976). 23 tests were carried in approximately rectangular shaped tunnel some 4 m high, 5 m wide and 390 m long. The fire sources were 200 litre and 400 litre petrol placed at approximately 108 m from the South portal which was closed throughout the test. Longitudinal ventilation from the South to North portal was available from a further fan at the South portal supplying up 7 m/s in the tunnel. The objectives of the tests were to determine the effects on human being, structures, and possibility of controlling products of combustion by the use of ventilation system. Temperature, velocity, gas sampling and smoke density instrumentation were spaced at intervals down the tunnel. A major uncertainty was that the HRRs from the fires were not measured.

EUREKA Programme : The EUREKA tests were performed in Norway and were reported by Haack (1995). 21 fire tests were performed which included 5 tests directly concerning road vehicles. The research programme was intended above all to provide information on several aspects of tunnel fires which includes fire phenomena, escape, rescue and fire - extinguishing, the effect of the surrounding structural parts on the fire.

Memorial tunnel: The Memorial test programmes were carried out in the Memorial tunnel, West Virginia, USA during 1993 to 1995 in a 850 m long disused two lane road tunnel. The programme consisted of over 100 trials to investigate relevant parameters

such as tunnel ventilation and configurations of such systems, air velocity, temperature and gas concentrations.

Newman et al (1983, 1984) studied stratification in a ventilated duct fire. The experiments were performed in large scale duct of 2.4 m x 2.4 m x 61 m long. The heat releases rate from various fire sources examined ranged between 10 kW and 20 MW. The ventilation velocity was varied between 0.5 m/s to 4.0 m/s. The fire sources in the experiment were heptane, coal with kerosene, and neoprene with coal and with methanol. Gas temperature measurements were made.

Kwack et. al (1990) performed a series of tests to study the flow of smoke through aircraft cabin interior. The model was 1/3 rd of the scale model with the dimensions of 0.76 m high and 0.52 m wide and 9.2 m long. There is uncertainty into the actual shape of the model. The work involved a series of 4 tests with Turbojet A fuel which produced fire sizes from 246 kW to 335 kW. The ventilation velocities range from 0.58 m/s to 0.87 m/s. Temperature and velocity measurements were reported.

Apte et al (1991) studied on the effect of ventilation flow towards the backlayering flow in a mine roadway of 5.4 wide x 2.4 m high. The purpose of the experiment was for model validation of the stratification flow for both upstream and downstream of the tunnel. Octane pool fires were used with the heat output varying from 0.5 MW to 12 MW and the ventilation velocity from 0.2 m/s to 2 m/s . The temperature measurements were made.

Recent series of tests which provide the most comprehensive data set available to date were done in Health and Safety Laboratory, Buxton (Bettis et al, 1993,1994). The tests were carried out in a 2.56 m high arch-shaped tunnel some 366m long. Kerosene pools of sizes from 0.3 MW to 20 MW were used and the ventilation velocities from 0.5 m/s to 4 m/s. Several measurements were made such as time varying temperature distributions,

smoke and gas concentrations (O_2, CO_2 and CO), counter-flow layer lengths and multi-point velocities.

2.1.2 Small Scale Tests

Hwang and Wargo (1986) made the most detailed study of the movement of backlayering flow layers in a small scale tunnel. The tunnel was 4.9 m long with a uniform cross-section 0.4 m wide by 0.3 m high. The tunnel can be tilted up to $\pm$ 18° from the horizontal, so that a ventilation current can be either ascending and descending. Natural gas was burned with an air - fuel ratio of 10:1. The HRR was not reported. The ventilation velocity was between 0.202 m/s to 0.309 m/s, produced by a blower. The temperature and velocity distributions inside the tunnel were measured at various positions. The effect of tunnel slope on the hot layer movement was also investigated.

Grant et al (1988) performed a series of small scale experiments. The wind tunnel consisted of several sections of smooth plastic tube, (nominal internal diameter 150 mm). The total length of the tunnel was approximately 15 m. The fire source used in the experiments consisted of a pool burning mineralised methylated spirit. The HRRs varied from 0.07 kW to 1.783 kW. The ventilation velocity ranged between 0.96 m/s to 6.72 m/s. Temperature and velocity distributions in the tunnel were reported.

Xue et al (1993) performed a small scale experimental tests in a circular duct of 0.25 m radius and 8.45 m long. Two tests were performed using ventilation velocities of 0.46 m/s and 0.92 m/s, both were at heat output of 3 kW by a pre-mixed gas burner. For both cases, the downstream temperatures profiles were measured.

Chaiken et al (1979) carried out coal fire experiments in a tunnel of a 9m long, 0.27m x 0.27m square cross-section. The entrance of the tunnel was open to the atmosphere while an exhaust fan was fixed at the downstream end of the tunnel. The HRR was not reported. The main objective was to investigate the backlayering layers and validated the result with a mathematical model.

Lee et al (1979a) used the same experimental facility as Chaiken et al (1979) to perform further experiments to investigate the interaction between duct fires and the ventilation. The tunnel walls and roof were lined with wood along the entire duct length and about 1 m of the initial length was ignited to produce the fire. 4 tests were performed. Lee et al (1979b) also performed another experiment in a model tunnel of 0.4 m high x 0.3 m width x 5 m long to investigate the stratification of the backlayering flow inside the tunnel. A gas burner was used to generate hot plume backing up against a longitudinal ventilation. Gas volumetric flow rate and air to gas ratio of the burners were varied for various fire sizes. The range of fire sizes and ventilation velocity were not reported.

Vantelon et al (1991) used a laser light to investigation the smoke backlayering in the 1/30 scale which consisted of a 0.15 m radius semi-circular tunnel of 3 m long. 5 fire sizes were used in the range between 0.325 kW to 0.800 kW by using a flat burner. The velocity of ventilation was between 0.195 m/s to 0.225 m/s· Correlation between the smoke backlayering with two main parameters; the ventilation speed and rate of HRR was established.

Oka and Atkinson (1995) investigated the critical ventilation velocity in an arch shaped tunnel (244 mm high x 274 mm wide, 15 m long) which was 1/10 of the HSL Colliery arch tunnel. The fire was produced by burning propane gas in air. The critical ventilation velocity for the range of HRRs from 0.45 kW to 29 kW which correspond to approximately 2 to 150 MW in a tunnel with a diameter around 5m was systematically determined. Oka and Atkinson also studied the effect of fire locations and burner geometries towards controlling the backlayering flow.

Atkinson and Wu (1996) further used the experimental facility as Oka and Atkinson to systematically measured the critical ventilation velocity for the tunnel with downhill slope between $0°$ and 10°. Correlation to calculate the critical ventilation velocity for a sloping tunnel was derived.

The extensive reviews on tunnel fires was done by Lea (1993, 1994). Table 2.1 summarises the details of the experimental tunnel fire tests for both reduced and large scales tests.

2.2 Aspects of Tunnel Fires

Before further discussions on the aspect of tunnel fires, it is important to define several related terms that are commonly used in tunnel fires study.

(1) Backlayering

Backlayering flow is defined as the layer of hot products which travel against the air flow. Some of the authors in section 2.1 used different terms such as reversed - flow and back-up-layer. In the present works, the term backlayering flow will be used through out the thesis.

(2) Critical ventilation velocity

Critical ventilation velocity is defined as the minimum ventilation velocity at which the backlayering flow is suppressed completely. The unit for critical ventilation velocity is m/s.

(3) Fire power

Fire power is defined as the heat release rate (HRR) by the combustion during the fire. The unit of HRR is either kilowatt (kW) or megawatt (MW)

(4) Fire Seat

Fire seat is defined as the position where the fire originated in the tunnel.

2.2.1 Fire power

Fire power is the main parameter which is considered to design ventilation system in the tunnel. Unfortunately, there are very few test programmes have included real vehicles in tunnel.

In the EUREKA 'Firetun' programme, 21 fire tests were performed, but only 5 tests directly concerned road vehicles. The rail car fires mostly amounted to between 15 and 20 MW. The burning of the heavy good vehicle was measured more than 100 MW. In another experiment, Malhotra (1995) reported that the magnitude of HRR for a single heavy good vehicle (HGV) carrying furniture was in excess of 100 MW.

Most of the ventilation designs are based on the fire power from Heselden (1978). Heselden gave values of 3 MW for an ordinary car, 10 MW for a van, 20 MW for a lorry or coach, 50 MW-100 MW for petrol spill. World Road Association (PIARC) recommended that for a passenger car the HRR is approximately 5 MW. For a Bus/Truck and petrol tanker, the HHRs are 20 MW and 30 - 100 MW, respectively.

The HRR for the HGV is considered as the upper limit for fire power in designing the ventilation velocity. Thus, any ventilation system which is going to be used must take the consideration to be able to control the smoke given by HRR approximately 100 MW. The summary of the fire power from Eureka tests and PIARC are shown in Tables 2.2 and 2.3, respectively.

2.2.2 Behaviour of the Fire

The spread of a fire inside a tunnel is different from in an open place. Flames from a substantial fire reaching the tunnel ceiling can no longer travel upwards and must therefore travel horizontally. Since they are very hot and therefore light gases, they travel under the ceiling and in this situation they can elongate to a surprising extent, as much as 5-10 times of an open fire (Heselden, 1978). This elongation arises because the

mixing of air into the flame under the ceiling is by a much slower process than when the flame is travelling vertically, so that in order for enough air to be entrained to burn all the volatile fuel, the horizontal flame has to be much longer. A stable situation of a light gas above a heavier one is created, so that the turbulent eddies are damped down by buoyancy forces and the rate of air mixing is very much reduced. In addition, mixing into horizontal flame can only take place over one side of the flame.

In the presence of the longitudinal ventilation system, the air flow forced 'torch like' flame over the edge of the fuel through where the flaming region is generally inclined at certain angle from the vertical (Haerter, 1965; Bettis et al, 1993, 1994; Apte et al, 1991).

The duration of the fires fluctuated considerably depending on external circumstances and could last between 30 minutes and several hours. The fire flash-over point was reckoned to occur after some 7 to 10 minutes (Haack, 1992). With petrol fire, the peak temperature was reached 1 to 2 minutes after ignition and remained during 2 to 15 minutes. The highest temperatures at the site of the fire was approximately 1400 °C.

With rail road and car fires, there was a fast development during 10 to 15 minutes. The temperatures during most of the rail car and bus fires reached maximum values of about 800 to 900 °C. The maximum fire durations for both cases were 128 minutes and 75 minutes, respectively. The fire duration for maximum temperature were 42-46 minutes for rail car and 20-25 minutes for the bus (Haack, 1992, 1995).

2.2.3 Behaviour of Smoke Flow

The general movement of the smoke inside the tunnel during the fire has been illustrated in Chapter 1. It has been pointed out that during the fire, the smoke moves under the influence of forces due to pressure gradients within the bulk of the fluid (Drysdale, 1985). The forces are created by:

1. Buoyancy arising from differences between internal and external ambient temperatures. As long as the smoke is at higher temperature than the surrounding air, it will rise, the buoyancy for per unit volume being given by the product $g(\rho_0 - \rho)$.

2. Buoyancy created directly by the fire. Burning in a compartment or tunnel generates high temperatures which produce the buoyancy for hot gases.

A detailed discussion on the movement of smoke was done by Heselden (1978). Later, Liew et al (1988) briefly discussed the problems of the movement of the smoke and devised the solutions to control the movement.

(1) Smoke Generated in Tunnel Fires

With regard to the smoke flow, it was found that during tunnel fires a large quantity of smoke was generated (Heselden & Hinkley,1970, Haerter,1965). Under natural ventilation, the layer was initially 1-2 m thick depending on the size of the fire, reaching 3 -4 m deep for the largest fire after 10 minutes. The velocity of the advance layer was in the region of 1 - 1.5 m/s. The smoke 'nose' travelled 414 m from the fire and the layer was then quite define even though it would have been some 5° C above the air beneath. A layer or plug of smoke reaching to the ground level was often formed at the tunnel entrance.

With a longitudinal ventilation system, the smoke stratification was rapidly destroyed and lead to a quick development of a steep smoke front which filled the total traffic space. The smoke spread approximately with the same velocity as the longitudinal flow on the exhaust air side. Even if the fumes were highly diluted, the visibility in the smoke area was extremely low or lacking completely.

Hinkley (1970) ' proposed equations (2.1) and (2.2) to calculate the production of the smoke during the fires. M is the smoke production rate and d is the depth of the smoke.

$$M = 0.05P(H - d)^{3/2} \rho_0 g^{1/2} \tag{2.1}$$

$$d = M / \rho_s V_s W \tag{2.2}$$

g is gravity, P is the perimeter of the fire, H is the height of the tunnel, ρ_s is the smoke density, V_s is the velocity of the smoke and W is the width of the tunnel.

Table 2.2 also gives the measured smoke flowrates produced by various HRRs in the Eureka tests. The measured smoke flowrate for a plastic car (5 MW) was estimated to be 30 m^3/s. For a 40 seaters bus and a HGV loading, the smoke flow rates of 60 m^3/s and 50 m^3/s were estimated, respectively. However, the predicted smoke flowrates from PIARC shown in Table 2.3 gives slightly lower smoke flowrate for 5 MW fire (20 m^3/s). For petrol tanker (100 MW), the smoke flowrate was in the range of 100 - 200 m^3/s.

(2) Backlayering Flow and its Interaction with Ventilation

The majority of the experimental programmes in Section 2.1.1 concerned with the backlayering flow. It has been established that the backlayering flow of the smoke occurred when the ventilation velocity in the tunnel was low. The backlayering was characterised stratified in nature, created due to different temperatures between the hot and cold layers. The driving force of these layers was the buoyancy forces due to different densities.

The temperature of the layers decrease as the backlayering flow moves upstream (Hwang & Wargo, 1986). Furthermore, the layer of thickness of the backlayering remains approximately constant until the end, where the layer disappears abruptly. The depth of the layer also decreases with increasing ventilation speed. Further investigation from Kwack et al (1990) also showed that a strong backlayering flow ceiling jets of hot gases were detected well upstream of the fire for all tests. The thickness of the backlayering flow ceiling jet and smoke layer remain relatively constant in the test which was similar smoke layers shapes observed by Hwang and Wargo (1986).

The mixing between layers was found to be characterised by a dimensionless number which known as Richardson number (Ellison and Turner, 1959). The Richardson number is the ratio of the buoyancy forces to the inertial forces,

$$\frac{gH\Delta T}{T(V - V_o)^2} \quad\quad (2.3)$$

where g is the gravitational acceleration, H is tunnel height, ΔT is the temperature difference, T is the smoke temperature, V is the smoke velocity and V_o is the initial smoke velocity.

It was reported that when this number is large, that is for deep, hot smoke layers, then the mixing of the hot layers with the fresh air is very slight. Mixing only occurs when Richardson number falls below a critical value of about 0.8.

(3) Incipient Conditions for Backlayering

One of the main criteria of the ventilation design is to set the correct ventilation flow in order to suppress the backlayering from moving upstream for evacuation during tunnel fire. In order to do this, the critical conditions at which the incipient smoke backlayering occurred has to be investigated and determined.

Thomas (1968) studied the effect of the ventilation velocity on fire plume and defined the modified Froude Number in equation (2.4). Thomas considered the only forces in the fluid are buoyancy, the viscous and the Reynolds stresses due to turbulent mixing. If the molecular diffusion, viscosity, heat loss and friction at the walls are neglected, the flow pattern can only be function of the ratio of buoyancy and inertial force over a cross-section of the tunnel. This ratio could be described by a global parameter having the form of a modified Froude number, Fr_m

$$Fr_m = \left(\frac{gH\Delta T}{U^2 T}\right) \quad\quad (2.4)$$

17

where U is the ventilation velocity. From equation (2.4), Thomas considered the buoyancy head as $gH\Delta T/T$ and the velocity head as U^2/g. Thomas assumed that the critical condition occurs when Fr_m is equal to 1. At this condition, the magnitude of pressure head and velocity head is the same, thus the backlayering does not occur.

Lee et al (1979a) further defined modified Froude number, Fr_m which important as a criterion for the occurrence of backlayering flow. The relationship was similar to Thomas, but instead of using temperature, Lee et al considered the density difference in the equation.

$$Fr_m = \left(\frac{gH\Delta\rho}{U^2\rho_0} \right) \qquad (2.5)$$

where $\Delta\rho$ is the density difference, ρ_0 is the ambient density.

Lee et al found that Fr_m equal to 4.5 for incipient smoke backlayering. Lee et al also found that the critical Fr_m for the smoke backing up at specified distance from the fire, is independent of the length of the fire zone and the fan, only depends on the local interactions between the buoyant flow of hot gases upstream and the forced ventilation flow,U. For longer duct or tunnel, where fire related pressure drops are less significant when compared to the total pressure drop, U will approach the cold ventilation velocity. In their further experiments on the stratified backlayering flow (Lee et al, 1979b), Lee et al defined two further modified Froude numbers to characteristic the backing up phenomenon replacing U by Uv which is a velocity immediately upstream from the fire,

$$Fr_m = \left(\frac{gH\Delta\rho}{U_v^2\rho_0} \right) \qquad (2.6)$$

The second modified Froude number shown in equation (2.7) was based on tunnel height(H) and ventilation velocity(U), proposed as a more practical modified Froude number than Fr_m, being more easily determined from experimental data.

$$Fr_{m(a)} = \left(\frac{gH}{U^2}\right) \qquad (2.7)$$

Fr_m was found to be approximately unity and $Fr_{m(a)}$ was found to be approximately 10 when backlayering flow in the small scale experiments occurred.

Ris (1970) proposed another modified Froude number based on Prandtl's mixing length hypothesis to explain the separation between hot and cold layers in the interaction of ventilation flow in duct fire. The resulting equation is as below:

$$\frac{\Delta\rho g\overline{H}}{\rho U^2} \leq \frac{\overline{w}'^2}{U^2}\frac{\overline{H}}{\ell} \qquad (2.8)$$

where $\overline{H}$ is the mean flow width, w' is the characteristic vertical velocity and l is the characteristic vertical length. It was found that the turbulent mixing is completely suppressed when $\Delta\rho gH/(\rho U^2) \geq 0.8$.

The magnitude of the modified Froude number for the incipient occurrence of the backlayering flow remains debatable and these values vary with each authors. These differences arise because the experimental measurements, on which they are based, derived from a wide variety of tunnel shapes, sizes and fire scenario. The modified Froude number from Lee et al for example, was based on several aspects. The most important are:

- The fire was not a discrete floor source, but emanated from 3 elongated surfaces forming the roof and side walls of the duct.

- A relatively high rate of mass injection from the fuel was recorded, giving $m_f/m_a = 1$.

However, Thomas imposes the following restrictions upon the applicability of this criterion:

- Molecular diffusion and viscous stresses are neglected for a fire source on the floor of the duct.

19

- The fire is assumed to produce a low mass injection rate such as that m_f/m_a = 10^{-3}.

- The temperature rise in the hot gas remains small, so that $(T_f-T_a)/T_a \ll 1$.

The conditions of the assumptions used in Thomas (1968) was further verified by Grant et al (1988) in their small scale experiment.

2.2.4 Throttling Effect

As a fire develops in the tunnel, it interacts with ventilation air flow and generates aerodynamic disturbances in the ventilation flow. The interaction and disturbance may lead disturbances such as throttling of the air flow which result an overall increase in the flow resistance in the tunnel. When the ventilation velocity was throttled down, backlayering flows tends to occur in the tunnel.

Hwang and Chaiken (1978) produced a simple one dimensional quasi-steady mathematical model for simulating the throttling effect on longitudinal ventilation. Their model was tailored to a specific experimental facility which had a short duct length between the fire and exhaust fan. The model correctly predicted the throttling effect for a constant volumetric flowrate at the fan. Application of this model is only useful when the fire seat is close to an exhaust fan.

Chaiken et al (1979) performed experimental works to study the throttling effects in tunnel fire. Data from these experiments on flow throttling down to the point where flow reversal and substantial smoke backlayering occurs, was found to be in broad agreement with the model developed by Hwang and Chaiken (1978). It was found that the flow resistance in the fire zone was increased by a factor of 6, and upstream and downstream of fire by approximately 1.5. The ventilation air velocity was thus throttled to less than half of its initial value before the fire.

2.3 Critical Ventilation Velocity

2.3.1 Critical Ventilation Velocity Relationship

Thomas (1968) then proposed the relationship between the ventilation velocity and the HRR. From the modified Fr_m (equation 2.4), Thomas deduced a critical ventilation which at the backlayering flow is just suppressed by assuming that at equilibrium, the two forces will be equal. He then substituted the expression that relate ΔT and Q, the HRR (convective component only, into (2.4), becomes:

$$U_c = k \left(\frac{gQ'}{\rho_0 C_p T} \right)^{\frac{1}{3}}$$ (2.9)

where U_c is the critical ventilation velocity, Q' is HRR per unit width of the tunnel W, ρ_0 is the ambient air density, C_p is the specific heat capacity, k is a constant of order unity and T is the smoke temperature. The value of k can be found from suitable experiments by assuming that a representative value for T can be identified.

Hinkley (1970) derived another formula for calculating the velocity of hot gases travelling along the roof of a shopping mall. Hinkley used the same theory as Thomas to give the velocity of these gases as in equations (2.10). The magnitude of this velocity was assumed similar to the magnitude of the ventilation velocity.

$$U_c = K' \left(\frac{gQT}{C_p \rho_0 T_0^2 W} \right)^{\frac{1}{3}}$$ (2.10)

The value of K' was found to be 0.8, taken from experimental data on the movement of the hot gas layers in relatively short corridors, without forced ventilation. The velocity of 'nose' or 'smoke front' is given by a similar relationship. He includes an algebraic function of the depth of the layer and the height of the mall, noted by "K".

$$U_c = CK \left(\frac{gQT}{C_p \rho_0 T_0^2 W} \right)^{\frac{1}{3}}$$ (2.11)

where C is a constant equal to 0.82.

Based on Hinkley's theory, Heselden (1978) derived another formula for calculating the critical ventilation velocity.

$$Uc = CK\left(\frac{gQT}{C_p\rho_o T_o{}^2 W}\right)^{1/3}$$ (2.12)

Heselden assumes that K is equal to unity and fixes C at 0.8. Both values were obtained by experiments in a disused rail tunnel (Heselden and Hinkley, 1970). The heat output and the critical ventilation velocity were estimated. The value of C was determined by taking just three sets of experimental data.

In 1982, The Subway Environment System (SES) derived a simple model, to calculate the critical ventilation velocity devised by Danziger and Kennedy (1982). The critical ventilation velocity is given by, Uc

$$Uc = K_g k\left(\frac{gQ}{C_p\rho_o T\ W}\right)^{1/3}$$ (2.13)

$$T = \left(\frac{Q}{C_p\rho_o A U_c}\right) + T_o$$ (2.14)

The value of k is set to 0.61, calculated based on modified Froude number equal to 4.5, obtained by Lee et al (1979).

The most recent models derived to calculate the critical ventilation velocity were from Oka and Atkinson (1995) based on their small scale experimental results. The following general expression were reported for the critical ventilation velocity in the model:

$$U_c = V^* \sqrt{gH} \left(\frac{Q^*}{0.12} \right)^{1/3} \quad \text{for } Q^* < 0.12 \qquad (2.15)$$

$$U_c = V^* \sqrt{gH} \qquad \text{for } Q^* > 0.12 \qquad (2.16)$$

where Q^* and V^* are the dimensionless HRR and dimensionless critical ventilation velocity obtained in equation (2.17 and 2.18), respectively.

$$Q^* = \frac{Q}{\rho_0 T_0 C_p g^{\frac{1}{2}} H^{\frac{5}{2}}} \qquad (2.17)$$

$$V^* = \frac{U_c}{\sqrt{gH}} \qquad (2.18)$$

The values of V^* are between 0.22 and 0.38 depending on various burners in the smaller models.

It should be noted that the above models are derived based on data at which the backlayering will not occur. They cannot be extended to be used to predict the ventilation velocity at which the backlayering propagating at certain distance from fire source.

2.3.2 Measured and Predicted Critical Ventilation Velocity

Table 2.4 summarises the critical ventilation velocity for large scale tunnels based on experimental tests and predictions. There were still lack of critical ventilation measurements in large scale tunnels. The critical ventilation data were limited to only one or two HRRs and scattered especially at higher HRRs.

It was difficult to justify the exact value of the critical ventilation velocity for a specific HRR due to insufficient data. However, for the worst possible scenario in tunnel fire, HRR of 100 MW should be considered as the upper limit. Indeed, the overall data in Table 2.4 shows that PIARC gave a wide range of critical ventilation velocities, from 5

m/s to 8 m/s, for 100 MW fire. However, the predicted value from Heselden (equation 2.12), suggested lower velocity for a fire of this size (6.7 m/s). Above all, the measured values from Eureka and Memorial tunnel tests for HRR 100 MW were much lower, approximately 2.8 m/s and between 2.5 m/s to 3.0 m/s, respectively.

2.3.3 Parametric Analysis of Critical Ventilation Velocity

(1) Effect of Fire Sizes

The empirical models derived by Thomas (1968), Hinkley (1970) and Heselden (1978) suggested the value of the critical ventilation velocity for the horizontal tunnel varies with the one third power of the heat output from fire. The present of variable T in the numerator of equation (2.13) in the SES model shows that at large heat outputs the critical ventilation velocity tends to an asymptote of near-constant velocity.

Through experiments, the most valuable results were from Memorial tests and Gallery tests (Bettis et al, 1993, 1994). Both results showed that the critical ventilation velocity varied with one third power of HRR. However, the above variations were only limited to lower heat release in the Gallery tests. Instead, the critical ventilation velocity was found to be nearly independent of heat output over a wide range of fire sizes. These behaviour has been confirmed by Oka and Atkinson (1995) in their small scale experiments.

Kennedy (1997) made further comparison between SES program and Memorial test results. The variations of the critical ventilation velocity with fire HRR was in a good agreement. However, it reported that SES overpredicted the required air velocity by 4 to 20 percent for large fires. SES also underpredicted the critical ventilation velocity for a small fire.

(2) The Effect of Tunnel Slope

When the fire seat is located in the low part of the tunnel, buoyant plume of combustion products, smoke and hot gases resulted from the fire will rise and impinge the tunnel roof, then spreading of the hot smoke along the roof will take form of a gravity current which has the characteristic features of a deep head at the leading edge, followed behind by a shallower layer.

The magnitude of the ventilation velocity and the inclination angle of the tunnel greatly influence the orientation and location of the leading edge of the plume (Hwang and Wargo, 1986). The backlayering layers are stable but their appearance and disappearance is very sensitive to the magnitude of the ventilation velocity and the inclination angle of the tunnel. The layer maintains its thickness almost to the end, where the thickness decreases rapidly.

Atkinson and Wu (1996) found that the effect of slope on critical ventilation velocity to control the smoke flow was modest. The magnitudes of the critical ventilation velocities were found to be very sensitive for the downhill slope between 0° to 4°. The critical ventilation velocities were then became independent of the slope when the downhill slope greater than 4°. Correlations to obtain critical ventilation velocity for a sloping tunnel were then suggested as in equations (2.19) and (2.20).

$$U_c = [gH]^{1/2} \times V^*_{max} \times \left[\frac{Q^*}{0.12} \right] \times [1 + 0.008\theta] \qquad \text{for } Q^* \leq 0.12 \qquad (2.19)$$

$$U_c = [gH]^{1/2} \times V^*_{max} \times [1 + 0.008\theta] \qquad \text{for } Q^* \geq 0.12 \qquad (2.20)$$

where θ is the tunnel slope expressed in percentage. The grade correction factor recommended in the U.S. department of Transport Subway Environment Simulation (SES) Program to predict the critical ventilation velocity in slopings tunnels is:

$$V(\theta) = V_o \times \left[1 + 0.0374\theta^{0.8} \right] \qquad (2.21)$$

(3) The Effect of Fire Geometry and Locations

The vehicles that occupy the tunnel can present the blockage in the tunnel. Oka and Atkinson (1995) found in their experimental tunnel that a solid blockage produced sizeable decreases in the critical ventilation velocity. In a tunnel of the experimental shape (Colliery Arch), a vehicle with a height around half the tunnel height occupying around 12% of the tunnel cross section should cause a decrease of around 15% in the critical ventilation velocity. Oka and Atkinson gave further example to state that if the vehicle occupies 32% of the tunnel cross section the critical ventilation velocity should be reduced by 40-45%. They also found that the fire geometry has a relatively minor effect on the critical ventilation velocity.

However, both findings were limited to only small scale model. Further studies in larger experimental test facilities are required to confirm the above variations.

(4) The Effect of Tunnel Aspect Ratio

The effect of tunnel aspect ratio (cross-section) have not been studied in detail. Most of the previous experimental data obtained by performing tests on one tunnel geometry.

2.4 Tunnel Fire Study by Computational Fluid Dynamics

2.4.1 CFD Simulations

The most recent technique to study the behaviour of tunnel fires is by using Computational Fluid Dynamics (CFD). This approach is capable of modelling multi-dimensional, time-dependent nature of fire in both obstructed and un-obstructed tunnel of arbitrary geometry. This approach is based on equations for the conservation of mass, momentum and energy. CFD models are built based on many complex interactive processes such as convection, buoyancy, radiation, three-dimensional effects and combustion. The performances of CFD simulations depend on the accuracy of the physical models to describe turbulence, heat transfer, combustion process and smoke transportation.

Table 2.5 summarises some of published CFD works that obtained from the literature.

2.4.2 Aspects of Tunnel Fires Studied by CFD

Although CFD is at the earlier stage in tunnel fire studies, there are several aspects that have been investigated by several researchers listed in Table 2.5.

(1) Validation of the computer codes

The first hurdle in CFD modelling is to study the flow problem and the combustion model. Much of work has been done in these fields. The use of the two - equations k - ε model has been shown to be quite valid. However, the current turbulence model was reported can only produce the accuracy of about 15 - 20 percent in the prediction of smoke velocities and temperature (Rhode, 1995).

The present combustion models are not matured enough to simulate the fire. Alternatively, some of CFD publications used heat source to represent the fire inside the tunnel. However, despite the limitations, all authors in Table 2.5 successfully simulated the qualitative behaviours of tunnel fire similar to the experimental observations.

Kumar and Cox (1987) reported that the qualitative features of the forced-ventilated Zwenberg fire trial were successfully captured such as the absence of any backlayering flow against the longitudinal ventilation was correctly mimicked. In addition, the measured average downstream velocity of the hot gas layer was accurately simulated and the temperature field was adequately predicted except very close to the fire.

Woodburn and Britter (1996) found that the inclusion of the buoyancy-related modifications in standard k-ε turbulence model strongly affected the extent of upstream propagation of the backlayering against the ventilation. They also found that with the exclusion of radiative model, the length of an upstream propagating smoke layer was

very sensitive to the ventilation velocity. This was in agreement with experimental results.

Fletcher et al (1994) also found similar findings as Woodburn and Britter. With the inclusion of the buoyancy-related modifications in standard k-ε turbulence model, the hot layer extent double the length which was in a close agreement with experimental data. In addition, the amount of backlayering flow calculated using the model was found to be relatively insensitive to the radiation model.

Fletcher et al also studied the flow behaviour in the fire zone. They found that flow within the fire zone was dominated by three-dimensional which confined within 2 metres upstream and 5 metres downstream. The flame tilt angle appeared to be well captured. However, the temperatures downstream from the fire in Fletcher's simulation was over-predicted and Fletcher et al were not able to find the reason for this. However, the heat output from these fires was estimated from measured fuel mass loss rate, so this is one possible source for the discrepancy. The effect of varying the prescribed soot fraction was found to be small on both the downstream temperature field and backup layer length. One of the main findings was that the observed stratification in the downstream temperatures field was only captured if the buoyancy modifications were incorporated in the standard k-ε turbulent model. When these modifications were removed, the stratifications were also greatly reduced.

Lea (1995) found that the upstream flow was very sensitive to small changes in velocity which was consistent with the behaviour found in both the Phase 1 and 2 HSE-Buxton tunnel fire trial (Bettis et al, 1993 & 1994). The plume of the hot combustion products was inclined at a large angle to the vertical. The simulated tilt angle was nearer 75°. A similar patterns were observed in the HSE-Buxton Phase 1 fire trials. Lea reasoned that the large tilt angles was not due to the differential rates of entrainment on the upwind and downwind sides of the plume. The large tilt angles was claimed found due to local accelerations of the incoming air around the fire plume.

In the following simulation on a one-third scale model of Channel tunnel heavy goods vehicle shuttle Lea (1997) found that the extent of a hot layer 'backlayering' against imposed longitudinal ventilation was adequately captured. However, the simulation did not adequately measure temperatures closer to the fire, in particular immediately downstream from the fuel tray. The simulated velocity around the locomotive and amenity coach was also over- predicted. However, the qualitative behaviour (negative velocity) above the loader wagon was reported to be correctly captured - indicating the presence of a hot layer.

Other CFD publications related to tunnel fires have been published in Bennardo et al (1997), Bettis (1995), Brandies et al (1983) and Van de Leur et al (1989).

(2) Prediction of Critical Ventilation Velocity

There has been very little publications concerned with the prediction of critical ventilation velocity. The first simulation was performed by Kumar and Cox (1987) for Zwenberg model tunnel. Others simulations were from Gaffney and Kynaston (1992), Woodburn and Britter (1996) and finally Lea (1995) who gave the most comprehensive prediction for HRRs between 1 MW to 15 MW for the Gallery tunnel, Buxton.

(3) Sensitivity Analysis on the Critical Ventilation Velocity.

The empirical models, discussed in Section 2.3 show that the critical ventilation velocity depends on several parameters such as fire size, tunnel slope and tunnel geometry. Simulations to investigate the sensitivity analysis of the critical ventilation relationship have been made.

(a) Effect of Fire Sizes

Tuovinen et. al (1996) indicated that the bigger the fire size, the bigger the hazardous region. The pattern of the variation of the critical ventilation velocity however could not be justified since in their simulations, only two fire sizes were considered. Similarly, Lacroix (1997) reported that the critical velocities greatly depend on the fire sizes. However, its variation was also not reported.

Lea (1995) correctly predicted the critical ventilation velocity pattern similar to the established empirical models. However, he found that the critical ventilation velocity was essentially independent of HRR at larger HRR, a similar results obtained the experimental tests for the Gallery tunnel, in Buxton.

(b) Effect Tunnel Slope

Britter and Linden (1980) showed that the travelling speed of the current front was sensitive to small changes in the slope angle when the slope was less than 5°. However, the front speed was much less dependent on the slope when the slope was greater than 5°. These findings were in a good agreement with the simulated results from Kawabata et al (1991) who showed that at certain ventilation velocity, there was no backlayering regardless of the grade of the tunnel.

Woodburn and Britter (1996) indicated that the backlayering flow behaves as gravity current when the length of the flow was greater than 5 times of the tunnel height. When the flow was less than 5 times of the tunnel height, the flow was strongly influenced by the impingement and deflection at the tunnel roof.

Tuovinen et. al (1996) also compared the progress of smoke between 3 slope angles of 0°, 2.5° and 5°. The results showed that the hazardous smoke region began to move very rapidly in the upward direction, for slope 2.5° and 5.0°. The larger the slope, the faster the movement of the zones.

(c) Effect of Tunnel Width (Aspect Ratio)

With regard to the effects of tunnel width on the critical ventilation velocity, Lea (1995) found that for a given fire HRR, as the tunnel width increases the critical ventilation velocity also increases. This was in direct contradiction to the trends suggested by any of the simple models for critical ventilation velocity in section 2.3, which indicate that the critical ventilation velocity should decrease in these circumstances.

To test on the effect of tunnel width Tuovinen et. al (1996) performed 6 cases for fire growth $\alpha = 0.1$, 1.54, and 3.5 kW/s^2 on both 6 m and 12 m wide tunnels. The results showed that hazardous regions moved faster in 6 m wide tunnel than in 12 m wide tunnel for the small fires with the same HRR. For larger fire (3.5 kW/s^2), the model predicted the hazardous regions moved faster in the 12 m wide tunnel.

However, there is no experimental data to verify these findings from Lea and Tuovinen et al.

2.5 Conclusions

There were a number of major experimental tests and reduced scale tests in tunnel fires. However, the majority of the data were not adequate. In most cases, the HRR produced by the fire was not measured. This was one of the major discrepancies. The duration of the fire also was reported to be short. Thus it cannot be ensured that steady state conditions has reached. There were also limited studies in tunnel fire tests which involved real vehicles. As consequences, the actual data of HRRs from the real vehicle have to be estimated.

The flow behaviour of the backlayering has been theoretically modelled. The relationship between the critical ventilation velocity to prevent smoke backlayering flow has been derived by several workers. However, the critical ventilation velocity data were limited

in numbers and scattered, especially at higher HRR. Some of the values obtained from large scale experiments were in doubt because it was unclear whether the smoke layer was controlled exactly at the leading edge of the fire. In the real case, it was very difficult to control the layer at exactly the critical conditions. This lead to the uncertainties on the value of the critical ventilation velocity.

The influence of fire HRR on the critical ventilation velocity has also been studied. The empirical models suggest that the critical ventilation velocity varies with the one third to the power of the HRR. This relationship was confirmed in the experimental tests. However, uncertainty arises from to the most recent results from HSL, Buxton. The critical ventilation velocities at higher HRRs appeared to be less dependence on the HRRs. Thus, in future, it is necessary to confirm the findings by carrying out further experiments in different tunnel geometries and provides the information for understanding the behaviour.

There are limited studies on the effect of tunnel slope on the critical ventilation velocity. Furthermore, the literature showed that no studies were carried out on the effect of tunnel geometry on the critical ventilation velocity and yet this is very important issue. In the present empirical models, the critical ventilation velocity was calculated based on the fire HRR per tunnel width. However, the shapes of the tunnels are not considered.

CFD simulations on tunnel fire are at the initial stage. The field model approach, however, has not yet reached the stage of describing complete air flow in a tunnel fire. The buoyancy effect in turbulence model is the most focused issue in CFD simulations. The hot plume induced by a local fire, its interaction with the ventilated air flow, and the secondary flow in cross-sections have significant influence on flow turbulence distribution. These effects have to be taken into account in the turbulence model. Further studies on the flow behaviour and computer validations are urgently required. Finally, the combustion and radiation models are not mature enough to be used effectively in the

simulation of tunnel fire. Some of the published CFD works used heat source to represent the combustion rather than to model real combustion. Due to its complexity, under some circumstances most of the researchers try to avoid radiation models in their simulations.

Table 2.1: Summary of selected experimental tunnel fire tests

Authors	Scale		Tunnel				Reported Measurements						
	Large	Small	Slope	Height (m)	Width (m)	Shape	Qmax	Qmin	Umax (m/s)	Umin (m/s)	Temp	Vel	Gas
Heselden &Hinckely (1970)	✓		-	5.2	7.6	(1)	8MW	2MW	1.5	1.0	✓	-	✓
Haerter (1965)	✓		-	6.0	4.0	(1)	not reported		1.7	1.7	✓	-	✓
Feizlmayr (1976)	✓		3.9	4.0	5.0	(2)	not reported		7.0	-	✓	-	-
Ventalon et al (1991)		✓	-	radius = 0.15m		(3)	800W	325W	0.225	0.19	✓	-	-
Kwack, E.Y (1990)		✓	-	0.76	1.52	(5)	335kW	246kW	0.78	0.58	-	-	-
Xue, Hihara (1993)		✓	-	radius = 0.25m		(3)	3kW	3kW	0.92	0.46	✓	✓	
Hwang & Wargo (1980)		✓	±18	0.3	0.4	(2)	not reported		0.309	0.202	✓	✓	
Oka & Atkinson (1995)		✓	-	0.244	0.274	(4)	28.1kW	2.8kW	0.10	0.60	-	✓	-
Atkinson & Wu (1996)		✓	0-10	0.244	0.274	(4)	14.1kW	2.8kW	0.10	0.60	✓	✓	-
Bettis et al (1993, 1994)	✓		-	2.44	2.74	(4)	20MW	0.3MW	4.0	0.50	✓	✓	✓
Newman et al (1993, 1994)	✓		-	2.4	2.4	(2)	20 MW	10 kW	4.0	0.5	✓	✓	✓
Grant et al (1988)		✓		radius = 0.15 m		(3)	1.783 kW	0.07 kW	6.72	0.96	✓	✓	
Apte et al (1991)	✓		-	2.4	5.4	(2)	12MW	0.5MW	2.0	0.5	✓	✓	✓
Chaiken et al (1979)		✓	-	0.27	0.27	(2)	not reported		not reported		✓	✓	✓
Lee et al (1979)		✓	-	0.40	0.30	(2)	not reported		not reported		✓	✓	✓

Keynotes: (1) Horse shoe   (2) Rectangular   (3) Circular   (4) Arch   (5)The shape is uncertain

34

Table 2.2: Measured fire powers obtained from Eureka tests (Haack, 1995)

Test No	Fire Source	Release Energy	Ventilation (m^3/s)	HRR (MW)	Smoke Flow Rate (m^3/s)
C11	Metal car	6 GJ	0.3	-	-
C21	Plastic car	7 GJ	0.5	5	30
B11	Bus(40seats)	48 GJ	0.3	25	60
LF1	HGV loading	65 GJ	0.7	15	50
HF1	Loaded HGV	87 GJ	6/0.5/3	40-150	-

Table 2.3: Proposed fire powers by PIARC in 1987 (Lacroix, 1997)

Cause of fire	Equivalent gasoline pool (m^2)	Heat Release Rate (MW)	Smoke Flow Rate (m^3/s)
Passenger car	2	≈ 5	20
Bus/Truck	8	≈ 20	60
Petrol tanker	30-100	≈ 100	100-200

Table 2. 4: Measured and predicted critical ventilation velocity based on larger scales

Authors	Methods	Tunnel	Minimum critical ventilation (m/s)	Fire sizes (MW)
Feizlmayr (1976)	measured	Zwenberg	2.0	20
Haack (1995)	mesured	Repparfjord	2.8	100
Lacroix (1997)	measured	Memorial	2.5 - 3.0	10 - 100
Jagger (1996)	measured	Gallery	1.6	5.4
Lacroix (1997)	measured	Puymorens	2.0 , 3.0	2-3 , 4 -5
Lacroix (1997)	measured	Grand Mere	2.0 , 2.5-3.0, 3.5 -4.0	5, 10, 20
Kennedy et al (1988)	predicted	Mount Lebanon	2.5 - 11.0	not stated
Heselden (1978)	predicted	hypothetical tunnel	5.3 , 6.7	50 , 100
Kennedy *et al* (1982)	predicted	Glenwood	2.8	50
Chow & Leung (1988)	predicted	Zwenberg	2.5	14.45 - 20
Jones *et. al* (1988)	predicted	Dartford	3.0	not stated
Lowndes *et.al* (1988)	predicted	Route 5	5.0	not stated
Pope *et al* (1988)	predicted	Great Belt	5.0	not stated
Wood, D (1993)	predicted	Limehouse	4 .0	50 MW
Mizuno *et al* (1992)	predicted	Tokyo Bay	2.0 - 3.0	not stated
Berner (1992)	predicted	Gottard	5.0 - 8.0	100
World Congress (1987)	guideline	.	1.0-2.0, 2.0-3.0, 5.0-8.0	5, 20 ,100
PIARC (1987)	guideline		3.0 - 6.0	not stated

Table 2.5: Summary of selected CFD simulations

Author	Code		Tunnel				CFD sub-models			Reported Values			
			Model	Height	Width	Shape	Flow	Fire	Radiation	Qmin	Qmax	Umin	Umax
Kumar & Cox (1987)	Jasmine	3D	Zwenberg	4.0	5.0	(2)	k - ε	Comb.	✓	14.45 MW	20.25 MW	2	4
Fletcher et al (1994)	Furnace	3D		2.4	5.4	(2)	k - ε	Comb	✓			0.5	2.0
Woodburn & Britter (1996)	FLOW3D	3D	Gallery	2.44	2.74	(4)	k - ε	Comb	✓	1.5 MW	2.3 MW	1.72	1.85
Lea (1994,1997)	FLOW3D	3D	Gallery	2.44	2.74	(4)	k - ε	Comb	✓	1 MW	15 MW	1.15	1.3
Tuovinen et al (1996)	Jasmine	3D	Ofnegg	6.0	4.0	(1)	k - ε	Comb	✓	not reported		not reported	
Brandies et al (1983)	TDC	2D	Caldecott	7.64	L = 100	(2)	not reported	Comb	not report	not reported		2.0	2.0
Chow & Leung (1988)	Simpler	3D	Ofnegg	4.0	5.0	(2)	k - ε	Comb	not report	14.45 MW	20.25MW	2.5	4.0
Kawabata et al (1991)	not reported	2D	model	6.9	L = 8.31	(2)	k - ε	Comb	not report	2MW	2MW	2.0	4.5
Bennardo et al (1997)	FLUENT	3D	model	0.1	0.2	(2)	k - ε	Heat source	not report	10 MW	12 MW	not reported	
Xue et al (1993)	SIMPLER	3D	model	radius = 0.25		(3)	k - ε	Heat source	not report	1.42×10^5 (W/m^2)		0.46	0.92
Apte et al (1991)	Furnace	3D	model	2.4	5.4	(2)	k - ε	Comb	not report	not reported		0.5	2.0

Keynotes: (1) Horse shoe   (2) Rectangular   (3) Circular   (4) Arch   Comb = combustion

Chapter 3

Scaling

Many engineering problems have been resolved satisfactorily by applying modelling procedures. These procedures permit full scale behaviour to be predicted from the result of small scale tests. Scaling the models is achieved by identifying the important parameter of the system and expressing these in the form of relevant dimensionless parameter of the system.

Of course, the real and exact experimental data can only be obtained in a large scale tests. However to organise full scale tests to study fires in tunnels is very expensive and requires much time. In addition, it will be very difficult to control the experimental parameters since the geometry is quite large. The reduced scale experiments are far less costly than full size tests in special facilities. They are also more flexible and allow to test a great number of situations. Visualisation is generally better than in an actual site, measurements are easier and principally more reproducible, since the laboratory conditions enable to monitor all parameters.

The only rigorous method in the scaling technique is to use similarity laws that define the scale ratio for all physical and chemical quantities. Fluid dynamics similarity is possible because the equations which govern heat transfer in tunnel air on the one part and transportation of a second fluids in the model on the other part are identical under an non-dimensional form. However, there are some restrictions since the detailed structures of the flow such as turbulent scale and intensity and the energy exchange such as flame radiation, may not comparable between a small and a large scale. Hence this restriction leads to partial scaling techniques.

Table 3.1 summarises capabilities and limitations of real tunnel tests with full size fire test in specialised facilities (Lacroix,1995). Table 3.2 summarises the comparisons of two types of reduced scale model (Lacroix, 1995).

3.1 Froude Scaling

The relationship in the scaling laws in fire studies were published in details by Emori et al (1983) and Quintiere (1989) who solved the governing equations of momentum, energy and species. There are more than 28 dimensionless groups were derived.

Regarding a tunnel fire, there are two non-dimensional groups that are important because they determine flow dynamics in forced convection to which the air movements inside the tunnel at certain distance from the fire can be assimilated.

(1)   Reynolds number $$R_e = \frac{VD}{\nu} = \frac{\text{inertia forces}}{\text{viscosity forces}}$$ (3.1)

where V and D respectively characteristic values of speeds and length, and ν the kinematic viscosity of the fluid. This number characterises the laminar or turbulent regime of the flow.

(2)   Froude number $$Fr = \frac{V^2}{gD} = \frac{\text{inertia forces}}{\text{gravity forces}}$$ (3.2)

This number characterises the effects of gravity and is therefore very important to take into account the lower density of hot gases. It may sometimes be combined with relative difference of the smoke density ($\Delta\rho/\rho$) to investigate its stratification. It is then called the Richardson number. Most authors in Chapter 2 defined as modified Froude number.

$$R_i = \frac{gD}{V^2} \cdot \frac{\Delta\rho}{\rho} = \frac{1}{F_r} \cdot \frac{\Delta\rho}{\rho}$$ (3.3)

Many other non-dimensional groups must be considered due to many physical phenomena involved, such as thermal transfers, including radiation and chemistry. In practice it is never possible to preserve the totality of similarities at a scale other that full size.

For essentially all steady state-burning fire problems, reaction are fast enough to burn all the oxygen before it reaches the fuel surface. Thus, combustion rate can be regarded as independent of (fast) chemical kinetics and all dimensionless groups related to chemical kinetics, such as activation energy number can be ignored.

In a fire situation when turbulent conditions prevail and the Reynolds number is sufficiently large, there is no need for R_e number to be equal in full scale and reduced scale models The Reynolds number must be kept beyond a critical value warranting a well-established turbulent regime, at least 10000 to 20000 (Lacroix, 1995).

Radiation effects, if considered important, can only be included in this scaling approach as a constant fraction of convective heat release rate. Under such circumstance, the fluid dynamics of the convection dominated fires can be modelled by Froude number.

3.1.1 Dimensionless Heat Release Rate and the Critical Ventilation Velocity in Froude Scaling

Comparisons between two different scales are always in the form of dimensionless forms. For tunnel fire study, the dimensionless forms are expressed in the terms of dimensionless heat release rate and velocity based on Froude modelling by Thomas, (1968) as follows:

(1) Dimensionless velocity

$$V^* = \frac{Uc}{\sqrt{gH}} \qquad (3.4)$$

(2) Dimensionless heat release rate

$$Q^* = \frac{Q}{\rho_0 T_0 C_p g^{\frac{1}{2}} H^{\frac{5}{2}}} \qquad (3.5)$$

Alternatively, the dimensionless groups can be derived from the critical ventilation velocity relationship shown in equation 3.6. A simple dimensionless technique namely, Buckingham technique to obtain dimensionless groups can be used as follows:

$$U_c = \left(\frac{gQ'H}{\rho_0 C_p T_0 A_T}\right)^{1/3} \qquad (3.6)$$

In equation (3.6), there are 8 variables identified: U_c, g, Q, ρ, C_p, H, T and A_T

The dimensional unit for each variable : $[LT^{-1}]$, $[LT^{-2}]$, $[ML^2T^{-3}]$, $[ML^{-3}]$, $[L^2T^{-2}\theta^{-1}]$, $[L]$, $[\theta]$ and $[L^2]$, respectively.

The general form in the Buckingham Π Theorem is,

$$[LT^{-1}][LT^{-2}]^a[ML^2T^{-3}]^b[L]^c[ML^{-3}]^d[L^2T^{-2}\theta^{-1}]^e[\theta]^f[L^2]^g = [M]^0[L]^0[\theta]^0[T]^0 \quad (3.7)$$

Equating exponents of each dimension,

For M	$b + d = 0$	(3.8)
For L	$1 + a + 2b + c - 3d + 2e + 2g = 0$	(3.9)
For T	$-1 - 2a - 3b - 2e = 0$	(3.10)
For θ	$-e + f = 0$	(3.11)

By solving d, e, f and g in term of a, b, and c

$$d = -b \tag{3.12}$$

$$e = -1/2 - a - 3/2b \tag{3.13}$$

$$f = -1/2 - a - 3/2b \tag{3.14}$$

$$g = 1/2a - b - 1/2c \tag{3.15}$$

$$[U_c]\,[g]^a\,[Q]^b\,[H]^c\,[\rho]^{-b}\,[Cp]^{-1/2-a-3/2b}\,[T]^{-1/2-a-3/2b}\,[A_T]^{1/2a-b-1/2c} \tag{3.16}$$

Thus, the dimensional group can be expressed in term of Π,

$$\Pi_1 = \left(\frac{g}{C_p T_o A_T^{1/2}}\right) \quad \Pi_2 = \left(\frac{Q}{\rho_o C_p^{3/2} T^{3/2} A_T}\right) \quad \Pi_3 = \left(\frac{H}{A_T^{1/2}}\right) \quad \Pi_4 = \left(\frac{U_c}{C_p^{1/2} T^{1/2}}\right)$$

By combining $\Pi 1$ and $\Pi 4$ obtained

$$\Pi_5 = \left[\frac{v}{\sqrt{gl}}\right],$$

represents the dimensionless critical ventilation velocity.

Combining $\Pi 2$, $\Pi 4$ and $\Pi 5$, obtained

$$\Pi_6 = \left[\frac{Q}{\rho_o Cp_o T_o g^{1/2} \ell^{5/2}}\right].$$

represents the dimensionless heat release rate.

3.1.2 Scaling Relationship for Tunnel Fire

Froude number scaling has been used extensively to simulate aerodynamics effects of tunnel fires (Oka and Atkinson ,1995 ; Wu et al, 1997, Bakar et al , 1999; Lee et al, 1979; Vantalon et al, 1991).

The fundamental of Froude scaling involves maintaining the same Froude number at each of scaled involved. To preserve the Froude number both heat release rate and air velocity need to be altered if the geometry is scaled linearly. In order to achieve this requirement the following expressions must be kept constant.

$(Q/l^{5/2})$ = constant, in order to maintain similar flame shapes and temperatures

$(V/(gl))^{1/2}$ = constant

where l is the characteristic length, is the height of the tunnel.

Oka and Atkinson (1995) further derived heat release and velocity scaling relationship by using Froude model. For the heat release scaling, it is established by Thomas that heat release, Q is scaled to $H^{5/2}$. Thus the relationship becomes,

$$\frac{Q_{model}}{Q_{fullscale}} = \left[\frac{H_{model}}{H_{fullscale}}\right]^{5/2} \tag{3.17}$$

where H is the tunnel height

For critical ventilation relationship,

$$\left[\frac{V_{model}}{V_{fullscale}}\right] = \left[\frac{H_{model}}{H_{fullscale}}\right]^{1/2} \text{ (for large or small Q)} \tag{3.18}$$

43

3.2   Problems Arising in Froude Scaling

In the established scaling law, the characteristic length of the buoyant flow is taken as the height of the tunnel. However, there are some uncertainties arises from this technique. First, the validity of the established technique might be only for the tunnels which have the same cross - sectional area. Since the characteristic length in equations (3.18) is taken as the tunnel height, it would be expected that the same critical ventilation velocity will be predicted for tunnels having the same height but different cross-sectional geometries.

A good example of the validation of the current established technique was when Oka and Atkinson (1995) compared the small scale results with the Gallery tunnel (which has the same cross-sectional shape). The results showed a good agreement between the two scale tunnels. However, when the small scale results were compared with the Memorial tunnel results (vaulted cross-sectional with 60 m^2 area and 7.86 m maximum height) by Lacroix (1997), the results did not completely fit the derived models obtained by Oka and Atkinson.   The critical ventilation velocity for the Memorial tests kept on slowly growing with the high heat release rates, above the reported Q* = 0.12 limit. However there was no strong disagreement in the critical ventilation velocity when V* values around 0.35 were used.

A plausible answer for the difference is that the cross-sectional area of the Memorial tunnel is not exactly the same as the model of Oka and Atkinson and hence further investigation on the characteristic length in the scaling relationship which includes the cross-sectional shape of the tunnel is required.

The use of characteristic length varies from many authors. Most authors (Chapter 2) used tunnel height as the characteristic length. However, in the work of Ris (1970), the characteristic length was taken as the mean hydraulic tunnel height. In this work, this researcher thinks that the use of hydraulic tunnel height is more accurate than tunnel height. The dynamic flow of air inside the tunnel is more to a function of the hydraulic

diameter of the duct which also include the effect of tunnel width, rather than depend solely on the height of the tunnel.

The preliminary results of the effect of cross-sectional shape on the critical ventilation velocity from the present study were published in Wu et al (1997) and Bakar et al (1999). In the papers, it was found that there are variations of the critical ventilation velocity for the tunnels which have the same height but different width. To some extent, these results proved that the current scaling law which uses H as characteristic length may not be valid to predict the heat output and critical ventilation velocity for large tunnel which have the same height but different cross-sectional shapes. It was suggested through the preliminary study that the mean hydraulic tunnel height should be used in the analysis of the experimental data to be plotted in the dimensionless forms of heat release rate and dimensionless critical ventilation velocity for the model tunnels. To prove the arguments, the calculated dimensionless heat release rate and critical ventilation velocity obtained by different tunnel shapes must follow approximately the same variation. This is one of the investigations carried out in the present works.

Table 3.1: Capabilities and limitations of real tunnel tests with full size fire tests in specialised facilities(Lacroix, 1995)

In Real Tunnel	In Experimental Facility
Advantages: - very demonstrative - rather easy organisation	**Advantages:** - any type of fire - excellent instrumentation - indisputable data
Limitations: - limited power - imperfect instrumentation - unchecked boundary conditions	**Limitations:** - heavy organisation - unique geometry
Case for use: - qualitative data - checking the installation - personnel training	**Case for use:** - quantitative data - characterisation of fires - validation of other methods

Table 3.2: Comparison of two types of reduced scale model (Lacroix, 1995)

Reduced Scale Tests	
Actual Fires At Medium Scale (>1:3)	**Actual/Adiabatic Models At Small Scale (<1:10)**
Advantages: -cost much lower than full size -reproducible and high-quality measurements -several possible layouts	**Advantages:** -cost lower than medium scale -reproducible and high-quality measurements -numerous possible layouts
Limitations: -no real thermal similarity, therefore risky extrapolation	**Limitations:** -imperfect similarity - no thermal losses (Adiabatic)
Case for use: -qualitative studies	**Case for use:** -qualitative or semi-quantitative studies

Chapter 4

Objectives and Approaches of the Present Study

The outcomes from the literature search show that the studies related to the critical ventilation velocity are still limited. There are three main areas which required further investigations.

(1) The effects of tunnel cross sectional geometry on the critical ventilation velocity have not been studied yet by experiment. Furthermore, the recent results on the behaviour of weakly dependent of critical ventilation velocity on HRRs obtained from both large and small scale fire tests in Health and Safety Laboratory, Buxton should be further verified by performing fire tests in different tunnel shapes.

(2) In the present scaling technique, the height of the tunnel is taken as the characteristic length in the relationship associated with buoyancy force. This means that the current scaling technique predicts the same critical ventilation velocity for tunnels which have same height but different cross-sectional areas. If the critical ventilation velocity does vary with the cross-sectional area, this presents an uncertainty in the technique.

(3) The CFD modelling in tunnel fire is at an early stage. Although previous publications (Lea, 1995; Woodburn & Britter, 1996; Fletcher et al, 1994) have confirmed that CFD can capture the behaviour of tunnel fires, further validations against the real experimental results are urgently required.

For these reasons, the main objectives of the present study are aimed at: a) verifying the effects of tunnel geometry or tunnel aspect ratio on the critical ventilation velocity, b) proposing new scaling techniques used in tunnel fires data analysis and finally, c) validating the CFD modelling results with the experimental results.

4.1 Approaches of the Present Study

The investigations in the present study can be divided into two parts; experimental work and computational fluid dynamics modelling.

(1) Experimental Investigation

Small scale models were proposed to be used to measure the critical ventilation velocity. As a continuation to the previous works in Buxton from Oka and Atkinson (1995) and Atkinson and Wu (1996), it was decided to build the first model tunnel of the square cross - sectional geometry of height 250 mm and width 250 mm, approximately similar cross - sectional geometry to previous colliery arch model. Three more tunnel models which have the same height (250 mm) but different widths were built to investigate on the effect of tunnel aspect ratio. The widths of the other three tunnels were 125 mm, 500 mm and 1000 mm, respectively.

The utility of small scale models provide the ability for the observation, measurement and control of the experiment.

Type of Fuel and its Flow Rate

The type of fuel used in the present work was propane gas. This provides a good model comparisons with previous works. In addition, the combustion process could be simply simulated in CFD modelling in the second approach.

The selections of propane flow rates were similar to Oka and Atkinson and Atkinson and Wu. In both works, propane flow rates between 0.1 to 20 litre per minute were estimated to produce fires between 2 MW to 150 MW in a large tunnel of diameter 5 m when the scaling technique is applied. In the present work, with the range of propane flow rates, it were estimated to produce fires between 2.5 to 100 MW in a tunnel of diameter around 5.0 m.

Instrumentation

Detection of smoke : K-type thermocouples were used to detect the smoke. It is expected that the upstream backlayering flow in the tunnel should be very sensitive to the ventilation flow. To detect the upstream flow, fine K type thermocouples were used. The temperature measurements in the other regions in the were made by using normal K type thermocouples.

Velocity Profiles: Simultaneously, the Orifice plate and Hot Wire Anemometer were used to measure air velocity inside the tunnel. Laser Doppler Velocimetry (LDV) was used to measure the velocity profiles within the fire region.

Data acquisition: A Windows based data logging system namely MicroLink was used to acquire the data from the experiment. This provides the advantage in the visualisation of the progress of the smoke, which was represented by the voltage difference

Measurement Technique

Critical ventilation velocity : To systematically measure the critical ventilation velocity, the ventilation velocity was measured at least 4 places upstream from the fire where the backlayering was controlled. Then extrapolation to obtain the critical ventilation velocity at zero tunnel height was made. The extrapolated value was then used back in the experiment for the confirmation.

Temperature profiles: The temperature measurements were made in three main regions; fire region, upstream and downstream at least at two ventilation velocities. Special software was used to transform the temperature data into contours.

(2) Computational Fluid Dynamics

The second approach of the present work was to use CFD package to predict the variations of the critical ventilation velocity with tunnel aspect ratio similar to the experimental model tunnels. The flow inside the tunnel were examined in detail. The simulations were performed in three dimensions by modelling propane combustion in air.

Chapter 5

Experimental Investigation

This chapter describes the experimental investigations carried out in the present work. The model tunnels have been built in the Health and Safety Laboratory since this project was supported by both the Health and Safety Executive and the Department of Chemical and Process, University of Sheffield.

5.1   Experimental Rig

The schematic front view and cross-section of the tunnel is shown in Figure 5.1. The tunnel was mounted on a steel platform of approximately 15 metres long with a height of 1 m and a width of 0.7 m (Figure 5.2).

5.1.1 Model Tunnels

A total of 5 model tunnels were used in this study. The dimensions of the tunnels are as follow:

Tunnel	Height (m)	Width (mm)	Aspect Ratio (W/H)	Cross-sectional area (m^2)
A	0.250	0.136	0.5	0.03125
B	0.250	0.250	1	0.0625
C	0.250	0.500	2	0.03125
D	0.250	1.00	4	0.2500
E	0.244	0.274	1.12	0.0569

Each model tunnel was formed from Perspex (PMMA) with the thickness of 6.25 mm with the length of up to 5.5 m from the tunnel entrance. Beyond this point, the tunnel was formed from 18 SWG (1.25 mm thick) stainless steel with the length of up to 10 m, including the burner section. The total length of the tunnel was around 15 m. Perspex was used because not only it is less expensive but also provides the visualisation due to

its transparency. The length of each section made by Perspex was approximately 1.5 m. For the stainless steel section, the length for each section was approximately 3.0 metres. Each section was joint to each other by using tape which can resist high temperature.

5.1.2 Ventilation Supplier

A straight PVC pipe of diameter 101.1 mm fitted with an orifice plate was used to channel the inlet flow. Orifice plate construction and inlet conditions were in accordance with BS 1042. The flow was driven by a jet of compressed air, acting as a momentum pump. Relatively coarse adjustments in the ventilation rate could be made by varying the compressed air supply. Fine adjustments in velocity by amounts as low as 0.3% were possible by using an iris, partially obstructing the inlet to the momentum pump.

Orifice plate pressures were measured and recorded using two different techniques, a differential pressure transducer which was connected to the datalogger and an inclined spirit Manometer. The calibrations of the Manometer was traceable to a National Standard. Therefore it can provide the reading with a good degree of accuracy. The orifice plate provides a measure of the total volumetric flow. The velocities reported are calculated by dividing the volumetric flow by the model cross-sectional area.

5.1.3 The Fire Source

Propane gas was used as the fuel, metered through a rotameter to the burner. The gas was supplied from the cylindrical bottle placed outside the laboratory. A porous bed burner of diameter 106 mm was used. The burner was filled with small glass beads in order to distribute propane gas. The top surface of the burner set flush with the tunnel floor. The burner was placed at approximately 5.75 m from tunnel entrance, in the stainless steel section.

5.1.4 Instrument for Velocity Measurement

Hot Wire Anemometer was used to measure the upstream velocity inside the tunnel without the presence of fire. The Hot Wire has been calibrated by Health and Safety Laboratory and required a power supply of 12 V. The output of the Hot Wire was directly connected to the datalogger.

The velocity profiles with the presence of the fire were measured by using Laser Doppler Velocimetry (LDV) facility performed by Allen et al (1999).

5.1.5 Instrument for Temperature Measurement

The upstream backlayering flow of hot gases was detected by using K-type stainless steel sheathed thermocouples of diameter 0.25 mm. Thermocouples were fixed 10 mm below the roof at distances equal to 1, 3, 5 and 10 times tunnel heights upstream of the centre of the fire.

Three arrays of K type thermocouples of diameter 1.25 mm were built to measure the temperature in the fire region, downstream and upstream from fire seat. The distances where each thermocouple was set in each array were 40 mm, 70 mm, 100 mm, 130 mm, 160 mm, 190 mm, 220 mm and 240 mm above the tunnel floor. The arrays were attached to a long rod and inserted into the tunnel from the exhaust end. Various distances downstream from the burner were marked on the rod.

5.1.6 Instrument for Data Collection

Datalogging system called MicroLink 3000 which required a Windows based software, WINSPEED in the Health and Safety Laboratory was used to acquire the experimental data. The Microlink 3000 has 3 boards with the capacity of 16 channels each. The channels in the first board were set to differential pressure transducer, the Hot Wire Anemometer and four upstream thermocouples. The second and third boards were used for 24 thermocouples which measure the temperature in downstream and fire regions.

The MicroLink was set to take 100 samples at the frequency of 1 Hertz for temperature and velocity profiles measurements. The voltage range for pressure transducer and Hot Wire Anemometer were set to 0 to 10 Volts. The voltage range of the thermocouple was set to 0 to 20 mmVolts, according to the manual.

5.2   Experimental Procedure

Before the experiments were carried out, there were certain safety rules and risk assessments which required to be followed. The lists of safety rules and risk assessments can be seen in Appendix A. Table 5.1 shows the summary of the experimental tests and conditions.

5.2.1   Calculation of the Average Ventilation Velocity in the Tunnel

The average ventilation velocity was measured by both Hot Wire Anemometer and orifice plate. The orifice plate enabled the volumetric rate of flow to be measured by using the pressure difference and the characteristics of the flowing fluid. The orifice plate in the 101.1 mm diameter PVC pipe causes a static pressure difference between the upstream and downstream side of the plate. As stated earlier, the orifice plate was designed according to BS 1042: section 1.1 and thus the equations contained within the British Standard can be used with a degree of confidence.

The mass flow is related to the pressure differential by equation

$$q_m = C_d E \varepsilon \frac{\pi}{4} d_o{}^2 \sqrt{2 \Delta p \times \rho} \qquad (5.1)$$

where q_m = mass flow rate (kg/s)

$\quad$ C_d = discharge coefficient

$\quad$ E   = velocity of approach factor

$\quad$ ε = expansion factor = 1 for incompressible fluids

$\quad$ d_o = diameter of the orifice throat (mm) = 0.072 m (2.828 ")

$\quad$ Δp = differential pressure (Pa)

$\quad$ ρ = mass density of the fluid (kg/m^3)

The velocity of approach factor may be calculated by using equation

$$E = \frac{D_p{}^2}{\sqrt{D_p{}^4 - d_o{}^4}} = \frac{4^2}{\sqrt{4^4 - 2.828^4}} = 1.1546 \qquad (5.2)$$

The relationship between the mass flow rate and the average velocity as follow:

PAGE(S) MISSING IN

ORIGINAL

$$V_p A_p = U A_T \qquad (5.7)$$

The calculated average velocity inside each tunnel are shown in Tables B1 to B5 in Appendix B.

5.2.2 Calculation of HRR from Fire

The HRR corresponding to the propane flow rates was calculated using the heat of combustion of propane reacting in air. The stoichiometric reaction of propane considered as follows:

$$C_3H_8 + 5CO_2 \quad \Rightarrow \quad 3CO_2 + 4H_2O$$
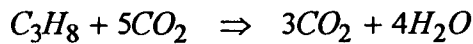
The heat of combustion of Propane (ΔHc) considered is 46.4 MJ/kg taken from Fire Protection Engineering Handbook (1995). The relative molecular weight is 44 kg/kmol.

Calculation of propane HRR

1 mol of C_3H_8 occupy 22.4 litre at standard conditions (1 atmosphere, 273K)

$$\text{1 l/min propane} \quad = \frac{1}{22.4} \times 44.0 \ \text{g/min}$$

$$= \frac{1}{22.4} \times 44 \times 46.4 \times \frac{1}{60} \ \text{kJ/s}$$

$$= 1.50 \ \text{kW}$$

Thus, 1 l/min of propane corresponds to approximately 1.50 kW of HRR.

5.2.3 Testing the Velocity Distributions in Tunnel

(1) Velocity Distribution Without Fire

Before the critical ventilation velocity measurements were made, it was necessary to measure the velocity profiles inside each tunnel in order to ensure uniform air flow distribution. As being discussed in section 5.1.2, the compressed air from the straight 4 inch pipe was positioned at the central point of the tunnel entrance. As the tunnel becomes wider, it would be expected that the horizontal profiles were not uniform. Thus, the installation of the flow straightener should be made.

The measurements were performed at 10 tunnel heights upstream of the burner. A series of holes were drilled in the cross - sectional span on the tunnel roof at various distances from tunnel axis. The Hot Wire Anemometer was inserted from these holes at various points inside the tunnel.

The measured values of the velocity distributions at 35 points of the cross - sectional span for tunnel **A** are presented in Table 5.2. The Manometer reading was set to 0.48 kPa at the bottom scale. The velocity profiles are shown in Figure 5.3. It can be seen that the flow inside the tunnel was uniform, especially at the tunnel centreline as illustrated in Figure 5.3(c). The horizontal profiles at 125 mm above tunnel floor indicated in Figure 5.3(f) also shows that the flow was uniform. Hence, there was no need for the installation of the flow straigthener. The average velocity inside the tunnel measured by the Hot Wire Anemometer was calculated to be 0.56 m/s. This value was in good agreement with the calculated average velocity using orifice (0.54 m/s) presented in Table B1.

The measured velocity distributions in tunnel **B** are shown in Table 5.3. The ventilation air flow was adjusted to give Manometer reading of 1.70 kPa, also at the bottom scale. Figure 5.4 shows the velocity profiles at 10 tunnel heights in the tunnel **B**. Again, the measured profiles show that the velocity inside the tunnel was uniform and the flow straigthener was not required. The average velocity given by the Hot Wire was calculated to be 0.58 m/s compared to 0.53 m/s calculated in Table B2.

For the larger aspect ratio tunnels, the horizontal profiles are more important. Several modifications were made to obtain relatively uniform velocity. The ventilation air inlet pipe was replaced to the bigger one in order to supply more air. The horizontal velocity profiles were measured at 125 mm above tunnel floor. The Manometer scale was positioned at the top scale and the reading was set to 2.00 kPa which lead to the average air velocity inside the tunnel 0.57 m/s. Figure 5.5(a) shows the velocity profiles inside tunnel **C** without any modification. As expected the velocity was not uniform. The profiles at the both sides of the tunnel were lower.

To improve the profiles, a circular block was placed at 100 mm from the air inlet. The solid blockage was designed to split the core into two ways so that the flow from both cores gradually developed as the air flow further downstream. Figure 5.5(b) shows the new velocity profiles. It can be seen that the profiles on the left side were improved. In Figure 5.5(c), the inlet pipe was pushed to the left so that more air would flow to the right side. However, there was no significant changed to the profiles. Finally Figure 5.5(d) shows the improved velocity profiles by using a flow straigthener that was placed at about 100 mm from the air inlet. A piece of wood of the same dimension of the tunnel cross-sectional was used and divided into 3 regions with both end sections were drilled with holes of 1 inch diameter.

A bigger ventilation air flow rate was expected in tunnel **D**. To supply more air inside the tunnel, series of 1 inch holes were drilled at approximately 100 mm from the compressed air inlet pipe to withdraw the air from the surroundings. Figure 5.6(a) shows the horizontal velocity profiles without the flow straightener It can be seen that the velocity profiles at the right side of the tunnel were the lowest. The flow straightener was then installed and the new profile is shown in Figure 5.6(b). However, more air flow in the left side of the tunnel. Figure 5.6(c) shows the profiles when the pipe was pushed to the left and finally Figure 5.6(d) shows the profiles when 7 holes were blocked at the left sides. The profiles was almost uniform although the velocity at both ends of the tunnel were slightly low. Table 5.4 and 5.5 give the tabulated horizontal profiles along the mid - tunnel height for tunnels **C** and **D**, respectively.

(2) Velocity Distribution With the Presence of Fire

In the LDV techniques, the tunnel floor within the fire region (500 mm upstream and 500 mm downstream from the burner) was replaced with a special glass which resisted to higher temperature. The laser facilities were setup below the tunnel. Four laser beams were used and the measurements were made at which the intersection of two corresponding beams. The intersection was carefully adjusted for the specified distance above tunnel floor. The measurements were made at least two times to obtain the average value.

5.2.4   Critical Ventilation Velocity Measurement

Upstream flow of hot gases was detected using K type stainless steel sheathed thermocouples with a diameter of 0.25 mm. Thermocouples were fixed 10 mm below the roof at distances equal to 1, 3, 5 and 10 tunnel heights upstream from the fire. The progress of a hot layer upstream to engulf a thermocouple was obvious from temperature records. Convective heating of the thermocouples could in all cases be easily and unambiguously differentiated from radiative effects, which were small and did not vary significantly during small changes. The procedures for the critical ventilation velocity measurement were as follows:

(1) The exhaust system (exhaust ventilation) was activated.

(2) A small amount of air was passed through the tunnel in order to clear the tunnel from any accumulated gases.

(3) The butane pilot flame was ignited and introduced into the tunnel just downstream of the burner through the burner hole while a small amount of propane gas was made available by opening the valve on the propane flow meter. The pilot flame was then removed and the burner was placed in its hole.

(4) Cooling water was then applied to the stainless steel section to restrict the metal temperature.

(5) The propane flow rate was set according to the required value

(6) The initial air velocity can now be set to the required value.

(7) After approximately 5 minutes of the burning time, the data logging software was then initiated.

(8) The ventilation velocity for the smoke to reach 1, 3, 5 and 10 tunnel heights for each propane flow rate was determined. The air flow was reduced by gradually closing the iris plate.

(9) Procedure (8) was repeated for propane flow rates 0.5, 1.0, 2.0, 5.0, 7.0, 8.0, 10.0, 15.0 and 20.0 litre/min propane.

After each test described above, the result obtained by the datalogging was reviewed. If the satisfactory result was not achieved, another test was then repeated. The value of the critical ventilation velocity which would prevent any 'back-layering' flow past the fire was obtained by extrapolating the results to 0 tunnel height. Then the critical ventilation

velocity was applied in the tunnel to confirm that no backlayering existed in the upstream of the fire.

It was found that the flame in the tunnel was not steady. The flame wandered from left to right. This behaviour to some extent affected the backlayering to move forward and backward. As a result, it was expected that there was some instability of the reading from the thermocouples. Because of the nature of the flame which has been discussed, the measurements of the critical ventilation velocity were performed more than one for the specific test in order to obtain an average value.

The cooling water in the fire region was assumed that it did not give great effect on the movement of the backlayering flow. The cooling water was used to protect the stainless steel walls especially when higher HRRs were used. The sprinkling system was specially designed such that the water did not accumulate on top of the tunnel and remove too much heat from the tunnel walls.

Altogether there were 136 tests for the critical ventilation velocity measurements for 1, 3, 5 and 10 tunnel heights of the smoke to travel upstream for HRRs between 1.50 kW to 30.0 kW. In addition to the determination from the thermocouples, some of the tests were determined by visualisation especially for the backlayering to travel up to 5 and 10 tunnel heights.

5.2.5 Temperature Measurement

Temperature measurements were performed in three main regions; fire region, downstream and upstream.

(1) Fire Region

The measurements were performed up to 400 mm downstream from the burner. The thermocouple arrays were pulled downstream from the mid point of the burner in a step of 25 mm. The measurements were made on three HRRs, 3.0 kW, 7.50 kW and 15.0 kW. The ventilation were set at three conditions; critical ventilation velocity, twice of

the critical ventilation velocity and the velocity at which the backlayering flow travelled at 10 tunnel heights upstream. Measurements were started after 5 minutes of fires.

(2) Downstream Region

The procedures employed were similar to fire region temperature measurement. A step of 250 mm was used starting from the mid-point of the burner. The measurements were made up to 4000 mm downstream from the burner.

(3) Upstream Region

In the upstream measurement, only one thermocouple array was used in both tunnels **A** and **B**. For tunnel **D**, three thermocouple arrays were used. The measurements were made in step of 100 mm starting from the burner centreline up to 1000 mm upstream. The ventilation velocity was set at with the smoke front reached 10 tunnel heights upstream from the burner.

5.3   Data Processing

Logging of all the measuring devices to the Microlink provides a convenient result was achieved. The datalogger recorded the voltage change from each measuring equipment (differential pressure transducer, Hot Wire Anemometer and thermocouples) and converted into standard reading such m/s and degree Celsius for velocity and temperature, respectively. All data were then saved in the form of ASCII files.

(1) Critical ventilation velocity data

Logging to the differential transducer provides a step changed when the ventilation velocity was systematically reduced. The interval when the critical ventilation velocity occurred can be determined when the corresponding thermocouple was engulfed by the smoke indicated by a sudden rise in the temperature. The corresponding reading from the Manometer can be obtained.

A sample of the critical ventilation velocity determination for tunnel **B** for HRR 1.50 kW when the smoke backlayering at 1, 3, 5 and 10 tunnel heights is shown in Figure 5.7. The plots of voltage output and temperature for various thermocouples were obtained by

the WINDSTREAM software. Initially, it can be seen that a high ventilation velocity was set. Then it was reduced systematically by the adjustment of the iris. This will correspond to the voltage change in the data logging. For each step, the Manometer reading was recorded so that the critical ventilation velocity reading can be determined.

It can be seen in Figure 5.7(a) that at an output up to 4.20 V, the backlayering is intermittently reaching 1 tunnel height as the temperature is fluctuating. By reducing the output to 4.01V the temperature indicated at one tunnel height increases thus suggesting that the backlayering is engulfing the thermocouples. Thus, the critical ventilation velocity is estimated lies between the values of 4.20 V and 4.01 V. The corresponding Manometer reading is between 0.78 kPa and 0.74 kPa. The ventilation velocity is between 0.35 m/s and 0.36 m/s shown in Table B2.

Figure 5.7(b) shows the voltage reading and the corresponding pressure reading for the backlayering to reach 3 tunnel heights. The critical ventilation velocity lies in between output 3.00V and 2.50V. The corresponding Manometer reading is between 0.48 kPa and 0.47 kPa, whilst the ventilation velocity is between 0.29 m/s to 0.30 m/s (Table B2).

Figure 5.7(c) indicates the output data for the backlayering to reach 5 tunnel heights. The backlayering engulfs the thermocouples between output 2.16V and 2.02V. The corresponding Manometer reading is between 0.39 kPa and 0.36 kPa. The ventilation velocity is between 0.25 m/s to 0.26 m/s (Table B2).

Finally Figure 5.7(d) shows the output data for the backlayering to reach 10 tunnel heights. Initially, the ventilation velocity is quite low. It can be seen that the thermocouples has already been engulfed by the smoke. Then, the ventilation velocity is increased at the output of 1.01V and reduced systematically in steps by gradually closing the iris plate. The critical ventilation velocity is between the output of 0.95V and 0.92V. The corresponding Manometer reading is between 0.15 kPa to 0.14 kPa. The ventilation velocity is between 0.16 m/s to 0.17 m/s (Table B2).

The above procedure for analysing the results was repeated for all of the propane flowrates considered. However, for the larger aspect ratio tunnels (**C** and **D**), the procedure of identification of the interval steps of the reduction of the air flow was slightly changed. This is because the maximum limit of the differential transducer has reached due to higher air flow rates. Thus, to identify the step, a voltage supplier was connected to the datalogging. The voltage can be switched on and off. For each step changed, the voltage was on and off for the following step. The typical diagram obtained by datalogging can be seen in Figure 5.8.

(2) Temperature data

A simple QBASIC programme was made to process the data in each file and assemble in certain format to be plotted (Appendix C). The temperature contours were plotted using a software called ORIGIN which is available in the Health and Safety Laboratory.

(a) Front View

Water cooling

To exhaust

Upstream
Thermocouples

10TH 5TH3TH   1TH

Thermocouples
Arrays

Iris
plate

101.1mm

y

Orifice
plate

Propane to burner

Burner

Compressed
air supply

3000mm   5000 mm   2420mm   7500mm

(b) Cross -section

136 mm   250mm   500mm   1000mm   274 mm

250mm   250mm   250mm   250mm   244 mm

A   B   C   D   E
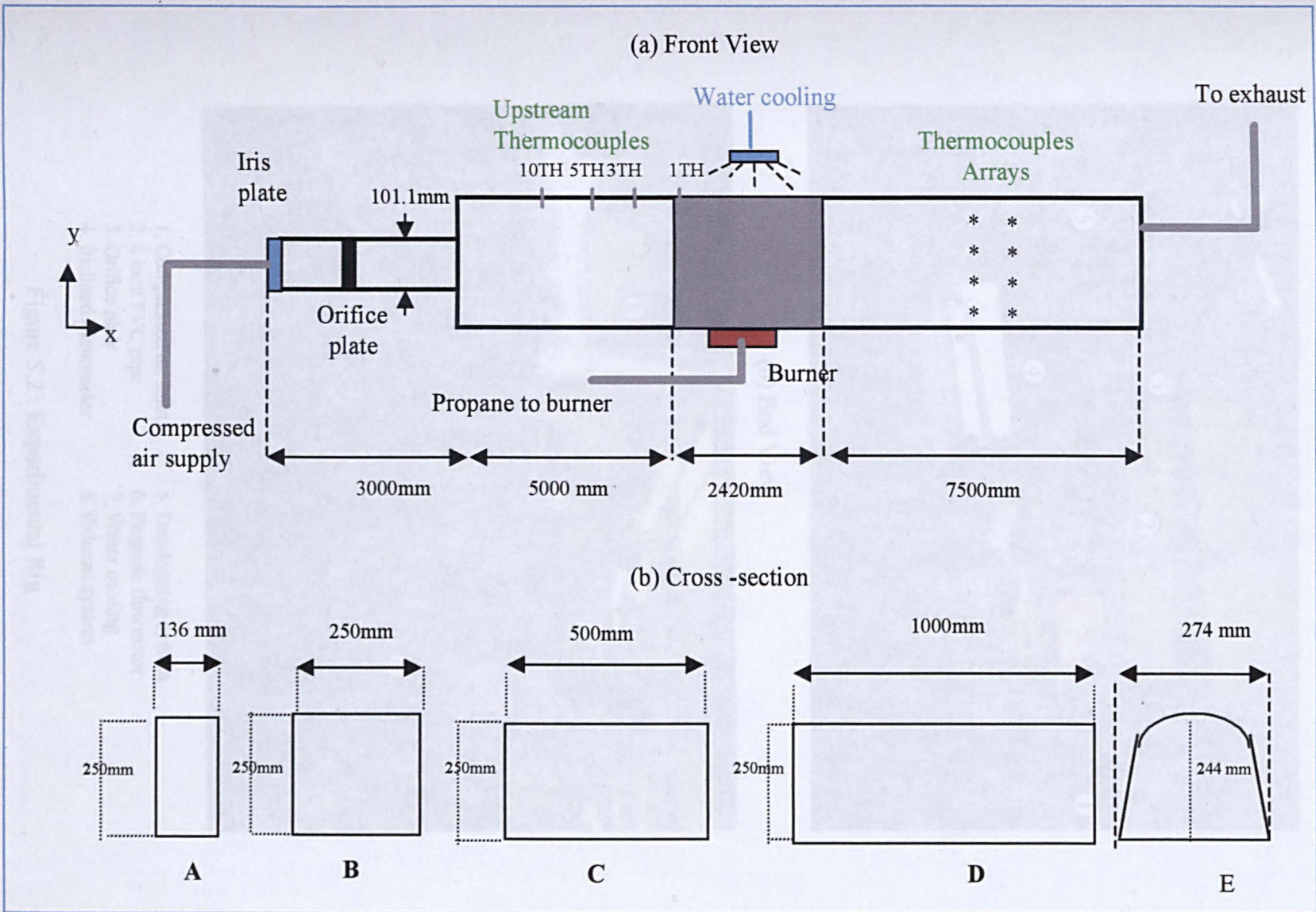
Figure 5.1 : Schematic front view and cross-section of experimental rig
(not to scale)

(a) Front View
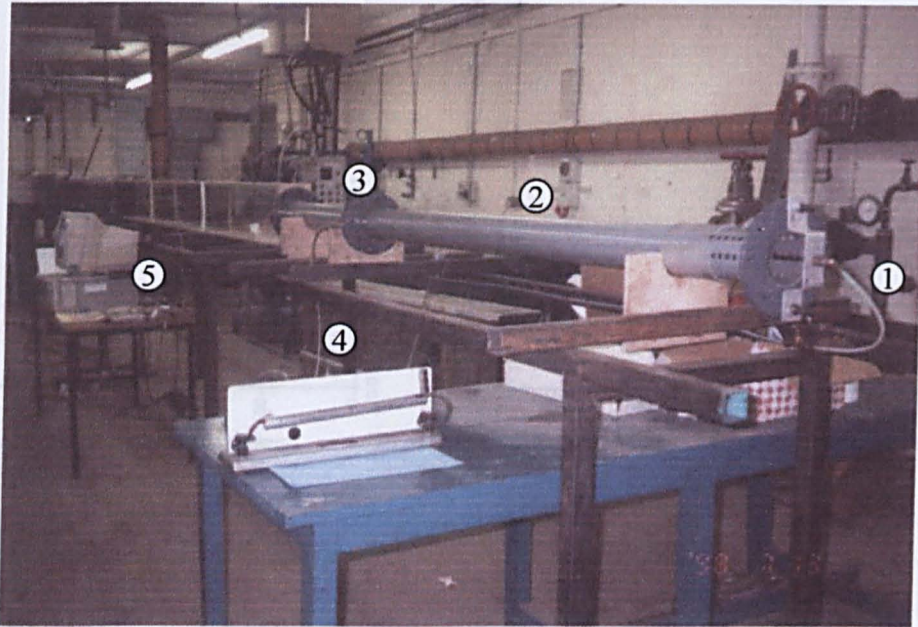
(b) End View
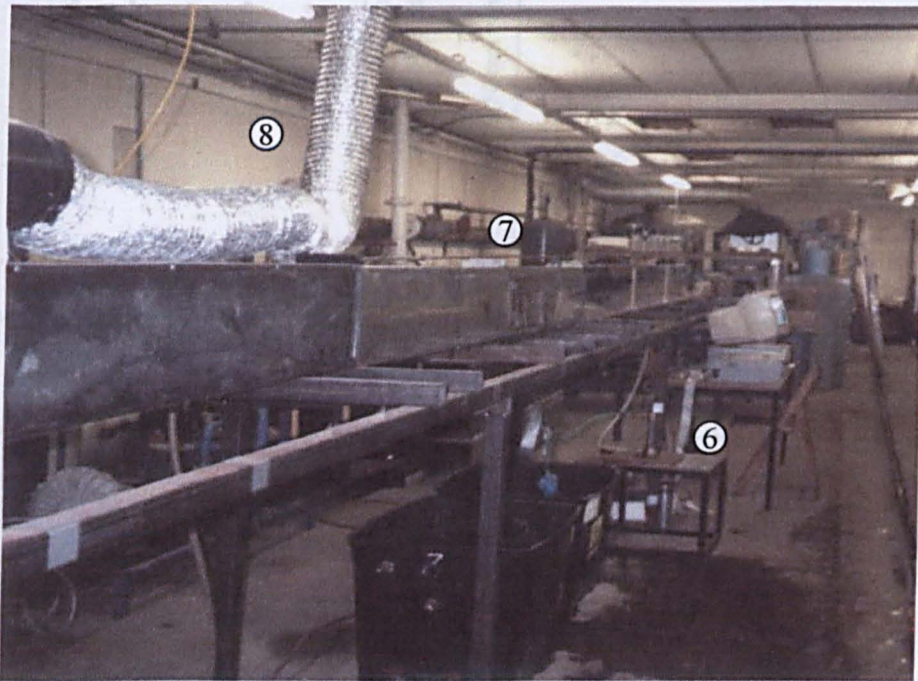
1. Compressed air inlet
2. 4 inch PVC pipe
3. Orifice plate
4. Inclined Manometer

5. Datalogging system
6. Propane flowmeter
7. Water cooling
8. Exhaust system

Figure 5.2 : Experimental Rig
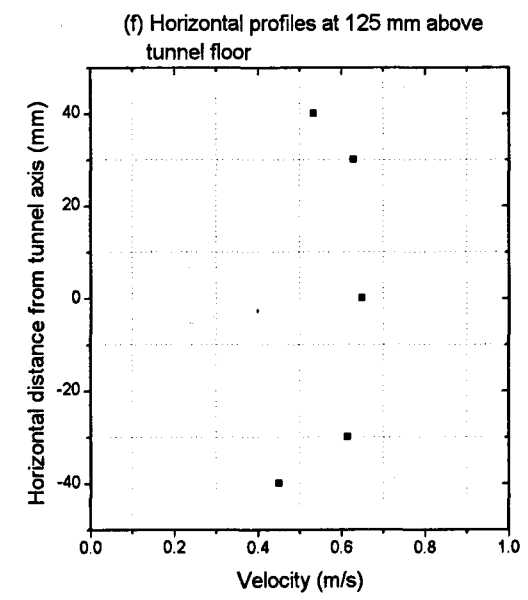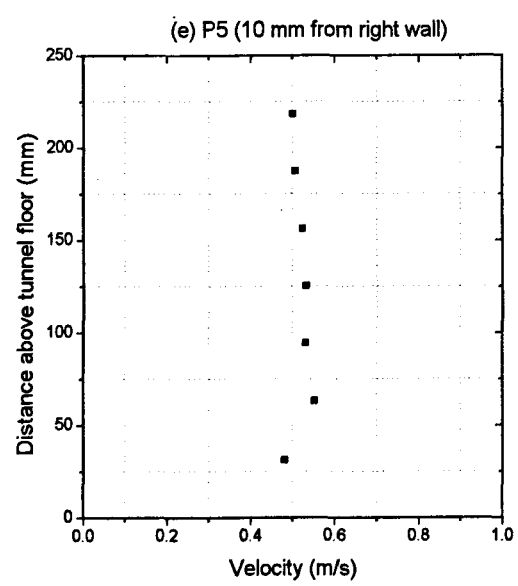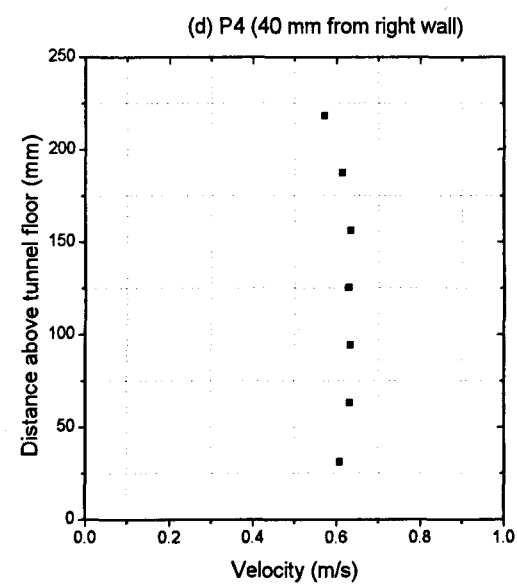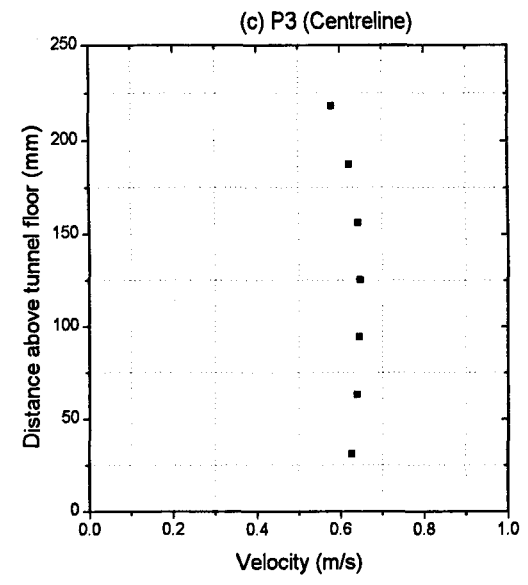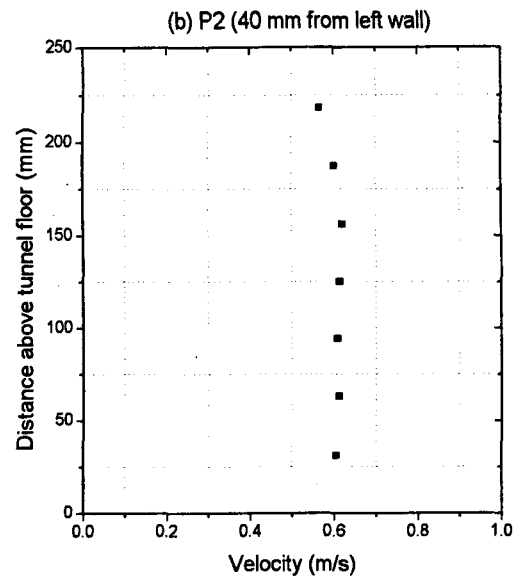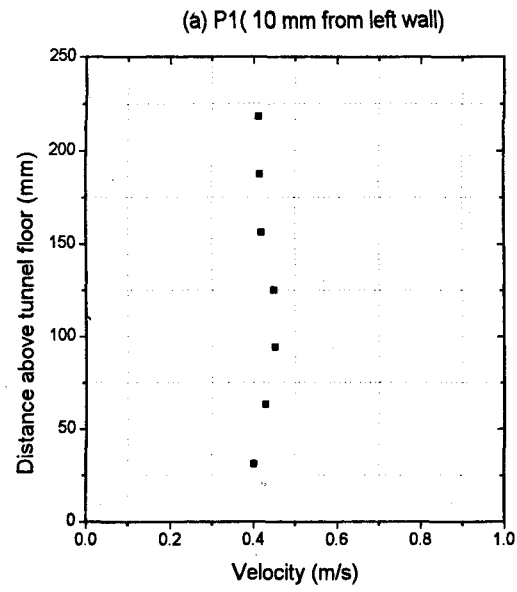
Figure 5.3: Velocity profiles at 10 tunnel heights upstream in tunnel A
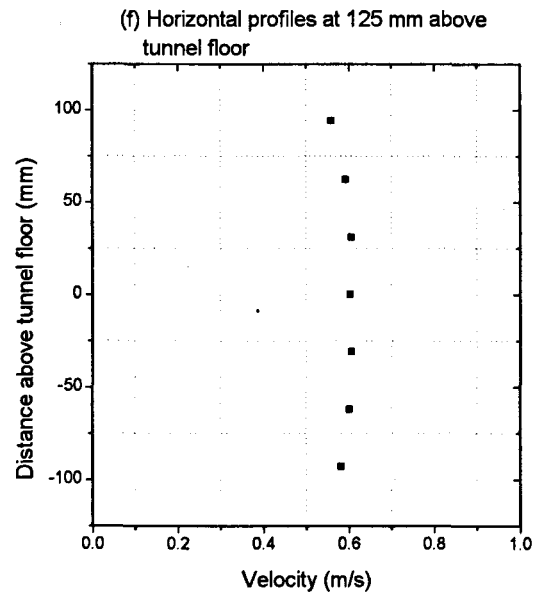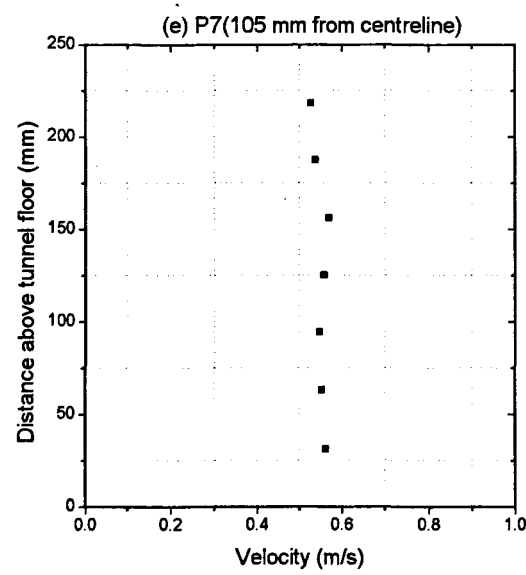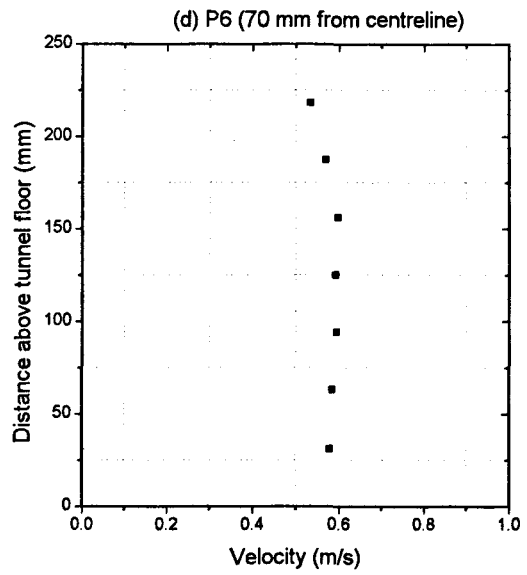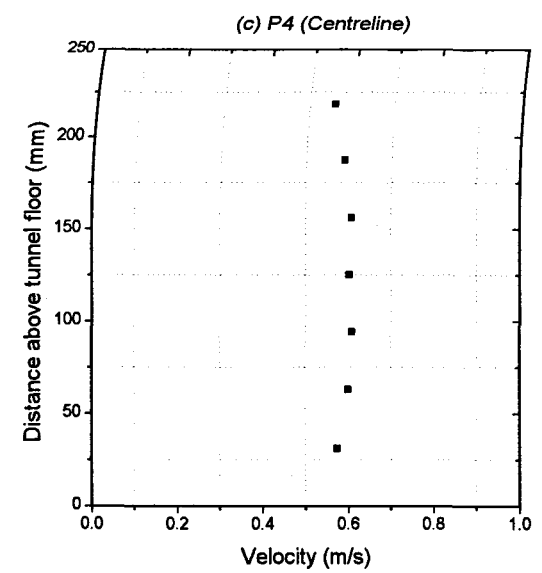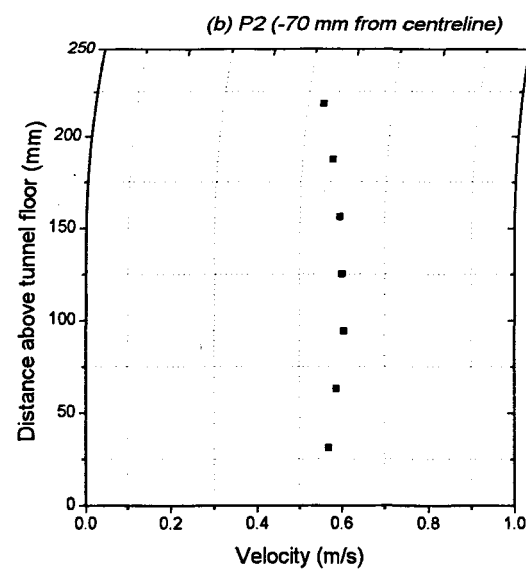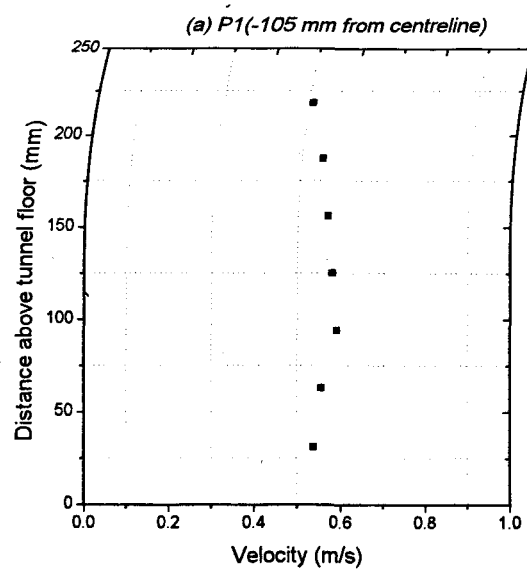
Figure 5.4 : Velocity profiles at 10 tunnel heights upstream in tunnel B

(a) No modification

(b) Blockage: 100mm from inlet, 185mm from left side, 165mm from right side

(c) Blockage : pipe pushed to left

(d) flow straigthener
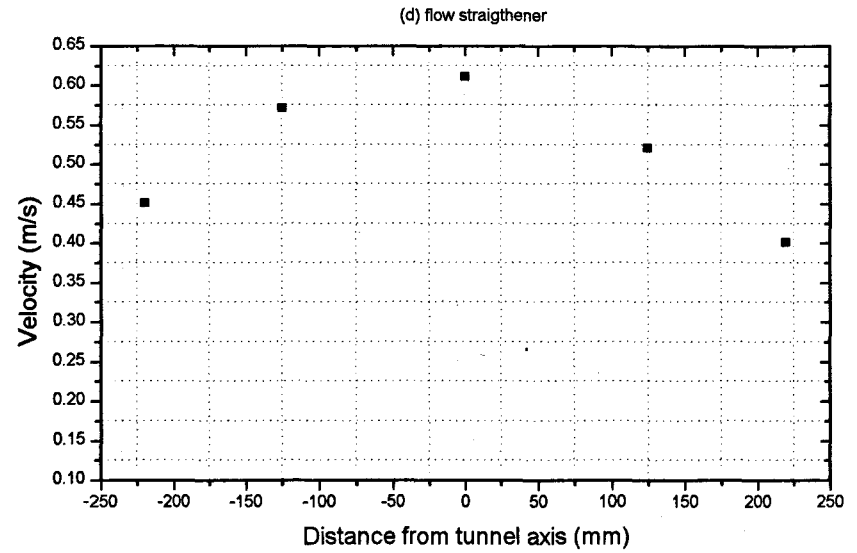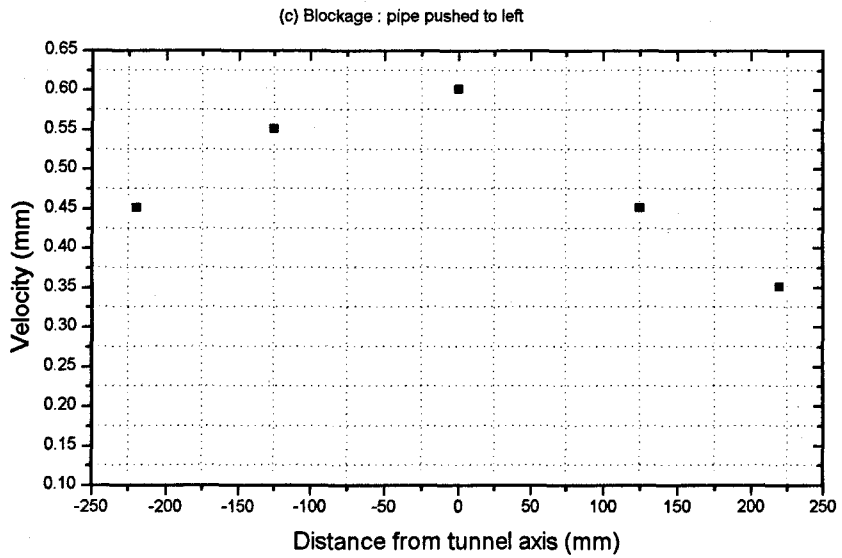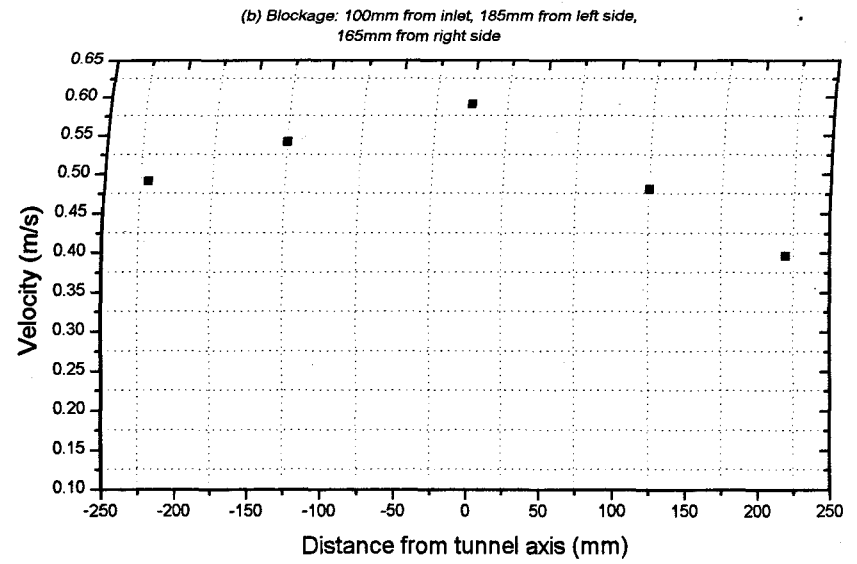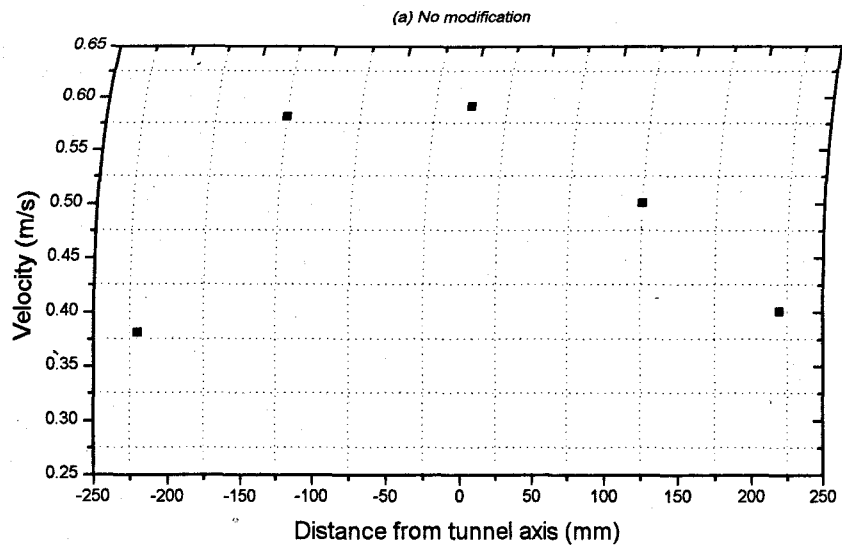
Figure 5.5 : Horizontal velocity profiles at 10 tunnel height upstream in tunnel C
(125 mm below tunnel roof)
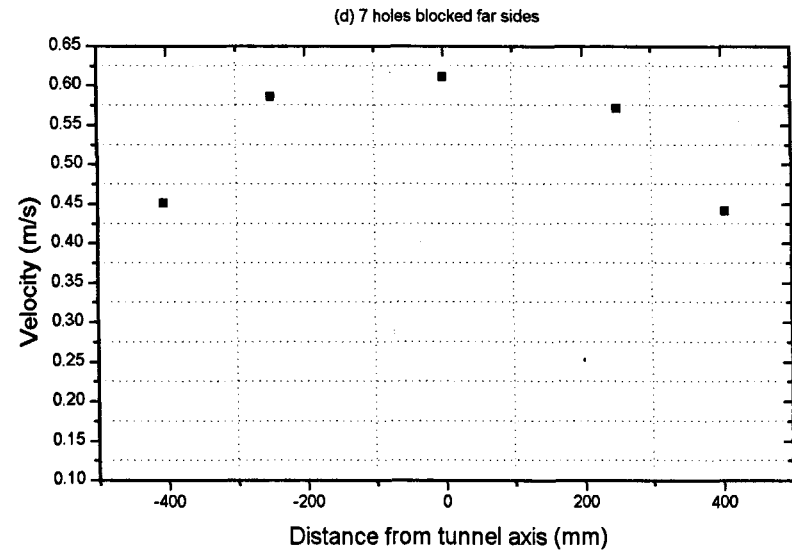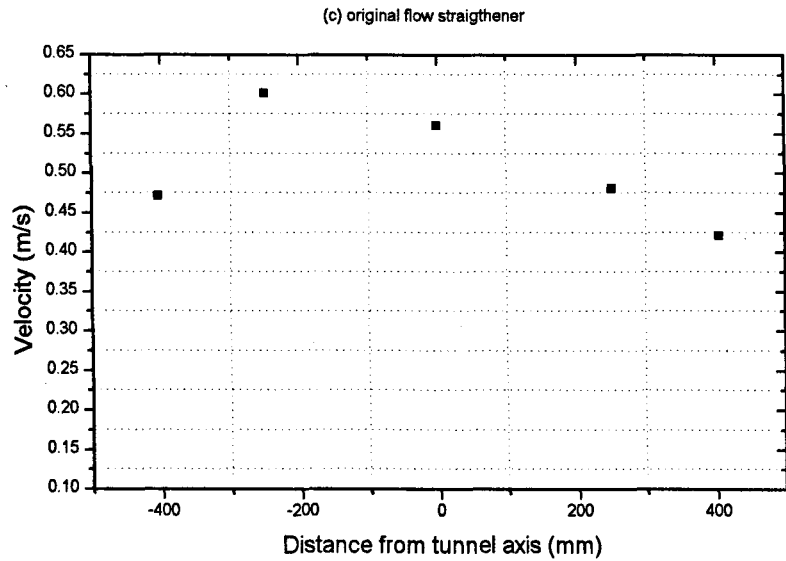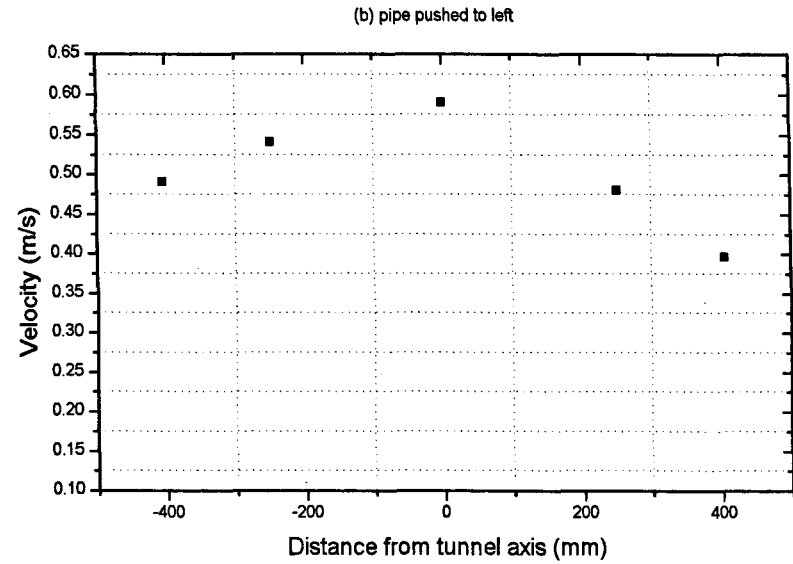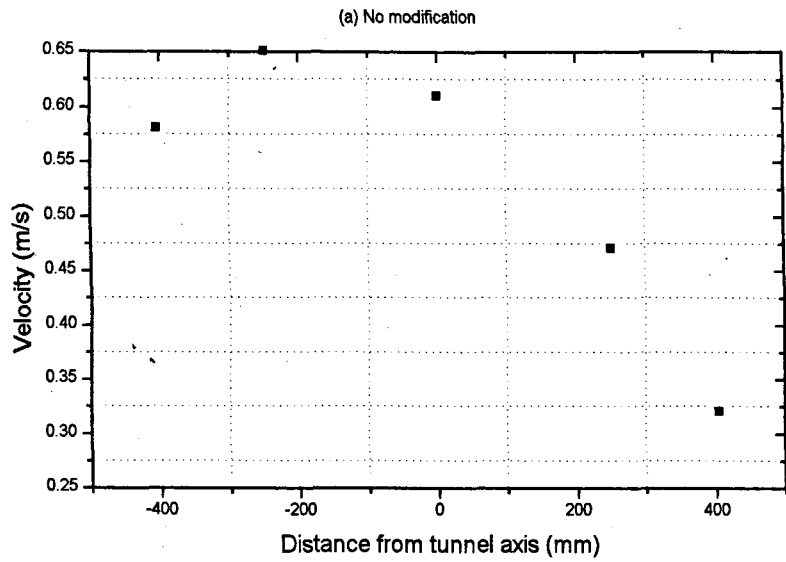
Figure 5.6 : Horizontal velocity profiles at 10 tunnel heights upstream in tunnel D
(125mm below tunnel roof)
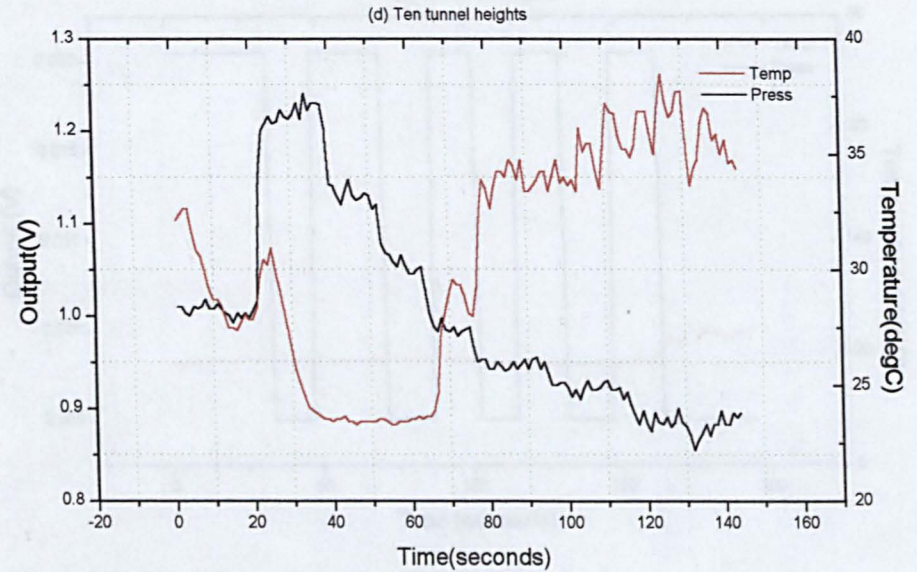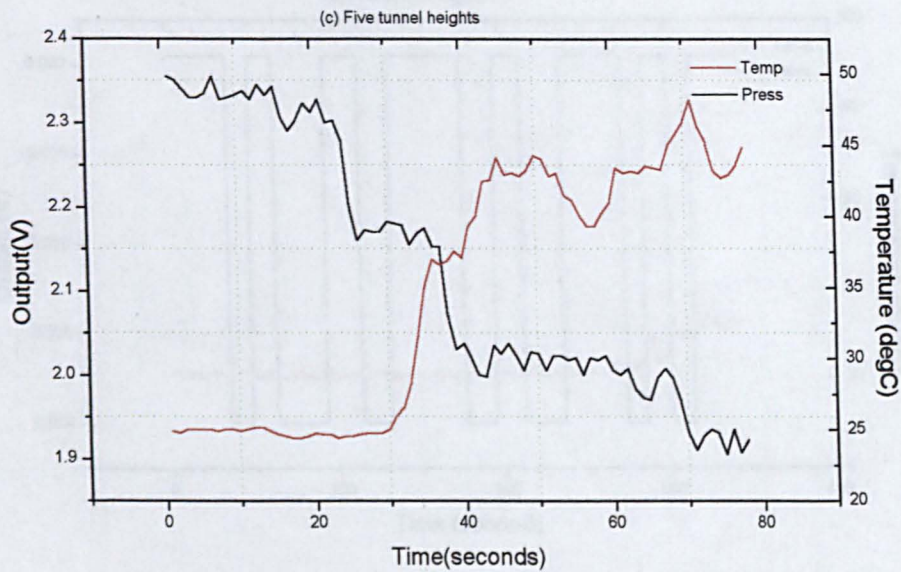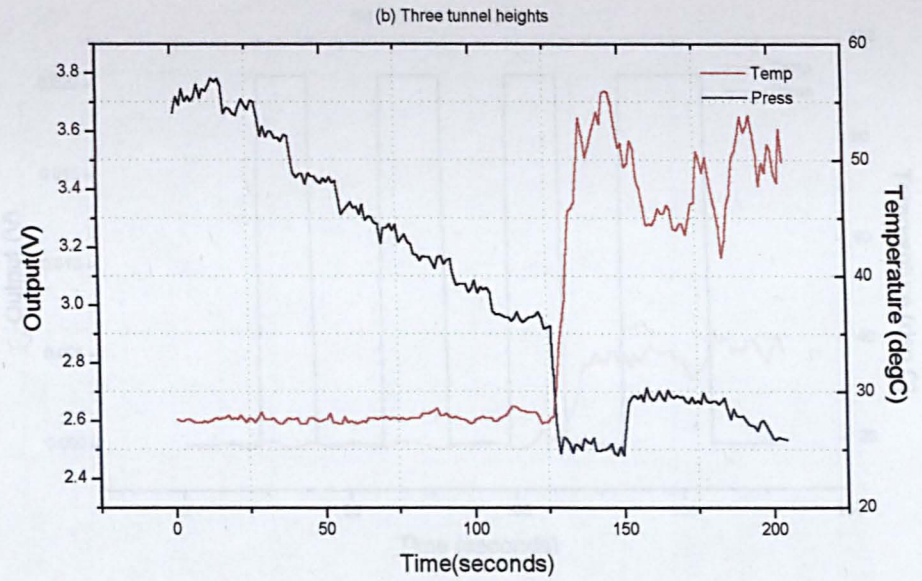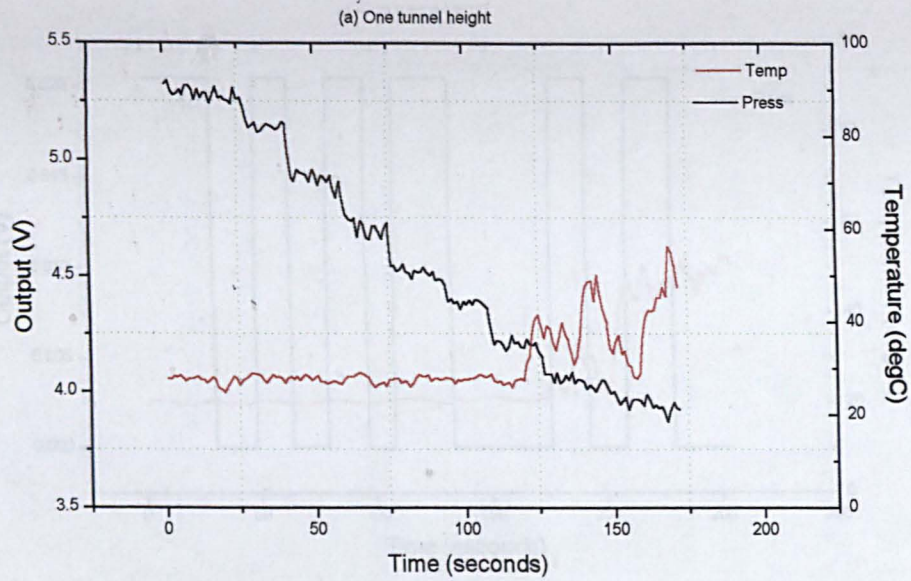
Figure 5.7 : A sample of critical velocity determination in tunnel B at 1.50 kW fire
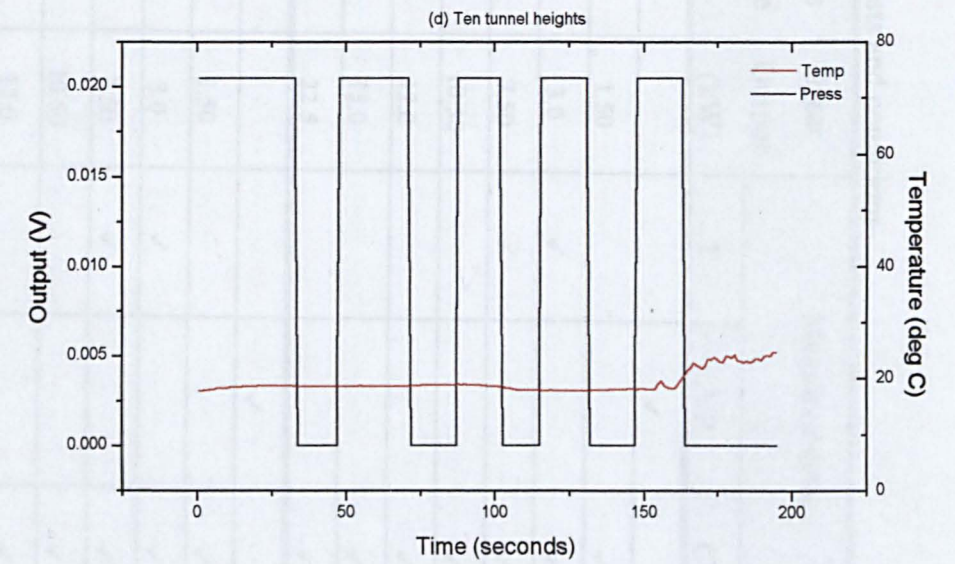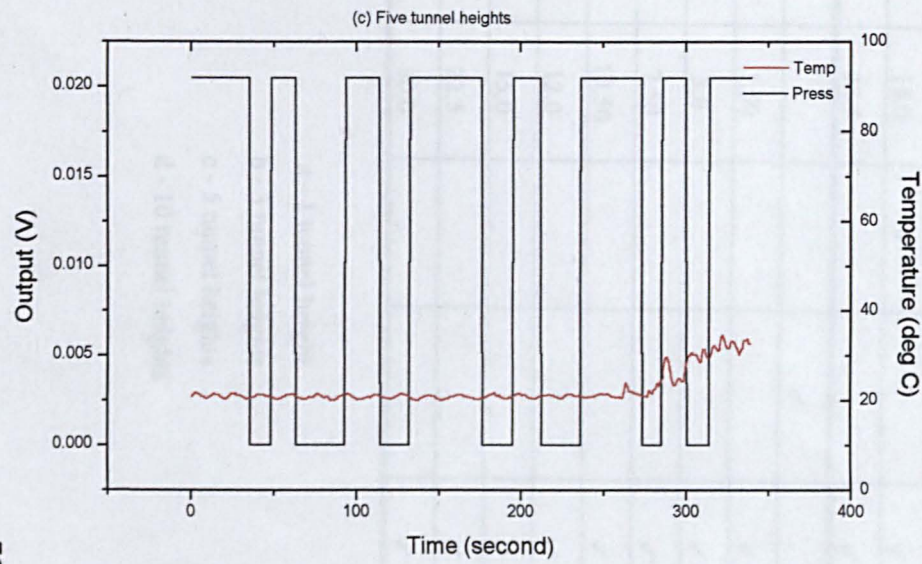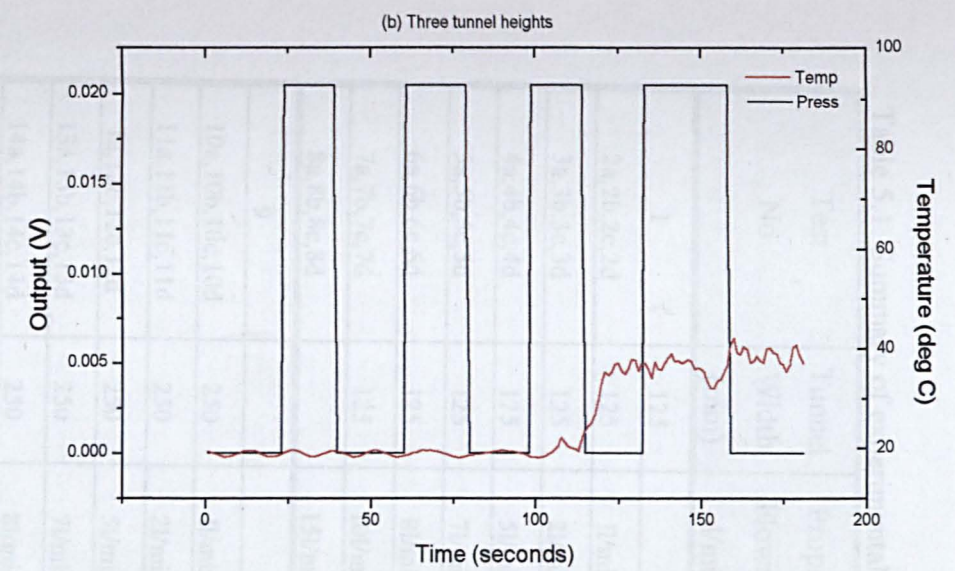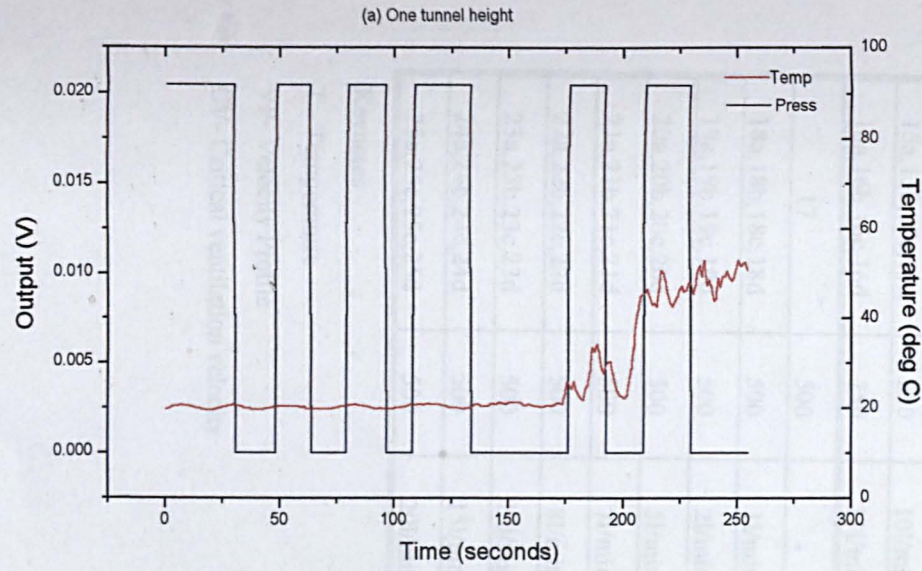
Figure 5.8 : A sample of critical velocity determination in tunnel D at 1.50 kW fire

Table 5.1: Summary of experimental tests and conditions

Test No	Tunnel Width (mm)	Propane Flowrate l/min	Heat Output (kW)	Measurements		
				T	VP	CV
1	125				✓	
2a,2b,2c,2d	125	1l/min	1.50			✓
3a,3b.3c,3d	125	2l/min	3.0	✓		✓
4a,4b,4c,4d	125	5l/min	7.50	✓		✓
5a,5b,5c,5d	125	7l/min	10.50			✓
6a,6b,6c,6d	125	8l/min	12.0			✓
7a,7b,7c,7d	125	10l/min	15.0			✓
8a,8b,8c,8d		15l/min	22.5			✓
9					✓	
10a,10b,10c,10d	250	1l/min	1.50			✓
11a,11b,11c,11d	250	2l/min	3.0	✓		✓
1a,12b,12c,12d	250	5l/min	7.50	✓		✓
13a,13b,13c,13d	250	7l/min	10.50			✓
14a,14b,14c,14d	250	8l/min	12.0			✓
15a,15b,15c,15d	250	10l/min	15.0	✓		✓
16a,16b,16c,16d	250	15l/min	22.5			✓
17	500	-			✓	
18a,18b,18c,18d	500	1l/min	1.50			✓
19a,19b.19c,19d	500	2l/min	3.0			✓
20a,20b,20c,20d	500	5l/min	7.50			✓
21a,21b,21c,21d	500	7l/min	10.50			✓
22a,22b,22c,22d	500	8l/min	12.0			✓
23a,23b,23c,23d	500	10l/min	15.0			✓
24a,24b,24c,24d	500	15l/mni	22.5			✓
25a,25c,25c,25d	500	20l/min	30.0			✓

Keynotes:

T - Temperature

VP- Velocity Profile

CV- Critical ventilation velocity

a - 1 tunnel height

b - 3 tunnel heights

c - 5 tunnel heights

d - 10 tunnel heights

Table 5.1a: Summary of experimental tests and conditions

Test No	Tunnel Width (mm)	Propane Flowrate l/min	Heat Output (kW)	Measurements		
				T	VP	CV
26	1000				✓	
27a,27b,27c,27d	1000	1l/min	1.50			✓
28a,28b.28c,28d	1000	2l/min	3.0	✓		✓
29a,29b,29c,29d	1000	5l/min	7.50	✓		✓
30a,30b,30c,30d	1000	7l/min	10.50			✓
31a,31b,31c,31d	1000	8l/min	12.0			✓
32a,32b,32c,32d	1000	10l/min	15.0	✓		✓
33a,33b,33c,33d	1000	15l/min	22.5			✓
34	274				✓	
35a,35b,35c,35d	274	1l/min	1.50			✓
36a,36b,36c,36d	274	2l/min	3.0			✓
37a,37b,37c,37d	274	5l/min	7.50			✓
38a,38b,38c,38d	274	10l/min	15.0			✓
39a,39b,39c,39d	274	15l/min	22.5			✓

Keynotes:

T - Temperature

VP- Velocity Profile

CV- Critical ventilation velocity

a - 1 tunnel height

b - 3 tunnel heights

c - 5 tunnel heights

d - 10 tunnel heights

Table 5.2: Velocity distributions at 10 tunnel heights upstream in tunnel **A**

Distance below tunnel roof (mm)	Velocity Distribution (m/s)				
	-42.5 mm	-22.5 mm	Centreline (0 mm)	22.5 mm	42.5 mm
32	0.48	0.57	0.58	0.57	0.50
63	0.48	0.60	0.62	0.61	0.51
94	0.42	0.62	0.64	0.63	0.52
125	0.45	0.61	0.65	0.63	0.53
158	0.45	0.61	0.64	0.63	0.53
187	0.43	0.61	0.64	0.63	0.55
219	0.40	0.61	0.63	0.61	0.48

Table 5.3: Velocity distributions at 10 tunnel heights upstream in tunnel **B**

Distance below tunnel roof (mm)	Velocity Distribution (m/s)						
	-105 mm	-70 mm	-35 mm	Centreline (0 mm)	35 mm	70 mm	105 mm
32	0.51	0.54	0.55	0.56	0.58	0.53	0.53
63	0.55	0.57	0.57	0.59	0.61	0.57	0.54
94	0.57	0.59	0.59	0.61	0.61	0.59	0.57
125	0.58	0.60	0.60	0.60	0.60	0.59	0.56
158	0.59	0.60	0.61	0.61	0.61	0.59	0.55
187	0.56	0.59	0.60	0.60	0.61	0.58	0.55
219	0.54	0.57	0.57	0.57	0.58	0.58	0.56

Table 5.4: Measured velocity distributions along the mid-tunnel height in tunnel **C**

Modifications	Velocity Distribution (m/s)				
	-220 mm	-125 mm	Centreline	125 mm	220mm
No modification	0.38	0.58	0.59	0.50	0.40
Blockage: 100mm from inlet, 185mm from left, 165 from right	0.49	0.54	0.59	0.48	0.40
Blockage with pipe pushed to left	0.45	0.55	0.60	0.45	0.35
Flow straigthener	0.45	0.57	0.61	0.52	0.41

Table 5.5: Measured velocity distributions along the mid-tunnel height in tunnel **D**

Modifications	Velocity Distribution (m/s)				
	-405 mm	-250mm	Centreline	250 mm	405mm
No modification	0.58	0.65	0.61	0.47	0.32
Original flow straigthener	0.49	0.54	0.59	0.48	0.40
Pipe pushed to left with flow straigthener	0.47	0.60	0.56	0.48	0.42
7 holes bolcked at the left sides of flow straigthener	0.45	0.59	0.61	0.57	0.44

Chapter 6

Experimental Results

This chapter presents the experimental results obtained from the model tunnels in three sections, namely the critical ventilation velocity, temperature distributions and velocity distributions. The majority of the experimental results concerned with tunnels **A**, **B**, **C** and **D**. However, as part of on going project, the additional results from tunnel **E** were also included in this thesis.

6.1 Critical Ventilation Velocity

The critical ventilation velocities have been systematically measured. The ventilation velocities required for the backlayering to travel up to 1, 3, 5 and 10 times of the tunnel heights for tunnels **A** to **D** are shown Tables 6.1 to 6.4. The value of the ventilation velocity considered was taken from the average value between the upper and lower velocities corresponding to the Manometer readings.

The plot of ventilation velocity against the HRR and the plot of ventilation velocity required to control the length of the back layering flow to 1, 3, 5 and 10 times of the tunnel heights for tunnels **A** to **D** are depicted in Figures 6.1 and 6.2, respectively. It can be seen in Figure 6.1 that the ventilation velocity to control the backlayering at each tunnel height, increasing with the increase of HRR from the fire. For each tunnel, the variations follow similar pattern, thus indicated the test consistency.

The critical ventilation velocity for each HRR was obtained by extrapolating each plot in Figure 6.2. The value was reapplied in the experiments for the confirmations. Table 6.5 presented the critical ventilation velocity for each HRR in each tunnel. The variations of

the plot of the critical ventilation velocity against HRR for the five tunnels are shown in Figure 6.3.

The results in Figure 6.3 obviously show that there are variations of the critical ventilation results for tunnels **A** to **D** which have exactly the same height but different widths. It is shown that in tunnel **A**, the critical ventilation velocity increases with the HRR over the same range of HRR, however when the HRR reaches about 7.5 kW, the critical ventilation velocity become nearly independent of heat output. A similar pattern is obtained in tunnel **B**. However, the behaviour of independent of HRR occurs at HRR 10. 5 kW. On the contrary, this pattern has not been observed in tunnels **C** and **D**, the critical ventilation velocity still increases with the HRR up to 30 kW fire.

Comparing the values of the critical ventilation velocity for the same HRR, it is shown that tunnel **D** requires the smallest critical ventilation velocity, followed by tunnels **C** and **B** when the HRRs are less than 15 kW. In contrast, tunnel **A** requires the greatest critical ventilation velocity only when the HRRs less than 3.0 kW. However, when the HRRs are greater than 3.0 kW, the critical ventilation velocity for tunnel **A** are kept constant below 0.48 m/s. Whilst, in tunnel **B**, beyond HRRs 15.0 kW, the critical ventilation velocity are kept below 0.60 m/s. The critical ventilation velocities for tunnels **C** and **D** exceed 0.60 m/s and still increasing with fire HRR.

It is also shown in Figure 6.3 that the critical ventilation velocity for tunnel **E** increases with the HRR up to 7.5 kW. Beyond this HRR, the critical ventilation velocity becomes constant. The critical ventilation velocity in tunnel **E** at lower HRR was slightly greater than the critical ventilation velocity in tunnels **A**, **B**, **C** and **D** below 10 kW.

In summary, there are variations of the measured critical ventilation velocity for the five tunnels which have relatively the same height but different widths.

6.2   Temperature Distribution

Extensive temperature measurements have been made in two tunnels, **B** and **D**, representing a lower and a higher tunnel aspect ratio. Additional temperature measurements have also been made in tunnel **A**. The temperature inside the tunnels are focused on three main regions as being outlined in the experimental investigation. The tabulated values show the temperature at each position inside the tunnel represented by co-ordinate x-y-z. Co-ordinate x is the axial direction in the tunnel with reference to the burner centreline. Co-ordinate y represents the distance above tunnel floor, whilst co-ordinate z represents the horizontal distance from tunnel centreline. The negative sign indicates the distance upstream from the fire seat while the positive sign indicates the distance downstream from the fire seat. The unit for the temperature is degree Celsius.

Most of the temperature data have been analysed and plotted in the form of contours for better analysis. A contour interval of 50 °C was set in each figure. The direction of the ventilation flow in all contours is to the right side.

6.2.1 Temperature Distribution in Fire Region

The measured temperature distributions in the fire region in both tunnels **B** and **D** are presented in Tables 6.6 to 6.17. Figure 6.4 shows the temperature contours in tunnel **B** at 3.0 kW fire at three ventilation velocities. In Figure 6.4(a), the ventilation velocity was set to 0.25 m/s, the condition for the backlayering flow was controlled at 10 tunnel heights upstream from the fire. While in Figure 6.4(b), the ventilation velocity was increased to 0.48 m/s, the critical ventilation velocity for this HRR. In Figure 6.4(c) the ventilation velocity was set to 0.96 m/s, doubled the critical ventilation velocity.

It can be seen in Figure 6.4 that with the presence of ventilation flow, the fire plume deflects at certain angle from the vertical. When the ventilation is low, the backlayering occurs, indicated by the contour 100 °C on the left. When the ventilation velocity is increased, the backlayering flow is suppressed at the leading edge of the burner as shown

in Figure 6.4(b). Further increase in the ventilation velocity shown in Figure 6.4(c), the flame deflects at greater tilt angle from the vertical, resulting the majority of the HRR is released downstream from the burner.

Figure 6.5 depicts the contours in tunnel **B** at three HRRs (3.0 kW, 7.5 kW and 15.0 kW) at critical conditions . The critical ventilation velocities applied were 0.48 m/s, 0.56 m/s and 0.60 m/s, respectively. It can be observed that as the HRR increases, the fire inside the tunnel also grows in size. The maximum temperature recorded at 3.0 kW, 7.5 kW and 15.0 kW were in the order of 586.36 °C, 679.26 °C and 746.92 °C, respectively.

Figure 6.6 shows the contours in tunnel **B** with the presence of backlayering flow at 3.0 kW, 7.5 kW and 15.0 kW. The ventilation velocities were 0.25 m/s, 0.31 m/s and 0.34 m/s, respectively. Under these conditions, the backlayering flow was controlled at 10 tunnel heights upstream from the fire. It can be seen that as the HRR increases, the maximum temperature in the backlayering also increases. The contours at 200 mm above the floor for example is 100 °C for 3.0 kW fire , then increases to 150 °C at 7.5 kW fire. The magnitude further increases between 250 °C to 300 °C for 15.0 kW fire.

Figure 6.7 shows the cross-sectional temperature contours in tunnel **B** at various distances from burner at 3.0 kW fire at critical conditions (0.48 m/s). The temperature data in Table 6.6 show both centreline and second thermocouple arrays recorded higher temperature values. This suggests that the cross-sectional width of the flame at 3.0 kW was approximately 55 mm from the centreline. The thermocouples in the third array only recorded the hot combustion gases. Whilst, figure 6.8 shows similar cross-sectional contours at 15.0 kW fire. At this HRR, it can be seen that the flame was nearly reached the tunnel wall, judging by the high temperature contours near the wall.

Figure 6.9 depicts the contours in tunnel **D** at 3.0 kW fire at three ventilation velocities. The ventilation velocities were 0.18 m/s, 0.40 m/s and 0.50 m/s, respectively. While Figure 6.10 shows the contours at 3.0 kW, 7.5 kW and 15.0 kW fires at critical ventilation conditions. The critical ventilation velocities were 0.40 m/s, 0.50 m/s and 0.59 m/s, respectively. Similar to Figure 6.5 (tunnel **B**), it can be seen that as the fire increases, the size of the plume also increases. The maximum temperature measured at each HRR were 580.54 °C, 729.01 °C and 768.66 °C, respectively. However, it can be observed that the flame in tunnel **D** is less deflected from the vertical than the flame in tunnel **B**. In addition, the observed flame length in tunnel **D** is also slightly shorter.

Figure 6.11 depicts the contours in tunnel **D** at 3.0 kW, 7.5 kW and 15.0 kW with the presence of backlayering flow. The ventilation velocities were set to 0.18 m/s, 0.28 m/s and 0.33 m/s, respectively. The backlayering was controlled at 10 tunnel heights upstream from fire, similar to Figure 6.6 (tunnel **B**). Similarly, as the HRR increases, the contours show that the maximum temperature in the backlayering region increases. It can be also observed that the position of the first contour indicating the backlayering flow is at approximately 225 mm above tunnel floor, which is slightly higher than in tunnel **B**. This could suggest that the depth of the backlayering flow in tunnel **D** is slightly lower than in tunnel **B**.

The cross-sectional temperature contours at various distances from the burner in tunnel **D** at 3.0 kW and 15.0 kW fires at critical ventilation velocity are shown in Figures 6.12 and 6.13. It can be seen that the pattern of the contours are slightly different from tunnel **B**. Once the smoke reached the ceiling, it spread away to the wall. The contours also show that the wall did not give a significant effects on the flame geometry and smoke movement. The temperature data for 3.0 kW fire in Table 6.12 show that both second and third arrays recorded lower temperature value with the average temperature between 20°C to 40 °C. This suggests that the thermocouples in both arrays were only recorded the radiation or heated values. However at 15.0 kW fire, the second array recorded

higher temperature in the order of 250 °C. The highest temperature in the third array was in the order of 165 °C which suggests the temperature of the hot combustion gases.

Figure 6.14 shows the additional temperature contours measured in tunnel **A** at the critical ventilation velocities for HRR 3.0 kW, 7.50 kW and 15.0 kW. The critical ventilation velocity for each HRR were 0.40 m/s, 0.48 m/s and 0.48 m/s, respectively. Since the burner occupied the majority of the cross-sectional width, it would be expected that in this tunnel the fire would reach the tunnel walls. Therefore, it was decided to measure the temperature distributions only at tunnel centreline.

In conclusion, the present results clearly show the shapes and the sizes of the plume inside the tunnels. Further justifications on the fire plume such as the interaction between the plume with the ventilation flow and plume tilt angles will be discussed in the following chapter.

6.2.2 Temperature Distribution in the Upstream

The temperature distributions in the upstream region have been measured at 3.0 kW, 7.5 kW and 15.0 kW fires starting from the burner centreline up to 1000 mm upstream from the burner. The ventilation velocity was set at which the backlayering was controlled up to 10 tunnel heights upstream from the burner. In this region, the temperature measurements in tunnel **A** were used for lower aspect ratio tunnel.

The measured temperatures in tunnel **A** at 3.0 kW and 7.50 kW are shown in Tables 6.18 and 6.19, respectively. The temperature contours at both HRRs are shown in Figure 6.15. It can be seen that the backlayering flows are stratified and the maximum temperature decreases as the backlayering flow in the upstream. It can be also observed that the thickness of the backlayering flow is approximately the same regardless of the fire HRR for the same tunnel. The photograph of the backlayering flow in tunnel **A** at HRR 7.5 kW shown in Figure 6.16 further shows that the smoke thickness is

approximately half of the height of the tunnel with the end of the layer formed a sharp edge.

Tables 6.20 to 6.22 show the measured temperatures in tunnel **D** at 3.0 kW, 7.5 kW and 15.0 kW fires, respectively. Figure 6.17 shows the temperature contours for 3.0 kW and 7.5 kW fires. Similarly, the thickness of the backlayering flow is approximately the same for both fires in tunnel **D**.

Comparing the temperature contours in Figures 6.15(a) and 6.17(a), it can be observed that the depth of the backlayering flow was greater in tunnel **A** than in tunnel **D**. Further temperature comparisons at various distances upstream from fire seat for tunnel **A** and **D** at 3.0 kW in Figure 6.18 also confirmed the backlayering flow patterns.

6.2.3 Temperature Distribution in the Downstream

The measured temperature distributions in the downstream are presented in Tables E1 to E12 in Appendix E. The overall temperature distributions in downstream of the fire in tunnel **B** for 3.0 kW, 7.5 kW and 15.0 kW at critical ventilation velocity and velocity for the backlayering was controlled at 10 tunnel heights are shown in Figures 6.19 and 6.20. The measured temperature contours show that the downstream smoke flow is stratified. Figures 6.21 and 6.22 show similar temperature contours in tunnel **D** at the same conditions.

6.3 Velocity Distribution

The velocity distributions presented in this section have been measured in tunnel **B** by Allen et al. (1999) using Laser Doppler Velocimetry (LDA). Table 6.23 shows the average velocities for five HRRs (1.5 kW, 3.0 kW, 4.5 kW, 7.5 kW and 15.0 kW). The negative sign shows the direction of the backlayering flow. The velocity profiles for the five HRRs considered are shown in Figure 6.23. It can be seen that the ventilation velocity to control the backlayering flow up to 2.25 tunnel height increases with the

HRR up to 4.35 kW. Beyond this HRR, the ventilation velocities have becomes constant. Thus indicates the existence of the behaviour of the independent of the ventilation velocity on the HRR.

Another significant observation is that the velocity profiles in the backlayering region are almost similar regardless of the HRRs. This further indicates that the depth of the backlayering flow is almost constant in that particular tunnel.

Table 6.24 shows the velocity distributions at 3.0 kW when the ventilation velocity was set to 0.47 m/s. The velocity profiles at various positions upstream from the fire are shown in Figure 6.24. It can be observed that at this condition the smoke front travelled between 1.5 to 2 tunnel heights, consistent with previous determination using 0.25 mm sheathed thermocouple.
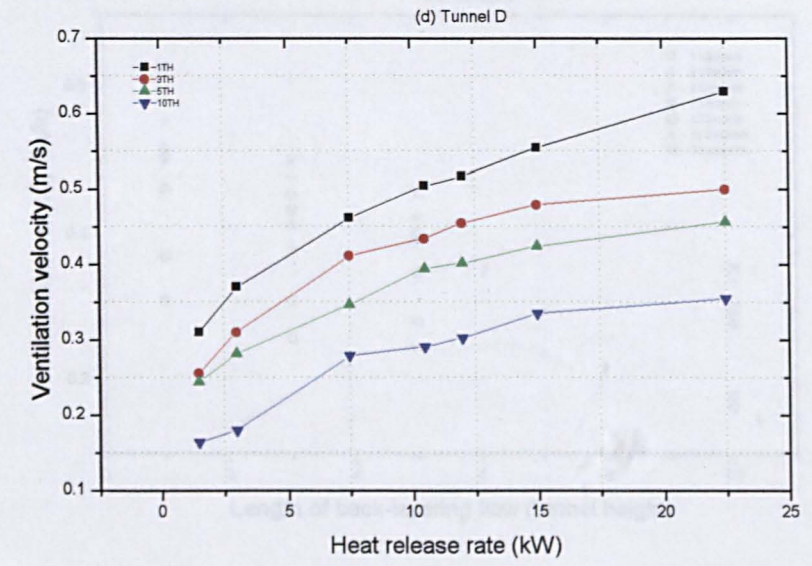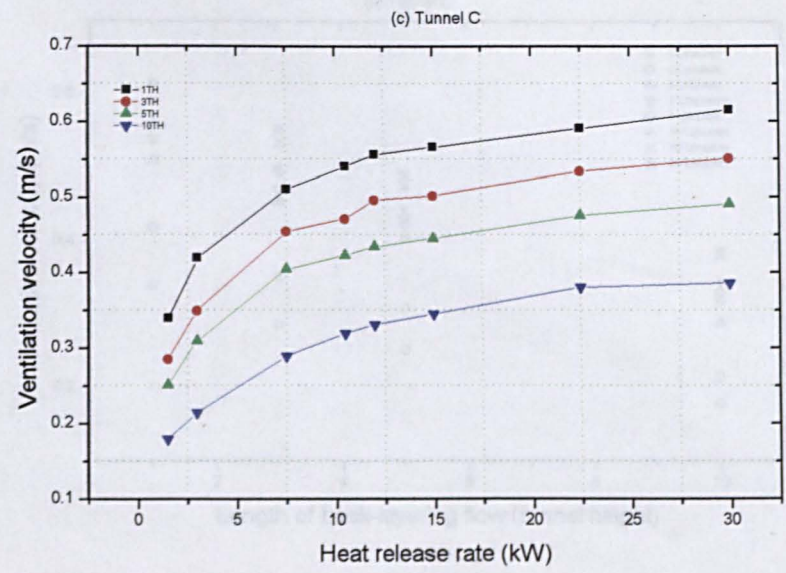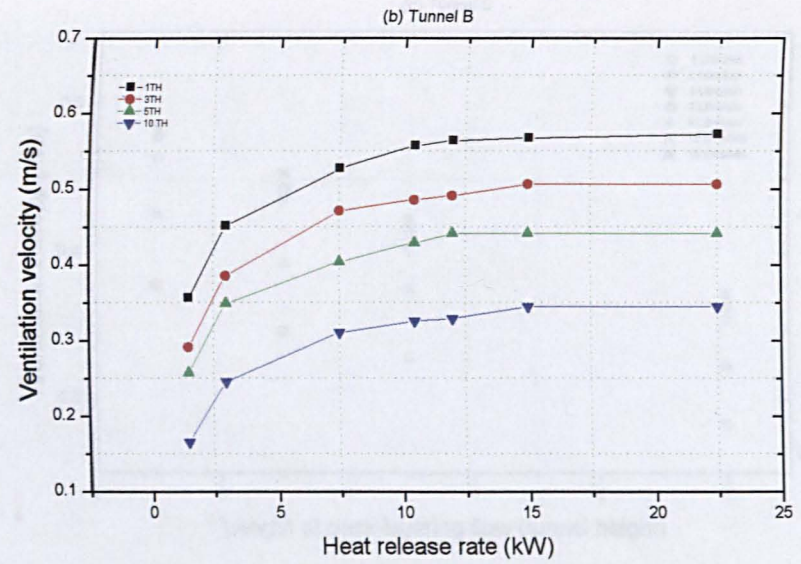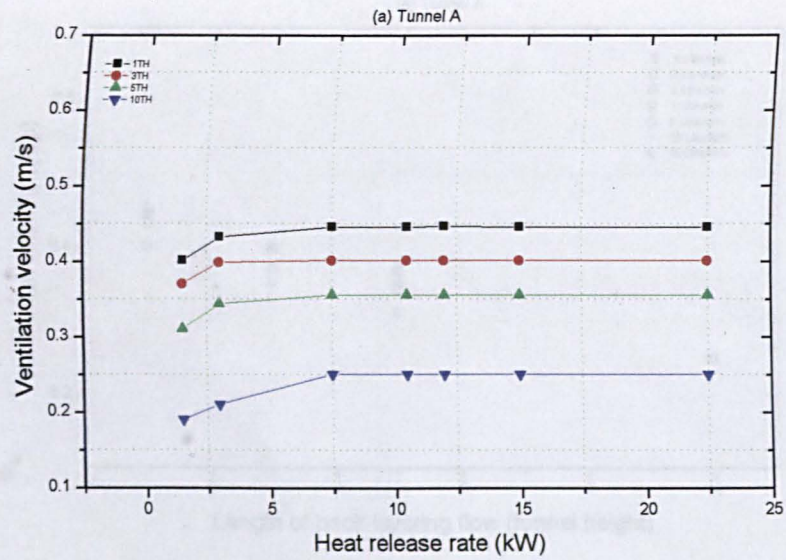
Figure 6.1 : Plot of ventilation velocity vs HRR at 1, 3, 5 and 10 tunnel heights backlayering
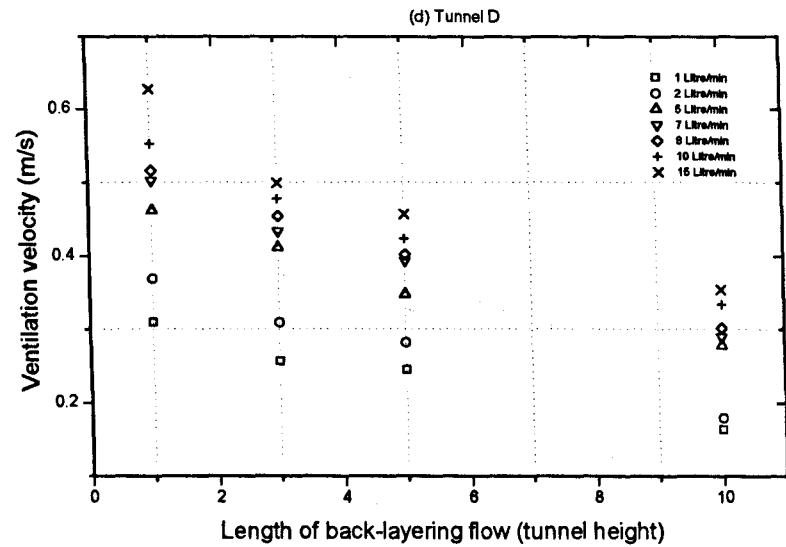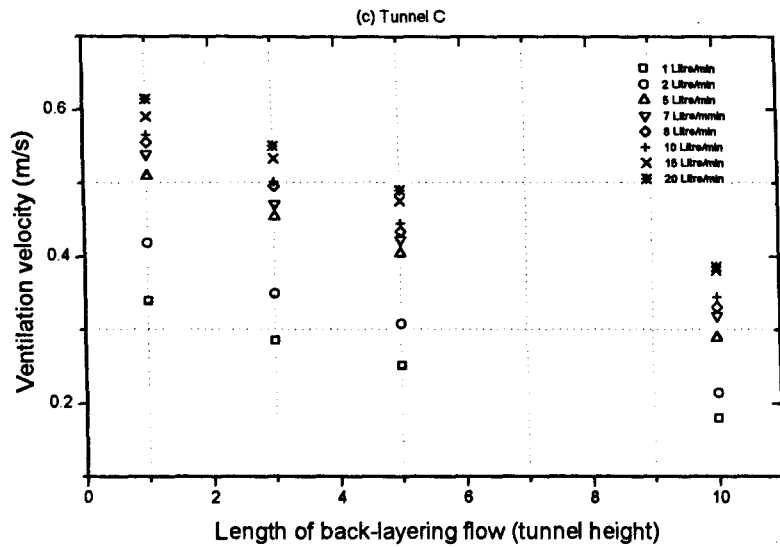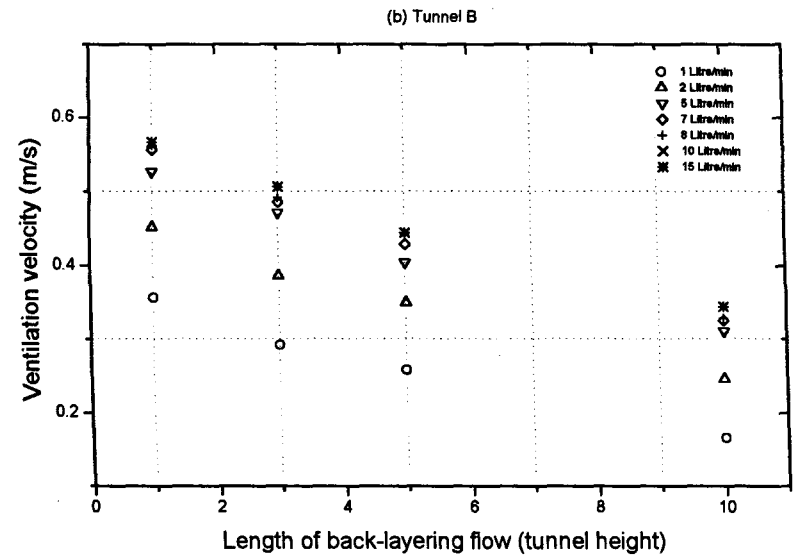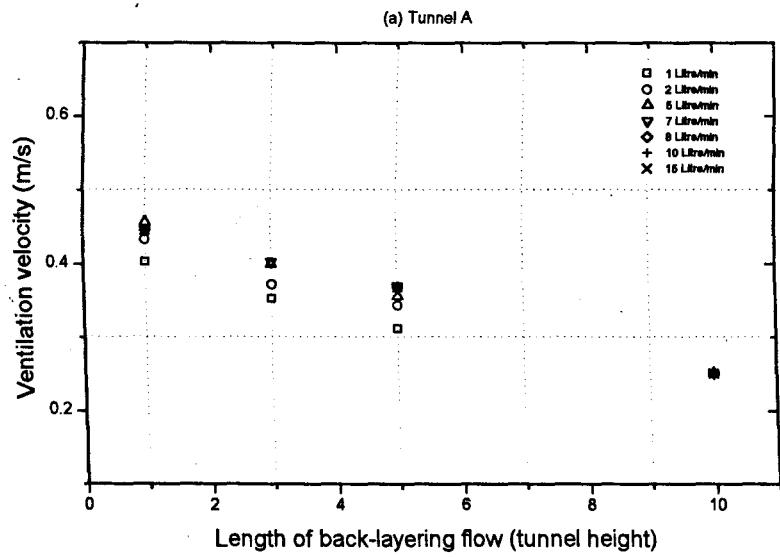
Figure 6.2 : Plot of ventilation velocity vs length of backlayering at various HRRs
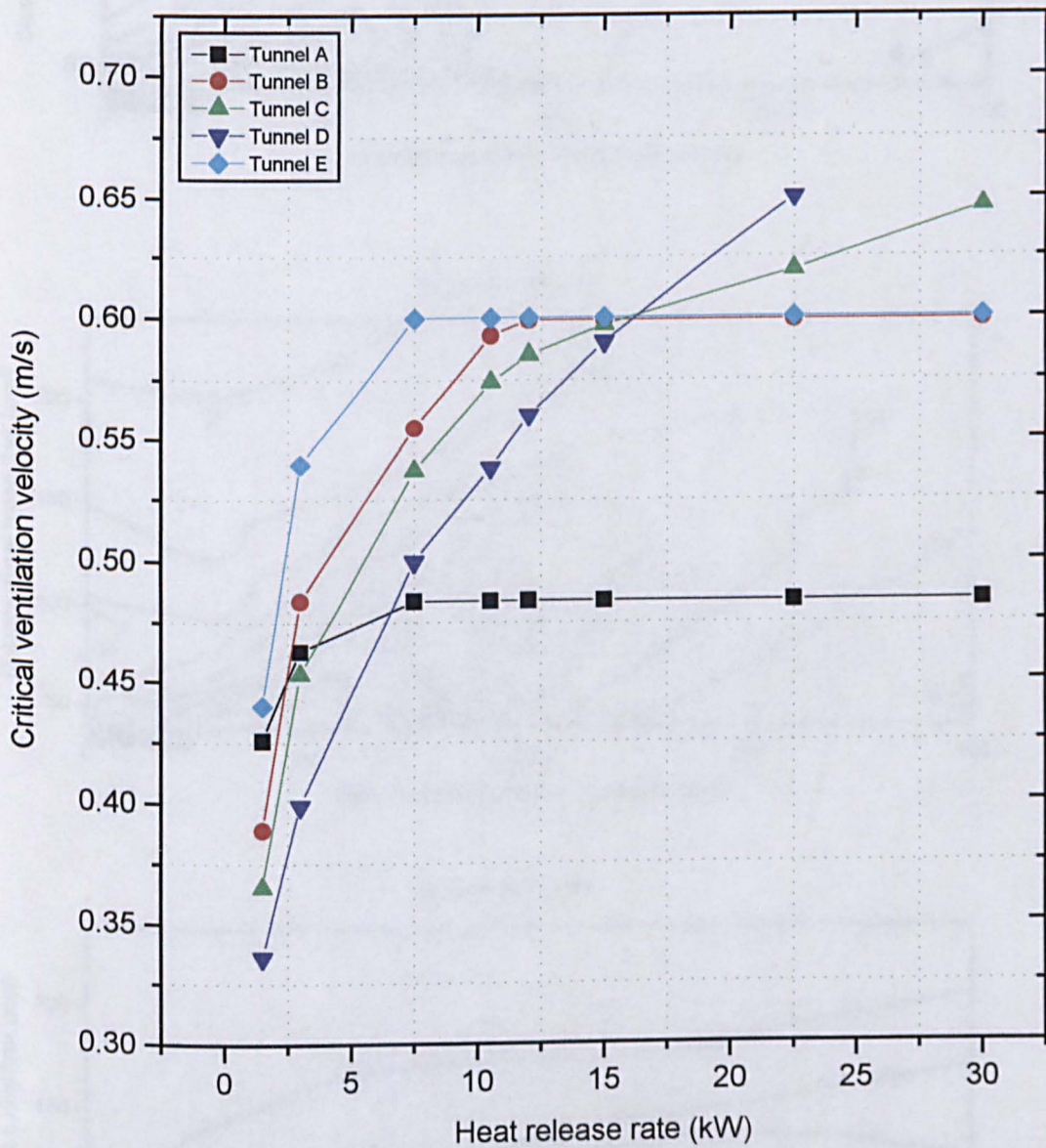
Figure 6. 3 : Critical ventilation velocity against heat release rate
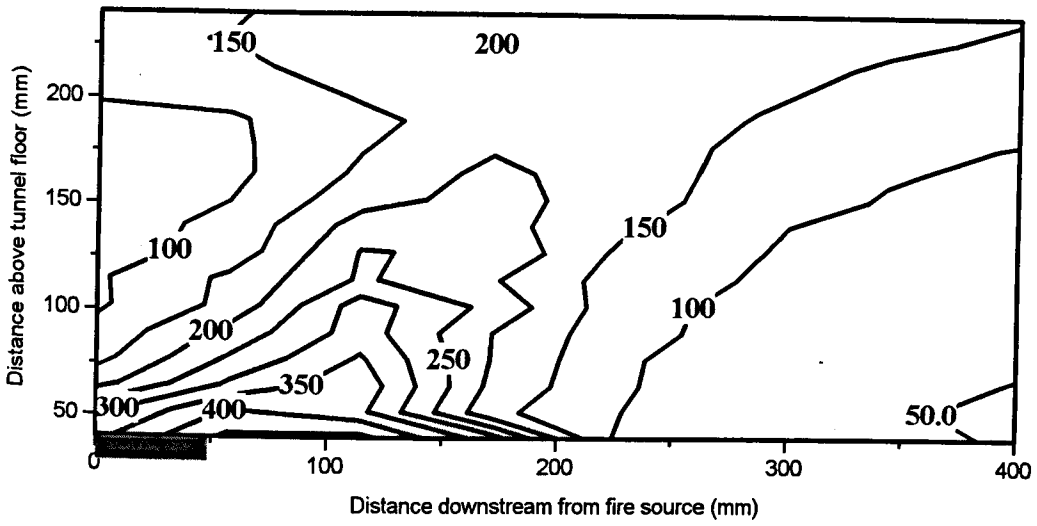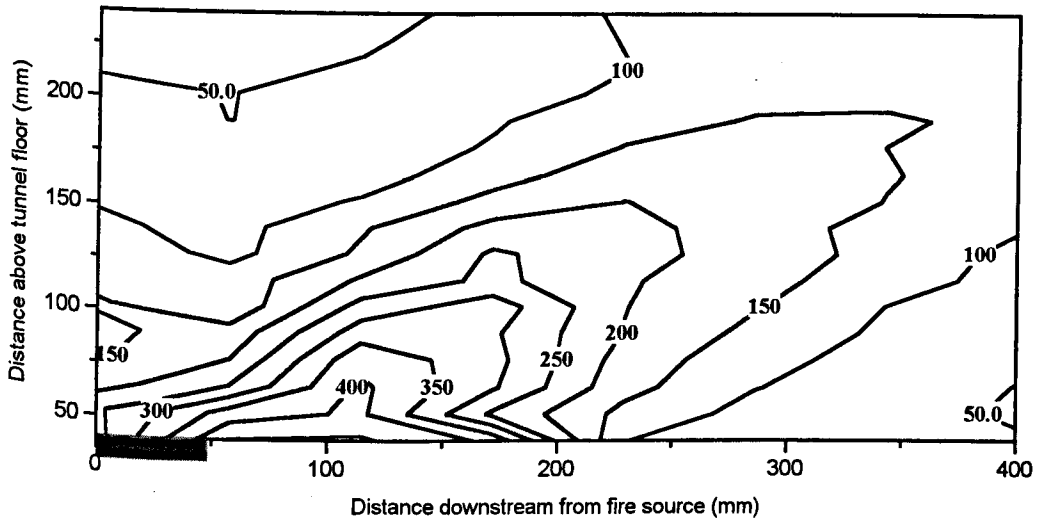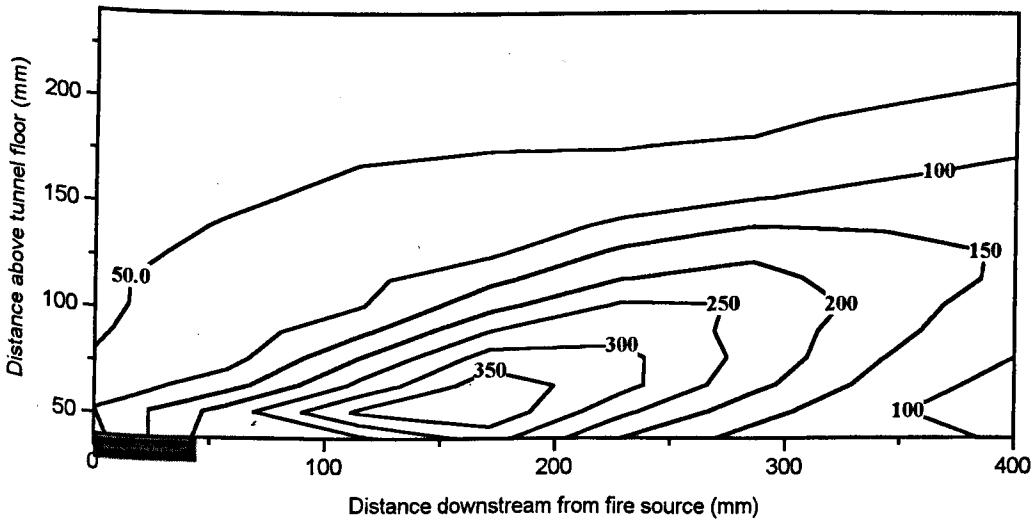
Figure 6.4 : Measured temperature contours in tunnel B at 3.0 kW fire

(a) Q = 3.0 kW, Uc = 0.48 m/s

(b) Q = 7.50 kW, Uc = 0.56 m/s

(c) Q = 15.0 kW, Uc = 0.60 m/s
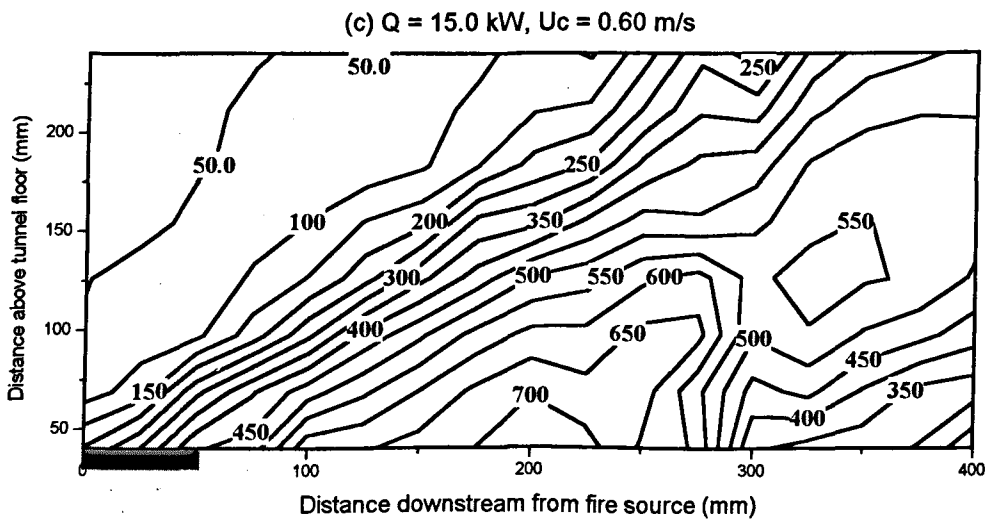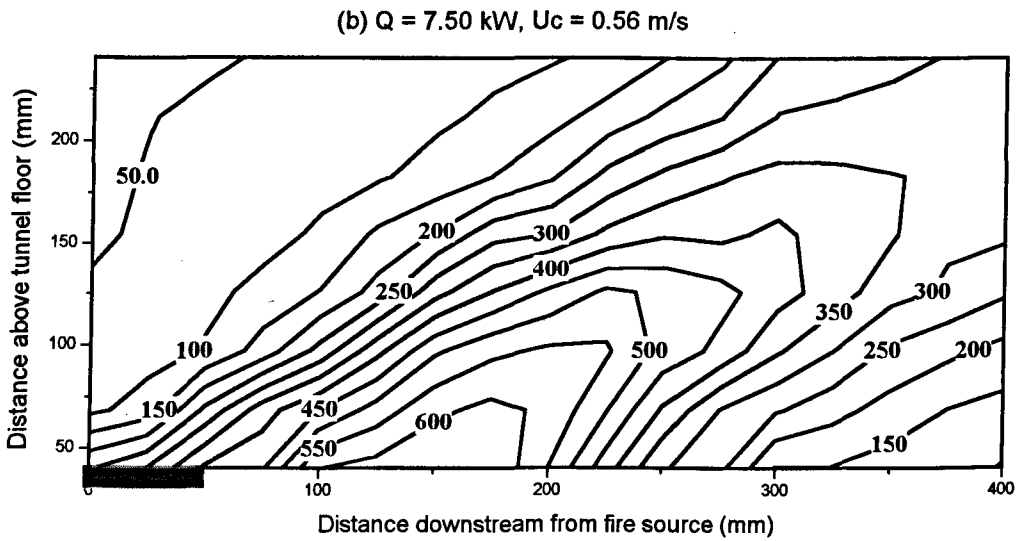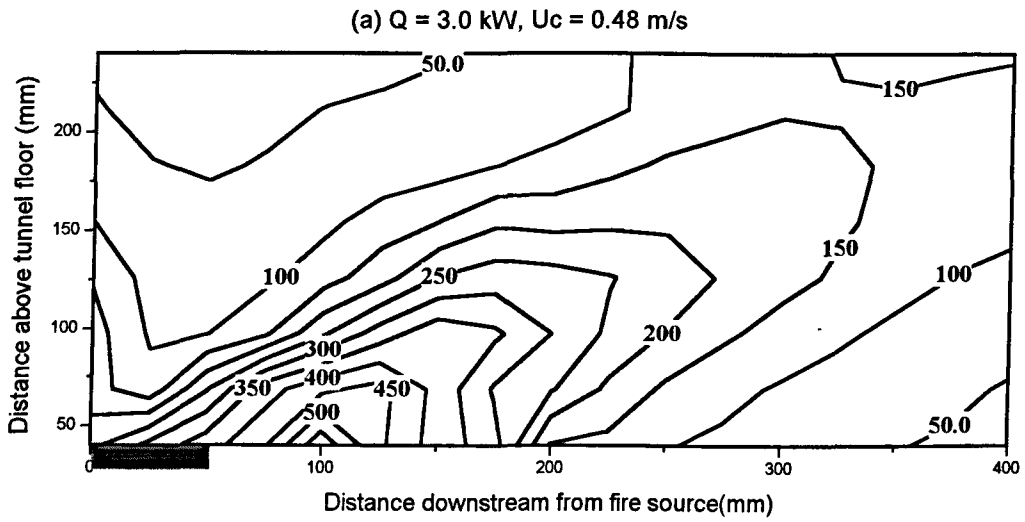
Figure 6.5 : Measured temperature contours in tunnel B for 3.0 kW, 7.50 kW and 15.0 kW at critical conditions

(a) Q = 3.0 kW, U = 0.25 m/s

(b) Q = 7.50 kW, U = 0.31 m/s

(c) Q = 15.0 kW, U = 0.34 m/s
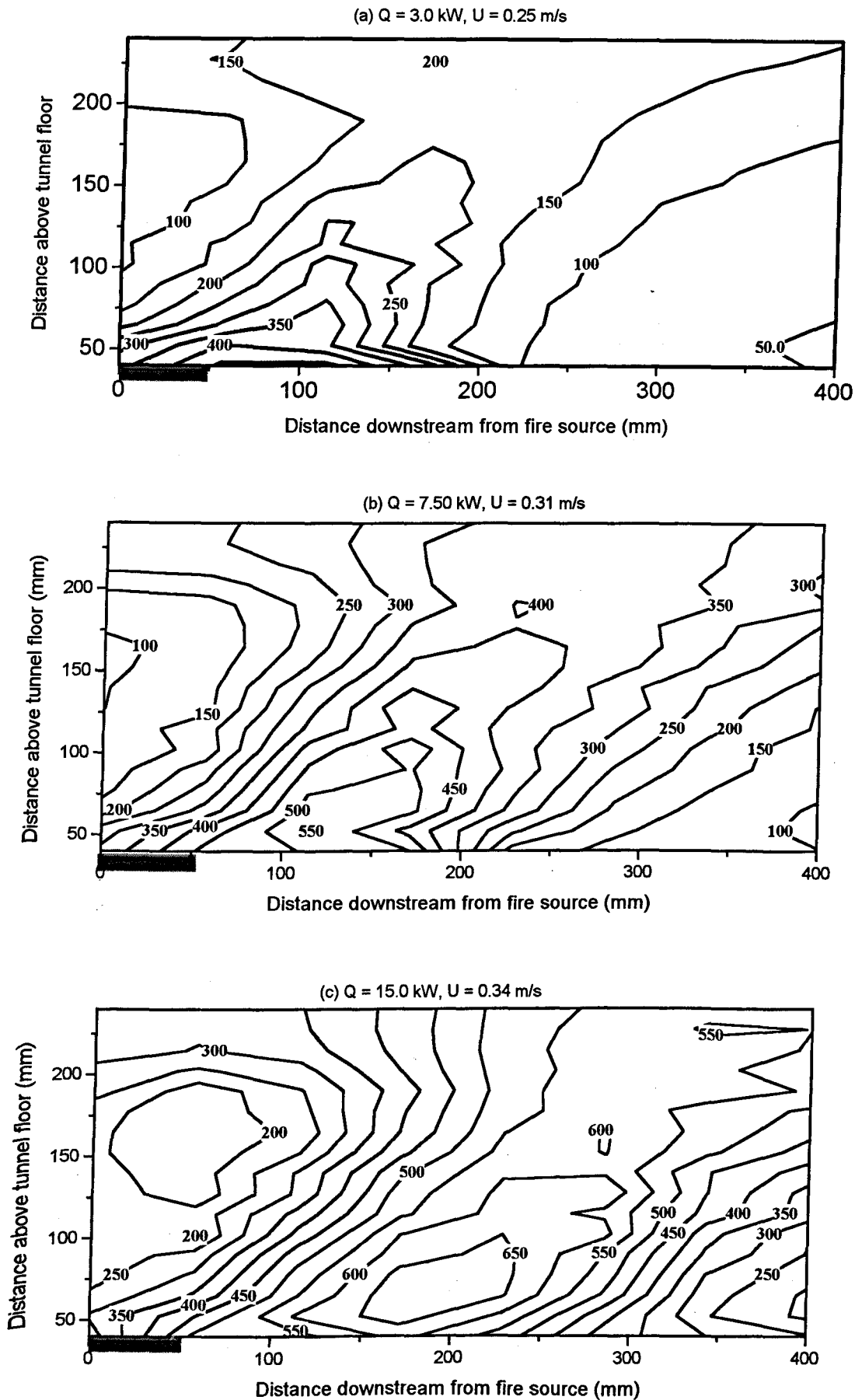
Figure 6.6 : Measured temperature contours in tunnel B for 3.0 kW, 7.50 kW and 15.0 kW. (Backlayering controlled at 10 tunnel heights upstream)

89
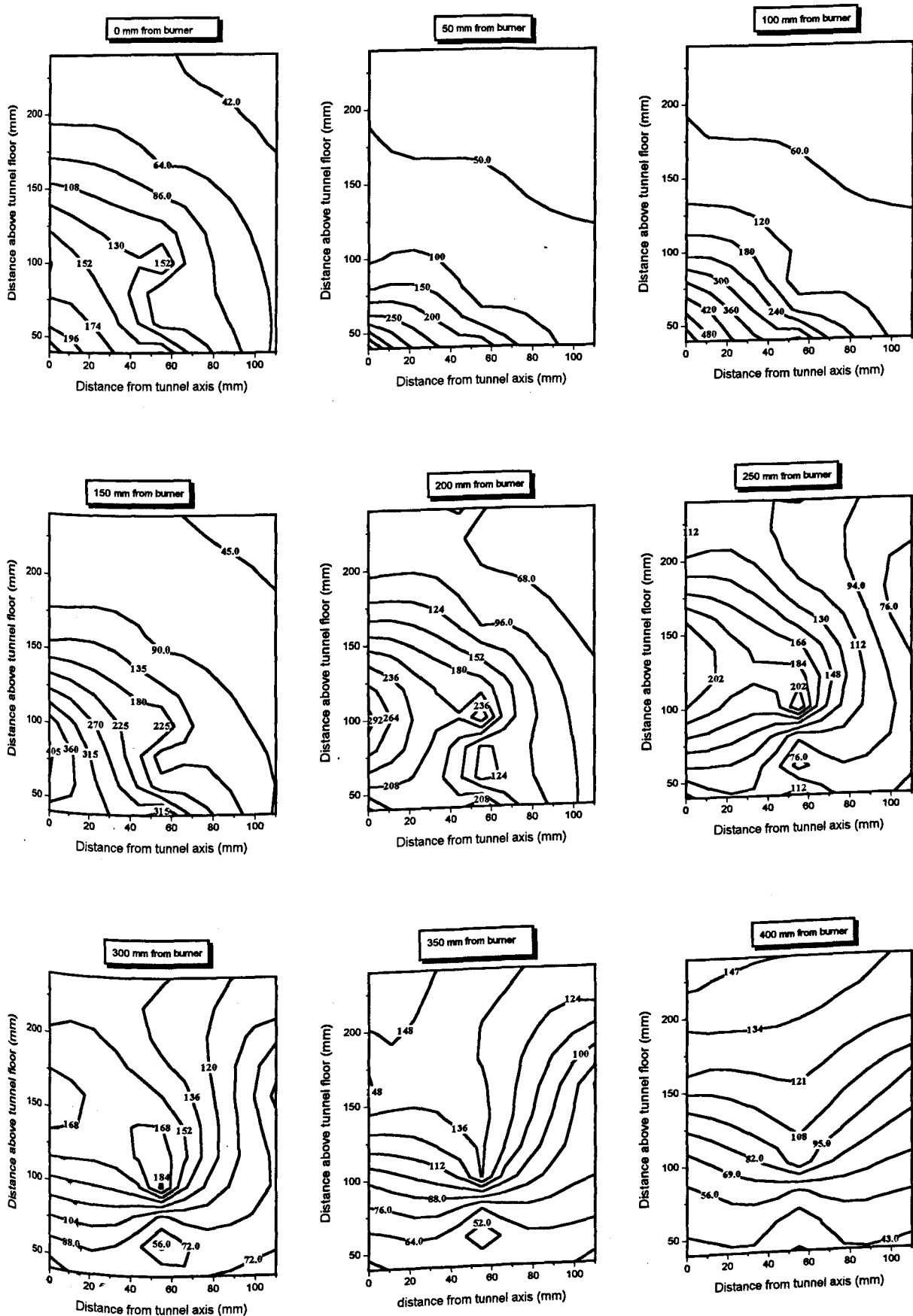
Figure 6.7 : Measured cross-sectional temperature contours at various distances from burner in tunnel B (Q = 3.0 kW, Uc = 0.48 m/s)
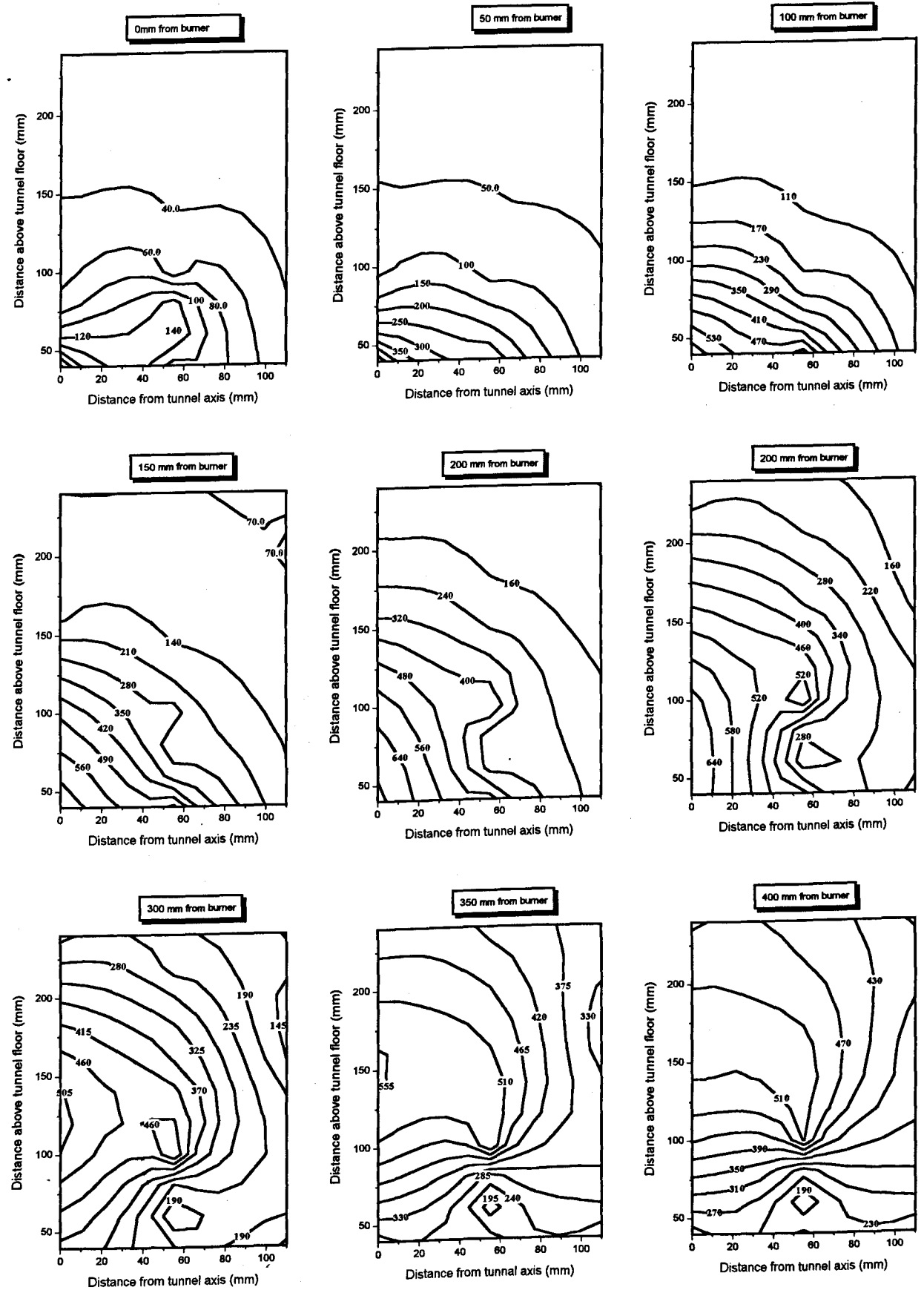
Figure 6.8 : Measured cross - sectional temperature contours at various distances from burner in tunnel B (Q=15.0 kW, Uc = 0.60 m/s)

91
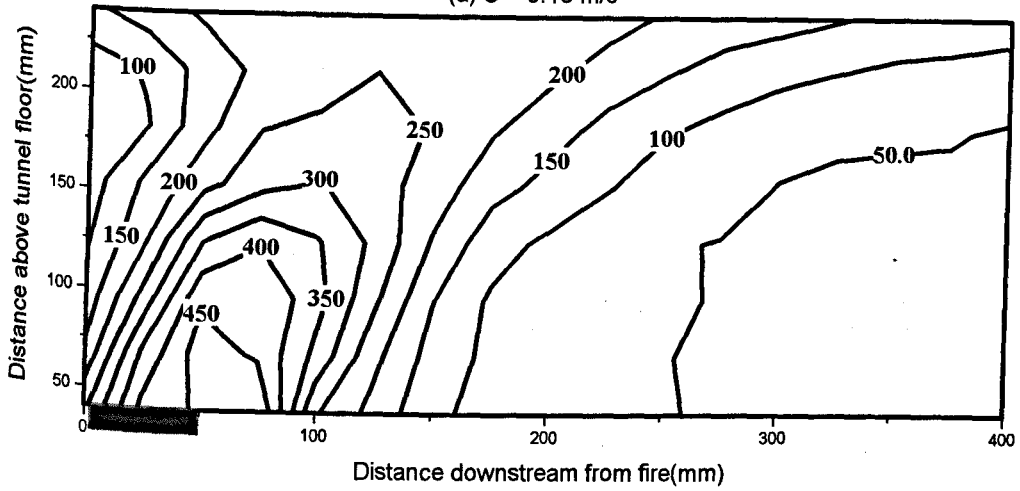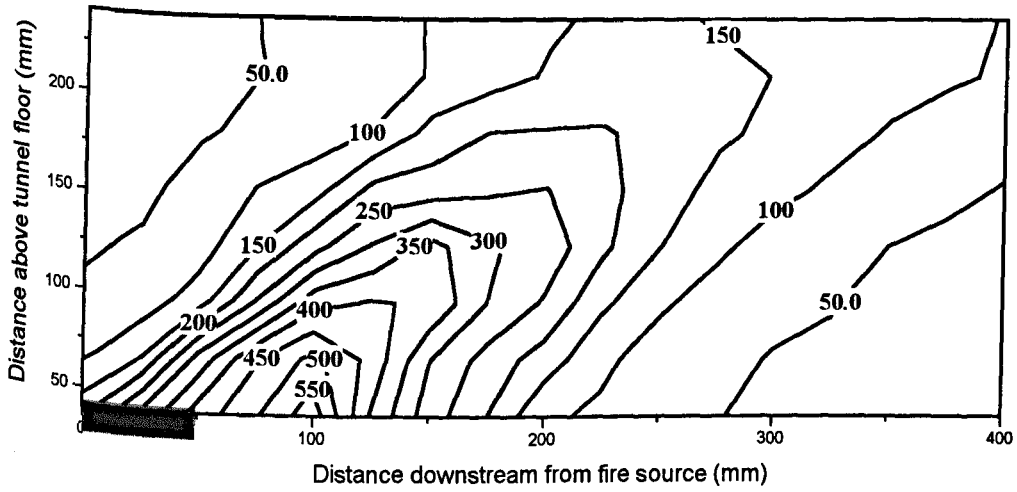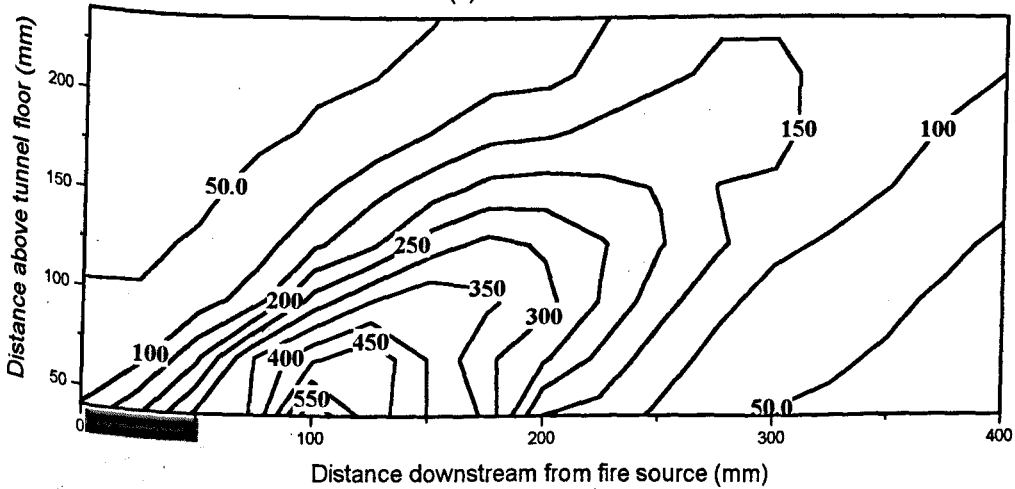
Figure 6. 9 : Measured temperature contours in tunnel D at 3.0 kW fire

(a) Q = 3.0 kW, Uc = 0.40 m/s

Distance above tunnel floor(mm)

Distance downstream from fire source(mm)

(b) Q = 7.50 kW, Uc = 0.50 m/s

Distance above tunnel floor (mm)

Distance downstream from fire source(mm)

(c) Q = 15.0 kW, Uc = 0.59 m/s

Distance above tunnel floor (mm)

Distance downstream from fire source (mm)
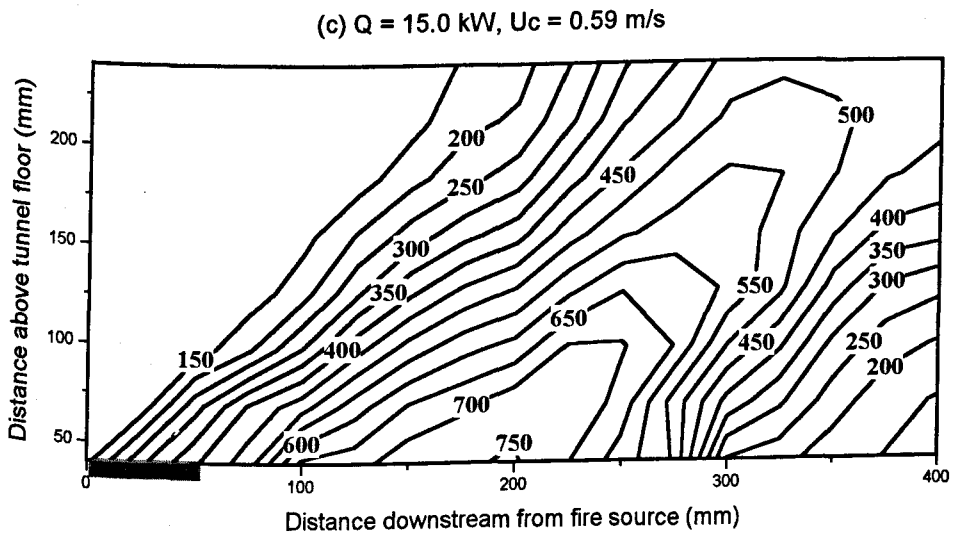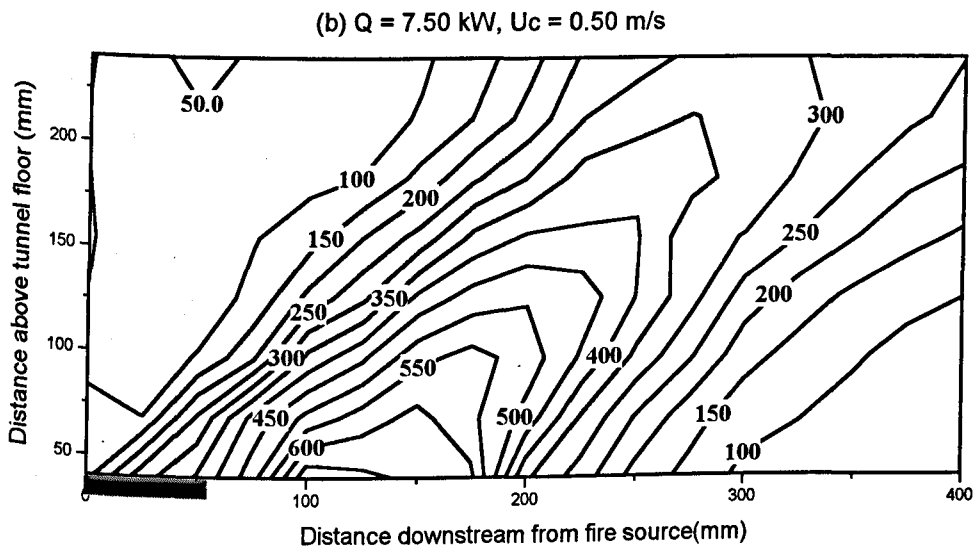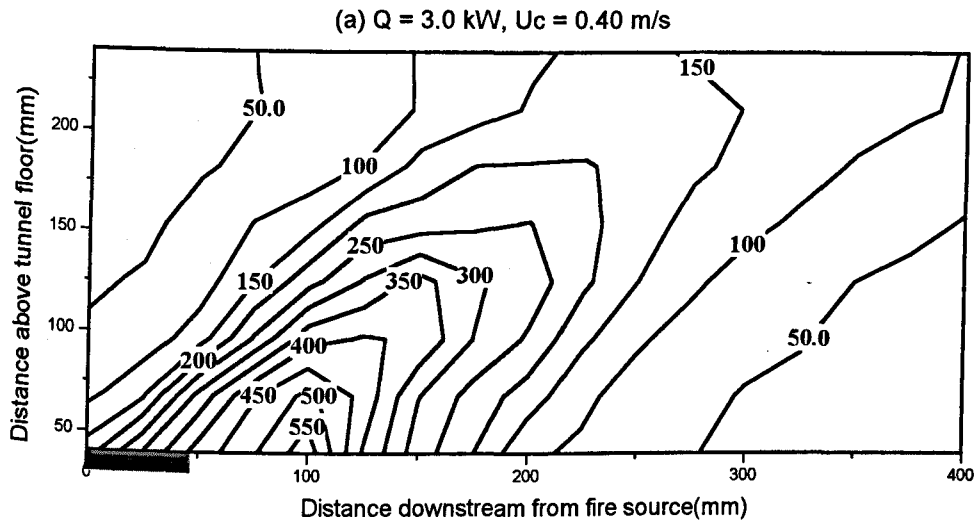
Figure 6.10 : Measured temperature contours in tunnel D for 3.0 kW,
7.50 kW and 15.0 kW at critical conditions

(a) Q = 3.0 kW, U = 0.18 m/s

(b) Q = 7.50 kW, U = 0.28 m/s

(c) Q = 15.0 kW, U = 0.33 m/s
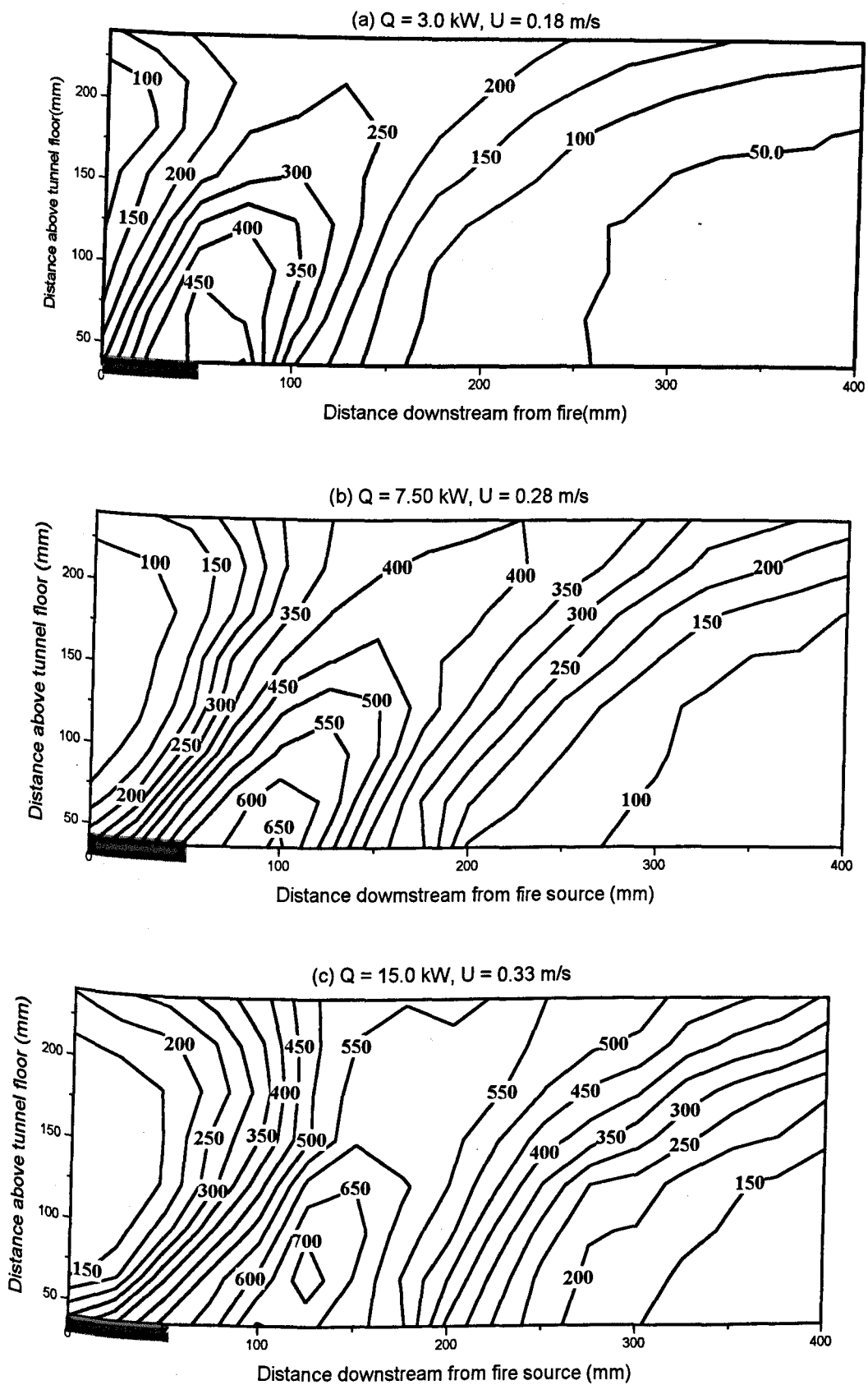
Figure 6.11 : Measured temperature contours in tunnel D for 3.0 kW,
7.50 kW and 15.0 kW (Backlayering controlled at
10 tunnel heights upstream)
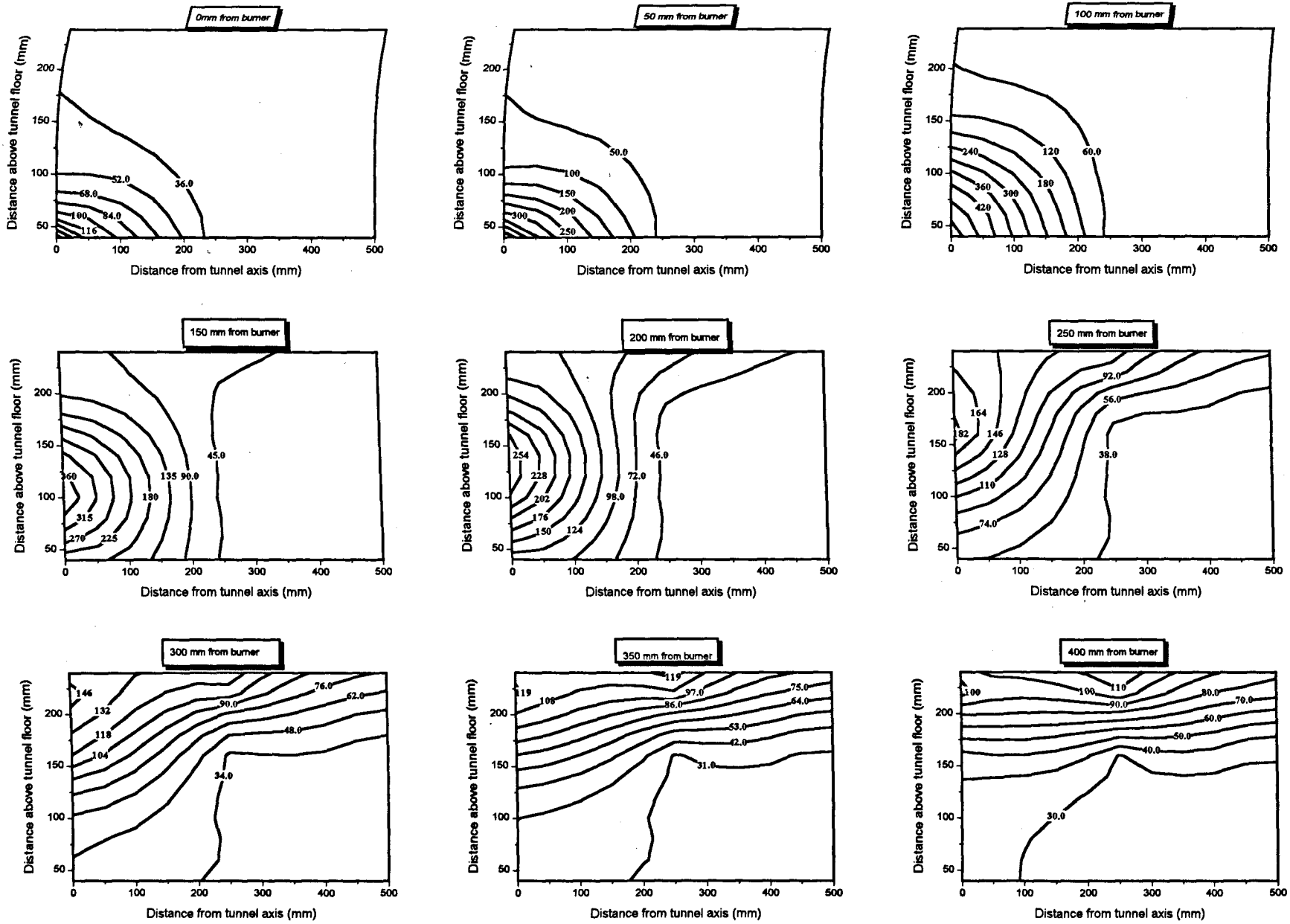
Figure 6.12 : Measured cross-sectional temperature contours at various distances from the burner in tunnel D [Q=3.0 kW, Uc = 0.40 m/s)

95
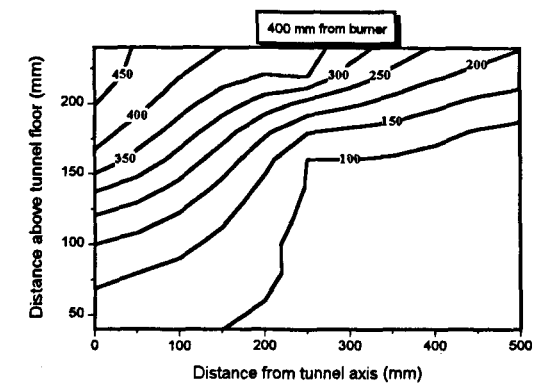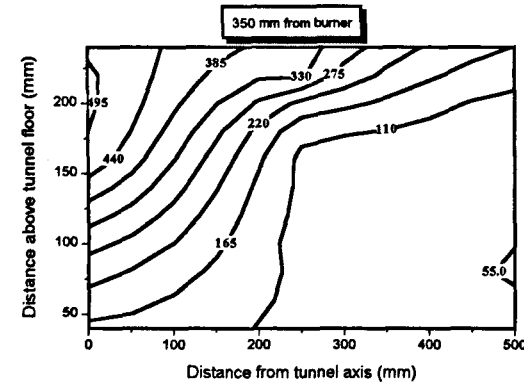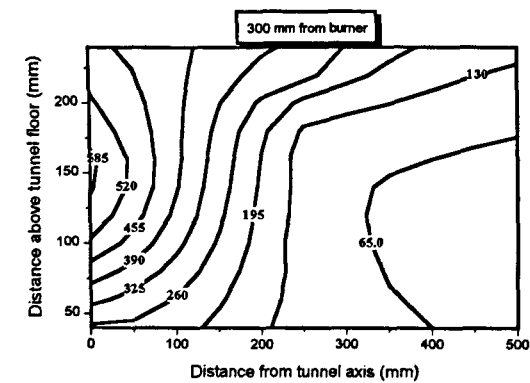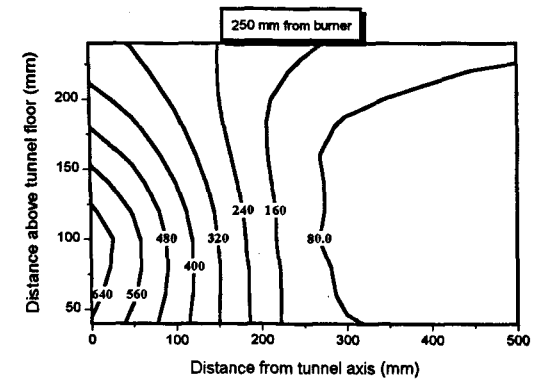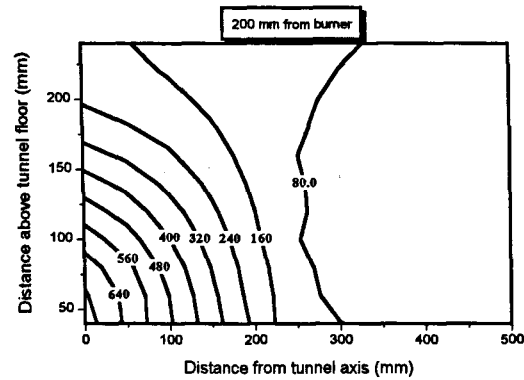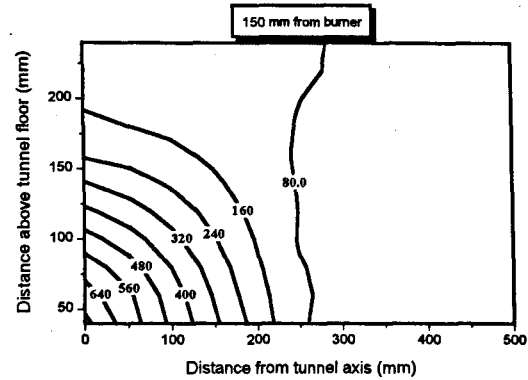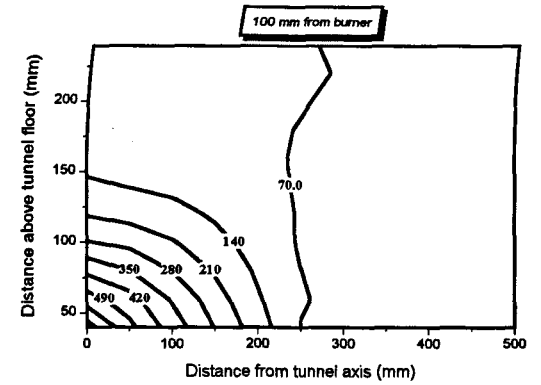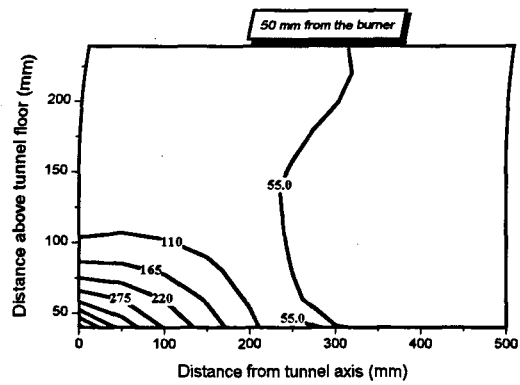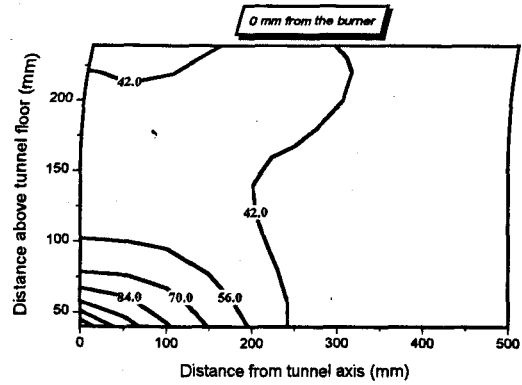
Figure 6.13 : Measured cross-sectional temperature contours at various distances from the burner in tunnel D [Q=15.0 kW, Uc = 0.59 m/s)
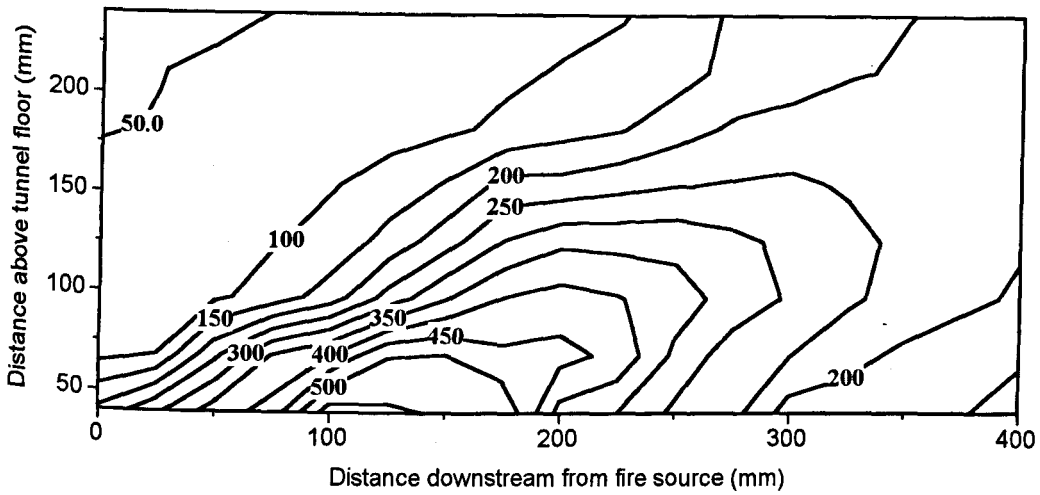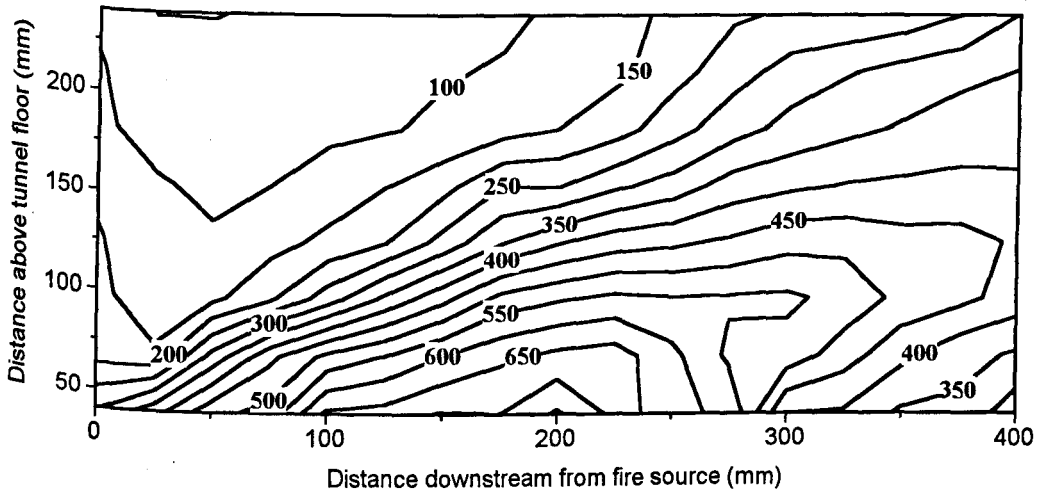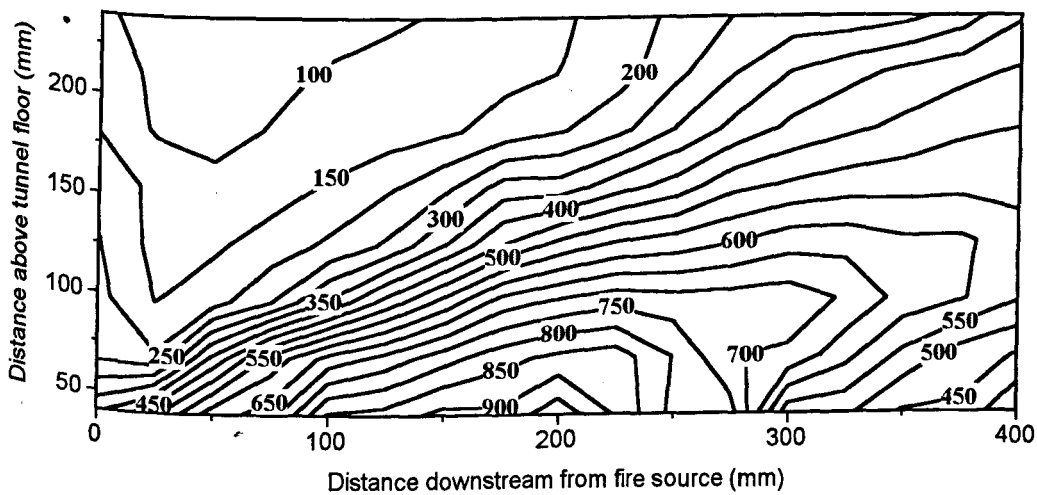
Figure 6.14 : Measured temperature contours in tunnel A for 3.0 kW,
7.50 kW and 15.0 kW at critical conditions

(a) Q = 3.0 kW, U = 0.25 m/s
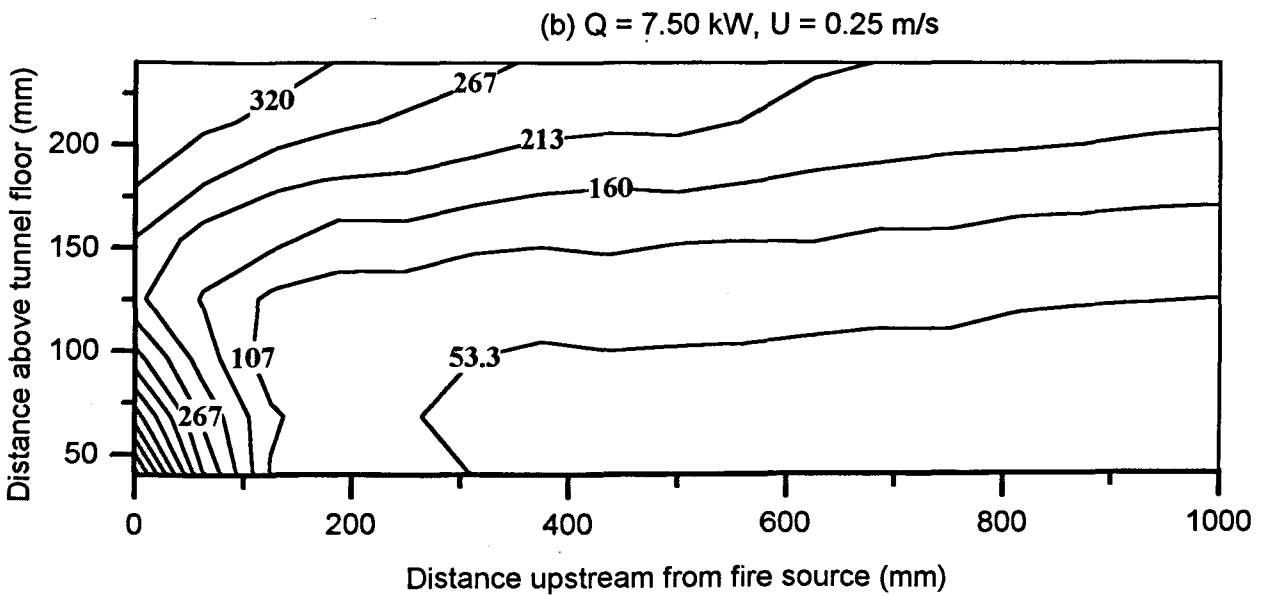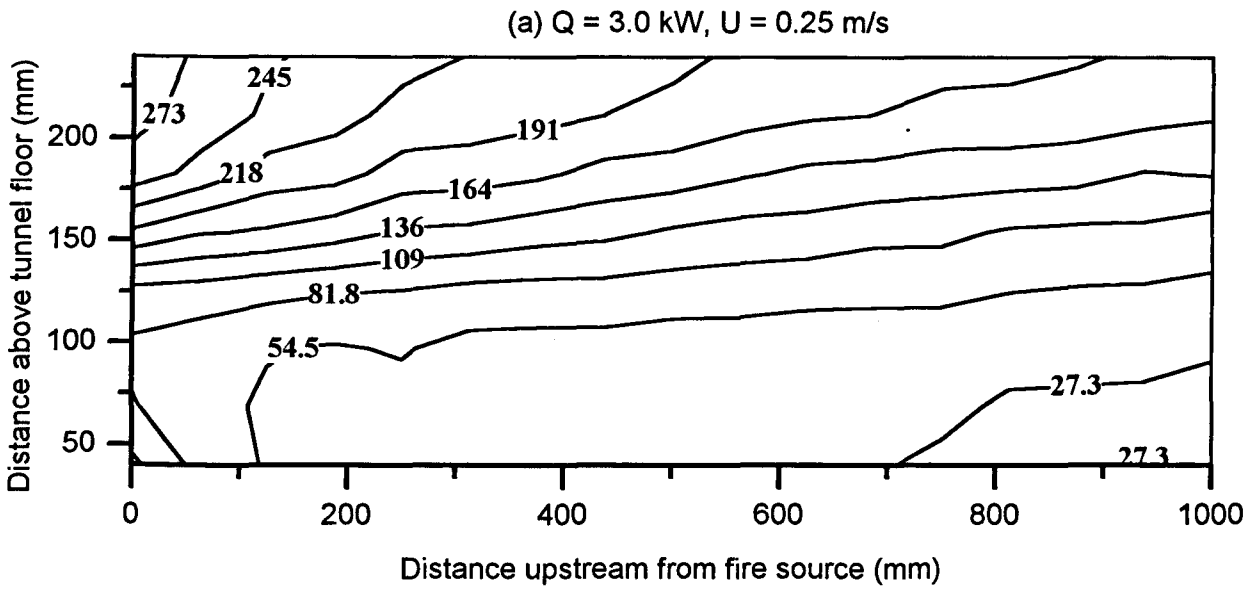
(b) Q = 7.50 kW, U = 0.25 m/s

Figure 6.15 : Measured upstream temperature contours in tunnel A
(Backlayering controlled at 10 tunnel heights)

(a)
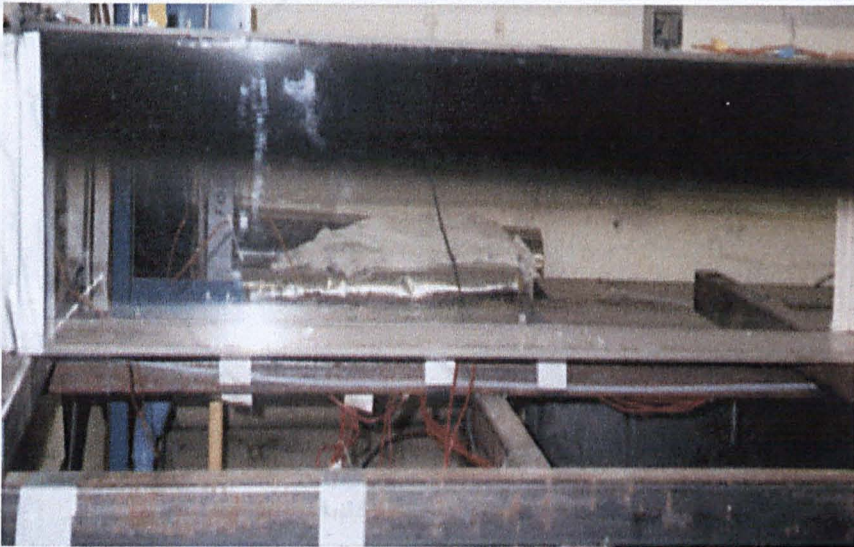
(b)

Figure 6.16 : Photographs of the backlayering layer in tunnel A

(a) Q = 3.0 kW, U = 0.18 m/s
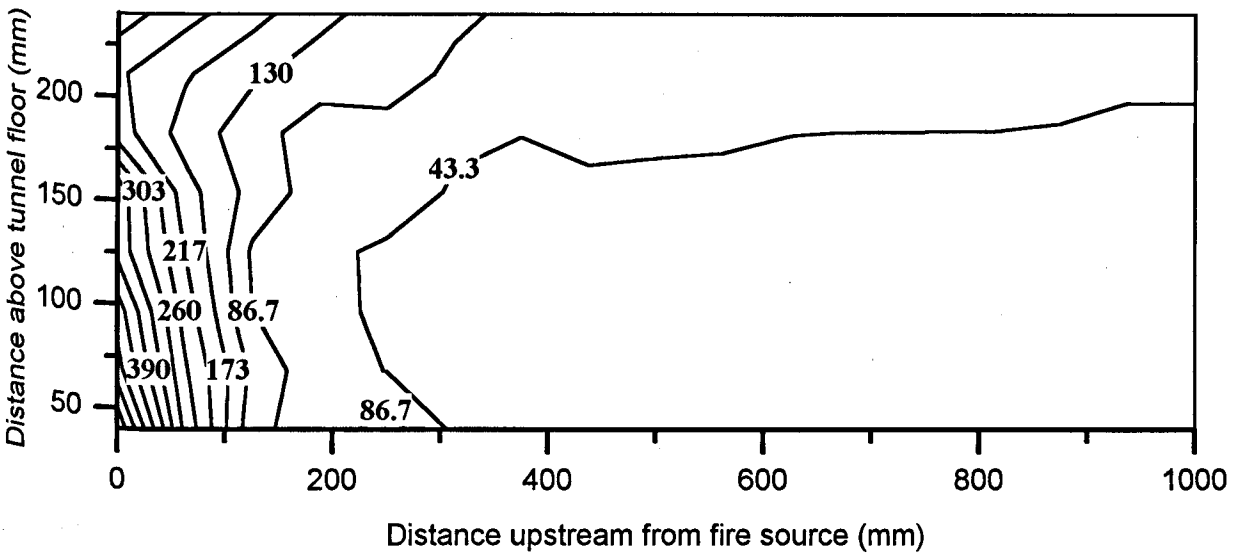
(b) Q = 7.50 kW, U = 0.28 m/s
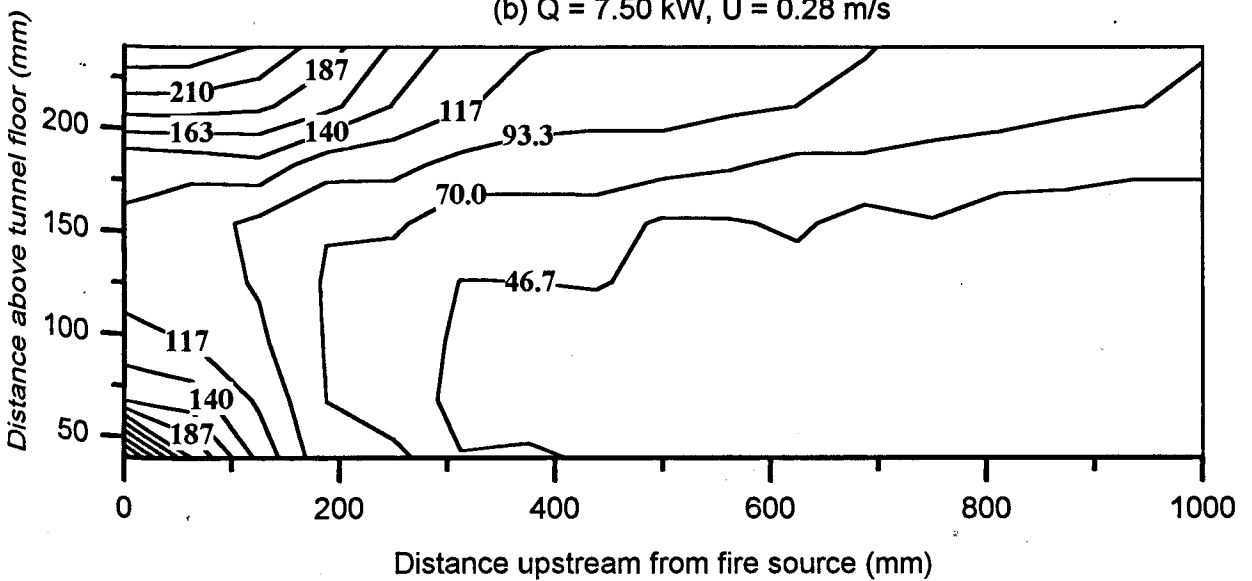
Figure 6.17   : Measured upstream temperature contours in tunnel D
(Backlayering controlled at 10 tunnel heights)

100
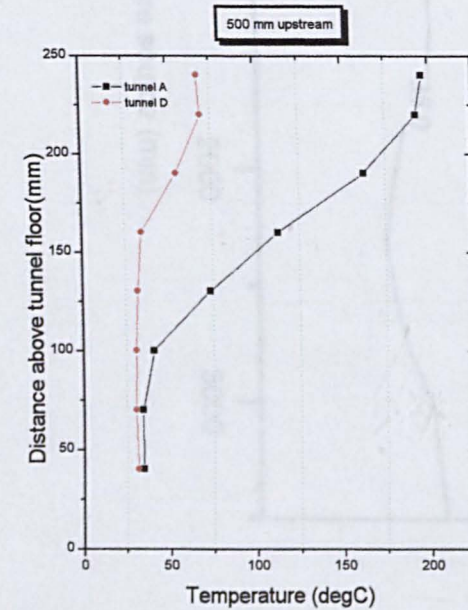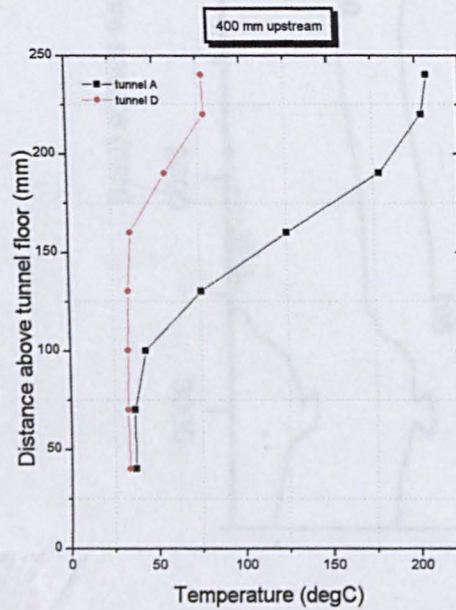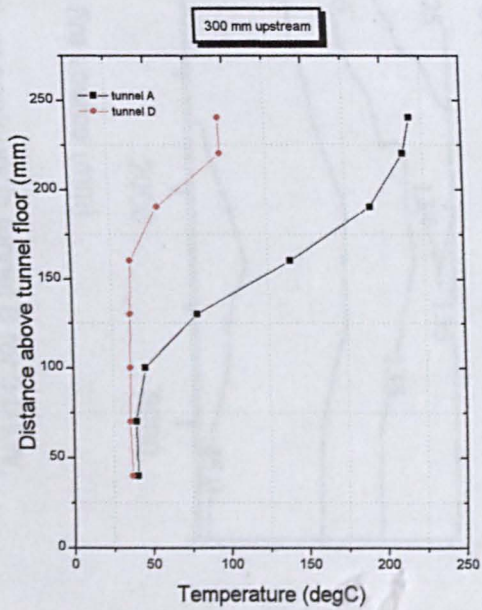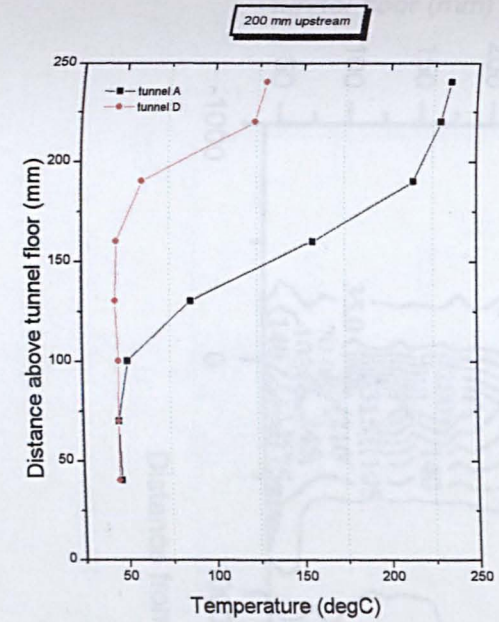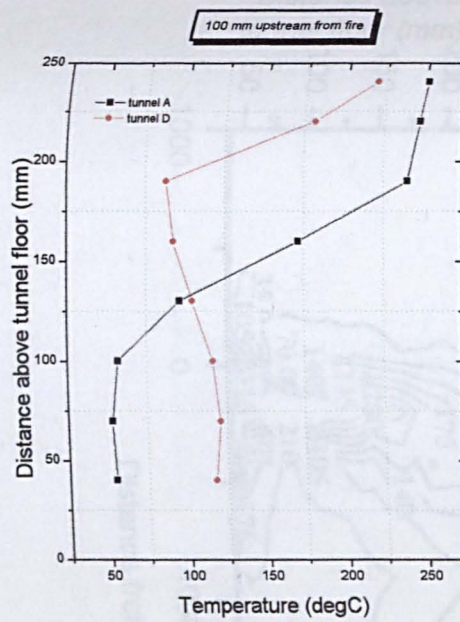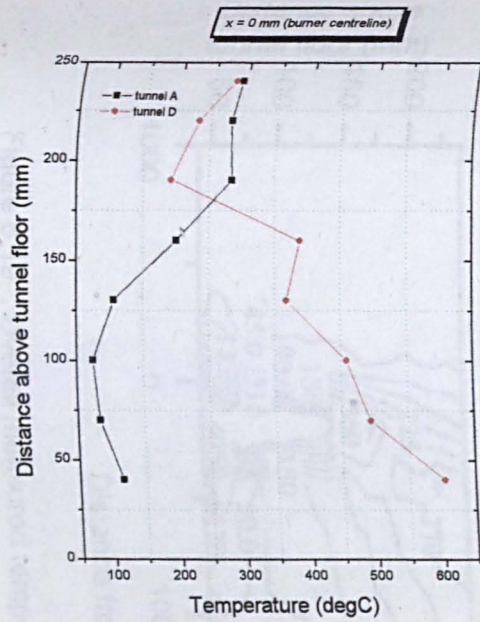
Figure 6.18 : Comparisons between measured upstream temperature distributions in tunnel A and D at 3.0 kW

(a) Q = 3.0 kW, Uc = 0.48 m/s
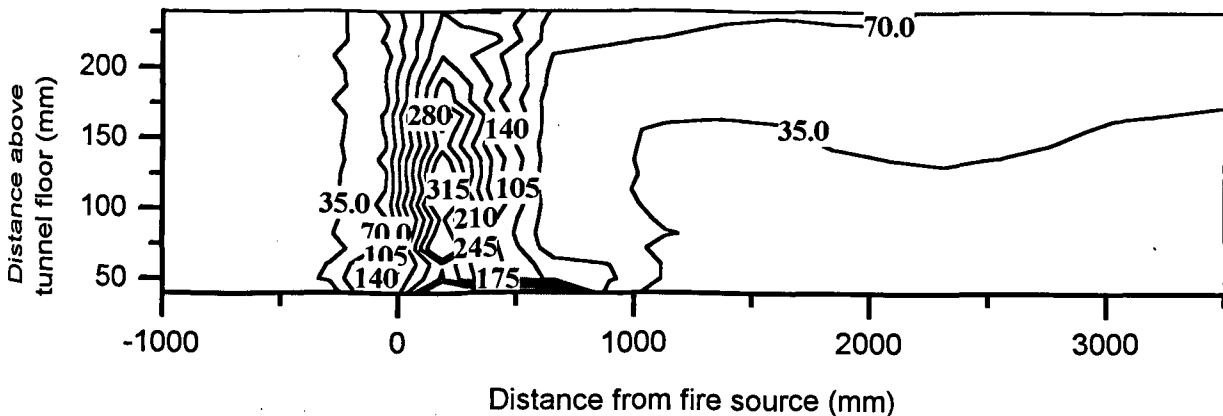
(b) Q = 7.50 kW, Uc = 0.56 m/s
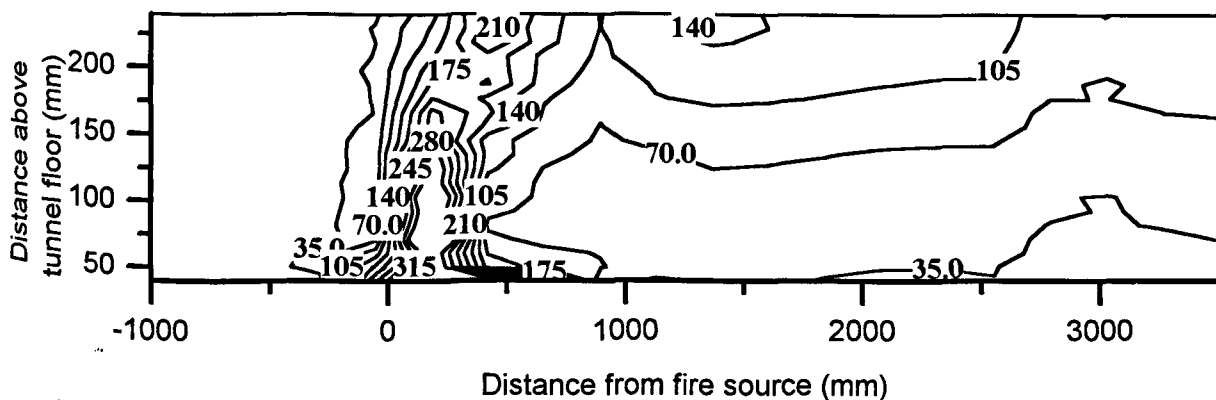
(c) Q = 15.0 kW, Uc = 0.60 m/s
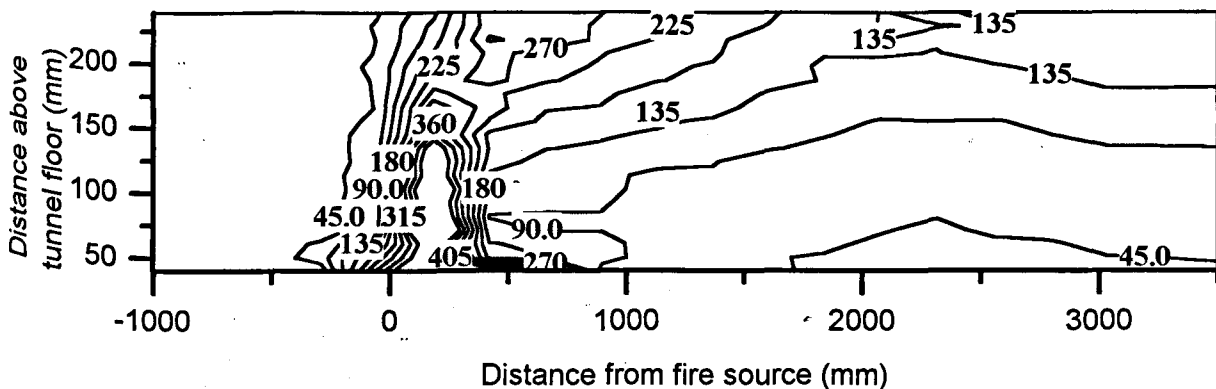
Figure 6.19 : Overall measured temperature contours in tunnel B for 3.0 kW, 7.50 kW and 15.0 kW at critical conditions

102

(a) Q = 3.0 kW, U = 0.25 m/s
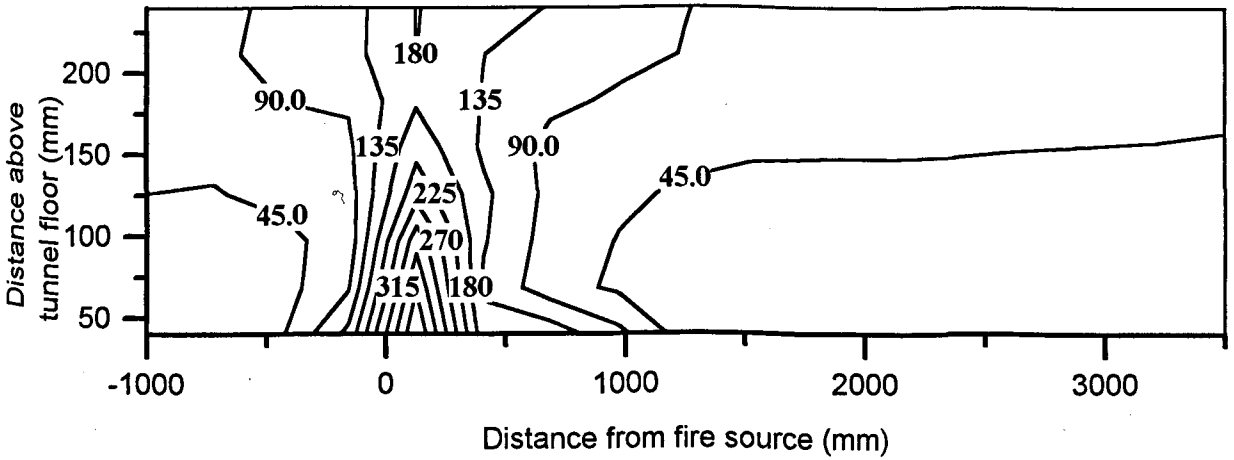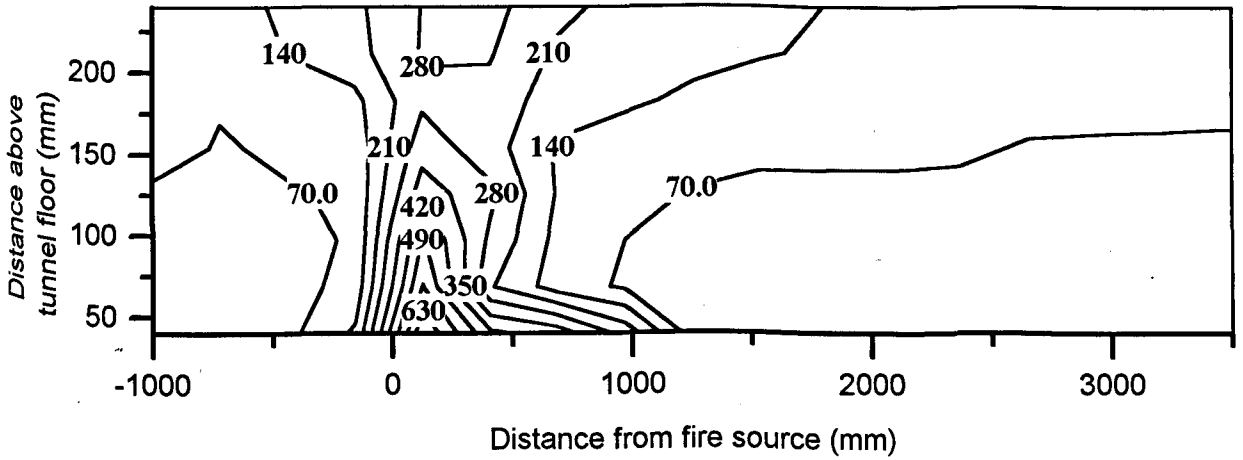
(b) Q = 7.50 kW, U = 0.31 m/s

(c) Q = 15.0 kW, U = 0.34 m/s
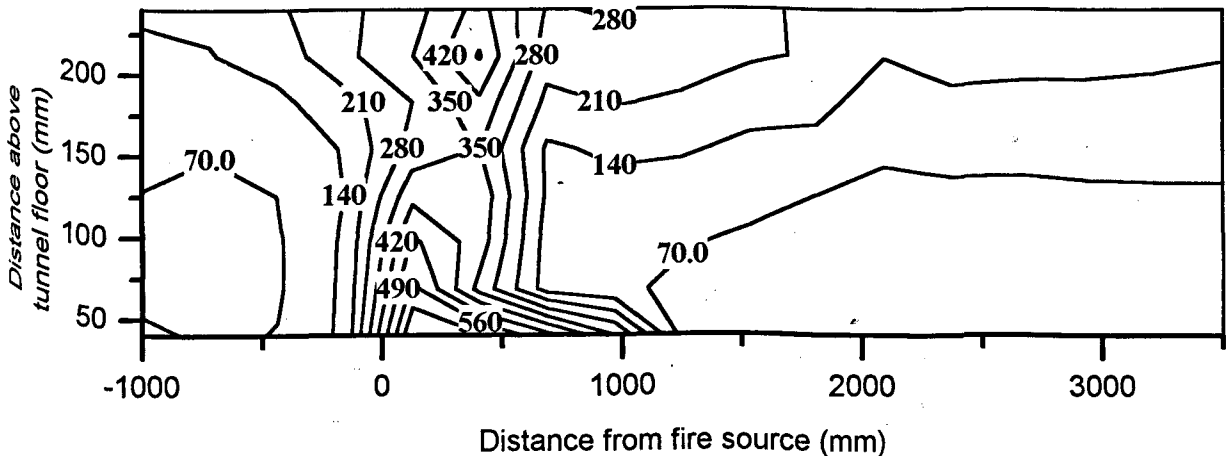
Figure 6.20 : Overall measured temperature contours in tunnel B for 3.0 kW, 7.50 kW and 15.0 kW (backlayering was controlled at 10 tunnel heights upstream)
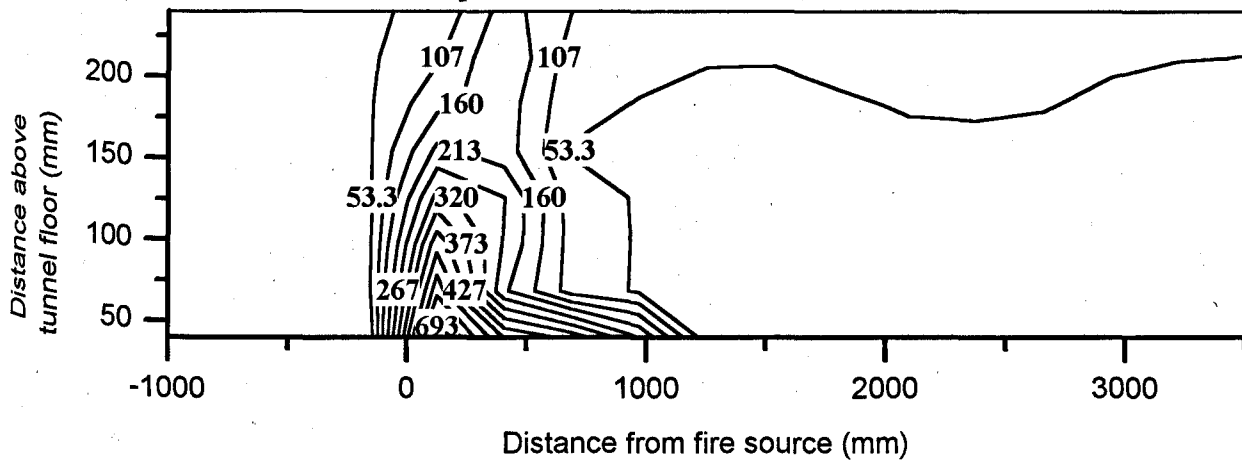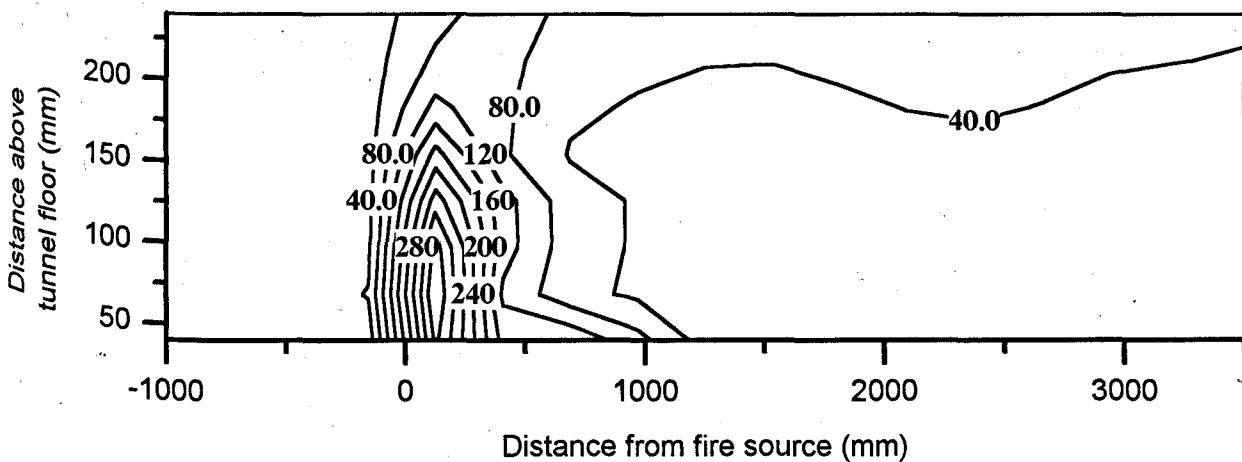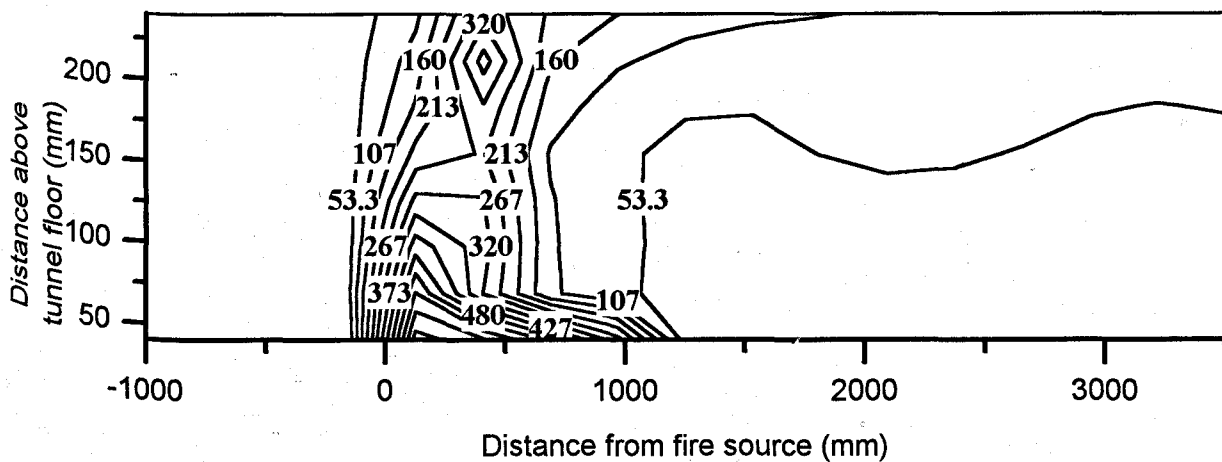
Figure 6.21 : Overall measured temperature contours in tunnel D for 3.0 kW, 7.50 kW and 15.0 kW at critical conditions

(a) Q = 3.0 kW, U = 0.18 m/s
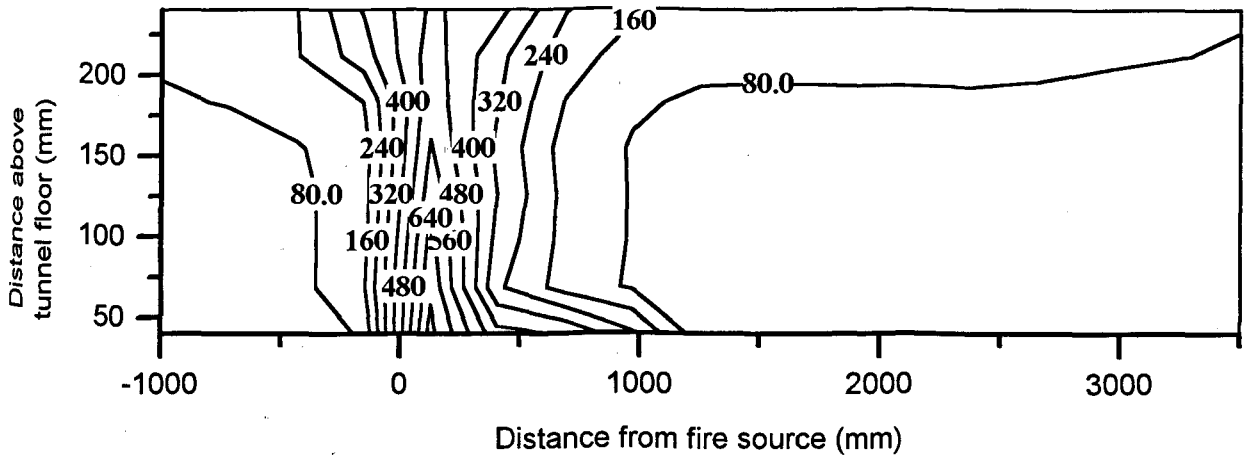
(b) Q = 7.50 kW, U = 0.28 m/s
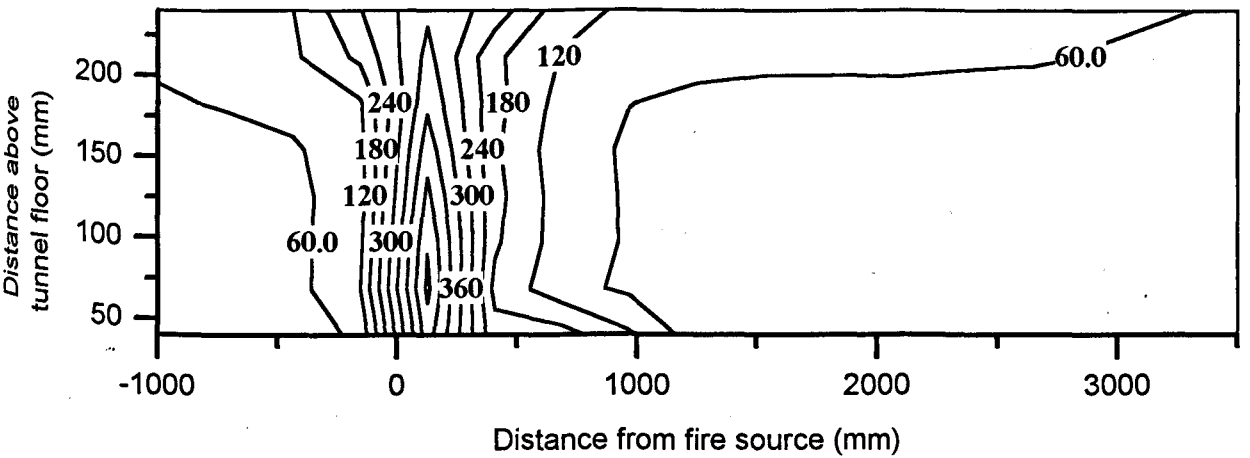
(c) Q = 15.0 kW, U = 0.33 m/s
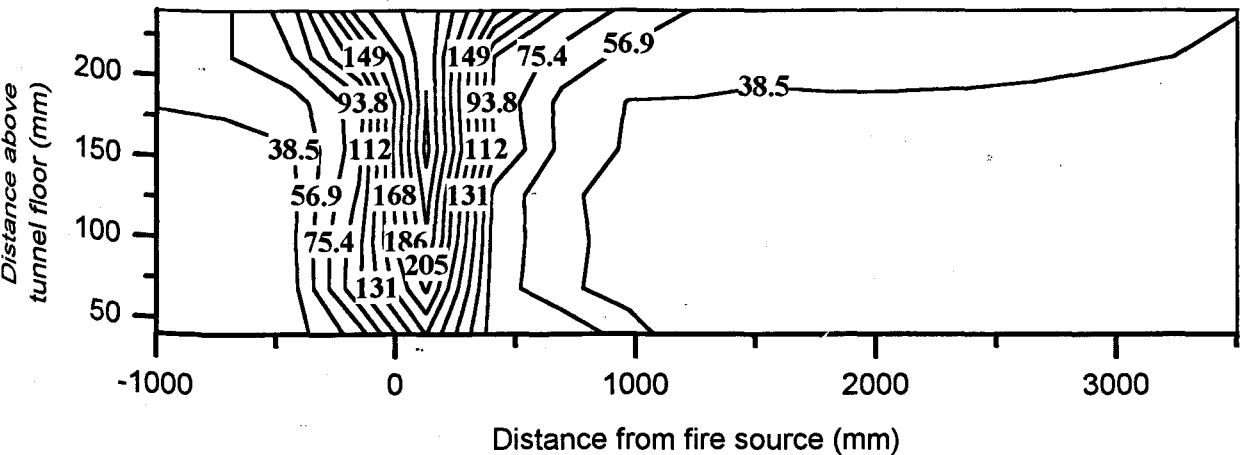
Figure 6.22 : Overall measured temperature contours in tunnel D for 3.0 kW, 7.50 kW and 15.0 kW (backlayering was controlled at 10 tunnel heights upstream)
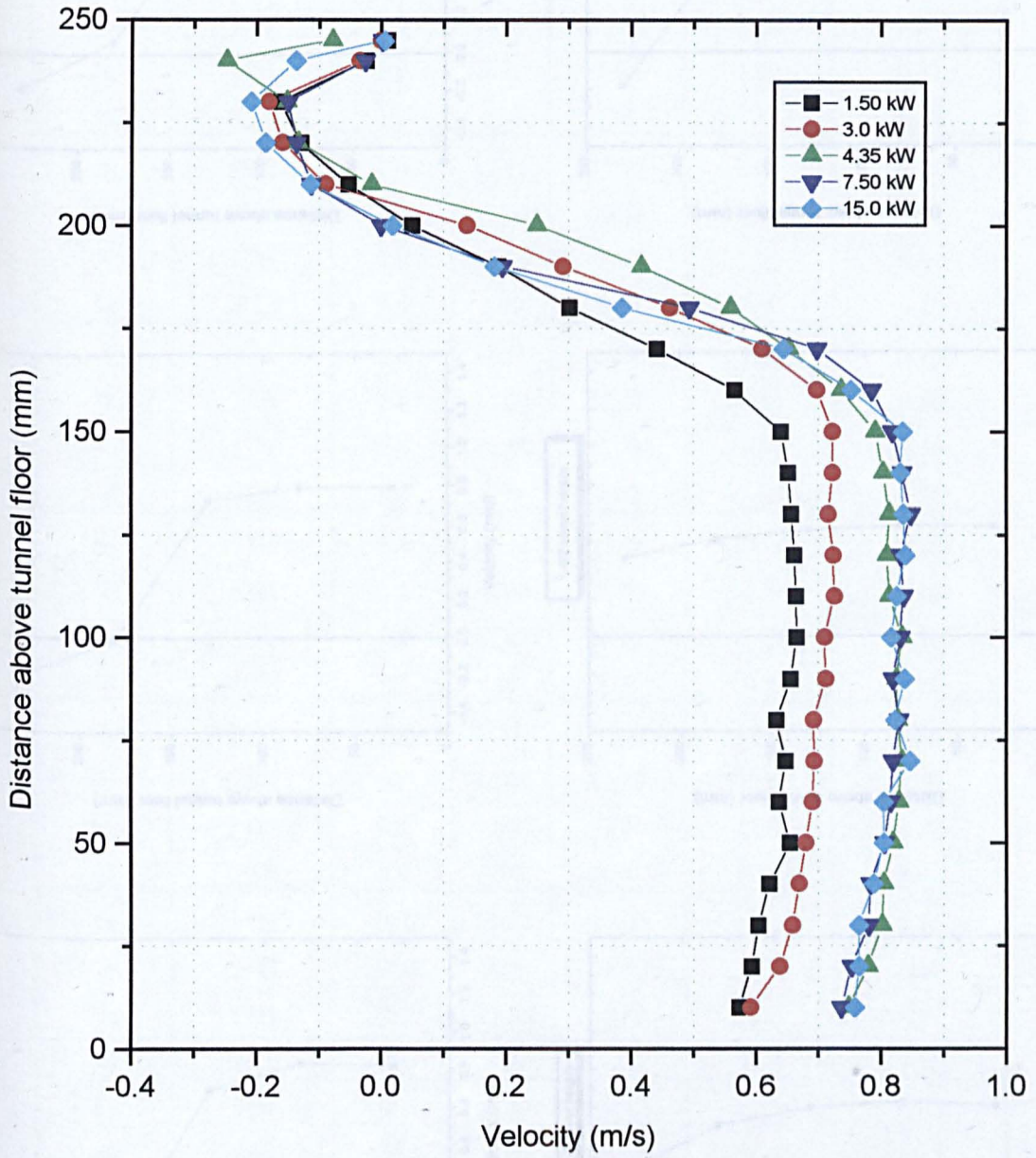
Figure 6.23   : Velocity profiles at 1.25 tunnel height upstream from fire
at various HRRs in tunnel B (Allen et al (1999))
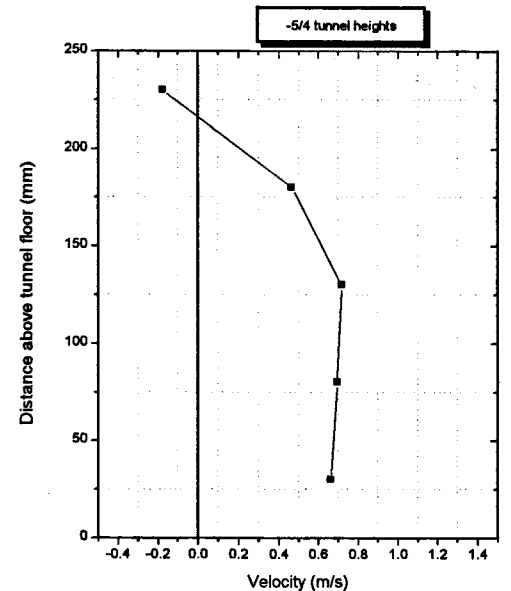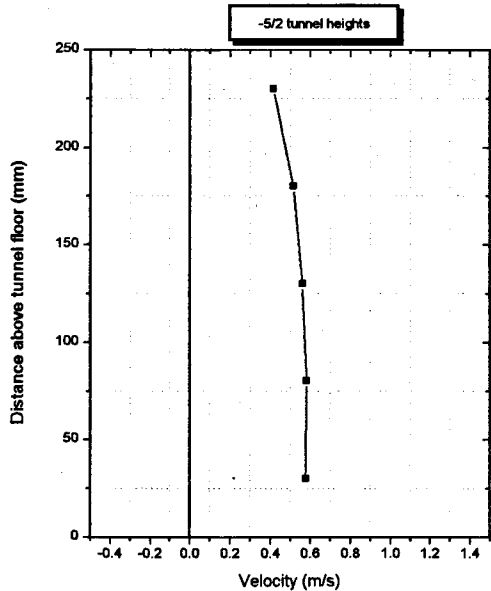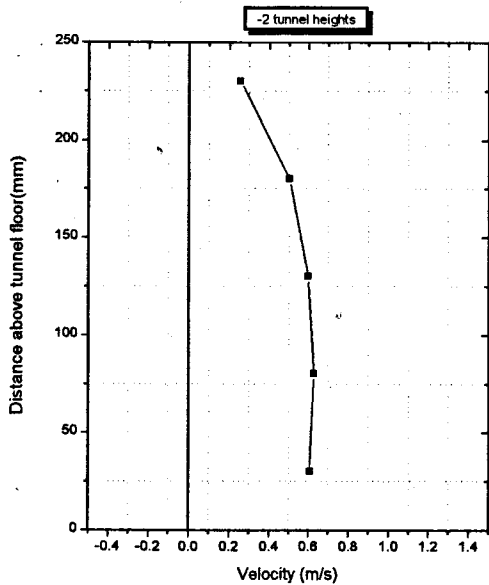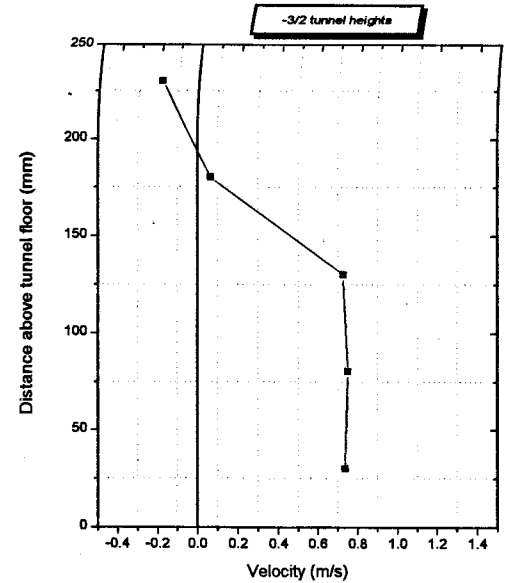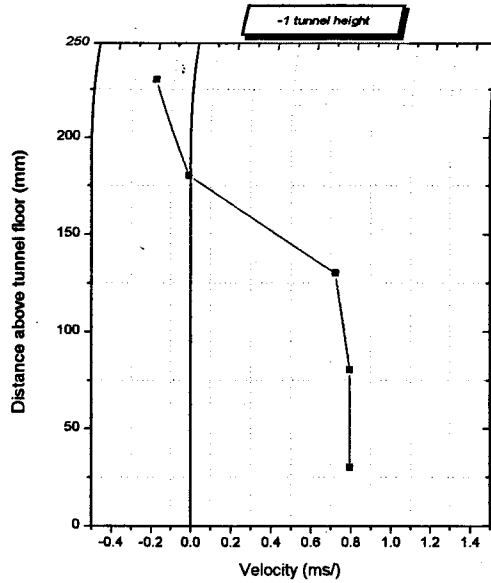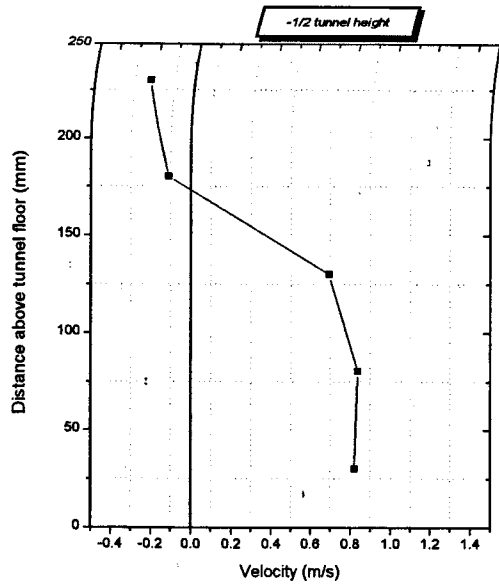
Figure 6.24 : Velocity profiles in the backlayering in tunnel B at various distances from the burner at 3.0 kW fire

Table 6.1: Measured ventilation velocity for 1, 3, 5 and 10 tunnel heights in tunnel A

Test No	Distance backup (TH)	Propane Flowrate (l/min)	True pressure reading (Pa) Upper	Lower	Heat output (kW)	Ventilation velocity (m/s)
2a	1TH	1.0	14.00	13.00	1.50	0.41
2b	3TH	1.0	10.00	10.00	1.50	0.35
2c	5TH	1.0	8.50	7.00	1.50	0.31
2d	10TH	1.0	5.00	5.00	1.50	0.25
3a	1TH	2.0	15.75	15.75	3.00	0.43
3b	3TH	2.0	12.00	10.75	3.00	0.37
3c	5TH	2.0	10.50	9.00	3.00	0.34
3d	10TH	2.0	5.00	5.00	3.00	0.25
4a	1TH	5.0	18.50	16.50	7.50	0.46
4b	3TH	5.0	14.00	12.50	7.50	0.40
4c	5TH	5.0	11.50	9.50	7.50	0.36
4d	10TH	5.0	5.00	5.00	7.50	0.25
5a	1TH	7.0	17.00	17.00	10.50	0.45
5b	3TH	7.0	14.00	13.00	10.50	0.40
5c	5TH	7.0	12.00	10.50	10.50	0.37
5d	10TH	7.0	5.00	5.00	10.50	0.25
6a	1TH	8.0	17.00	17.00	12.0	0.45
6b	3TH	8.0	14.00	13.00	12.0	0.40
6c	5TH	8.0	12.00	10.50	12.0	0.37
6d	10TH	8.0	5.00	5.00	12.0	0.25
7a	1TH	10.0	17.00	17.00	15.0	0.45
7b	3TH	10.0	14.75	12.50	15.0	0.40
7c	5TH	10.0	11.25	10.00	15.0	0.37
7d	10TH	10.0	5.00	5.00	15.0	0.25
8a	1TH	15.0	17.25	16.50	22.50	0.45
8b	3TH	15.0	14.75	12.50	22.50	0.40
8c	5TH	15.0	11.25	10.00	22.50	0.37
8d	10TH	15.0	5.00	5.00	22.50	0.25

Table 6.2: Measured ventilation velocity for 1, 3, 5 and 10 tunnel heights in tunnel B

Test No	Distance backup (TH)	Propane Flowrate (l/min)	True pressure reading (Pa)		Heat output (kW)	Ventilation velocity (m/s)
			Upper	Lower		
10a	1TH	1.0	38.89	37.0	1.50	0.36
10b	3TH	1.0	24.0	23.5	1.50	0.29
10c	5TH	1.0	19.5	18.0	1.50	0.26
10d	10TH	1.0	7.5	7	1.50	0.17
11a	1TH	2.0	63.5	58.0	3.00	0.45
11b	3TH	2.0	45.5	43.5	3.00	0.39
11c	5TH	2.0	36.0	34.8	3.00	0.35
11d	10TH	2.0	17.3	16.5	3.00	0.25
12a	1TH	5.0	84.5	83.0	7.50	0.53
12b	3TH	5.0	66.0	65.0	7.50	0.47
12c	5TH	5.0	49.0	48.0	7.50	0.40
12d	10TH	5.0	28.8	27.8	7.50	0.31
13a	1TH	7.0	93.0	92	10.50	0.56
13b	3TH	7.0	71.0	70.5	10.50	0.49
13c	5TH	7.0	54.0	53.5	10.50	0.43
13d	10TH	7.0	31.0	30.5	10.50	0.33
14a	1TH	8.0	95.0	94.5	12.0	0.56
14b	3TH	8.0	73.0	70.5	12.0	0.49
14c	5TH	8.0	58.5	58.0	12.0	0.44
14d	10TH	8.0	32.0	31.5	12.0	0.33
15a	1TH	10.0	97.0	96.3	15.0	0.57
15b	3TH	10.0	76.5	75.5	15.0	0.51
15c	5TH	10.0	59.5	58.8	15.0	0.44
15d	10TH	10.0	34.5	34.5	15.0	0.34
16a	1TH	15.0	97.0	96.3	15.0	0.57
16b	3TH	15.0	76.5	75.5	15.0	0.51
16c	5TH	15.0	59.5	58.8	15.0	0.44
16d	10TH	15.0	34.5	34.5	15.0	0.34

Table 6.3: Measured ventilation velocity for 1, 3, 5 and 10 tunnel heights in tunnel C

Test No	Distance backup (TH)	Propane Flowrate (l/min)	True pressure reading (Pa)		Heat output (kW)	Ventilation velocity (m/s)
			Upper	Lower		
18a	1TH	1.0	140.0	136.0	1.50	0.34
18b	3TH	1.0	97.0	94.0	1.50	0.28
18c	5TH	1.0	75.0	72.0	1.50	0.25
18d	10TH	1.0	37.0	34.0	1.50	0.18
19a	1TH	2.0	212.0	208.0	3.00	0.42
19b	3TH	2.0	150.0	147.0	3.00	0.35
19c	5TH	2.0	114.0	110.0	3.00	0.31
19d	10TH	2.0	53.0	51.0	3.00	0.21
20a	1TH	5.0	315.0	313.0	7.50	0.51
20b	3TH	5.0	249.0	246.0	7.50	0.45
20c	5TH	5.0	193.0	191.0	7.50	0.40
20d	10TH	5.0	98.0	96.0	7.50	0.29
21a	1TH	7.0	360.0	353.0	10.50	0.54
21a	3TH	7.0	278.0	278.0	10.50	0.47
21c	5TH	7.0	219.0	215.0	10.50	0.42
21d	10TH	7.0	120.0	118.0	10.50	0.32
22a	1TH	8.0	379.0	379.0	12.0	0.56
22b	3TH	8.0	296.0	294.0	12.0	0.50
22c	5TH	8.0	235.0	230.0	12.0	0.43
22d	10TH	8.0	130.0	128.0	12.0	0.33
23a	1TH	10.0	399.0	396.0	15.00	0.57
23b	3TH	10.0	310.0	304.0	15.00	0.50
23c	5TH	10.0	242.0	239.0	15.00	0.44
23d	10TH	10.0	142.0	139.0	15.00	0.34
24a	1TH	15.0	438.0	424.0	22.50	0.59
24b	3TH	15.0	354.0	348.0	22.50	0.53
24c	5TH	15.0	280.0	278.0	22.50	0.48
24d	10TH	15.0	176.0	170.0	22.50	0.38
25a	1TH	20.0	467.0	460.0	30.0	0.61
25b	3TH	20.0	373.0	366.0	30.0	0.55
25c	5TH	20.0	300.0	293.0	30.0	0.49
25d	10TH	20.0	180.0	180.0	30.0	0.39

Table 6.4 : Measured ventilation velocity for 1, 3, 5 and 10 tunnel heights in tunnel D

Test No	Distance backup (TH)	Propane Flowrate (l/min)	True pressure reading (Pa)		Heat output (kW)	Ventilation velocity (m/s)
			Upper	Lower		
27a	1TH	1.0	480.0	460.0	1.50	0.31
27b	3TH	1.0	335.0	310.0	1.50	0.26
27c	5TH	1.0	304.0	290.0	1.50	0.24
27d	10TH	1.0	139.0	133.0	1.50	0.16
28a	1TH	2.0	700.0	665.0	3.00	0.37
28b	3TH	2.0	490.0	455.0	3.00	0.31
28c	5TH	2.0	380.0	-	3.00	0.28
28d	10TH	2.0	170.0	145.0	3.00	0.18
29a	1TH	5.0	1090.0	1050.0	7.50	0.46
29b	3TH	5.0	850.0	805.0	7.50	0.41
29c	5TH	5.0	610.0	575.0	7.50	0.35
29d	10TH	5.0	390.0	360.0	7.50	0.28
30a	1TH	7.0	1280.0	1240.0	10.50	0.59
30b	3TH	7.0	965.0	920.0	10.50	0.43
30c	5TH	7.0	770.0	750.0	10.50	0.39
30d	10TH	7.0	420.0	420.0	10.50	0.29
31a	1TH	8.0	1360.0	1300.0	12.0	0.52
31b	3TH	8.0	1060.0	1020.0	12.0	0.45
31c	5TH	8.0	810.0	770.0	12.0	0.40
31d	10TH	8.0	450.0	450.0	12.0	0.30
33a	1TH	10.0	1565.0	1500.0	15.00	0.55
33b	3TH	10.0	1160.0	1110.0	15.00	0.48
33c	5TH	10.0	910.0	870.0	15.00	0.42
33d	10TH	10.0	560.0	560.0	15.00	0.33
34a	1TH	15.0	1900.0	1870.0	22.50	0.63
34b	3TH	15.0	1270.0	1245.0	22.50	0.50
34c	5TH	15.0	1070.0	1020.0	22.50	0.46
34d	10TH	15.0	635.0	600.0	22.50	0.35

Table 6.5: Critical Ventilation Velocity data for each tunnel

Test No	Tunnel	Propane flowrate (l/min)	Heat output (kW)	Critical ventilation velocity (m/s)
2	A	1.0	1.50	0.43
3	A	2.0	3.0	0.46
4	A	5.0	7.50	0.48
5	A	7.0	10.50	0.48
6	A	8.0	12.0	0.48
7	A	10.0	15.0	0.48
8	A	15.0	22.50	0.48
10	B	1.0	1.50	0.39
11	B	2.0	3.0	0.48
12	B	5.0	7.50	0.56
13	B	7.0	10.50	0.59
14	B	8.0	12.0	0.60
15	B	10.0	15.0	0.60
16	B	15.0	22.50	0.60
18	C	1.0	1.50	0.37
19	C	2.0	3.0	0.45
20	C	5.0	7.50	0.54
21	C	7.0	10.50	0.57
22	C	8.0	12.0	0.59
23	C	10.0	15.0	0.60
24	C	15.0	22.50	0.62
25	C	20.0	30.00	0.65

Table 6.5a: Critical Ventilation Velocity data for each tunnel

Test No	Tunnel width (mm)	Propane flowrate (l/min)	Heat output (kW)	Critical ventilation velocity (m/s)
27	D	1.0	1.50	0.34
28	D	2.0	3.0	0.40
29	D	5.0	7.50	0.50
30	D	7.0	10.50	0.54
31	D	8.0	12.0	0.56
32	D	10.0	15.0	0.59
33	D	15.0	22.50	0.65
35	E	1.0	1.50	0.44
36	E	2.0	3.0	0.54
37	E	5.0	7.50	0.60
38	E	10.0	15.0	0.60
39	E	15.0	22.50	0.60

Table 6.6: Temperature data in the fire region in tunnel B (Q = 3.0 kW, Uc = 0.48 m/s)

x	(40, 0)	(70, 0)	(100, 0)	(130, 0)	(160, 0)	(190, 0)	(220, 0)	(240, 0)
0	233.44	167.23	175.23	144.95	98.44	62.76	48.33	44.55
25	326.40	101.55	88.96	74.67	60.10	46.58	39.96	33.83
55	470.29	164.08	92.84	73.41	59.51	48.42	41.07	33.66
75	530.07	270.77	126.41	84.39	66.15	53.16	44.01	36.17
100	586.36	430.39	222.13	113.65	75.86	58.94	48.01	39.77
125	500.21	468.17	310.42	157.07	85.61	63.47	51.54	42.96
150	341.46	443.65	381.74	235.91	112.43	69.80	55.41	48.05
175	219.17	357.77	360.44	264.65	138.52	77.61	60.13	58.30
200	145.69	262.38	303.33	262.70	168.06	96.60	68.35	71.43
225	108.28	193.94	243.53	251.74	196.12	120.26	84.05	91.53
250	87.66	147.44	201.20	231.92	200.97	143.27	109.86	118.81
275	74.82	117.55	162.11	197.43	193.41	150.46	124.92	129.91
300	63.64	96.06	133.02	170.36	180.25	156.88	145.68	145.67
325	54.78	78.80	112.79	146.87	162.00	147.66	148.84	151.04
350	47.81	65.69	89.55	124.68	149.42	145.99	151.06	151.68
375	43.54	55.80	71.95	102.54	131.46	139.95	149.56	151.85
400	39.20	47.83	61.65	86.43	120.48	132.86	147.82	151.45

x	(40, 55)	(70, 55)	(100, 55)	(130, 55)	(160, 55)	(190, 55)	(220, 55)	(240, 55)
0	176.98	49.64	152.61	105.13	66.59	51.86	43.25	43.87
25	149.16	54.73	79.85	64.55	50.61	43.71	37.48	35.38
55	234.71	50.72	76.39	62.87	51.03	45.41	38.31	35.3
75	376.32	46.12	88.09	69.02	55.62	49.1	40.6	36.92
100	369.31	44.19	113.48	79.66	62.41	54.06	44.09	40.51
125	379.23	42.32	167.99	92.26	68.94	58.33	46.86	43.8
150	344.06	40.09	227.14	120.59	74.76	61.28	50.4	49.04
175	284.98	39.43	271.63	161.89	85.4	65.05	54.11	56.75
200	235.03	38.48	257.77	172.73	96.97	72.03	60.97	69.81
225	165.74	36.37	239.96	194.23	123.6	86.21	73.14	88.56
250	123.44	31.93	217.57	188.7	137.69	104.54	95.02	114.27
275	106.76	27.13	200.87	193.27	155.52	121.52	109.57	125.2
300	87.27	28.7	187.46	178.8	152.85	132.18	126.85	139.46
325	79.15	28.29	158.88	159.81	146.56	135.18	135.42	143.86
350	63.86	26.88	136.93	142.39	137.97	133.45	138.1	144.64
375	48.29	27.55	112.47	123.95	135.41	135.43	144.08	148.77
400	44.24	27.01	104.11	114.29	122.91	131.22	141.95	146.81

x	(40, 110)	(70, 110)	(100, 110)	(130, 110)	(160, 110)	(190, 110)	(220, 110)	(240, 110)
0	58.83	62.12	58.58	54.41	46.11	36.69	38.19	33.57
25	49.52	51.73	49.2	46.42	41.02	33.2	33.22	30.81
55	55.48	57.14	53.48	49.44	42.52	33.9	33.77	31
75	64.3	66.01	60.58	54.77	45.75	35.69	35.62	32.04
100	72.75	75.11	68.06	60.52	48.8	37.79	38.12	33.81
125	80.7	84.08	74.21	66.19	52.18	40.24	40.9	35.56
150	83.85	89.49	77.29	70.03	54.83	42.59	44.15	37.12
175	82.06	93.77	81.44	74.83	57.45	44.72	47.1	38.61
200	78.81	87.45	77.77	72.18	56.37	45.39	51.04	44.04
225	71.5	84.68	79.03	75.48	57.5	48.67	62.53	62.12
250	66.19	91.04	87.75	78.02	58.49	55.09	85.74	88.13
275	61.23	90.83	96.04	88.13	67.03	65.26	97.27	100.63
300	57.84	83.93	86.42	83.28	67.47	79.35	112.87	113.78
325	51.95	73.01	84.44	82.61	73.5	91.19	123.5	123.22
350	47.36	65.41	76.73	77.77	75.33	102.65	127.47	125.56
375	41.09	61.46	73.98	81.76	89.11	114.78	131.32	128.72
400	39.34	50.62	66.75	79.32	94.26	118.66	132.84	129.28

114

Table 6.7: Temperature data in the fire region in tunnel B (Q = 3.0 kW, U = 0.25 m/s)

x	(40, 0)	(70, 0)	(100, 0)	(130, 0)	(160, 0)	(190, 0)	(220, 0)	(240, 0)
0	332.12	130.70	91.83	77.03	72.44	84.24	143.30	141.79
25	357.01	158.91	100.68	78.77	71.10	82.64	143.88	142.62
55	470.86	204.67	116.04	89.88	78.69	87.28	145.81	144.97
75	574.93	401.08	260.15	148.72	97.91	95.71	150.90	159.10
100	610.79	455.52	315.90	201.23	120.26	109.27	156.93	163.17
125	448.95	456.73	385.78	280.88	173.48	141.28	172.89	180.88
150	184.60	289.00	318.18	297.39	247.43	206.21	203.40	205.11
175	127.78	207.69	252.80	256.70	234.80	206.72	206.28	205.61
200	104.19	153.79	193.85	219.52	223.15	203.96	202.88	205.10
225	79.56	106.30	140.91	175.71	196.97	194.55	195.54	195.45
250	71.54	90.81	110.96	141.74	174.55	181.58	188.89	191.98
275	61.51	77.35	91.04	114.09	143.33	158.54	177.36	185.44
300	50.72	62.35	72.00	84.75	110.59	128.42	154.18	172.84
325	50.72	62.35	72.00	84.75	110.59	128.42	154.18	172.84
350	48.01	57.96	65.37	77.58	98.37	118.54	147.43	169.10
375	43.59	51.25	59.59	70.72	88.33	109.10	138.60	160.23
400	41.89	49.45	56.02	64.74	82.28	102.15	133.41	153.59

x	(40, 55)	(70, 55)	(100, 55)	(130, 55)	(160, 55)	(190, 55)	(220, 55)	(240, 55)
0	173.86	45.58	79.65	70.68	68.04	82.01	142.79	143.29
25	213.12	48.64	81.88	71.42	67.15	81.35	144.04	145.71
55	331.88	51.21	93.78	77.61	71.55	84.21	144.55	145.06
75	376.21	46.88	145.42	98.81	83.04	91.48	149.39	156.35
100	426.28	45.88	191.84	126.44	95.82	103.67	154.94	159.65
125	397.29	43.67	292.00	189.90	130.86	131.55	168.38	172.52
150	230.84	39.94	285.78	233.57	184.58	177.37	186.76	192.28
175	195.23	38.27	255.93	234.10	209.05	192.50	192.18	193.43
200	147.16	36.39	224.39	213.51	199.19	187.38	184.79	189.47
225	101.72	25.45	197.87	190.49	185.46	181.12	181.75	184.21
250	79.85	24.48	161.79	166.14	177.73	176.55	179.34	184.19
275	62.75	24.66	132.29	136.56	148.15	155.66	168.81	179.79
300	52.80	24.72	97.49	102.57	115.20	126.27	151.18	167.79
325	52.80	24.72	97.49	102.57	115.20	126.27	151.18	167.79
350	49.51	25.94	85.75	93.09	106.51	117.30	144.36	162.90
375	46.49	27.99	74.79	83.61	98.05	109.42	137.55	154.56
400	43.99	28.97	65.72	73.84	88.41	102.75	132.42	147.41

x	(40, 110)	(70, 110)	(100, 110)	(130, 110)	(160, 110)	(190, 110)	(220, 110)	(240, 110)
0	54.72	57.51	56.27	59.45	63.22	90.29	142.13	131.51
25	58.75	61.35	58.90	60.92	63.11	96.85	146.60	133.68
55	67.61	69.75	65.77	66.25	66.97	97.47	144.21	132.84
75	80.87	84.21	78.44	76.54	74.35	111.68	149.10	141.19
100	89.96	93.64	87.02	84.00	81.13	122.35	151.84	138.72
125	97.77	105.29	98.72	97.73	101.37	136.24	159.49	146.04
150	88.11	102.49	107.65	111.99	125.92	151.23	166.89	158.01
175	84.12	113.64	122.90	129.23	138.52	156.66	170.21	160.89
200	79.01	110.58	130.30	138.82	141.30	152.21	163.89	154.97
225	69.51	89.71	104.18	122.70	134.65	148.70	161.66	153.73
250	64.97	89.20	105.58	125.08	137.73	151.97	162.94	158.19
275	58.89	75.63	92.46	116.66	130.30	143.08	160.06	157.71
300	51.55	61.76	75.77	104.00	121.67	136.29	152.21	149.90
325	51.55	61.76	75.77	104.00	121.67	136.29	152.21	149.90
350	49.32	59.31	73.93	100.35	118.96	133.78	146.05	143.62
375	46.14	56.60	72.41	94.42	111.58	127.40	140.89	137.65
400	43.82	53.68	71.57	93.59	110.78	123.60	135.73	131.78

Table 6.8 : Temperature data in the fire region in tunnel B (Q = 7.50 kW, Uc = 0.56 m/s)

x	(40, 0)	(70, 0)	(100, 0)	(130, 0)	(160, 0)	(190, 0)	(220, 0)	(240, 0)
0	252.03	419.98	485.15	489.64	399.58	290.02	189.40	150.11
25	349.98	513.27	563.85	501.44	362.33	240.74	146.12	111.90
55	549.98	593.42	554.56	443.76	265.16	164.41	119.24	96.06
75	192.76	349.71	446.09	467.93	402.30	305.64	222.60	191.87
100	684.41	621.77	530.82	379.93	204.31	133.54	100.79	89.26
125	147.78	261.46	366.03	429.69	416.77	351.73	290.08	254.41
150	132.56	222.68	308.16	385.10	397.06	347.37	300.51	269.69
175	679.26	586.66	482.59	310.12	151.99	108.64	88.05	74.33
200	117.02	174.87	247.48	326.85	358.27	338.32	312.21	287.37
225	107.44	154.34	218.40	304.57	354.60	340.39	329.42	303.70
250	624.06	514.80	371.28	193.70	115.41	92.95	78.39	62.99
275	97.09	135.50	189.45	270.71	321.57	323.70	324.73	306.00
300	598.76	442.91	246.73	135.96	98.44	82.55	71.18	57.85
325	547.42	315.01	157.38	108.81	84.36	72.87	64.72	52.80
350	453.68	161.91	98.47	84.55	67.93	60.65	55.79	45.95
375	361.30	110.65	79.03	70.62	57.45	52.37	48.96	41.14
400	243.42	77.77	58.04	51.37	43.26	39.97	38.92	34.94

x	(40, 55)	(70, 55)	(100, 55)	(130, 55)	(160, 55)	(190, 55)	(220, 55)	(240, 55)
0	315.12	470.14	491.66	406.14	295.43	227.79	142.09	136.99
25	348.30	470.52	465.63	360.30	233.91	174.90	113.15	102.01
55	401.40	485.51	423.20	293.38	167.44	125.06	93.09	89.09
75	274.94	419.28	472.47	407.30	306.20	234.08	164.80	176.78
100	465.46	480.63	372.23	236.22	138.97	111.27	85.52	88.86
125	208.65	360.13	436.05	397.81	325.93	276.32	235.97	242.70
150	187.68	336.42	413.50	407.37	360.25	310.34	259.80	261.69
175	483.46	460.17	315.84	175.22	112.99	97.30	77.66	81.11
200	152.48	287.90	365.26	372.13	349.69	316.13	285.43	280.06
225	130.99	250.04	337.46	357.14	358.59	333.87	306.05	293.81
250	506.24	393.80	214.98	126.23	96.32	85.07	70.50	65.71
275	117.00	223.48	303.00	336.10	351.24	333.47	313.20	292.40
300	443.34	268.21	136.39	101.49	84.27	76.68	66.05	60.74
325	434.77	196.29	109.37	88.59	74.28	69.17	61.06	57.02
350	308.03	110.59	85.85	73.34	62.30	59.75	54.46	51.56
375	147.32	85.92	72.20	62.59	53.64	52.23	48.47	45.75
400	100.04	64.23	53.48	46.60	41.00	39.63	37.56	36.05

x	(40, 110)	(70, 110)	(100, 110)	(130, 110)	(160, 110)	(190, 110)	(220, 110)	(240, 110)
0	134.40	186.60	178.90	165.26	119.22	91.37	101.94	97.19
25	133.82	164.07	151.79	143.28	107.25	82.37	84.60	72.52
55	132.85	162.03	144.64	129.05	97.33	73.59	76.54	68.50
75	130.19	187.64	189.27	177.14	127.20	103.30	128.90	125.28
100	126.22	144.17	127.47	115.98	91.25	70.00	75.14	79.88
125	125.59	180.47	178.70	175.90	135.29	134.35	193.58	176.55
150	120.02	184.04	193.47	190.45	144.36	160.25	218.35	199.07
175	118.02	129.58	115.42	105.26	83.36	63.98	67.93	73.87
200	112.59	177.55	190.94	194.75	164.88	197.10	241.93	217.66
225	108.56	166.25	194.29	208.35	183.80	222.60	261.20	239.85
250	101.90	109.99	99.98	91.20	73.92	56.69	59.00	58.39
275	101.48	162.39	191.77	208.95	205.33	237.58	271.03	253.46
300	85.96	92.37	87.22	80.49	67.69	52.54	54.66	51.29
325	75.31	80.41	77.07	71.46	61.30	48.11	50.67	45.87
350	60.75	65.44	63.67	59.85	52.05	41.89	44.86	39.49
375	51.10	55.14	53.90	50.83	44.51	36.84	39.84	34.97
400	39.70	42.58	40.99	37.91	33.71	28.78	30.82	28.79

Table 6.9: Temperature data in the fire region in tunnel B (Q = 7.50 kW, U = 31 m/s)

x	(40, 0)	(70, 0)	(100, 0)	(130, 0)	(160, 0)	(190, 0)	(220, 0)	(240, 0)
				(y,z)				
0	313.28	131.10	104.98	97.56	89.02	111.84	239.40	238.81
25	362.36	152.55	111.83	102.79	92.89	113.86	239.68	239.13
55	475.10	225.89	134.15	114.56	100.30	118.38	239.55	237.92
75	558.67	375.26	224.50	148.52	114.90	127.55	240.22	241.75
100	649.73	516.71	374.97	227.78	142.40	138.88	239.37	249.34
125	690.32	567.48	478.98	363.05	247.98	212.86	273.93	281.30
150	622.87	611.46	562.56	460.53	322.88	268.98	303.14	303.04
175	482.04	576.60	571.03	516.10	405.80	348.01	350.21	340.36
200	330.79	475.17	521.58	525.64	464.99	413.73	395.26	369.50
225	238.79	413.55	484.01	488.17	455.54	411.76	390.02	365.55
250	163.04	282.06	373.15	423.61	440.28	416.04	396.68	374.13
275	145.45	227.84	315.20	374.88	411.61	400.66	395.66	376.42
300	120.66	161.67	220.54	299.45	360.95	377.13	383.44	368.67
325	111.94	144.46	190.31	259.58	324.98	348.30	362.80	356.94
350	99.92	123.55	155.63	215.40	288.18	324.31	350.96	352.85
375	88.17	104.58	128.19	175.41	241.77	291.36	331.67	338.94
400	80.15	93.09	112.20	143.55	205.00	253.12	309.67	332.44

x	(40, 55)	(70, 55)	(100, 55)	(130, 55)	(160, 55)	(190, 55)	(220, 55)	(240, 55)
				(y,z)				
0	162.43	112.29	94	89.33	86.73	111.15	237.51	246.11
25	177.6	118.09	98.79	93.16	89.93	115.33	236.83	243.17
55	330.91	156.43	110.93	101.13	95.96	119.64	236.13	240.38
75	412.33	255.37	146.41	117.66	107.17	126.9	238.56	242.04
100	448.49	346.14	211.53	143.05	119.52	133.33	242.51	247.23
125	468.44	420.56	301.51	212.91	163.4	173.88	264.49	268.31
150	453.3	491.96	413.99	306.35	219.46	230.25	292.27	289.2
175	419.12	521.13	493.36	404.21	314.9	313.65	333.36	324.06
200	343.34	468.65	482.1	418.35	355.35	356.97	362.21	352.15
225	290.7	429.88	469.64	417.4	353.87	350.1	351.22	343.31
250	231.28	374.25	449.17	435.78	407.61	391.25	375.32	354.99
275	182.43	308.62	402.7	409.57	402.67	387.65	374.98	361.54
300	143.74	245.52	329.69	366.74	395.76	392.19	379.11	360.98
325	129.94	210.42	283.46	318.21	351.37	356.87	359.97	347.97
350	115.09	188.2	250.78	288.38	326.18	334.51	346.28	345.24
375	100.48	151.1	201.02	230.75	264.12	292.34	324.82	337.04
400	89.54	126.36	162.86	190.61	233.96	259.61	309.03	325.47

x	(40, 110)	(70, 110)	(100, 110)	(130, 110)	(160, 110)	(190, 110)	(220, 110)	(240, 110)
				(y,z)				
0	64.43	71.32	73.11	78.34	90.65	126.12	258.24	236.54
25	67.63	74.54	76.55	81.47	94.42	130.9	253.82	229.75
55	76.76	84.12	84.47	88.33	99.17	144	248.57	219.96
75	91.66	99.78	98.15	101.32	107.45	157.35	247.44	216.4
100	106.4	115.72	110.55	111.27	109.65	156.61	246.65	214.67
125	126.29	138.99	130.69	130.56	126.93	188.35	260.75	213.69
150	138.26	158.6	150.73	149.83	150.6	220.53	283.89	210.3
175	148.79	190.7	196.17	194.89	202.83	259.06	301.51	226.59
200	147.24	184.7	197.03	205.86	227.97	281.08	319.27	253.83
225	142.73	189.18	198.85	211.25	234.38	267.35	300.74	250.98
250	133.88	178.96	209.38	243.79	267.91	302.7	327.35	277.74
275	127.95	189.25	230.77	274.93	288.58	312.31	330.09	285.64
300	120.1	171.47	218.86	267.09	282.48	318.08	336.19	301.55
325	110.93	151.94	197.62	245.12	263.78	302.87	322.52	294.88
350	103.62	142.47	183.55	239.53	258.41	293.82	316.42	294.76
375	94.53	124.88	156.28	212.19	239.43	277.58	303.69	286.82
400	85.13	111.41	141.9	193.6	224.37	262.12	293.55	280.88

117

Table 6.10: Temperature data in the fire region in tunnel B (Q = 15.0 kW, Uc = 0.60 m/s)

x	(40, 0)	(70, 0)	(100, 0)	(130, 0)	(160, 0)	(190, 0)	(220, 0)	(240, 0)
				(y,z)				
0	203.56	66.38	53.36	47.00	35.16	32.75	33.36	29.46
25	426.33	111.38	74.60	67.34	49.60	44.75	45.57	36.91
55	487.12	176.37	80.57	64.05	46.81	41.32	40.47	32.58
75	567.48	367.20	156.74	100.31	70.94	60.92	59.42	46.85
100	634.83	470.10	269.44	134.73	89.70	75.81	73.39	58.17
125	626.19	535.48	408.59	204.95	80.67	63.17	59.23	45.83
150	699.35	582.09	480.27	316.43	133.79	94.56	88.13	70.16
175	734.65	642.82	561.42	399.98	185.07	120.14	107.91	90.93
200	746.92	693.68	609.66	490.03	306.98	190.31	137.07	119.78
225	674.25	661.11	602.68	513.73	348.59	217.45	125.16	94.57
250	697.47	696.61	662.25	578.27	460.93	345.44	222.83	182.64
275	597.18	659.44	675.18	614.75	531.69	429.58	328.44	288.45
300	357.89	431.07	503.88	527.82	477.34	400.15	288.67	222.23
325	359.76	473.77	555.33	594.22	562.57	494.31	426.11	365.74
350	265.83	400.53	501.54	560.73	559.65	516.99	468.97	424.54
375	234.21	353.92	477.84	553.44	557.63	519.33	484.54	442.54
400	211.21	327.99	432.19	504.12	529.69	518.42	489.10	463.42

x	(40, 55)	(70, 55)	(100, 55)	(130, 55)	(160, 55)	(190, 55)	(220, 55)	(240, 55)
				(y,z)				
0	90.55	173.99	48.22	41.62	36.07	37.42	32.95	30.81
25	178.19	285.04	69.24	60.75	51.51	52.69	46.36	42.06
55	296.20	161.35	66.29	55.66	47.55	47.09	39.18	35.41
75	462.77	222.10	102.94	85.21	70.98	69.72	58.53	52.39
100	556.62	231.06	147.09	108.02	89.35	85.45	71.21	63.89
125	542.46	142.83	218.48	105.09	74.86	70.89	55.39	48.92
150	574.28	171.44	310.98	166.12	109.02	101.57	82.00	75.80
175	564.15	167.09	404.87	234.32	138.18	123.04	99.01	102.35
200	516.68	154.00	479.82	334.99	186.68	150.21	118.17	126.95
225	427.71	105.37	498.39	382.76	208.16	151.68	96.10	91.25
250	416.99	125.07	576.44	484.73	342.48	268.02	180.30	178.95
275	380.04	121.49	577.04	511.40	407.15	335.35	260.81	266.89
300	239.29	81.15	503.04	460.31	368.24	315.87	215.95	198.67
325	290.15	102.12	571.27	547.48	471.51	430.93	360.85	344.65
350	257.23	105.53	549.89	552.68	513.34	483.81	435.36	407.85
375	243.97	101.02	544.05	557.42	516.40	491.27	456.06	427.43
400	236.82	98.07	513.69	539.97	521.49	493.20	465.54	447.79

x	(40, 110)	(70, 110)	(100, 110)	(130, 110)	(160, 110)	(190, 110)	(220, 110)	(240, 110)
				(y,z)				
0	42.01	41.34	37.98	34.82	31.82	27.14	29.74	25.99
25	61.80	59.69	55.01	50.77	45.36	36.63	41.33	33.82
55	59.68	57.76	51.95	46.32	39.87	31.75	34.54	27.51
75	92.28	87.12	78.75	70.14	59.91	46.69	51.70	41.84
100	117.75	110.32	98.03	86.27	72.69	55.49	61.52	52.66
125	102.82	99.09	83.82	72.62	59.30	46.28	49.68	42.55
150	148.80	141.62	119.15	105.42	86.29	65.53	71.47	64.33
175	175.23	176.46	142.91	128.00	104.78	79.01	87.98	74.92
200	195.56	205.80	173.90	149.48	120.10	90.40	102.64	78.87
225	142.84	187.47	149.33	117.29	87.71	69.47	76.67	67.32
250	198.24	267.08	241.92	203.15	148.06	113.37	139.73	126.54
275	210.22	294.60	277.23	251.88	186.56	149.53	214.84	186.94
300	134.26	219.01	218.11	203.88	143.53	114.66	157.86	142.04
325	189.37	289.56	298.89	291.33	223.16	215.36	285.32	262.38
350	205.36	321.89	342.69	353.19	304.93	299.61	363.25	338.03
375	208.32	308.92	340.00	354.64	320.70	344.56	397.38	360.54
400	197.06	296.68	337.93	371.57	361.10	388.78	420.59	379.86

Table 6.11: Temperature data in the fire region in tunnel B (Q = 15.0 kW, U = 0.34 m/s)

x	(40, 0)	(70, 0)	(100, 0)	(130, 0)	(160, 0)	(190, 0)	(220, 0)	(240, 0)
0	275.19	259.97	266.04	258.37	232.85	271.75	371.72	322.31
25	377.19	167.04	144.73	144.65	144.65	169.32	303.56	296.87
55	526.40	278.44	160.01	143.16	137.46	156.51	300.58	308.94
75	568.46	411.10	242.50	171.42	151.11	165.60	310.50	303.21
100	651.82	510.16	385.32	242.99	172.66	181.76	322.90	291.06
125	696.27	570.76	467.85	318.40	206.69	208.70	345.05	320.17
150	742.34	657.71	568.48	459.61	336.21	327.37	402.47	342.59
175	739.84	712.13	626.40	536.00	417.65	387.04	421.52	393.55
200	710.14	726.33	677.90	581.13	485.62	453.19	468.21	463.97
225	648.34	717.85	711.63	632.01	556.74	522.53	529.62	519.78
250	548.35	657.37	686.88	657.06	582.28	552.40	550.40	533.54
275	410.51	562.17	655.46	663.92	616.85	589.12	582.76	559.35
300	324.24	477.26	582.72	631.34	624.38	604.79	592.37	563.61
325	242.88	356.87	455.76	542.55	599.72	598.23	597.34	577.88
350	162.67	220.30	309.17	418.05	504.71	539.53	547.96	529.34
375	160.94	202.73	268.54	378.39	474.71	525.39	557.93	552.24
400	149.09	177.56	231.50	322.42	438.49	501.49	551.94	549.82

x	(40, 55)	(70, 55)	(100, 55)	(130, 55)	(160, 55)	(190, 55)	(220, 55)	(240, 55)
0	229.44	188.53	258.89	256.01	115.76	279.50	246.01	71.28
25	212.58	227.83	142.53	142.58	158.71	174.42	299.65	238.52
55	357.21	242.07	139.03	133.78	181.38	162.61	304.44	308.69
75	448.40	247.76	170.55	150.50	192.99	171.51	315.47	300.91
100	493.24	233.92	234.01	177.89	195.28	187.83	327.14	272.74
125	557.19	210.99	309.34	219.72	173.80	204.23	338.91	305.91
150	555.88	178.90	416.29	312.43	177.73	295.63	393.50	311.73
175	469.27	143.21	458.03	374.93	123.15	330.68	392.43	358.06
200	425.38	125.64	530.54	455.57	62.06	392.17	435.69	443.49
225	407.63	134.69	570.25	518.84	87.87	484.94	506.65	495.91
250	362.40	135.81	585.42	550.23	105.41	525.54	530.59	508.26
275	308.12	126.96	587.16	588.39	113.78	562.07	555.79	523.84
300	290.41	124.88	583.78	593.80	115.10	580.45	568.99	544.26
325	237.90	111.15	516.80	561.92	117.32	587.00	576.36	560.34
350	198.58	74.66	442.07	502.43	52.38	534.90	526.74	515.55
375	190.81	80.31	399.24	474.80	69.80	537.68	547.75	542.43
400	172.29	78.74	362.07	432.08	77.88	516.19	542.46	539.65

x	(40, 110)	(70, 110)	(100, 110)	(130, 110)	(160, 110)	(190, 110)	(220, 110)	(240, 110)
0	134.81	155.30	177.09	209.41	239.99	272.70	359.83	206.02
25	97.34	103.37	110.63	121.48	128.26	173.78	315.89	214.17
55	107.34	110.50	111.88	116.11	128.14	166.12	313.42	265.07
75	127.95	129.38	127.61	127.17	140.08	176.77	318.07	247.23
100	147.18	149.17	144.43	142.13	152.83	201.11	331.95	193.36
125	164.37	170.35	158.16	152.59	157.36	235.02	350.84	192.76
150	189.82	205.04	191.95	188.14	205.80	341.70	392.34	169.90
175	165.72	193.38	180.26	176.99	189.75	309.62	377.69	173.56
200	184.95	245.93	240.32	242.81	254.73	342.59	411.61	362.07
225	212.42	269.41	289.42	305.38	339.59	421.63	468.05	391.77
250	216.53	282.27	304.41	338.66	376.21	441.46	481.75	391.32
275	215.60	288.56	335.27	391.94	426.44	483.65	501.06	417.77
300	216.62	291.09	346.22	405.32	451.70	498.86	505.62	444.42
325	211.37	287.02	346.46	420.23	464.56	506.37	506.38	480.58
350	175.23	259.09	325.85	397.77	427.15	474.85	487.67	439.14
375	188.94	260.27	323.44	394.12	429.19	482.13	505.59	480.43
400	179.44	245.81	305.21	375.09	415.42	477.68	503.94	477.49

Table 6.12 : Temperature data in the fire region in tunnel D (Q = 3.0 kW, Uc = 0.40 m/s)

x	(40, 0)	(70, 0)	(100, 0)	(130, 0)	(160, 0)	(190, 0)	(220, 0)	(240, 0)
				(y,z)				
0	169.52	78.88	52.17	43.22	38.72	33.84	32.51	32.42
25	337.71	126.56	66.55	52.06	45.23	38.06	35.03	35.19
55	494.40	246.59	107.41	68.12	54.98	44.05	38.80	39.12
75	577.82	408.35	236.93	133.46	84.15	58.35	49.48	50.28
100	580.54	514.23	372.08	208.73	104.21	65.16	51.78	54.10
125	368.97	438.10	400.44	288.62	157.20	84.62	60.50	64.67
150	188.64	339.81	400.13	369.76	260.11	143.05	98.41	108.03
175	140.70	241.67	303.89	301.42	247.68	162.27	116.37	122.99
200	108.20	182.20	251.50	285.38	256.09	187.98	142.30	143.36
225	71.45	111.67	163.18	214.86	232.72	194.73	167.54	159.15
250	57.10	76.07	110.30	155.41	188.62	181.37	165.29	155.47
275	49.43	60.51	81.81	113.40	155.42	160.28	157.17	146.71
300	45.35	47.75	59.85	80.34	117.46	139.63	152.40	139.84
325	43.24	45.37	52.99	68.15	95.34	122.82	138.89	130.54
350	37.45	37.93	42.19	51.36	74.27	101.86	121.23	116.20
375	35.09	35.02	36.13	40.93	55.87	85.38	115.82	109.73
400	33.17	33.09	34.19	36.96	47.05	70.58	102.99	97.89

x	(40, 250)	(70, 250)	(100, 250)	(130, 250)	(160, 250)	(190, 250)	(220, 250)	(240, 250)
				(y,z)				
0	27.99	28.25	26.96	25.63	27.28	27.46	29.51	29.10
25	30.93	31.30	29.62	27.75	29.87	29.95	31.02	30.37
55	33.93	34.42	32.31	29.80	32.28	32.05	32.82	32.17
75	37.37	38.09	35.40	32.30	34.59	35.06	38.09	40.29
100	38.41	39.12	36.50	33.10	35.21	35.15	35.84	35.60
125	39.45	40.38	37.36	34.12	35.61	35.96	36.63	38.55
150	37.18	38.53	35.64	33.11	34.26	35.84	48.54	64.24
175	37.75	39.32	36.15	33.61	34.82	35.93	50.75	66.40
200	37.45	39.36	36.03	33.58	34.65	38.78	69.07	90.02
225	35.92	38.38	34.82	32.92	33.70	40.77	88.77	109.86
250	34.65	37.47	33.65	32.30	33.09	41.66	100.92	120.77
275	32.95	35.75	32.21	31.04	31.98	44.62	107.20	125.27
300	31.57	34.29	30.82	30.04	31.30	52.88	110.61	127.30
325	31.59	34.06	30.87	31.11	32.81	60.43	116.57	134.54
350	29.14	31.42	28.36	28.02	29.89	55.42	106.01	123.42
375	27.84	29.95	27.31	27.00	29.10	60.22	104.79	119.98
400	27.26	28.96	26.52	27.09	29.23	63.62	107.09	119.50

x	(40, 480)	(70, 480)	(100, 480)	(130, 480)	(160, 480)	(190, 480)	(220, 480)	(240, 480)
				(y,z)				
0	26.33	21.70	21.84	22.01	22.20	21.68	21.67	21.63
25	27.21	22.49	22.72	22.96	23.17	22.44	22.40	22.38
55	29.03	24.36	24.56	24.85	25.03	24.07	24.08	24.24
75	29.31	24.46	24.76	25.07	25.25	24.65	26.42	31.66
100	29.56	24.67	24.93	25.28	25.37	24.06	24.87	29.90
125	30.96	26.01	26.32	26.65	26.71	25.37	26.54	30.14
150	30.99	26.13	26.38	26.81	26.88	26.34	30.40	37.89
175	31.19	26.35	26.61	27.02	27.11	25.85	28.18	34.44
200	31.47	26.56	26.81	27.28	27.39	27.23	35.16	44.86
225	31.57	26.69	26.90	27.41	27.45	27.05	36.09	48.74
250	31.66	26.72	26.99	27.51	27.60	29.17	45.43	61.09
275	31.49	26.60	26.83	27.27	27.48	31.56	51.07	69.02
300	31.40	26.52	26.71	27.10	27.59	35.47	61.47	77.44
325	31.29	26.36	26.61	26.88	27.62	38.67	69.92	84.83
350	30.90	25.96	26.11	26.33	27.19	39.64	70.52	84.72
375	30.54	25.65	25.76	25.93	27.93	43.50	74.63	85.17
400	30.28	25.37	25.51	25.64	28.40	44.65	78.04	84.79

Table 6.13: Temperature data in the fire region in tunnel D (Q = 3.0 kW, U = 0.18 m/s)

x	(40, 0)	(70, 0)	(100, 0)	(130, 0)	(160, 0)	(190, 0)	(220, 0)	(240, 0)
0	236.64	147.71	108.28	88.02	68.26	65.59	78.59	140.66
25	480.78	353.29	254.40	177.77	101.10	89.19	109.58	176.77
55	625.71	527.92	436.89	337.56	224.55	181.71	177.73	208.60
75	448.23	466.74	449.28	388.27	300.70	238.68	207.48	221.77
100	256.63	341.49	372.44	352.72	301.67	245.95	220.39	218.62
125	149.36	216.83	263.03	290.97	304.16	267.77	246.77	237.09
150	88.71	115.97	153.99	196.70	248.02	238.27	246.03	243.12
175	69.95	80.46	94.20	120.05	177.86	199.86	235.13	236.27
200	62.81	67.51	75.58	91.31	139.41	179.92	219.71	229.14
225	56.10	58.72	62.26	68.71	99.90	140.30	192.34	216.08
250	51.14	52.39	54.46	56.03	74.94	111.39	167.83	193.83
275	46.31	47.06	48.48	47.73	56.16	84.69	140.78	178.91
300	43.00	43.30	43.90	42.86	47.29	70.35	123.92	166.54
325	40.23	40.68	40.94	40.17	43.89	62.99	113.44	153.14
350	36.76	37.43	37.80	36.84	38.76	54.04	99.95	133.89
375	35.04	35.62	36.11	35.60	37.69	51.43	95.82	127.75
400	34.58	34.94	35.22	34.83	36.21	46.85	86.01	121.14

x	(40, 250)	(70, 250)	(100, 250)	(130, 250)	(160, 250)	(190, 250)	(220, 250)	(240, 250)
0	34.49	34.96	32.64	34.44	38.04	44.30	111.93	125.67
25	38.60	39.04	35.80	37.90	41.61	48.45	117.00	133.30
55	43.30	43.99	39.72	42.07	45.62	52.98	122.44	138.20
75	44.97	46.11	41.21	43.78	47.98	55.49	122.72	139.82
100	44.84	46.28	41.35	44.17	48.08	55.55	122.18	139.67
125	44.35	46.18	41.18	44.11	48.19	54.84	125.86	142.50
150	43.16	45.45	40.28	43.51	47.64	55.49	121.39	138.91
175	41.38	43.82	38.88	42.25	46.41	55.08	122.16	139.18
200	40.29	42.33	37.67	41.19	45.27	53.59	118.28	135.24
225	38.76	41.01	36.48	40.01	44.30	52.03	115.39	133.64
250	37.41	39.30	35.24	38.86	43.23	50.68	105.99	121.20
275	35.85	37.61	33.71	36.93	41.01	47.96	98.51	114.27
300	34.52	36.09	32.50	35.68	39.48	46.18	93.15	109.83
325	33.00	34.47	31.30	34.33	38.14	43.47	91.05	106.64
350	31.81	32.74	29.94	32.50	36.09	41.35	83.56	100.11
375	30.92	31.87	29.43	31.76	35.03	40.45	80.56	93.25
400	30.53	31.25	28.94	31.35	34.42	39.12	77.06	90.79

x	(40, 480)	(70, 480)	(100, 480)	(130, 480)	(160, 480)	(190, 480)	(220, 480)	(240, 480)
0	28.81	23.83	24.42	26.04	28.73	58.77	88.80	90.37
25	30.24	25.21	25.88	27.67	30.30	61.39	91.29	93.10
55	32.01	26.92	27.61	29.81	33.19	70.36	92.36	91.78
75	32.89	27.77	28.75	31.13	35.62	78.22	95.07	93.49
100	33.41	28.30	29.24	31.87	36.69	80.19	97.41	96.22
125	34.77	29.52	30.62	33.45	38.59	82.33	99.79	99.64
150	34.21	28.91	29.97	32.74	38.30	79.04	96.87	98.58
175	34.02	28.78	29.66	32.24	38.11	77.67	94.59	94.82
200	33.79	28.65	29.48	31.90	37.77	75.43	92.87	94.11
225	33.83	28.59	29.28	31.77	37.74	76.00	93.52	94.19
250	33.79	28.58	29.37	31.78	37.69	76.90	90.37	90.91
275	33.77	28.59	29.03	31.22	38.96	74.49	87.59	87.79
300	33.61	28.42	28.81	30.98	37.41	73.56	88.94	88.51
325	32.78	27.77	27.88	29.49	35.27	72.15	85.65	85.74
350	32.42	27.30	27.54	29.16	36.24	71.30	83.77	82.85
375	32.22	27.21	27.39	28.85	36.19	68.85	79.89	78.62
400	31.73	26.65	27.10	28.63	36.09	68.00	78.34	77.33

Table 6.14 : Temperature data in the fire region in tunnel D (Q = 7.50 kW, Uc = 0.50 m/s)

x	(40, 0)	(70, 0)	(100, 0)	(130, 0)	(160, 0)	(190, 0)	(220, 0)	(240, 0)
0	129.81	103.99	96.39	102.44	109.77	102.06	99.54	104.44
25	226.79	89.67	68.37	61.48	61.02	55.62	53.44	52.87
55	480.51	214.12	92.05	71.76	63.09	55.42	51.17	46.39
75	558.11	339.33	171.88	98.90	76.99	65.04	58.31	51.90
100	686.51	508.34	355.35	194.28	107.73	82.64	69.27	62.29
125	729.01	565.35	429.15	265.03	137.37	92.44	75.64	66.80
150	681.21	616.77	529.46	402.13	226.91	129.42	95.12	92.73
175	557.76	626.30	565.55	459.53	327.22	200.12	132.42	128.13
200	359.43	492.29	532.31	490.29	395.75	271.24	193.94	184.09
225	211.80	352.18	451.18	483.77	440.84	355.86	287.01	260.39
250	142.48	250.94	345.59	404.25	418.49	365.08	312.54	283.20
275	116.14	193.07	264.43	328.28	389.85	377.23	343.64	309.04
300	88.69	122.38	171.76	236.16	313.38	335.44	338.48	316.96
325	83.39	103.37	135.08	182.23	264.03	301.01	317.55	303.39
350	72.50	85.17	107.18	145.55	217.44	266.53	285.23	275.50
375	69.55	78.19	90.37	113.68	170.11	233.51	269.28	263.71
400	62.89	70.69	82.08	102.62	145.58	204.61	247.35	251.32

x	(40, 250)	(70, 250)	(100, 250)	(130, 250)	(160, 250)	(190, 250)	(220, 250)	(240, 250)
0	36.51	37.43	35.21	36.14	37.45	39.13	74.87	81.55
25	36.62	37.52	35.81	36.68	38.05	39.44	49.87	50.88
55	41.10	41.96	39.61	40.54	41.73	43.03	47.13	45.92
75	46.06	46.66	43.59	44.33	45.14	46.51	49.13	47.24
100	50.20	50.94	47.43	47.63	47.48	48.49	51.62	50.22
125	53.34	54.35	50.08	50.13	49.69	50.53	53.59	52.29
150	56.40	57.73	53.05	52.94	52.05	52.57	56.52	57.28
175	59.12	60.88	55.93	55.53	54.00	54.24	64.95	72.73
200	60.55	63.80	57.93	57.86	56.06	56.46	85.98	104.04
225	59.27	63.53	57.13	57.58	55.65	55.35	92.70	121.83
250	58.98	64.31	57.22	58.17	56.29	56.46	133.50	163.59
275	57.34	64.27	56.22	57.80	55.99	56.85	166.40	193.47
300	54.29	61.75	53.29	55.68	54.80	61.71	199.34	225.79
325	53.24	60.93	52.19	55.27	54.99	74.45	218.21	242.40
350	49.77	57.44	48.75	52.01	52.40	74.82	217.97	235.70
375	47.95	55.49	46.92	50.83	52.54	91.81	224.04	238.52
400	45.77	52.44	44.31	48.12	51.26	96.85	220.43	232.46

x	(40, 480)	(70, 480)	(100, 480)	(130, 480)	(160, 480)	(190, 480)	(220, 480)	(240, 480)
0	32.57	27.43	28.20	28.72	28.96	28.41	34.61	41.67
25	32.01	27.05	27.87	28.63	29.10	27.91	30.22	32.77
55	32.90	27.97	28.76	29.59	30.02	28.60	30.01	31.31
75	34.16	29.10	29.88	30.73	31.14	29.51	30.72	32.27
100	35.63	30.29	31.11	32.01	32.29	30.52	35.20	43.56
125	36.57	31.20	31.92	32.71	32.87	30.81	33.02	37.14
150	37.80	32.34	33.06	33.87	34.04	31.92	36.36	45.28
175	38.91	33.41	34.07	35.01	35.05	33.23	42.78	56.51
200	40.08	34.58	35.33	36.23	36.28	33.98	44.94	61.42
225	40.41	34.84	35.61	36.63	36.52	34.11	43.91	60.74
250	41.54	35.89	36.63	37.70	37.28	36.17	48.64	68.68
275	42.00	36.48	37.00	38.12	37.55	36.10	51.52	77.40
300	42.36	36.63	37.23	38.17	37.97	39.96	72.20	100.85
325	42.56	36.89	37.55	38.23	38.37	49.26	97.76	124.59
350	42.15	36.61	37.11	37.85	38.21	51.75	103.43	134.09
375	41.88	36.41	36.96	37.40	38.22	59.88	119.67	145.97
400	41.17	35.74	36.27	36.54	38.21	64.05	127.85	151.32

Table 6.15: Temperature data in the fire region in tunnel D (Q = 7.50 kW, U = 0.28 m/s)

x	(40, 0)	(70, 0)	(100, 0)	(130, 0)	(160, 0)	(190, 0)	(220, 0)	(240, 0)
				(y,z)				
0	229.84	97.99	68.53	60.93	56.68	59.52	95.92	120.83
25	475.47	199.19	107.27	83.73	73.56	75.00	106.73	144.18
55	605.69	403.13	246.32	154.82	106.22	97.73	118.42	162.14
75	724.70	577.18	456.65	338.86	212.13	171.13	174.91	225.94
100	663.29	631.27	556.40	481.30	382.40	319.12	285.83	304.42
125	510.04	597.26	580.98	530.44	450.47	389.35	353.95	350.15
150	369.58	482.71	513.29	506.54	468.70	420.00	381.16	365.45
175	179.18	291.19	371.08	436.56	458.58	430.11	404.79	374.36
200	143.88	209.13	281.75	355.75	403.48	408.24	418.57	391.09
225	113.89	155.77	202.25	278.30	353.82	389.69	410.24	400.50
250	105.09	128.16	152.06	192.87	272.70	337.10	388.39	377.23
275	96.45	109.70	123.34	141.15	198.04	287.69	366.62	372.59
300	86.95	96.20	105.36	112.94	152.17	218.47	309.42	336.65
325	74.98	81.73	86.99	89.18	112.39	169.57	252.60	276.53
350	70.51	75.59	79.61	80.44	95.12	144.00	235.98	266.88
375	63.96	68.41	71.10	70.34	78.59	119.14	204.10	247.04
400	59.15	62.81	65.06	63.98	70.02	102.54	178.69	222.03

x	(40, 250)	(70, 250)	(100, 250)	(130, 250)	(160, 250)	(190, 250)	(220, 250)	(240, 250)
				(y,z)				
0	38.49	38.84	36.26	38.42	43.86	54.27	136.84	156.68
25	44.72	45.85	42.04	45.23	52.87	64.97	165.93	183.49
55	50.37	52.11	47.18	50.83	59.22	72.20	174.39	186.44
75	56.16	58.40	52.52	56.63	65.08	77.97	185.57	201.01
100	63.30	66.40	59.24	64.14	72.51	86.70	213.26	228.39
125	66.39	69.88	62.25	67.52	76.05	92.88	221.87	234.63
150	68.36	72.77	64.05	70.16	79.29	96.33	222.73	244.76
175	70.48	75.73	66.50	74.71	84.83	107.23	229.50	249.36
200	70.23	76.08	66.01	74.66	84.79	109.85	231.13	252.95
225	67.83	74.65	63.92	73.09	82.83	103.37	218.38	246.99
250	66.10	72.90	62.76	72.56	83.12	108.85	223.89	245.43
275	64.79	72.22	61.41	71.30	81.77	106.82	216.78	245.21
300	61.17	67.75	57.51	67.39	78.28	103.15	205.42	231.74
325	56.77	62.41	53.60	62.79	73.65	98.05	182.36	204.73
350	54.54	59.52	51.03	59.38	69.88	94.61	174.96	193.51
375	50.53	55.42	47.18	55.24	65.06	86.40	163.94	190.41
400	48.22	52.50	44.94	52.78	62.11	81.13	150.32	175.69

x	(40, 480)	(70, 480)	(100, 480)	(130, 480)	(160, 480)	(190, 480)	(220, 480)	(240, 480)
				(y,z)				
0	32.06	26.92	27.80	30.38	34.55	63.88	119.52	124.46
25	34.43	29.09	30.32	33.95	39.88	77.31	137.92	141.09
55	36.46	31.04	32.34	36.56	43.08	81.90	139.30	145.36
75	38.63	32.97	34.20	38.89	45.61	86.90	141.67	144.92
100	41.36	35.64	36.99	42.02	49.52	105.99	147.92	145.54
125	42.95	37.16	38.64	43.53	52.03	113.61	147.24	144.82
150	44.37	38.47	39.86	44.81	54.28	118.19	151.86	149.70
175	47.50	41.08	42.58	48.51	58.86	125.04	157.04	159.74
200	48.54	41.99	43.51	49.21	59.42	126.57	160.43	164.23
225	49.00	42.31	43.89	49.64	60.00	124.10	156.64	161.55
250	49.63	42.85	44.48	50.08	61.69	127.26	160.25	162.77
275	50.19	43.53	44.97	50.92	63.40	129.84	162.45	164.38
300	50.35	43.37	44.47	50.08	62.16	130.67	161.35	164.28
325	49.69	42.87	44.00	49.33	63.37	128.21	152.93	153.62
350	47.98	41.35	42.10	46.68	60.10	126.94	150.04	149.59
375	46.82	40.29	41.14	45.63	61.56	124.38	147.82	148.72
400	45.77	39.53	40.47	44.65	60.18	119.26	141.70	143.49

Table 6.16 : Temperature data in the fire region in tunnel D (Q =15.0 kW, Uc = 0.59 m/s)

x	(40, 0)	(70, 0)	(100, 0)	(130, 0)	(160, 0)	(190, 0)	(220, 0)	(240, 0)
				(y,z)				
0	135.81	72.72	56.44	50.23	48.02	44.34	42.24	38.41
25	291.05	107.17	72.91	63.30	59.84	53.98	50.96	45.96
55	507.41	220.00	112.88	85.04	76.67	67.19	62.26	56.14
75	577.16	347.60	176.52	113.08	95.42	81.08	74.85	67.78
100	663.11	470.06	283.89	161.79	119.09	96.76	88.59	80.92
125	718.28	570.81	422.73	272.69	160.98	120.29	104.01	94.92
150	742.50	663.62	511.45	372.44	230.01	153.08	124.34	115.57
175	768.66	726.71	570.53	447.32	317.56	229.16	177.56	157.88
200	755.43	737.11	602.62	488.11	352.29	247.02	190.89	180.33
225	740.14	750.87	704.17	573.24	459.22	359.48	266.28	252.55
250	632.98	690.66	707.34	640.98	538.21	453.54	380.10	345.73
275	476.71	603.88	658.66	645.79	573.59	489.29	427.84	401.03
300	247.09	390.62	509.19	604.07	600.33	546.59	502.80	469.96
325	198.88	318.03	421.08	528.38	564.24	544.90	514.32	488.61
350	152.53	220.00	293.52	388.11	482.20	512.21	504.77	485.24
375	125.17	165.75	228.69	300.31	413.05	472.29	492.15	484.48
400	117.77	146.82	199.77	272.93	388.16	446.47	472.74	467.83

x	(40, 250)	(70, 250)	(100, 250)	(130, 250)	(160, 250)	(190, 250)	(220, 250)	(240, 250)
				(y,z)				
0	39.50	39.18	38.25	39.00	41.32	44.35	46.22	43.02
25	46.12	46.35	44.76	45.76	48.29	51.78	54.94	50.99
55	53.55	53.55	51.31	52.65	55.24	59.28	63.20	58.80
75	60.72	60.47	57.67	58.95	61.52	66.10	69.97	65.51
100	67.82	67.50	63.64	64.39	66.33	71.13	76.20	71.58
125	73.24	72.50	67.99	68.71	69.91	74.52	80.23	76.22
150	81.20	79.29	74.88	74.00	74.42	79.19	87.26	85.40
175	85.69	85.08	78.99	78.76	78.98	83.88	92.67	94.62
200	89.97	88.94	82.29	81.46	80.72	84.85	95.24	98.55
225	94.26	94.24	86.53	85.58	84.43	88.68	106.85	116.66
250	97.32	100.98	91.58	91.08	89.82	94.50	146.62	175.40
275	98.92	103.84	93.97	93.93	93.33	99.15	182.09	216.33
300	97.69	106.93	95.31	97.79	98.46	115.73	282.11	309.56
325	92.64	103.20	89.96	93.64	93.89	107.39	269.92	304.36
350	90.21	102.66	88.06	93.60	95.76	129.31	338.62	358.04
375	86.55	99.98	85.50	94.42	98.57	159.06	358.95	377.77
400	83.80	97.80	82.59	91.80	98.64	168.75	352.02	372.67

x	(40, 480)	(70, 480)	(100, 480)	(130, 480)	(160, 480)	(190, 480)	(220, 480)	(240, 480)
				(y,z)				
0	35.87	30.49	32.04	33.08	32.92	32.24	34.18	33.72
25	39.10	33.45	35.50	37.02	37.21	36.02	38.80	39.43
55	41.11	35.34	37.57	39.40	39.73	38.08	41.59	43.22
75	43.01	37.15	39.48	41.37	41.74	40.20	43.74	46.08
100	44.72	38.66	40.99	43.03	43.40	41.69	45.57	51.50
125	45.95	39.67	41.87	43.63	43.96	42.13	46.42	53.95
150	49.06	42.00	44.29	46.42	46.26	44.61	53.20	69.65
175	50.29	43.49	45.64	47.61	47.58	45.76	52.31	71.23
200	51.66	44.82	46.85	48.82	48.49	46.67	52.51	70.82
225	53.92	46.67	48.54	50.53	50.00	48.07	59.94	80.08
250	56.59	49.10	51.05	53.41	52.52	52.44	72.05	102.64
275	58.58	50.78	52.67	55.23	54.53	55.60	80.55	112.56
300	60.76	52.89	54.88	57.19	56.96	70.23	123.40	152.79
325	60.83	53.23	54.95	57.34	56.85	61.77	114.75	149.48
350	61.60	54.05	55.92	58.05	58.01	70.60	137.23	170.41
375	61.74	54.67	56.63	58.08	59.05	88.11	170.43	198.02
400	61.64	54.81	56.61	57.90	59.28	96.24	181.47	209.35

Table 6.17: Temperature data in the fire region in tunnel D (Q = 15.0 kW, U = 0.33 m/s)

x	(40, 0)	(70, 0)	(100, 0)	(130, 0)	(160, 0)	(190, 0)	(220, 0)	(240, 0)
					(y,z)			
0	295.61	116.29	90.69	84.20	93.00	105.92	162.95	202.91
25	427.96	171.72	116.40	101.88	113.74	127.78	185.32	243.31
55	562.89	362.91	212.06	143.47	139.23	146.93	201.15	265.67
75	672.18	525.08	388.82	268.24	201.01	202.07	264.45	323.17
100	707.87	607.18	520.55	415.86	317.26	308.19	347.70	384.97
125	747.53	736.50	697.58	616.45	529.41	499.57	493.58	493.70
150	626.35	658.80	676.54	646.66	594.10	563.28	549.62	533.69
175	469.95	516.55	581.97	614.76	618.74	593.10	568.54	546.62
200	389.89	453.90	523.91	554.51	579.29	567.48	557.18	537.16
225	277.60	335.58	392.41	466.58	545.09	557.22	568.84	554.42
250	179.58	228.57	283.48	355.51	461.43	510.89	549.96	549.91
275	150.37	174.02	204.99	252.87	358.14	452.94	525.05	538.70
300	152.00	170.45	200.60	237.68	337.68	433.52	515.48	527.13
325	133.14	143.36	163.02	183.45	256.52	346.95	453.98	478.35
350	124.54	132.34	147.04	158.90	212.53	298.12	417.65	459.68
375	123.82	128.77	139.03	143.53	186.25	269.83	398.56	434.61
400	111.52	116.31	124.04	125.72	157.94	223.31	346.83	390.68

x	(40, 250)	(70, 250)	(100, 250)	(130, 250)	(160, 250)	(190, 250)	(220, 250)	(240, 250)
					(y,z)			
0	57.12	58.00	54.45	60.05	72.13	93.99	252.26	265.56
25	65.63	67.79	63.66	71.57	86.56	113.44	279.96	289.07
55	72.62	75.25	70.20	79.73	95.94	126.40	294.54	300.34
75	83.12	85.96	79.65	90.43	107.60	141.32	316.17	316.56
100	92.18	95.08	87.88	99.57	116.12	154.69	341.00	347.23
125	105.32	109.73	100.76	115.58	134.07	188.82	406.38	410.71
150	113.07	119.28	108.44	124.89	144.02	204.93	413.87	420.80
175	115.21	122.82	110.65	127.98	147.52	205.19	407.87	417.02
200	117.36	126.88	113.48	131.75	152.37	224.16	420.85	426.84
225	116.04	128.06	112.32	132.09	153.49	222.84	409.89	424.64
250	112.84	125.67	109.51	129.55	151.74	210.85	402.77	430.30
275	111.78	126.98	109.04	131.77	157.99	240.05	426.48	453.35
300	108.02	122.28	104.18	125.63	150.64	227.11	402.12	422.02
325	101.28	117.25	99.23	120.89	147.42	225.10	373.85	411.52
350	96.77	111.26	93.13	114.06	141.19	209.83	353.70	393.89
375	93.86	106.23	87.93	106.36	133.62	196.00	330.68	369.19
400	87.91	98.54	81.90	100.61	126.98	183.39	290.10	332.61

x	(40, 480)	(70, 480)	(100, 480)	(130, 480)	(160, 480)	(190, 480)	(220, 480)	(240, 480)
					(y,z)			
0	45.19	38.51	41.77	47.70	56.18	118.72	203.68	207.85
25	49.55	42.40	46.32	53.85	64.71	142.46	220.94	217.90
55	51.97	44.80	48.93	56.97	68.73	161.96	230.55	219.03
75	54.95	47.58	51.66	60.05	72.55	174.46	238.68	220.58
100	58.47	50.81	54.54	63.16	76.31	190.86	246.99	222.21
125	63.88	55.57	59.58	68.60	83.82	201.68	245.56	229.19
150	67.01	58.34	62.49	71.64	87.44	205.48	238.04	224.42
175	69.13	60.16	63.52	72.49	89.47	199.04	232.86	222.95
200	70.77	61.56	65.06	74.28	91.68	204.21	238.60	228.52
225	72.45	63.01	66.00	74.86	94.08	198.01	240.56	236.05
250	73.02	63.66	66.19	74.97	92.03	195.62	245.98	244.54
275	77.57	67.78	69.81	79.03	99.20	213.69	269.07	270.06
300	76.55	66.82	69.15	77.47	96.76	208.76	258.66	259.23
325	75.96	66.42	68.90	77.63	98.38	209.97	258.85	266.88
350	75.22	65.72	67.24	75.44	95.23	210.99	261.56	262.73
375	74.45	65.04	65.84	73.61	98.48	212.25	250.51	249.52
400	73.24	64.36	65.06	72.87	96.07	206.21	240.13	241.67

Table 6.18 : Temperature data in the upstream region in tunnel A (Q = 3.0 kW, U = 0.25 m/s)

x	(40,0)	(70,0)	(100,0)	(y,z) (130,0)	(160,0)	(190,0)	(220,0)	(240,0)
-100	54.22	52.64	56.77	96.16	171.32	240.07	247.33	250.82
-200	46.50	45.63	50.89	87.16	156.78	214.05	229.64	234.71
-300	40.21	39.39	45.71	79.37	139.54	190.94	212.66	217.49
-400	36.70	36.13	42.94	75.32	125.09	178.21	203.19	206.46
-500	34.52	34.06	40.59	73.46	112.74	162.49	192.83	196.33
-600	30.53	30.26	36.57	69.77	95.60	144.35	180.52	176.86
-700	28.55	27.90	34.67	67.01	91.06	138.98	171.98	175.87
-800	26.77	25.66	31.81	60.93	82.21	135.60	162.72	172.65
-900	25.78	24.57	29.78	56.72	74.26	132.44	155.25	164.13
-1000	24.67	23.70	28.28	53.16	67.05	124.80	145.18	151.59

Table 6.19: Temperature data in the upstream region in tunnel A (Q = 7.50 kW, U = 0.25 m/s)

x	(40,0)	(70,0)	(100,0)	(y,z) (130,0)	(160,0)	(190,0)	(220,0)	(240,0)
-100	111.01	99.30	93.97	108.61	159.34	277.58	335.72	361.33
-200	61.52	62.78	64.09	82.30	128.15	237.13	285.35	313.09
-300	51.33	52.08	55.82	75.58	122.61	217.62	262.85	281.88
-400	44.06	44.86	50.02	75.01	116.06	190.45	241.07	252.79
-500	44.06	44.86	50.02	75.01	116.06	190.45	241.07	252.79
-600	39.10	40.07	45.67	71.34	107.83	170.32	221.65	220.30
-700	35.00	34.71	41.38	68.86	100.58	159.90	201.48	211.16
-800	32.54	30.90	37.02	64.13	91.98	155.16	189.80	201.18
-900	30.83	28.75	34.02	59.58	84.09	152.06	182.16	193.29
-1000	28.92	26.94	32.07	56.87	77.94	144.96	172.46	182.94

Table 6.20: Temperature data in the upstream region in tunnel D (Q =3.0 kW, U = 0.18 m/s)

x	(40, 0)	(70, 0)	(100, 0)	(130, 0)	(160, 0)	(190, 0)	(220, 0)	(240, 0)
-100	117.13	120.92	116.70	104.32	92.38	87.81	181.47	218.98
-200	45.63	45.33	45.77	44.51	45.19	59.76	123.69	129.16
-300	36.85	35.96	36.10	36.44	37.43	55.66	96.15	95.77
-400	33.33	32.55	32.79	33.62	35.42	56.14	78.90	78.16
-500	31.37	30.39	30.69	31.68	34.41	54.96	69.49	67.97
-600	29.02	28.61	28.95	30.48	31.25	52.26	63.11	61.87
-700	24.41	24.57	26.23	27.17	27.65	48.45	55.36	53.04
-800	24.00	24.36	26.06	26.65	28.05	48.32	54.27	52.56
-900	23.64	24.29	25.83	26.30	28.09	46.71	51.76	50.00
-1000	23.32	24.20	25.70	25.91	27.04	43.51	48.70	46.76

x	(40, 250)	(70, 250)	(100, 250)	(130, 250)	(160, 250)	(190, 250)	(220, 250)	(240, 250)
-100	43.10	43.20	45.68	46.52	45.66	67.77	126.88	141.33
-200	37.88	37.05	37.61	39.13	41.34	69.97	106.07	115.86
-300	34.04	32.61	32.84	34.51	36.84	62.83	89.16	95.27
-400	31.70	30.05	30.43	32.04	34.64	60.36	76.79	79.64
-500	29.99	28.16	28.77	30.50	32.79	58.03	66.39	66.98
-600	28.26	26.78	27.24	29.05	31.22	53.53	57.98	58.67
-700	24.12	23.77	24.23	25.21	28.39	47.74	50.03	50.03
-800	23.81	23.68	24.06	24.84	28.06	45.46	48.17	47.96
-900	23.46	23.47	23.90	24.88	28.35	43.84	46.16	45.68
-1000	23.21	23.31	23.73	24.82	28.02	40.98	43.73	43.60

x	(40, 480)	(70, 480)	(100, 480)	(130, 480)	(160, 480)	(190, 480)	(220, 480)	(240, 480)
-100	34.86	30.63	32.56	33.14	35.37	53.43	89.94	99.91
-200	33.02	28.87	31.06	31.60	34.55	54.45	88.20	95.41
-300	31.49	27.24	29.03	29.82	33.30	53.03	78.52	83.33
-400	30.33	25.87	27.53	28.24	31.98	53.42	72.37	75.14
-500	29.13	24.80	26.32	27.09	31.24	52.97	64.79	66.56
-600	28.00	23.65	25.10	25.98	29.77	49.44	56.56	57.19
-700	26.71	22.33	23.46	23.96	27.86	45.00	49.56	49.60
-800	26.57	22.22	23.27	23.82	28.02	44.08	47.24	46.83
-900	26.48	22.08	23.08	23.65	27.78	42.96	46.59	46.25
-1000	26.41	22.05	22.91	23.55	27.06	40.58	43.61	43.43

Table 6.21: Temperature data in the upstream region in tunnel D (Q = 7.50 kW, U = 0.28 m/s)

x	(40, 0)	(70, 0)	(100, 0)	(130, 0)	(160, 0)	(190, 0)	(220, 0)	(240, 0)
				(y,z)				
-100	157.51	122.92	110.29	100.26	102.84	117.87	238.48	252.77
-200	62.10	63.38	63.23	64.15	68.46	107.61	188.28	189.20
-300	44.10	45.56	46.23	48.23	53.47	97.52	133.86	130.10
-400	38.31	38.37	39.47	43.01	42.98	89.12	110.83	109.17
-500	38.31	38.37	39.47	43.01	42.98	89.12	110.83	109.17
-600	34.88	35.29	36.16	40.24	38.76	81.51	101.47	100.53
-700	32.21	32.66	34.34	38.28	35.51	76.03	93.85	92.81
-800	30.25	30.45	33.07	35.51	32.63	69.22	83.72	82.36
-900	29.15	30.00	32.16	33.60	32.05	62.97	76.52	74.79
-1000	28.67	29.47	31.35	32.54	31.25	57.97	72.51	70.70

x	(40, 250)	(70, 250)	(100, 250)	(130, 250)	(160, 250)	(190, 250)	(220, 250)	(240, 250)
				(y,z)				
-100	58.99	63.49	62.22	64.38	65.34	137.92	186.69	194.34
-200	50.85	54.30	53.71	56.06	60.07	122.73	163.77	169.81
-300	41.50	42.19	42.54	45.21	49.63	103.34	127.19	130.57
-400	35.40	35.39	36.26	39.16	42.04	90.13	102.38	103.83
-500	35.40	35.39	36.26	39.16	42.04	90.13	102.38	103.83
-600	32.68	32.29	33.16	36.07	38.86	82.62	92.58	93.57
-700	30.55	30.08	30.75	33.35	36.54	75.34	82.86	83.26
-800	28.80	28.25	28.47	30.45	33.83	63.53	71.69	71.68
-900	27.82	27.29	27.54	29.33	32.98	58.79	66.33	66.52
-1000	27.23	26.72	26.86	28.66	32.55	56.36	63.49	63.72

x	(40, 480)	(70, 480)	(100, 480)	(130, 480)	(160, 480)	(190, 480)	(220, 480)	(240, 480)
				(y,z)				
-100	43.46	39.36	43.83	44.05	48.78	104.49	143.38	149.54
-200	41.24	36.95	41.52	41.50	46.94	99.87	133.82	138.15
-300	37.78	33.02	36.91	36.86	43.18	90.31	113.24	113.73
-400	33.56	28.83	32.44	33.13	39.26	81.96	96.52	97.85
-500	33.56	28.83	32.44	33.13	39.26	81.96	96.52	97.85
-600	31.62	26.98	30.18	31.14	36.73	74.71	87.96	89.35
-700	30.16	25.65	28.31	29.24	34.67	67.71	79.44	80.21
-800	29.05	24.54	26.62	27.47	32.54	60.48	69.02	69.68
-900	28.70	24.16	25.95	26.72	31.49	57.04	65.45	65.77
-1000	28.48	23.91	25.62	26.35	30.67	54.48	62.76	63.60

Table 6.22: Temperature data in the upstream region in tunnel D (Q =15.0 kW, U = 0.33 m/s)

x	(40, 0)	(70, 0)	(100, 0)	(130, 0)	(160, 0)	(190, 0)	(220, 0)	(240, 0)
				(y,z)				
-100	182.23	148.18	137.75	129.76	130.37	172.50	348.15	345.85
-200	86.78	88.82	90.02	93.48	98.23	164.75	268.22	266.23
-300	62.16	63.94	64.81	69.05	74.56	149.09	184.73	168.57
-400	49.66	50.62	51.42	56.58	55.72	128.02	154.32	145.75
-500	49.66	50.62	51.42	56.58	55.72	128.02	154.32	145.75
-600	43.87	45.12	45.73	52.14	49.37	113.53	140.09	135.25
-700	38.89	40.03	41.89	47.50	43.23	99.62	125.10	121.63
-800	36.39	36.88	39.50	42.39	39.57	91.39	112.52	107.92
-900	35.14	35.76	37.59	39.85	37.85	83.57	105.11	101.26
-1000	33.67	34.74	36.39	38.63	37.50	76.02	97.28	94.24

x	(40, 250)	(70, 250)	(100, 250)	(130, 250)	(160, 250)	(190, 250)	(220, 250)	(240, 250)
				(y,z)				
-100	85.88	94.35	90.13	96.94	98.01	213.62	269.87	283.18
-200	73.16	79.76	76.70	82.28	86.29	189.11	229.40	233.01
-300	56.75	58.60	58.11	63.40	69.48	151.76	174.90	175.10
-400	44.55	45.48	46.31	50.47	55.89	130.70	145.53	145.73
-500	44.55	45.48	46.31	50.47	55.89	130.70	145.53	145.73
-600	40.33	40.46	41.50	45.56	51.03	116.25	129.95	129.63
-700	36.24	35.72	36.38	39.84	45.41	102.61	114.81	114.60
-800	33.70	32.99	32.95	35.39	41.95	86.76	98.04	97.74
-900	32.28	31.86	31.58	33.81	40.20	81.07	92.00	91.67
-1000	31.34	30.58	30.36	32.57	38.87	75.89	86.90	86.95

x	(40, 480)	(70, 480)	(100, 480)	(130, 480)	(160, 480)	(190, 480)	(220, 480)	(240, 480)
				(y,z)				
-100	59.42	55.43	64.87	65.36	74.68	165.36	214.73	223.41
-200	55.55	50.81	59.50	59.56	69.64	151.95	197.95	201.23
-300	47.38	42.12	48.54	48.31	58.39	131.33	164.43	164.13
-400	41.17	35.64	41.79	42.58	51.72	119.00	146.26	147.57
-500	41.17	35.64	41.79	42.58	51.72	119.00	146.26	147.57
-600	36.48	31.33	36.76	37.70	46.75	105.73	128.27	130.05
-700	34.70	29.82	34.42	35.40	43.81	96.54	117.06	118.23
-800	31.47	26.72	29.98	30.84	38.70	83.06	99.41	100.91
-900	30.72	25.98	28.90	29.95	37.40	78.61	94.65	96.49
-1000	30.11	25.46	28.04	29.06	35.79	74.84	90.80	92.28

Table 6.23: Velocity distributions measured in tunnel B using LDV at 1.25 tunnel height from the burner when the backlayering flow was controlled at 2.25 tunnel height upstream (Allen et al, 1999).

Distance above tunnel floor (mm)	Velocity (m/s)				
	1.50 kW	3.0 kW	4.50 kW	7.50 kW	15.0 kW
10	0.574	0.592	0.748	0.737	0.758
20	0.594	0.638	0.779	0.753	0.765
30	0.604	0.659	0.802	0.780	0.765
40	0.622	0.669	0.805	0.783	0.788
50	0.655	0.680	0.819	0.806	0.805
60	0.637	0.691	0.829	0.815	0.805
70	0.648	0.694	0.834	0.819	0.846
80	0.633	0.693	0.827	0.829	0.823
90	0.656	0.712	0.825	0.819	0.838
100	0.666	0.710	0.834	0.831	0.816
110	0.665	0.726	0.813	0.836	0.825
120	0.662	0.724	0.809	0.832	0.839
130	0.657	0.716	0.813	0.847	0.836
140	0.652	0.723	0.804	0.834	0.831
150	0.640	0.723	0.791	0.818	0.835
160	0.566	0.698	0.737	0.785	0.752
170	0.442	0.610	0.653	0.698	0.644
180	0.302	0.462	0.560	0.493	0.386
190	0.188	0.291	0.417	0.194	0.181
200	0.050	0.138	0.249	0	0.018
210	-0.052	-0.089	-0.015	-0.112	-0.113
220	-0.128	-0.158	-0.133	-0.136	-0.185
230	-0.162	-0.179	-0.151	-0.149	-0.208
240	-0.024	-0.034	-0.247	-0.026	-0.137
245	0.010	0	-0.078	0.002	0.005

Table 6.24: Velocity distributions measured in tunnel B using LDV at various distances from the burner when the backlayering flow was controlled at 2.25 tunnel height upstream [Q = 3.0 kW, U = 0.47 m/s] (Allen et al, 1999).

Distance above tunnel floor (mm)	Velocity (m/s)					
	1/2TH	1TH	3/2TH	2TH	5/2TH	5/4TH
430	0.819	0.793	0.736	0.605	0.576	0.659
480	0.835	0.792	0.749	0.626	0.581	0.693
530	0.692	0.723	0.726	0.597	0.559	0.716
580	-0.111	-0.011	0.063	0.500	0.516	0.462
630	-0.222	-0.193	-0.185	0.253	0.415	-0.179

Chapter 7

Data Analysis and Discussion of

Experimental Results

In this chapter, the experimental results will be analysed and discussed. Firstly, the behaviour of the smoke flow is discussed in three aspects namely, the fire plume, backlayering flow and downstream smoke flow. The present study found the fire plume distribution in the tunnels is important in discussion of the variations of the critical ventilation velocity. Therefore detailed discussions on the fire plume distribution have been carried out. MacCaffrey's plume theory is extended in tunnel fire situations.

The main concern of the discussion is the critical ventilation velocity. The variation of the critical ventilation velocity is discussed in relation with fire power and tunnel cross-sectional geometry.

7.1 Fire Plume

The fire produced in the tunnels using 106 mm diameter porous bed burner in the present work was a turbulent diffusion flame. Figure 7.1 shows a photograph of a fire in tunnel E at 15.0 kW. There are two distinguished regions that can be observed; the flame and the buoyant smoke flow.

It can be observed that with the presence of longitudinal ventilation flow, the fire plume deflects at certain angle from the vertical, similar features as being found in the large scale experiments (Haerter, 1965; Bettis et al 1993; Apte et al 1991).

McCaffrey (1979) proposed fire plume theory by studying a fire plume above a 30 cm square porous burner. A free fire plume consists of three distinct regimes as illustrated in Figure 7.2. The three regimes are:

(1)   the near fire, above the burner, where there is persistent flame and accelerating flow of burning gas.

(2)   a region in which there is intermittent flaming and a near-constant flow velocity (the intermittent zone); and

(3)   the buoyant plume which is characterised by decreasing velocity and temperature with height

In the tunnels, the fire plume was confined by the tunnel walls. The fire interacted with the tunnel side walls and ceiling.   In addition, the longitudinal ventilation flow has strongly influenced the shapes of the fire plume. From the experimental observations, the present study extended McCaffrey's fire plume theory, to tunnel situations.   The fire plume was considered to have the three regimes. The feature of each regime is the same as described by McCaffrey.   However the fire plume shapes are completely different from a free fire plume.

Based on the measured temperature contours and experimental observations, at critical ventilation conditions, there are two different fire plume distributions in tunnel which are described in Figure 7.3 and Figure 7.4, respectively.

The first fire plume distribution occurred when fire power was relatively small. Examples are shown in Figures 6.5(a), 6.10(a) and 6.14(a) for tunnels **B**, **D** and **A**, respectively. In these tests, the fire plume was relatively small, the persistent and intermittent flame did not reach the tunnel ceiling. The fire plume was divided into three regimes as illustrated in Figure 7.3 where two parameters are proposed to describe the feature of the fire plume. The first parameter is the flame height (FH) which takes into account of the vertical flame height of the intermittent regime above tunnel floor. Next parameter is the deflection angle of the fire plume from the vertical which is defined as α.

In practice, it is quite difficult to define the temperature range with respect to the three regimes. This information is hardly found in the literature. To establish the basis for the discussion, the photograph in Figure 7.1 was compared with the measured temperature contours in Figure 6.5(c) for the tunnel **B**, at the same HRR.   The present work considered that the temperature in the persistent flame regime is greater than 500 °C. The temperature in the intermittent regime is between 250 °C to 500°C. The buoyant plume is considered to have temperature less than 250 °C.

The second fire plume distribution occurred when the fire power was increased to 15.0 kW. The measured temperature contours in Figures 6.5(c), 6.10(c) and 6.14(c) show that the intermittent flames have reached the ceiling. The fire plume was illustrated in Figure 7.4. However, upon increasing the fire power, the persistent flame elongated further downstream, from the fire seat. No experimental tests have demonstrated the persistent flame reached the ceiling when the ventilation velocity was set at critical conditions. Persistent flame did reach the ceiling when the ventilation velocity was much lower than the critical ventilation velocity.

7.1.1 Flame Height

Unlike in an open fire, the flame heights inside the tunnel were observed depend greatly on the interaction between the fire plume with the compartment geometry and the ventilation flow. An attempt was made to illustrate the flame height with two main parameters; the HRR and ventilation velocity. Since the exact regimes associated with the fire plume were difficult to determine, both temperature values of 250 °C and 350 °C were selected to justify the boundaries for the intermittent regimes, while the boundary for the persistent regime remains at 500 °C.

(1) Relationship of Flame Height and the HRR

Figure 7.5 shows the variations of the flame height against HRRs in tunnels **A**, **B** and **D** at critical ventilation velocities. The results show that for a small fire (3.0 kW), both intermittent regimes indicated by 250 °C and 350 °C are approximately at 125 mm above tunnel floor. Whilst, the persistent regimes in the three tunnels lay low. Both persistent and intermittent regimes are the highest in tunnel **D**, followed by tunnels **B** and **A**.

However at 7.50 kW fire, the intermittent regimes indicated by the 250 °C contours have definitely reached the ceiling, while the intermittent regimes indicated by 350 °C have nearly reached the ceiling for all tunnels. The persistent flame in the three tunnels are approximately at 125 mm above tunnel floor.

Finally at 15.0 kW fire, both intermittent regimes have already reached the ceiling, while the persistent flame have not yet reached the ceiling.

(2) Relationship of Flame Height with Ventilation Velocity

Figure 7.6 shows the variations of flame height against ventilation velocity in tunnels **A**, **B** and **D** at 3.0 kW, 7.50 kW and 15.0 kW with reference to the temperature 250 °C contours. Whilst, Figure 7.7 shows the same plot using 500 °C for the persistent flame regime. In both figures, the ventilation velocities were set at three conditions; velocity at which the backlayering was controlled at ten tunnel height upstream from fire seat, critical conditions and at the velocity twice of the critical ventilation velocity.

The results show that in all tunnels, the flame height decreases with the increase of ventilation velocity. It can be also observed that in both figures the flame heights in tunnel **D** are the highest, followed by tunnels **B** and **A**.

It is shown in Figure 7.6 that at lower ventilation velocity (between 0.15 m/s to 0.35 m/s), the intermittent regimes for a small fire (3.0 kW) have not yet reached tunnel ceiling for the three tunnels. However, when the fire HRRs increase to 7.50 kW and 15.0 kW, the intermittent regimes have already reached tunnel ceiling.

At the critical ventilation conditions (0.40 m/s to 0.65 m/s), the intermittent regimes at 3.0 kW, further reduce their heights. However, the intermittent regimes for 7.50 kW and 15.0 kW fires still reach the ceiling.

Similarly, it is shown in Figure 7.7 that at lower ventilation velocity (0.15 m/s to 0.35 m/s), the persistent flames are less than one third of the tunnel height for 3.0 kW fire. When the fire HRR increases to 7.50 kW, the persistent flames are approximately half the height of the tunnel. Further increases in the HRR to 15.0 kW, the persistent flame regimes nearly reach tunnel ceiling.

At the critical conditions (0.40 m/s to 0.65 m/s), the persistent flames for 3.0 kW fire are approximately the same height as in the previous condition. However, at 7.50 kW and 15.0 kW fires, the persistent regimes further reduce their heights.

7.1.2 Flame Angle (α)

The measured flame tilt angles from the vertical for three HRRs at least at two ventilation velocities are shown in Table 7.1. For each HRR, the first velocity was correspond to the velocity at which the backlayering flow was controlled at ten tunnel heights upstream. The second velocity was the critical ventilation velocity while the third velocity was the additional test that was carried out.

It was found that the deflection angles of the fire plumes in all tunnels were greater that 45 °. The tilt angles agreed with the results from the Gallery tunnel in the Health and

Safety Laboratory, Buxton (Bettis, 1993, 1994) which also showed that the flaming region was generally inclined at an angle greater than 45 ° from the vertical. A similar feature of the pattern was observed in another large scale experiment performed by Apte et al (1991). The measured tilts angles were in the range 54 ° to 66 °, depending on the ventilation velocity.

(1) The Relationship of Flame Angle with the HRR

The results in Table 7.1 also show that in a particular tunnel, for example tunnel **B**, the fire plume tilt angle increases as the fire power increases. The tilt angle for 3.0 kW fire at the critical ventilation velocity (0.48 m/s) was 70°. When the fire HRR was increased to 7.50 kW, the tilt angle at the critical ventilation velocity (0.56 m/s) further increased to 73°. Finally at 15.0 kW, the tilt angle further increased to 76°. A similar pattern occurred in both tunnels **A** and **D**.

(2)The Relationship of Flame Angle with the Ventilation Velocity

In order to investigate the relationship of the plume angle with the ventilation velocity, a few tests have been carried out on a specific HRR at least two ventilation velocities. Examples of the effect of the ventilation velocity on the fire plume angle can be seen in Figure 6.4. It can be observed that at ventilation velocity 0.25 m/s, the plume tilt angle was approximately 60°. When the ventilation velocity was increased to 0.48 m/s, the plume further deflected at approximately 70°. Finally, when the ventilation velocity was increased to 0.96 m/s, the deflection angle was approximately 78°.

(3) The Relationship of Flame Angle with Tunnel Aspect Ratio

The measured fire plume tilt angles in Table 7.1 also show that at specific HRR, the tilt angle decreases as the tunnel aspect ratio increases. It can be seen that at 3.0 kW fire at critical ventilation velocity, the tilt angle in tunnel **A** is 75°. The plume tilt angle decreases to 70° in tunnel **B**. Finally , the plume tilt angle further decreases to 60° in tunnel **D**.

Figure 7.8 shows the variations of flame tilt angles against ventilation velocity in tunnel **A, B, D** at 3.0 kW, 7.50 kW and 15.0 kW. It can be seen that for all HRRs, the flames in tunnel **D** have the lowest tilt angles from the vertical, while the flames in tunnel **A** have the highest tilt angles from the vertical.

7.1.3 Discussion of the Mechanisms for Fire Plume Distribution in Tunnels.

Having discussed the behaviour of the fire plume inside the tunnels, the next step is to understand the mechanisms for its behaviour. In the present work, the mechanisms for the fire plume distributions in the tunnels can be discussed into two main areas.

(1) Interaction Between Fire and Ventilation Flow

It has been pointed earlier that in the presence of the ventilation flow, the fire plume deflected at certain angle from the vertical. One of the mechanisms which should be considered for the observed behaviour is the air entrainment. Theoretically, in order to complete the combustion, the fire has to entrain the air from its surroundings. However, in tunnel, due to the presence of the walls and ceiling, the behaviour of the air entrainment would not be similar to an open fire.

In tunnel situation, since the fresh air is supplied through the ventilation in the upstream from the fire, it would be expected that there would be rapid air entrainment in the upstream positions compared to the downstream. This rapid air entrainment would cause local acceleration in the air velocity inside the tunnel. As a results, the air forced the fire to tilt at certain angle from the vertical. This phenomena would also explain the reason why the persistent flame was not observed to impinge the ceiling at the critical ventilation conditions, only elongated further downstream from the fire seat.

(2) Interaction Between Fire and Tunnel Walls.

The second mechanism for the distribution of the fire plume is the interaction between the fire and tunnel walls. It would be expected that in a lower aspect ratio tunnels, the fire would reach the tunnel walls. The examples of the measured cross-sectional fire geometry in tunnels **B** and **D** at HRR 3.0 kW and 15.0 kW can be seen in Figures 6.11 to 6.14, respectively. It can be observed that in tunnel **B** at 3.0 kW fire, the cross-sectional fire geometry at approximately closed to tunnel centreline. However, at 15.0 kW fire almost reached the walls. In contrast, in tunnel **D**, the fire cross-sectional geometry was confined near the centreline even at 15.0 kW fire.

Comparing the measured temperature contours in both tunnels, it can be seen that the flow patterns in tunnel **B** were slightly different from the patterns in tunnel **D**. The patterns in tunnel **B** indicated that the hot walls induced the cold air into the fire plume.

Referring back to the behaviour of air entrainment, due to the limited spaces at both sides, the flame has to elongate further downstream for the entrainment in a lower aspect ratio tunnel. In contrast, in the higher aspect ratio tunnels there are greater tendency for entrainment from both sides due to more spaces available. Therefore, it would be expected greater local acceleration near the fire seat. As a results, the fire would have less deflection angle from the vertical.

In addition to entrainment, there is another factor which cause the deflection of the fire plume. This factor is the obstruction of the fire to the air flow. In this case, the fire could be represented as a solid hot core which introduced the resistance to the air flow. It would be expected that in the lower aspect ratio tunnel, the deflection angle from the vertical would be greater than in the higher aspect ratio tunnels due to the limited spaces at both sides from the fire. To some extent, this variation has been confirmed by the experimental results.

To conclude, the air entrainment and flow acceleration around the fire determine the behaviour of the fire plume. It is hoped that CFD studies in the second part of the present work can examine the flow behaviours in the four tunnels in details.

7.2 Backlayering

The majority of the previous works concerned with the studies on the behaviour of the backlayering flow. In the present work, although most of the tests were carried out to study the critical ventilation velocity, there were a few tests that have been carried out to examine the behaviour of the backlayering and further confirm the previous findings.

The extensive backlayering temperature measurements were performed in both tunnels **A** and **D**. The measured backlayering temperature contours at 3.0 kW and 7.50 kW fires in tunnel **A** are shown in Figure 6.15. Whilst, the measured backlayering temperature contours for the same HHRs in tunnel **D** are shown Figure 6.17. The backlayering flows were found to have several characteristics similar to what have been previously found by other researchers such as Kwack et al (1990) and Hwang et al (1980). It was found that:

- The observed backlayering flows were stratified in nature. The maximum temperature in the backlayering region decreases as the backlayering moved in the upstream direction. This behaviour can be seen in Figures 6.15 and 6.17.

- The thickness of the backlayering layers remains approximately constant for the two HRRs in the same tunnel. The photograph in Figure 6.16 further shows that the smoke thickness in the backlayering was approximately half of the tunnel height with the end of the layer formed a sharp edge with the angle of inclination at approximately 25 - 30 ° of the tangent line to the tunnel ceiling. Comparing the backlayering flow in the two tunnels, it can be seen that the depth of the backlayering flows in tunnel **A** was greater than in tunnel **D**. This was expected due to different tunnel widths. The temperature plot in Figure 6.18 further confirmed the variations.

- The backlayering layers were very sensitive to the ventilation velocity. The critical results in Tables 6.1 to 6.4 clearly show that when a small changed in velocity, the backlayering length changed significantly from 1, 3, 5 and 10 tunnel heights.

In addition to the above findings, the present works also found that the backlayering flows filled the whole tunnel width although the depth was approximately half of the height of the tunnel. The plot of the measured temperatures at three cross-sectional distances from tunnel centreline in Figure 7.9 clearly show that at certain height above the floor, the temperatures at this position were almost the same.

7.3 Downstream Smoke Flow

There were also a few tests carried out to check the behaviour of the smoke flow in the downstream region. The results obtained in the experiment shown in Figures 6.19 to 6.22 indicate that the downstream smoke flow was stratified. When the fire was small (3.0 kW), the smoke only filled the top part of the tunnel. However, when the fire was large (15.0 kW), the smoke filled most of the tunnel.

7.4 Critical Ventilation Velocity

The most important from the experiment results in the present work are the measured critical ventilation velocities for various tunnel cross-sectional geometries. The results for the critical ventilation velocity between HRRs 1.50 kW to 30.0 kW fires are shown in Table 6.5. The variations of the critical ventilation velocity against HRR for the five tunnels are shown in Figure 6.3. The discussions on the critical ventilation velocity are discussed in relation to the tunnel cross-sectional geometry and fire power.

7.4.1 Effect of Tunnel Cross-sectional Geometry or Tunnel Aspect Ratio on the Critical Ventilation Velocity

Most of the previous studies on tunnel fires considered that the buoyancy force in the backlayering was directly associated with tunnel height. This resulted that the same critical ventilation velocity was predicted for the tunnels having the same height, but different cross-sectional geometries.

Some research (Lea, 1995 ; Touviven, 1996) considered the effect of the tunnel width. Lea (1995) in his CFD pointed out that the cross-sectional geometry may have effect on the critical ventilation velocity. The results in Figure 6.3 have shown that the cross-sectional tunnel geometry or tunnel aspect ratio did affect the magnitude of the critical ventilation velocity.

The results in Figure 6.3 have also shown that the relationship between the critical ventilation velocity and the tunnel width has two trends depending on the HRR. The first trend, the critical ventilation velocity decrease with the increase of tunnel width when the HRR is below 10 kW.

By taking tunnel **A** as a reference, the critical ventilation velocity at 1.5 kW fire in tunnel **B** was lower by approximately 9.3 percent. Likewise, the critical ventilation velocity for the same HRR reduced by 14.0 percent and 20.9 percent in tunnels **C** and **D**, respectively.

At 3.0 kW fire, the critical ventilation velocity for tunnel **A** has started to weakly dependent on HRR, whilst the critical ventilation in tunnel **B** had already exceeded the value in tunnel **A**. On contrary, the critical ventilation velocity for tunnels **C** and **D** were still lower by 2.2 percent and 13.0 percent, respectively.

At 7.50 kW, the critical ventilation velocity for tunnels **C** and **D** further dropped by 2.7 percent and 10.8 percent compared to tunnel **B**. The critical ventilation velocity further reduced consistently until HRR 10 kW.

The second trend is that critical ventilation velocity increases with tunnel width when the HRR was set higher than 10 kW. This was completely contradictory with the empirical models. It can be seen that at HRR 15.0 kW, the critical ventilation velocity in tunnel **C** has already exceeded the critical ventilation velocity in tunnel **B**. Similarly, at 22.50 kW, the critical ventilation velocity in tunnel **D** exceeded the critical ventilation velocity in tunnel **C**.

One of the most important observation was that the behaviour of near independent of the critical ventilation velocity occurred faster in the narrow tunnels than in the wider tunnels.

7.4.2 Effect of Fire Power on the Critical Ventilation Velocity

The relationship between U_c and Q will be easily applied and compared with different scales if plotted as the dimensionless variables suggested in Froude scaling as being discussed in Chapter 3. The relationships related to Q^* and V^* are shown in equations 3.4 and 3.5, respectively. For the calculation of V^* and Q^*, the values of the parameters are as follow:

The ambient air density ρ_o	$= 1.29 \text{ kg/m}^3$,
The heat capacity, Cp	$= 1.0 \text{ kJ/Kmol.K}$
The ambient temperature T_o	$= 298 \text{ K.}$
Characteristic length, H	$= 0.25 \text{ m}$

The calculated values of V^* and Q^* for the five tunnels are presented in Table 7.2 and Table 7.3. The individual plot of V^* and Q^* for first four tunnels is shown in Figure 7.10. The graph has been plotted in logarithmic scales (Log_{10}), so that the behaviour of independent of critical ventilation velocity on HRR can be easily distinguished.

As expected that there are two distinguished regions in both tunnels **A** and **B**. In the first region V* increases with Q*. In the second region V* becomes nearly constant with the increases of Q*. For tunnel **A**, the weak dependence of critical ventilation velocity on HRR can be seen at the second point where Q* is equal to 0.21. For tunnel **B**, the behaviour exhibits at approximately Q* equal to 0.33. However, although the two regions were not seen tunnels **C** and **D**, the last few points at higher Q* indicated that V* has started to become less dependent on Q* (transition region).

The points in the first region were linerised and the gradient gave the power law to the HRR in the critical relationship as discussed in Chapter 2. The values were 0.29, 0.33, 0.28 and 0.30 for tunnels **A**, **B**, **C** and **D**, respectively, consistent with 1/3 power in the empirical models.

The values of V*max were 0.31, 0.38, 0.41 and 0.41 for tunnels **A**, **B**, **C** and **D** whilst the corresponding values of Q*max at which the weakly independent occurred were 0.21, 0.33, 0.40 and 0.60, respectively. The values of V*max increases starting from the lowest tunnel aspect ratio and tends to become constant at higher tunnel aspect ratio. However, the value of Q*max is still increasing with the increase of tunnel aspect ratio.

Following to the determination of V*max and Q*max, the expressions for critical ventilation velocity relationship for the four tunnels in the forms of dimensionless critical ventilation velocity and dimensionless HRR can be derived as below:

- Tunnel A $\qquad V^* = 0.31\,[0.21]^{-1/3}\,[Q^*]^{1/3}$ for $Q^* < 0.21$ (7.1)

  $\qquad\qquad\qquad V^* = 0.31$ for $Q^* > 0.21$ (7.1a)

- Tunnel B $\qquad V^* = 0.38\,[0.33]^{-1/3}\,[Q^*]^{1/3}$ for $Q^* < 0.33$ (7.2)

  $\qquad\qquad\qquad V^* = 0.38$ for $Q^* > 0.33$ (7.2a)

- Tunnel C $\qquad V^* = 0.41\,[0.41]^{-1/3}\,[Q^*]^{1/3}$ for $Q^* < 0.41$ (7.3)

$$V^* = 0.41 \qquad \text{for } Q^* > 0.41 \qquad (7.3a)$$

- Tunnel D $\qquad V^* = 0.41 \, [0.60]^{-1/3} \, [Q^*]^{1/3} \qquad \text{for } Q^* < 0.60 \qquad (7.4)$

$$V^* = 0.41 \qquad \text{for } Q^* > 0.60 \qquad (7.4a)$$

Figure 7.11 shows the assembly of plot V* against Q* for the five tunnels. It can be observed that there are variations of V* against Q* for the five tunnels similar to Figure 6.3. The existing dimensionless analysis cannot correlate the experimental results into a simple form.

The overall effect of the fire power showed that for a small fire, the critical ventilation velocity vary with one third power of HRR, consistent with the empirical models. However, at higher HRRs, the critical ventilation velocity was found near independent of HRR. This further confirmed the findings from Oka and Atkinson (1995) and Bettis et al (1993, 1994) in HSL, Buxton.

7.4.3 Critical Ventilation Velocity and Velocity Distribution in Smoke Flow Measured Using LDV

The measured velocity distributions for five HRRs in tunnel **B** with the length of the backlayering was controlled at 2.25 tunnel heights are presented in Table 6.23. The LDV results in Figure 6.23 show that the magnitude of velocity inside the tunnel increases with the HRR when the HRR varied from 1.5 kW to 3.0 kW. However starting from 4.35 kW, the velocity profiles in the tunnel were similar. This directly showed the existence of the behaviour of independent of critical ventilation velocity on HRR. In addition, the velocity in the backlayering flow region was quite similar regardless the HRRs.

The results shown in Figure 6.23 also show the effect of flow acceleration approach the fire. It can be observed that the magnitudes of the maximum velocity profiles varied from 0.60 m/s to 0.80 m/s for 1.50 kW to 15.0 kW. The actual ventilation velocity set in

the experiment shown in Table 6.2 indicated that a velocity between 0.29 to 0.36 m/s was only required to control the backlayering up to 2 tunnel heights upstream for 1.50 kW fire. For 15.0 kW fire, the actual ventilation velocity required was between 0.51 to 0.57 m/s.

Thus, there are three important conclusions from the LDV measurements:

- The phenomena of the critical ventilation velocity becoming independent of the HRR at high HRR in tunnel fires. This confirmed the finding obtained from the thermocouple measurements.

- The velocity profiles showed that the velocity in the backlayering for all HRRs were similar. There were no significant difference in profiles between high and low HRRs. Thus, it can be concluded that studies on the backlayering flow itself could not explain the behaviour of weak dependence of the critical ventilation velocity on the HRR.

- There was an acceleration in the air flow near the fire. The air flow velocity to some extent was increased by approximately more than 50 per cent from the original magnitude.

7.4.4 Critical Ventilation Velocity and Flame Shape

The second conclusion arises from the LDV measurement gives important information regarding to the control of smoke flow in tunnel fires. It suggested that discussion of the behaviour of the critical ventilation velocity on HRR should be focused on another area other than the backlayering. In the present work, the researcher has tried to establish the relationship between the critical ventilation velocity and the flame shape.

The fire plume distribution inside the tunnel has been discussed in section 7.1. It was pointed out that there were two fire plume distribution patterns at critical ventilation condition according to the tunnel cross-sectional geometry and the fire power. Examination of the variations of the critical ventilation velocity with HRR against the fire plume distribution patterns has been carried out. It was found that there was strong link

between the change of the pattern in critical ventilation velocity against HRR and the change of the fire plume distributions.

It was suggested from the present work that when the HRR was relatively small, the flame laid low in the tunnel. Only buoyant plume reached the tunnel ceiling. In this case, the ventilation velocity is strongly affected by the HRR. The measured temperature contours for HRRs 3.0 kW in tunnels **B** and **D** in Figures 6.5(a) and 6.10(a) clearly shown that the fire plume at this HRR is relatively small. Under this conditions, it can be seen that the critical ventilation velocity for this HRR in Figure 6.3 is in the region of increasing with the power one third of the HRRs.

However, when the HRR was increased to a certain level, the intermittent flame region approached the ceiling at the critical ventilation conditions, the critical velocity became insensitive to the HRR. This was demonstrated in the tests with 7.50 kW shown in Figure 7.5 that the intermittent region has nearly reached the ceiling, indicated by contour 350 °C. At this HRR, the critical ventilation velocities in tunnels **A**, **B** and **E** were in the transition region, where they started to become weakly dependent of HRR. However, in tunnels **C** and **D**, although the intermittent flame approached the ceiling at 7.50 kW and 15.0 kW fires, the critical ventilation velocity slowly increases with the HRRs.

At very high HRR, the critical velocity became independent of the HRR. Again, this was demonstrated in the tests with 15.0 kW, shown in Figure 7.5, that the intermittent regimes have already reached the tunnel ceiling for all tunnels. At this condition, the critical ventilation velocities in tunnels **A**, **B** and **E** have become constant at 0.48 m/s, 0.60 m/s and 0.60 m/s, respectively. This situation has not been obtained in tunnels **C** and **D**. Tests with higher HRR should be carried out. Unfortunately, the present work did not carry out these tests due to simply the disturbance in the laboratory re-arrangement in the HSL. It is suggested that these tests should be carried out in future study.

The findings from this work have suggested that the Uc is determined by the interactions of the flame with the ventilation air and the tunnel walls. These interactions were reflected in the fire plume distribution inside the tunnel which had features of a larger tilt angle from the vertical and elongated flame in downstream from the fire seat. The fire plume has a way of coping with the large HRR by extending its longitudinal length.

Before the intermittent flame reaches the ceiling, the gases in the backlayering are mainly the buoyant smoke, the buoyancy force in the backlayering is determined by the smoke, therefore the value of the Uc is sensitive to the HRR. Once the intermittent flame reached the ceiling, the buoyancy force in the backlayering is mainly contributed by the intermittent flame which has almost constant velocity. Further increasing the HRR, will only results longer flame the nature of the intermittent flame under the ceiling does not change. Therefore the critical ventilation velocity becomes insensitive to the HRR.

7.5 Comparison of Measured Critical Ventilation Velocity with Predictions from Correlations

The critical ventilation velocities obtained in tunnels **A, B, C** and **D** in the present work were then compared with the three existing models [Heselden, 1978 (equation 2.12); Thomas, 1970 (equation 2.9); SES, 1982 (equations 2.13 & 2.14)]. In the calculations, the range of HRR was maintained between 0 to 30 kW. The correlations from Heselden and Thomas required the value of gas temperatures at each HRR in their empirical equations. Since the exact value of gas temperature at critical condition was not measured in the experiment, it was calculated by using equation 2.14 derived by SES.

Table 7.4 to Table 7.7 show the predicted critical velocities using the above correlations. Figure 7.12 illustrates the plot of the critical ventilation velocity with HRR for the four tunnels. It is clearly seen that the predicted critical ventilation velocities from Thomas and Heselden indicates that the critical ventilation velocity vary with the power of one third of the HRR at all HRRs. The correlation from SES predicted better match of the

critical ventilation velocity with the experiment. However the behaviour of weakly independent of critical ventilation velocity on the HRR was not predicted in tunnels **A** and **B** over the range of HRRs.

It is shown in Figure 7.12 that the established models do not predict the behaviour of weakly dependent of critical ventilation velocity on the HRRs. This is one of the drawbacks of the current established empirical models. In this case the model can be expected to over-estimate the critical ventilation velocity at higher HRRs.

The inability to predict the behaviour most probably due to the assumptions made in the empirical models that were quite simple, only taking consideration on the buoyant force in the backlayering as a function of the height of the tunnel. However, in real case, the phenomenon related to the fire plume is complex, and three dimensional in nature.

In addition, the existing models do not take the consideration on the shape of the tunnel. The critical ventilation velocity has been predicted based on the gross sense through an effective width. Thus, in future, it is necessary to derive new formulations with include the cross- sectional of the tunnel to predict the critical ventilation velocity.

7.6   Conclusions

The critical ventilation velocity in the five model tunnels have been systematically measured. In addition, the temperature distributions have been studied in three dimensions. The following are the summary of findings obtained in the present study.

- The critical ventilation velocity was found to vary with tunnel width in two trends. In the first trend, it decreases with the increase of tunnel width when HRR is below 10.0 kW. In the second trend, it increases with tunnel width when the HRR was set higher than 15.0 kW

- The relationship between the critical ventilation velocity with HRR was varying with the power of one third of the fire power at low HRR.

- The behaviour of the critical ventilation velocity becoming independent on the HRR occurred in tunnel fires, at higher HRRs.

- There were strong links between the change of the pattern in the critical ventilation velocity against HRR and the change of the fire plume distributions.

- McCaffrey's fire plume theory has been extended to tunnel fire. The fire plume is considered to have the three regimes but the shapes are completely different from a free plume. The two fire plume distributions at critical ventilation conditions, shown in Figure 7.3 and Figure 7.4, respectively.

- When the HRR was small, the flame laid low in the tunnel. Only buoyant plume reached the tunnel ceiling. In this case, the ventilation velocity is strongly affected by the HRR. However, when the HRR was increased to a certain level, the intermittent flame region approached the ceiling at the critical conditions, the critical ventilation velocity became insensitive to HRR. At higher HRR, when the intermittent flame definitely reached the ceiling, the critical ventilation velocity become totally independent on the HRR.

- The flame deflection angles in all tunnels were greater than 45 ° which agreed with the previous larger scale results especially from the Gallery tunnel tests, Buxton.

- The backlayering flow was found to be stratified in nature. The maximum temperature in the backlayering region decreases as the backlayering moved in the upstream direction. Another significant findings was that for a specific tunnel, the thickness of the backlayering flow was approximately the same regardless HRR. In two different tunnels, for a specific HRR, the depth of the backlayering in the higher aspect ratio tunnel was slightly lesser than in lower aspect ratio tunnel.

- The backlayering flow also was found to fill whole tunnel width at the top part of the tunnel. This is a crucial finding for the suggestion of the proposed new characteristic length for the buoyant flow which will be discussed in details in Chapter 9. The backlayering flow was also found to be very sensitive to the ventilation flow.

- In the downstream region, the smoke flow was also found to be stratified in nature. When the fire was small, the smoke was less stratified. However, when the fire was larger, typically 15.0 kW, the smoke filled most of the tunnel.

- The established empirical models predict the critical ventilation velocity increase one third of the power of HRR at all HRRs. However, they do not predict the behaviour of independent of critical velocity on the HRR. Thus, the models can be expected to over-estimate the critical ventilation velocity at higher HRR. Another major drawback is that the existing model do not also include the cross-sectional shape of the tunnel, only to consider the gross HRR per tunnel width.

- During dimensionless analysis on HRR and critical ventilation velocity, using tunnel height as the characteristic length, it was found that the values of Q*max increases with the increases of tunnel aspect ratio. Whilst, the value of V*max increases from 0.31 and becomes nearly constant at 0.41. Based on tunnel height, the critical ventilation results could not be co-ordinated into a single correlation. Thus, this emphasise the need to find a new characteristic length which takes into account the cross-sectional geometries of the tunnels.

To conclude, the present study is the first one to relate the behaviour of the Uc to the fire plume distribution inside the tunnel. CFD simulations have been carried out to examine the details of air entrainment and acceleration in the fire plume. The results will be discussed in the next chapter. Further discussions of the results and dimensionless analysis to the critical ventilation velocity and the HRR will be carried out in Chapter 9.

Figure 7.1: Photograph of a tunnel fire (Health & Safety Laboratory, Buxton, UK)

Figure 7.2: Schematic diagram of the fire plume (McCaffrey, 1979)
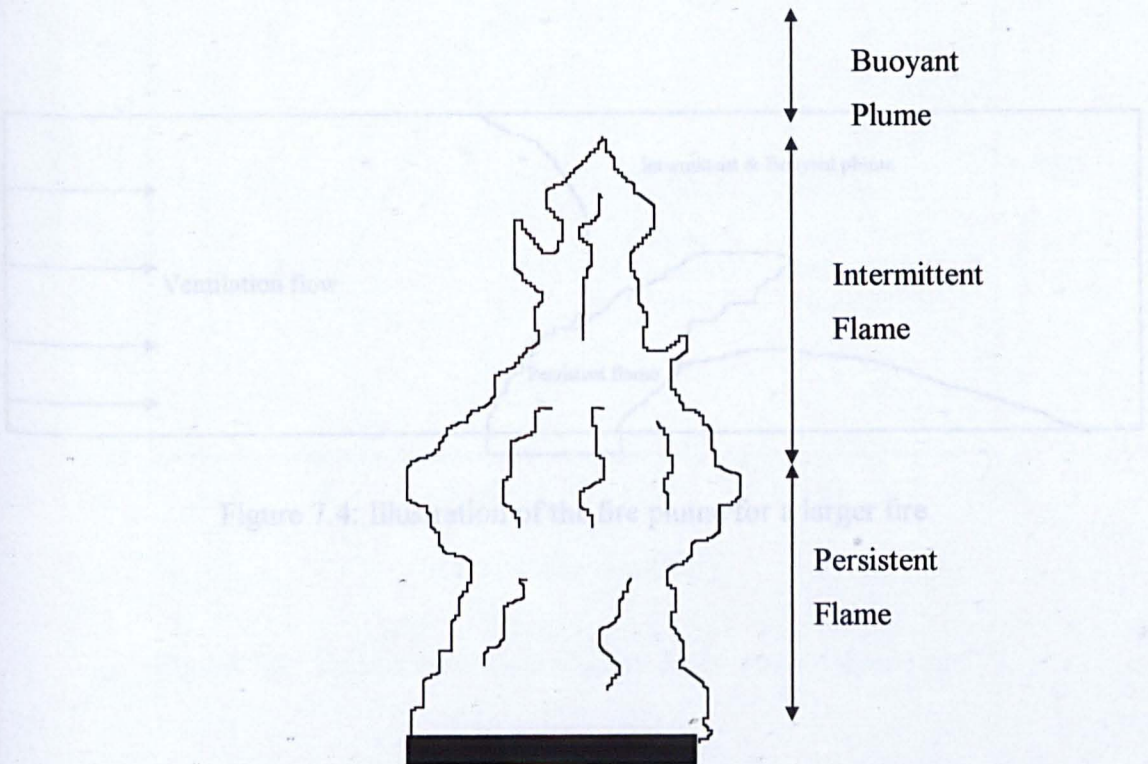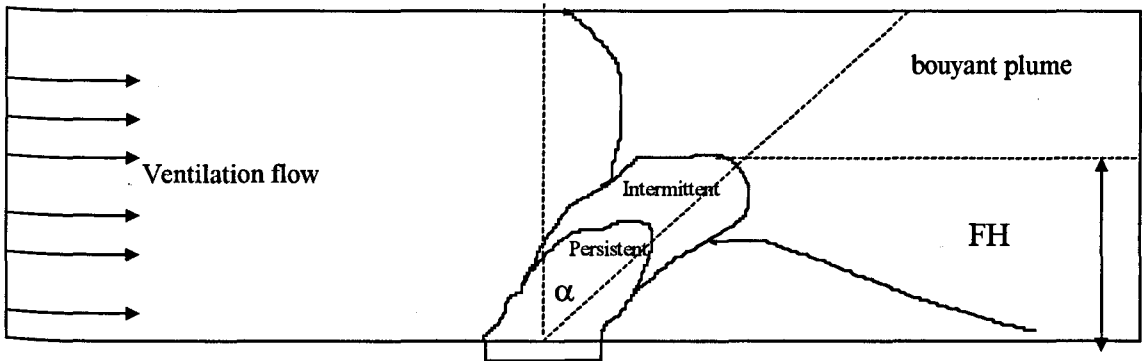
Figure 7.3: Illustrations of fire plume for a small fire
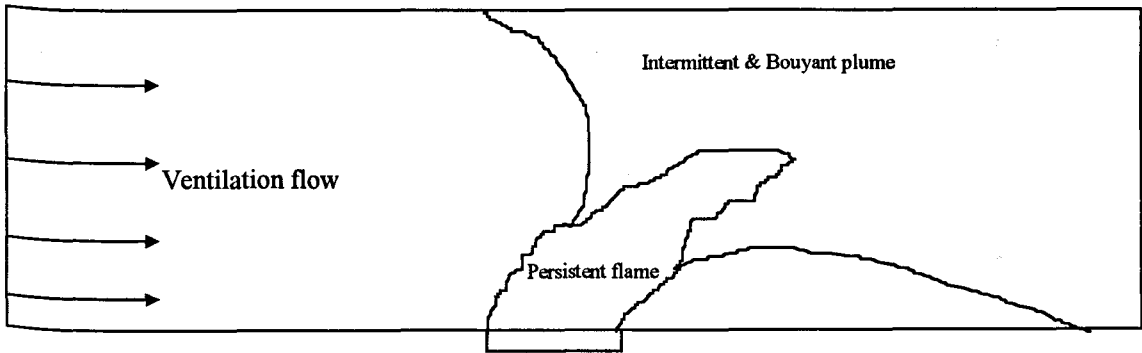
Figure 7.4: Illustration of the fire plume for a larger fire

Symbols	Colours
○ Tunnel A	Black - 250 °C
□ Tunnel B	Red - 350 °C
▽ Tunnel D	Blue - 500 °C
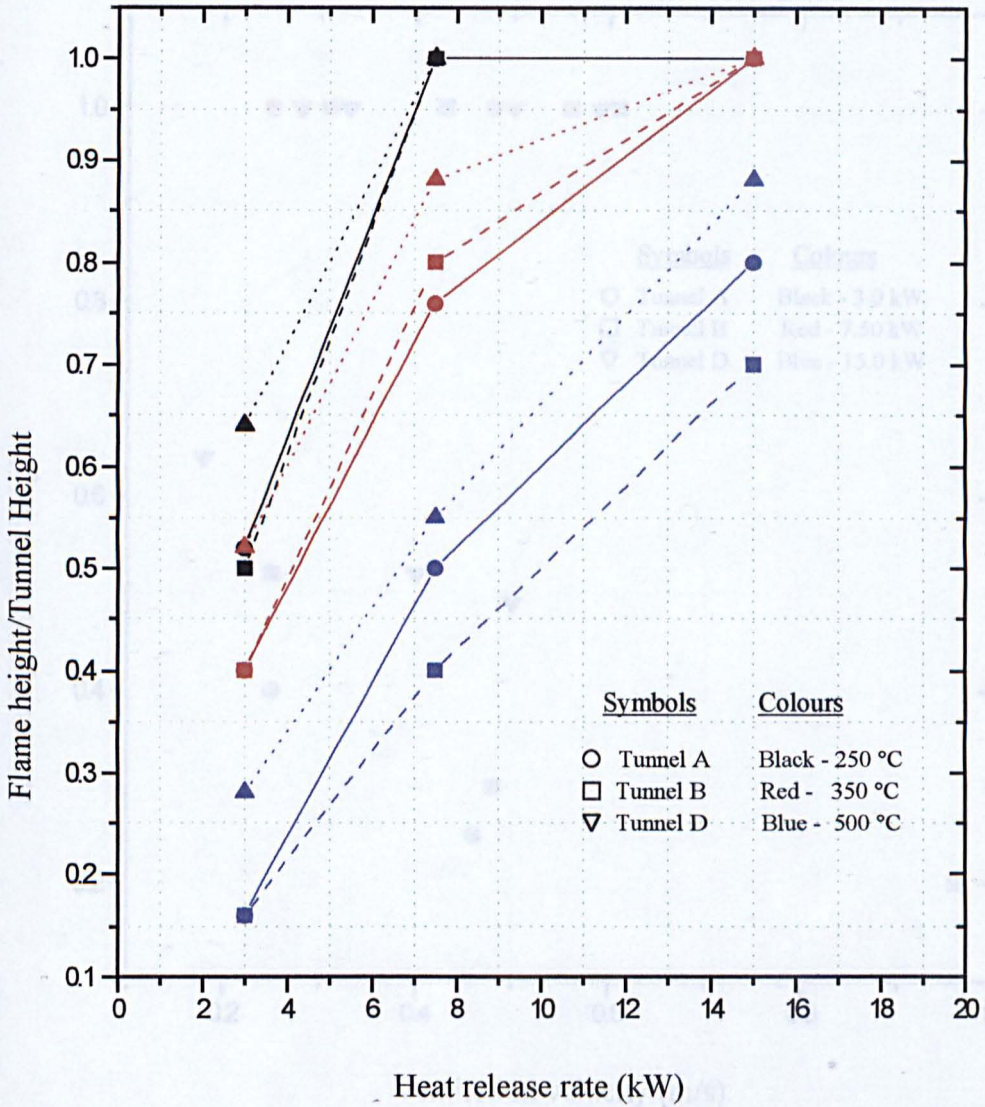
Figure 7.5 : Variations of flame height against heat release rate
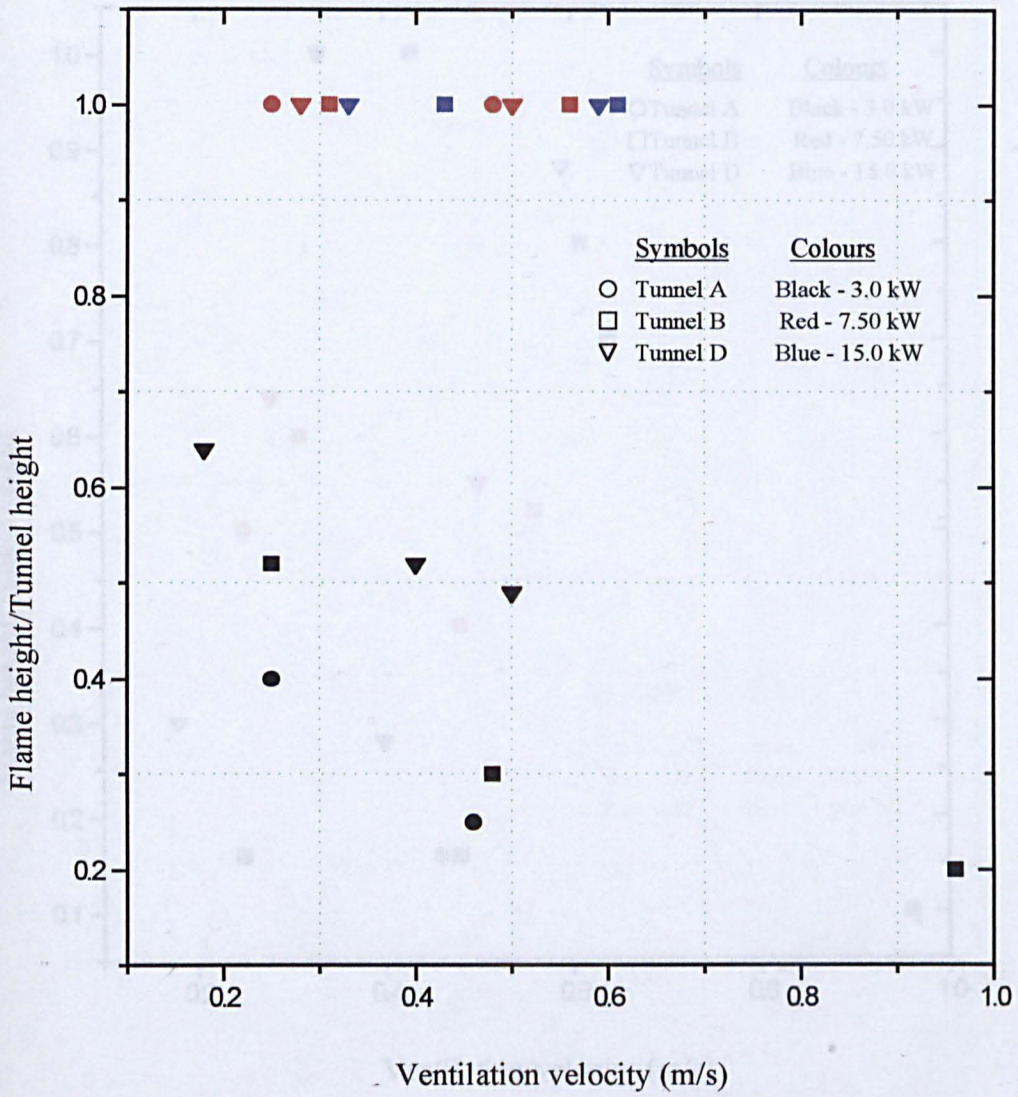
Figure 7.6 : Variations of flame height against ventilation velocity
based on 250 °C intermittent flame
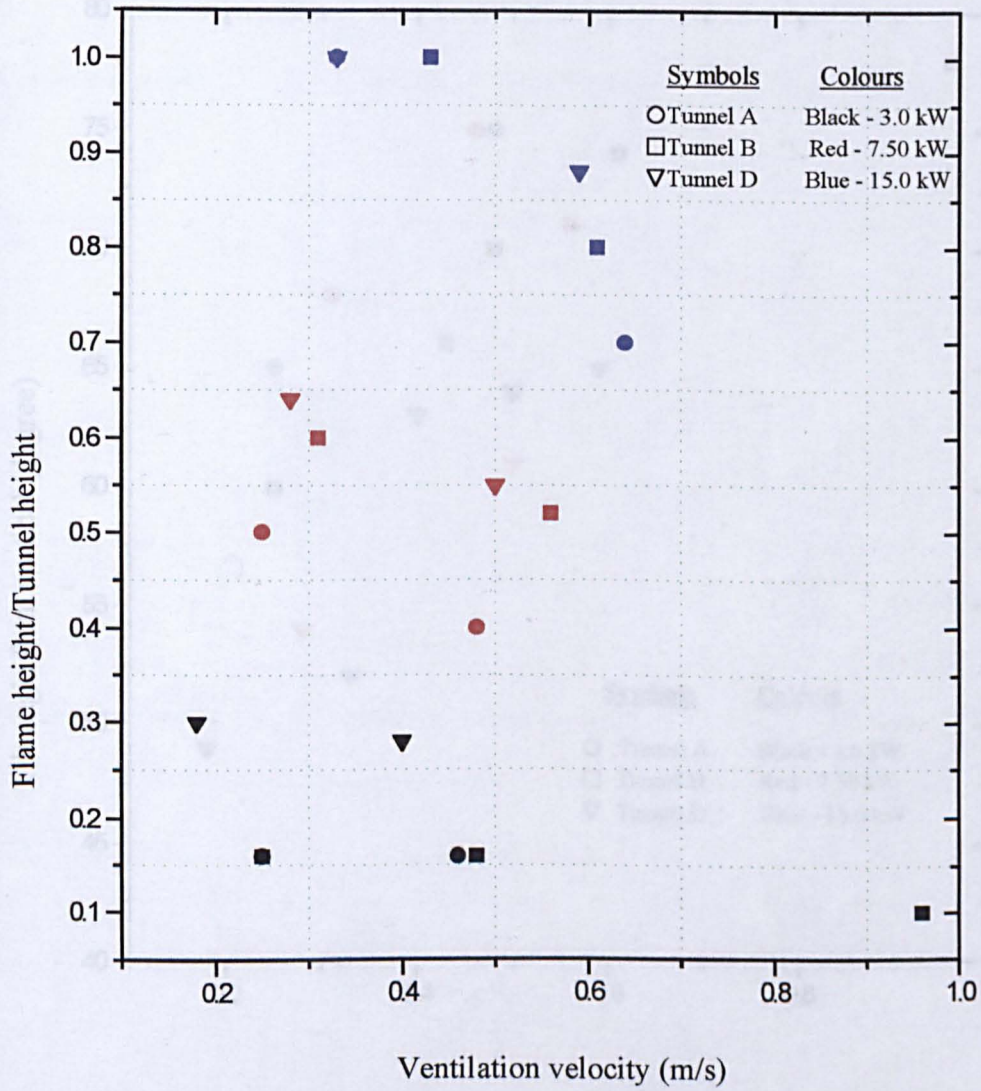
Figure 7.7 : Variations of flame height against ventilation velocity
based on 500 °C persistent flame
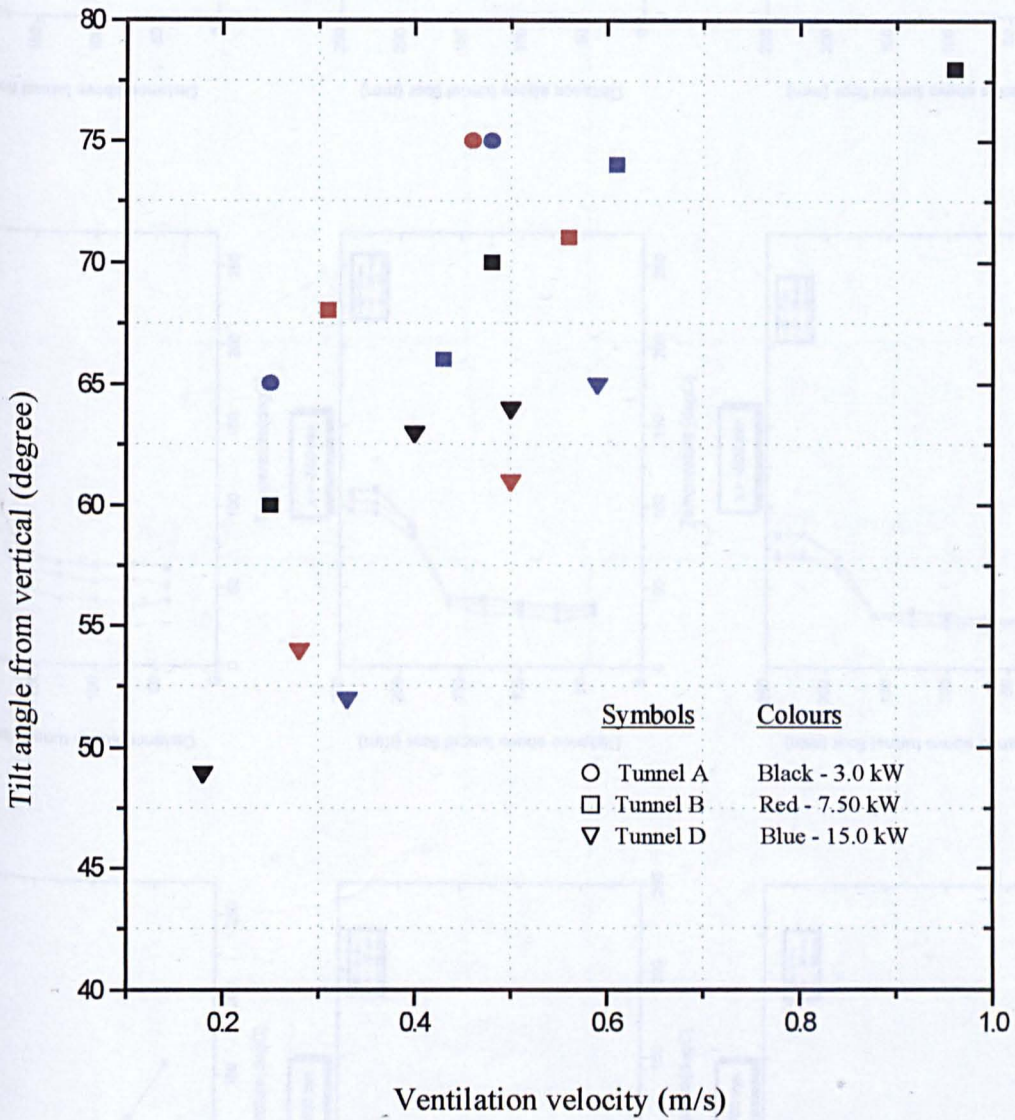
Figure 7.8 : Variations of flame tilt angle against ventilation velocity
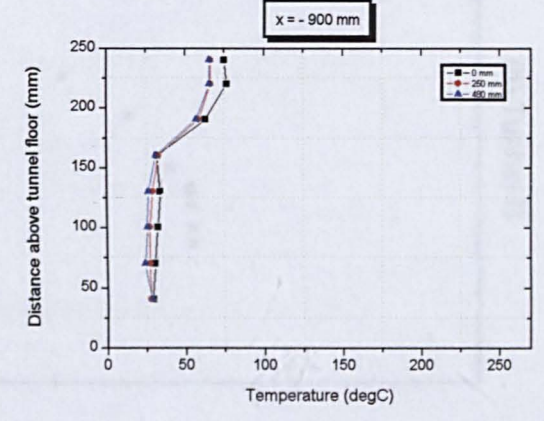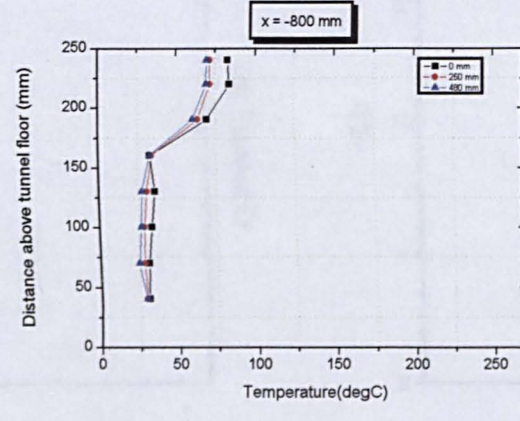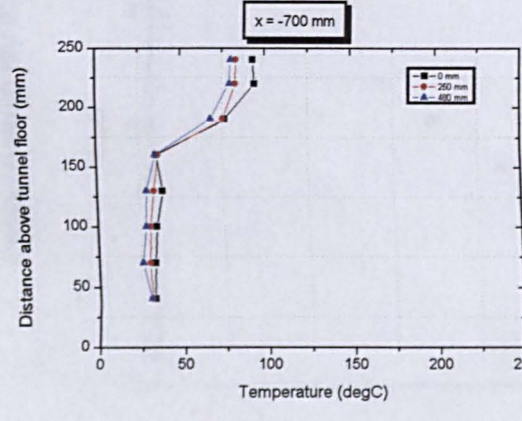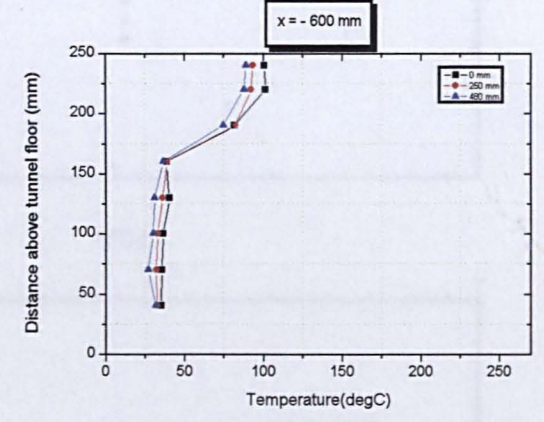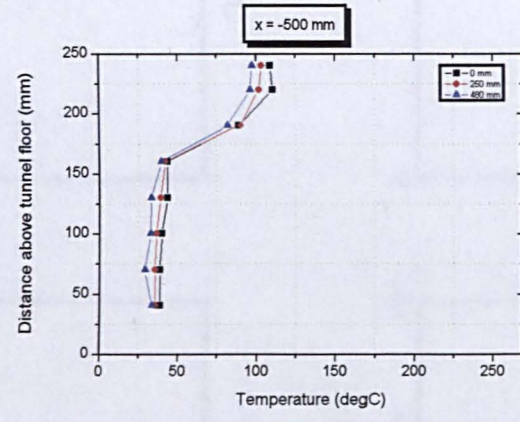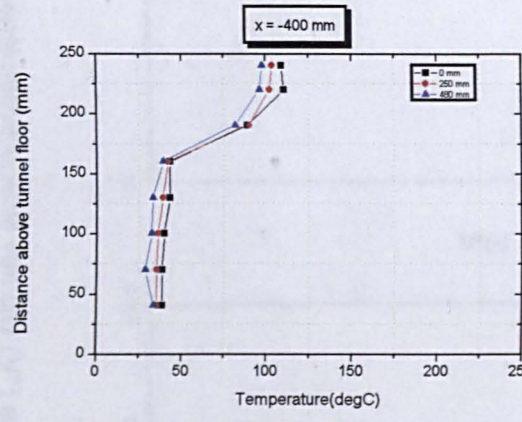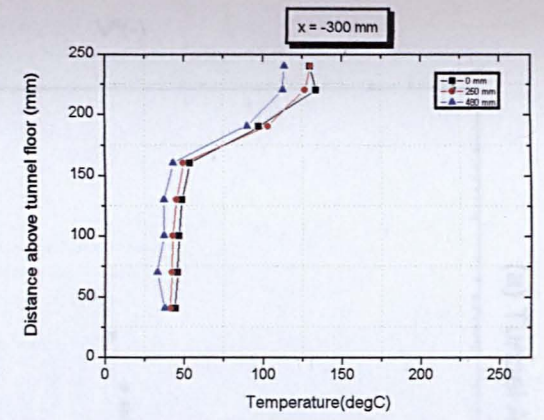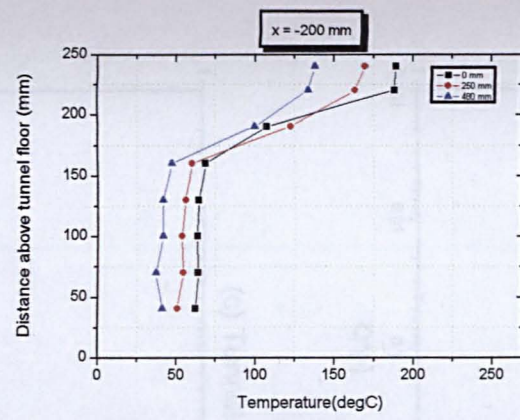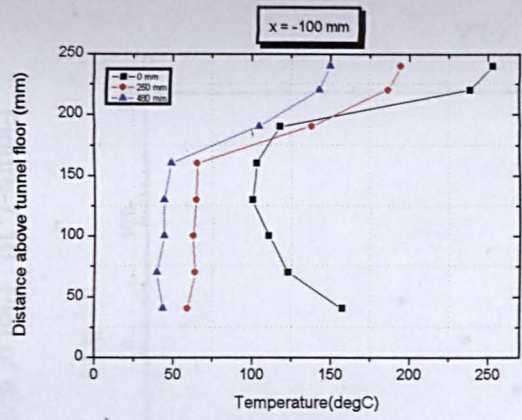
Figure 7.9 : Measured temperature distribution in the backlayering in tunnel D at 7.50 kW at three cross-sectional distances
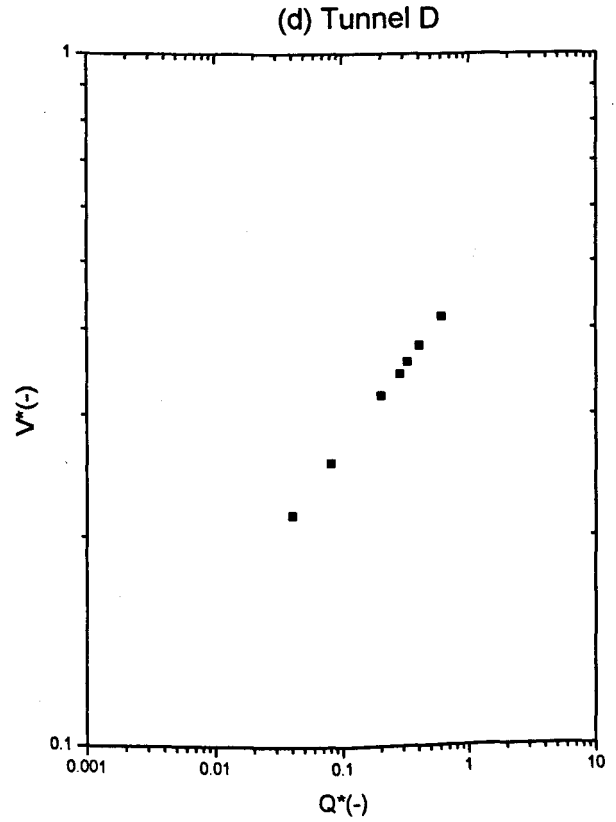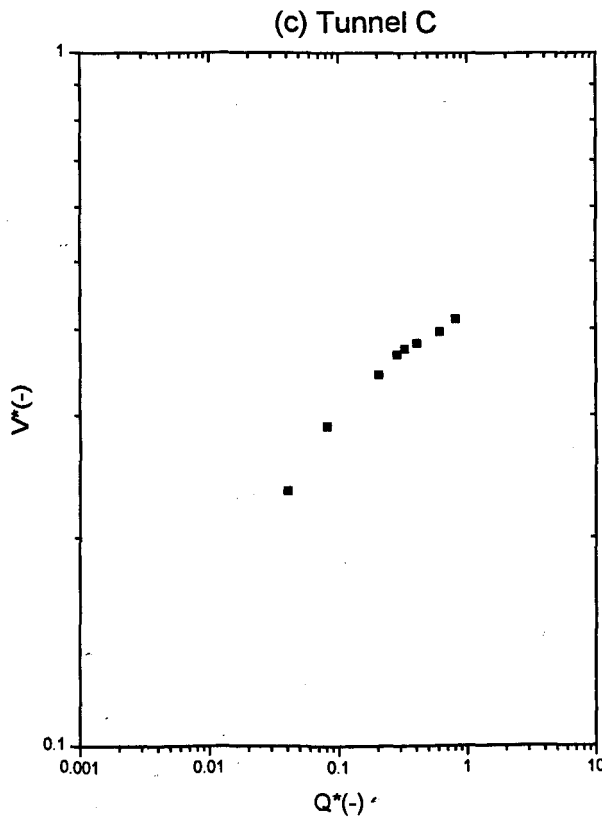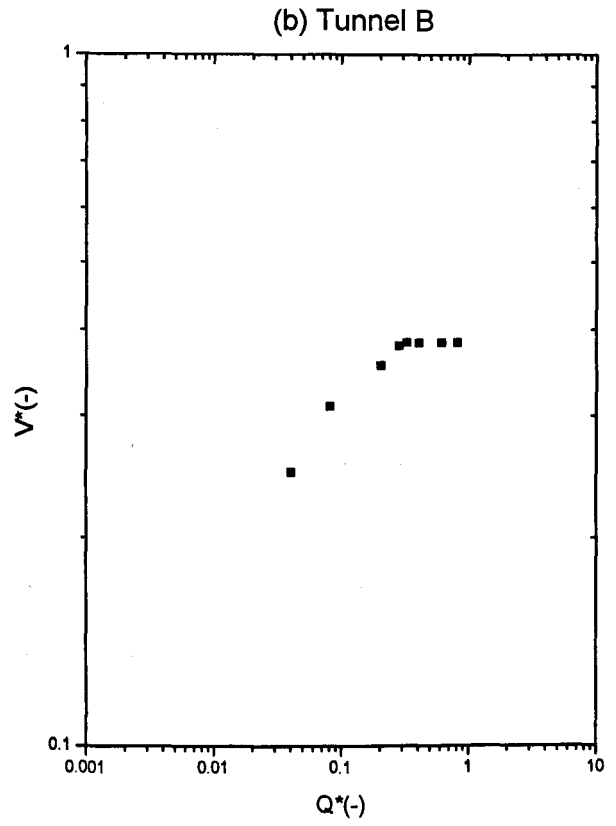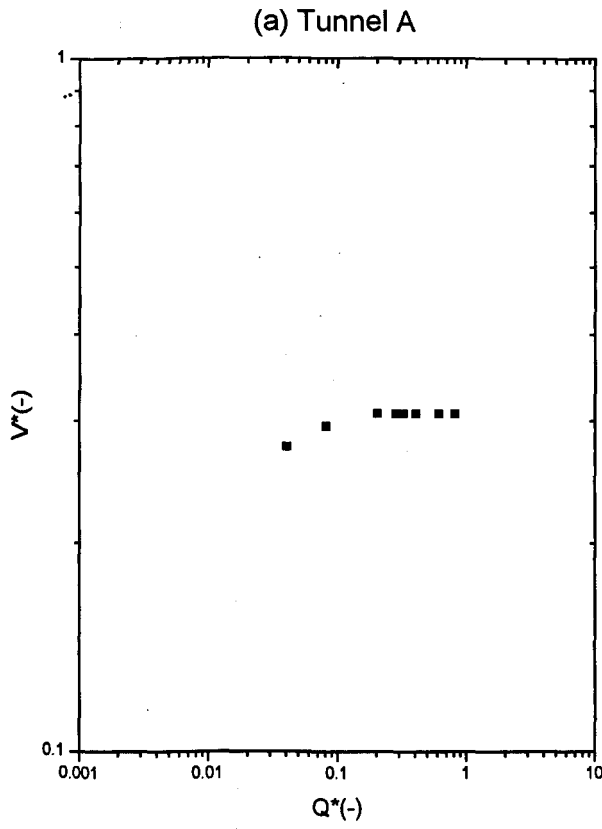
Figure 7.10 : Plot of dimensionless critical velocity (V*) against dimensionless
heat release rate(Q*) based on tunnel height
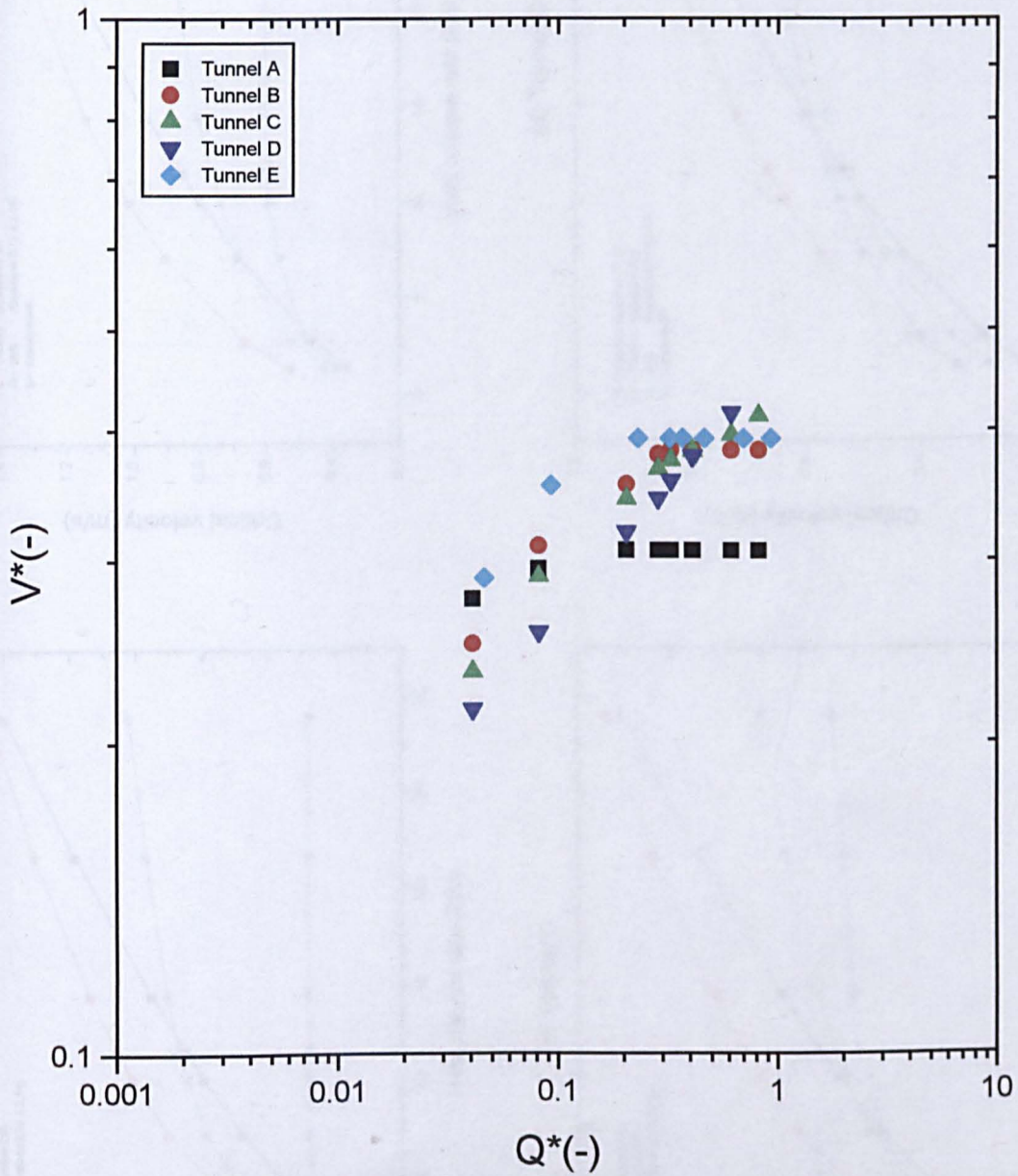
Figure 7.11 : Plot of dimensionless critical velocity (V*) against dimensionless heat release rate (Q*) for the five model tunnels
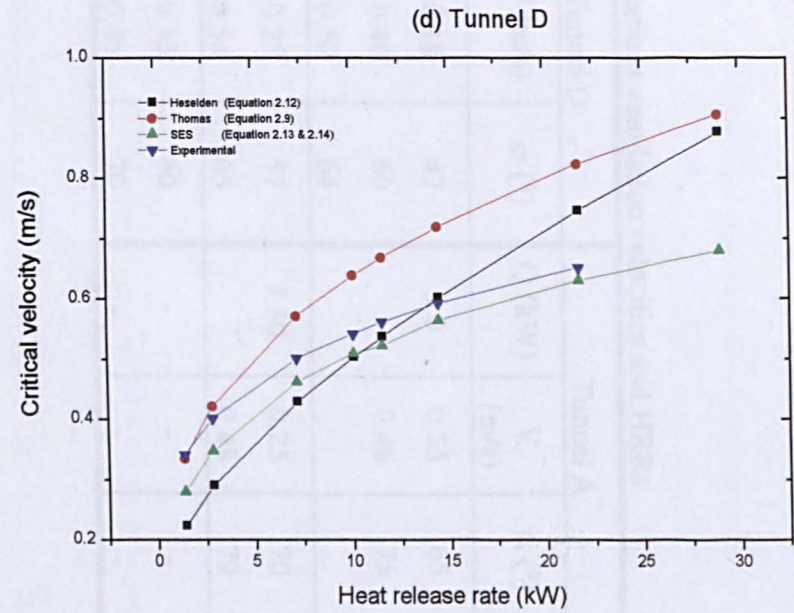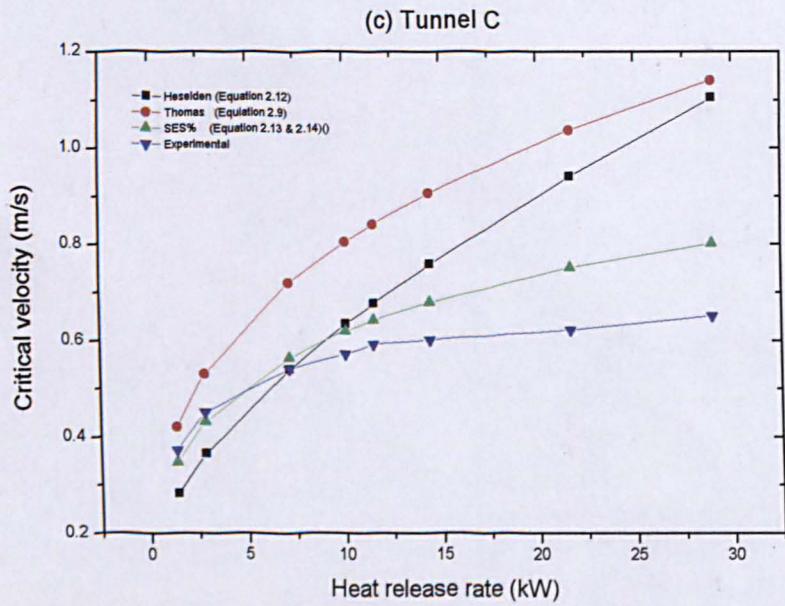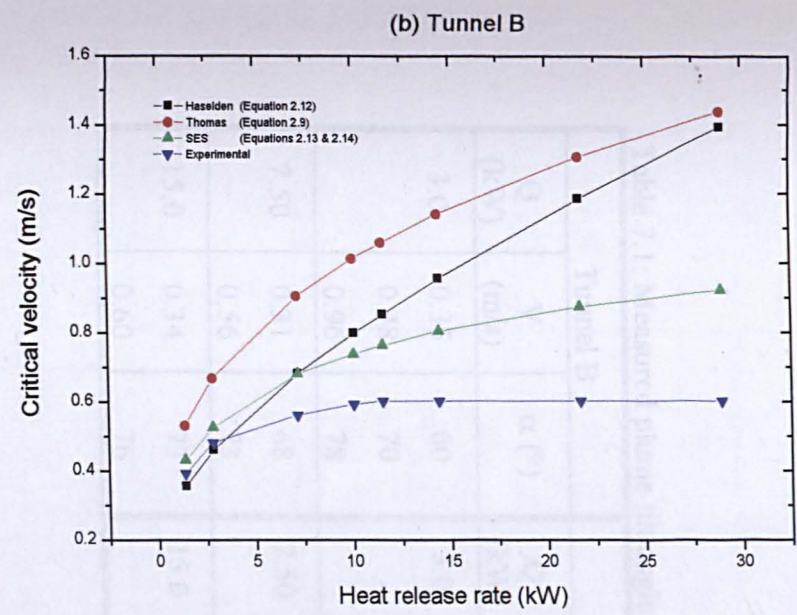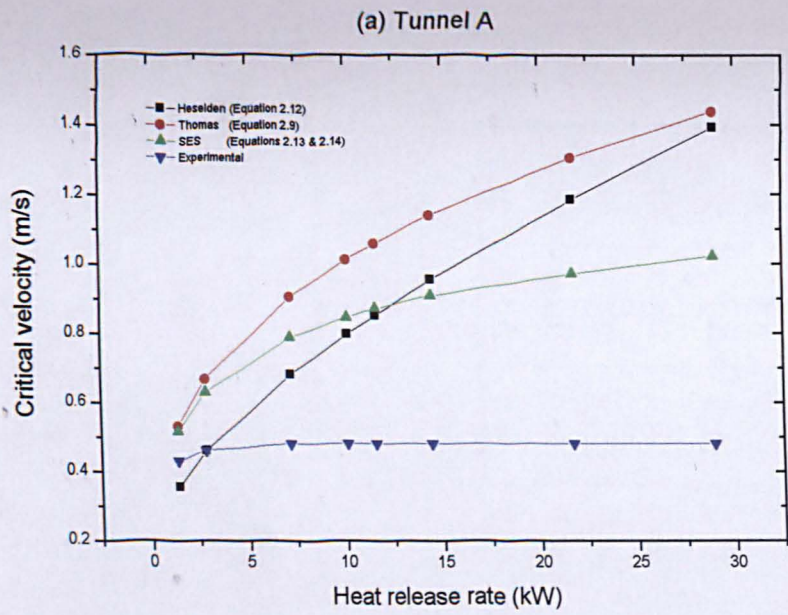
Figure 7.12 : Comparison of critical ventilation velocity obtained in the experiment with various correlations

Table 7.1: Measured plume tilt angle at various ventilation velocities and HRRs

Tunnel B			Tunnel D			Tunnel A		
Q (kW)	V (m/s)	α (°)	Q (kW)	V (m/s)	α (°)	Q (kW)	V (m/s)	α (°)
3.0	0.35	60	3.0	0.18	47	3.0	0.25	65
	0.48	70		0.40	60		0.46	75
	0.96	78		0.50	64			
7.50	0.31	68	7.50	0.28	57	7.50	0.25	70
	0.56	73		0.54	65		0.48	79
15.0	0.34	73	15.0	0.35	60	-	-	-
	0.60	76		0.65	70	-	-	-

Table 7.2: Dimensionless heat release rate (Q*)

Q (kW)	Tunnel A Q*	Tunnel B Q*	Tunnel C Q*	Tunnel D Q*	Tunnel E Q*
1.50	0.041	0.041	0.041	0.041	0.044
3.00	0.082	0.082	0.082	0.082	0.087
7.50	0.205	0.205	0.205	0.205	0.218
10.50	0.288	0.288	0.288	0.288	0.306
12.00	0.329	0.329	0.329	0.329	0.349
15.00	0.411	0.411	0.411	0.411	0.436
22.50	0.616	0.616	0.616	0.616	0.655
30.00	0.822	0.822	0.822	0.822	0.873

Table 7.3: Dimensionless critical ventilation velocity (V*)

Tunnel A V(m/s)	V*	Tunnel B V(m/s)	V*	Tunnel C V(m/s)	V*	Tunnel D V(m/s)	V*	Tunnel E V(m/s)	V*
0.43	0.275	0.39	0.248	0.37	0.233	0.34	0.215	0.44	0.288
0.46	0.294	0.48	0.309	0.45	0.289	0.40	0.255	0.54	0.353
0.48	0.307	0.56	0.354	0.54	0.343	0.50	0.319	0.60	0.393
0.48	0.307	0.59	0.379	0.57	0.367	0.54	0.344	0.60	0.393
0.48	0.307	0.60	0.382	0.59	0.374	0.56	0.358	0.60	0.393
0.48	0.307	0.60	0.382	0.60	0.381	0.59	0.377	0.60	0.393
0.48	0.307	0.60	0.382	0.62	0.395	0.65	0.415	0.60	0.393
0.48	0.307	0.60	0.382	0.65	0.413	-		0.60	0.393

$$Q^* = \frac{Q}{\rho_o T_o C_p g^{\frac{1}{2}} H^{\frac{5}{2}}} \qquad V^* = \frac{U_c}{\sqrt{gH}}$$

Table 7.4: Measured and predicted critical velocities for tunnel A

Q (kW)	Tf (K)	Critical Velocities (m/s)			
		Measured	Thomas[1]	Heselden[2]	SES[3]
1.50	373	0.43	0.65	0.45	0.52
3.00	435	0.46	0.82	0.59	0.63
7.50	635	0.48	1.11	0.91	0.79
10.50	770	0.48	1.24	1.09	0.85
12.00	837	0.48	1.29	1.17	0.87
15.00	972	0.48	1.39	1.32	0.91
22.50	1310	0.48	1.59	1.67	0.97
30.00	1647	0.48	1.76	1.98	1.02

Table 7.5: Measured and predicted critical velocities for tunnel B

Q (kW)	Tf (K)	Critical Velocities (m/s)			
		Measured	Thomas[1]	Heselden[2]	SES[3]
1.50	340	0.39	0.53	0.35	0.43
3.00	374	0.48	0.67	0.46	0.53
7.50	453	0.56	0.90	0.67	0.68
10.50	504	0.59	1.01	0.77	0.74
12.00	533	0.60	1.06	0.82	0.76
15.00	592	0.60	1.14	0.92	0.80
22.50	740	0.60	1.30	1.13	0.87
30.00	887	0.60	1.44	1.32	0.92

(1) $U_c = k \left(\dfrac{gQ'}{\rho_o C_p T} \right)^{1/3}$

(2) $U_c = CK \left(\dfrac{gQT}{C_p \rho_o T_o^2 W} \right)^{1/3}$

(3) $U_c = K_g k \left(\dfrac{gQ}{C_p \rho_o T \ W} \right)^{1/3}$

$$T = \left(\frac{Q}{C_p \rho_o A U_c} \right) + T_o$$

Table 7.6: Measured and predicted critical velocities for tunnel C

Q (kW)	Tf (K)	Critical Velocities (m/s)			
		Measured	Thomas[1]	Heselden[2]	SES[3]
1.50	321	0.37	0.42	0.28	0.35
3.00	337	0.45	0.53	0.35	0.43
7.50	379	0.54	0.72	0.50	0.56
10.50	404	0.57	0.80	0.57	0.62
12.00	415	0.59	0.84	0.60	0.64
15.00	443	0.60	0.90	0.66	0.68
22.50	505	0.62	1.04	0.79	0.75
30.00	566	0.65	1.14	0.90	0.80

Table 7.7: Measured and predicted critical velocities for tunnel D

Q (kW)	Tf (K)	Critical Velocities (m/s)			
		Measured	Thomas[1]	Heselden[2]	SES[3]
1.50	310	0.34	0.33	0.22	0.28
3.00	319	0.40	0.42	0.27	0.35
7.50	340	0.50	0.57	0.38	0.46
10.50	353	0.54	0.64	0.43	0.51
12.00	358	0.56	0.67	0.45	0.52
15.00	371	0.59	0.72	0.49	0.56
22.50	398	0.65	0.82	0.58	0.63

(1) $Uc = k\left(\dfrac{gQ'}{\rho_o C_p T}\right)^{1/3}$

(2) $Uc = CK\left(\dfrac{gQT}{C_p \rho_o T_o^2 W}\right)^{1/3}$

(3) $Uc = K_g k\left(\dfrac{gQ}{C_p \rho_o T\ W}\right)^{1/3}$

$T = \left(\dfrac{Q}{C_p \rho_o A U_c}\right) + T_o$

Chapter 8

Computational Fluid Dynamics Study

of the Smoke Flow

This chapter describes the three dimensional CFD simulations of the smoke flow in the tunnels. The main objectives are to study the flow behaviour in the tunnels and to investigate the dependence of the critical ventilation velocity on tunnel aspect ratio and the HRR. Detailed simulations have been carried out in the first four tunnels **A** to **D**, which have exactly the same height. The CFD simulations for the tunnel **E** were only performed during the initial stage where the fire was represented by heat source. The comprehensive comparisons between CFD results with experimental results have also been carried out.

The three dimensional simulations have been systematically performed. These include the selections of the combustion models and the optimisation in the buoyancy related term in the standard k-ε turbulence model. Finally, the numerical error was reduced by performing grid sensitivity tests.

8.1   Computational Models

In general, both Finite Rate Formulation (FRT) and Mixture Fraction Approach (PDF) combustion models have been tested. The flow inside the tunnel was modelled using standard k - ε turbulence model with the buoyancy force modification.

The FLUENT V.4.5 package which is available in the University of Sheffield has been used to model the flow and the combustion inside the tunnels. The governing transport equations of mass, momentum, energy and chemical species as follows:

(1) The Conservation of Mass

$$\frac{\partial \rho}{\partial t} + \frac{\partial}{\partial x_i}(\rho u_i) = 0 \qquad (8.1)$$

(2) The Conservation of Momentum

$$\frac{\partial}{\partial t}(\rho u_j) + \frac{\partial}{\partial x_i}(\rho u_i u_j) = \frac{\partial}{\partial x_i}\left(\mu\left[\frac{\partial u_i}{\partial x_j} + \frac{\partial u_j}{\partial x_i}\right]\right) - \frac{\partial p}{\partial x_j} + \rho g_i + F_j \qquad (8.2)$$

where:

ρ is the fluid mixture density; t is time variable; u_i is the velocity component in the i-direction; x_i is co-ordinates with $I = 1,2,3$ corresponding to rectangular co-ordinates x, y, z; p is fluid pressure; g is the gravitational acceleration and F_j is momentum transferred from second phase. The left hand side of equation (8.2) represents the convection term, and the first term on the right hand side represents diffusion. The remaining terms represent pressure, body force such as gravity, and the momentum interaction between the two phases.

(3) Standard k - ε Model and Buoyancy Effect

Standard k-ε turbulence model was used to model the flow inside the tunnels due to its simplicity and effectiveness. The standard k-ε turbulence model (Launder and Spalding, 1974) includes basic modifications for buoyancy based on Ljuboja and Rodi (1980, 1981) in the k-ε equation. The standard k-ε model is a two equations eddy viscosity turbulence model which transport equations for two variables: k the turbulence energy, and ε the rate of viscous dissipation of turbulence energy. The turbulent effective viscosity, μ_t, is related to k and ε, by a velocity scale ($k^{1/2}$) and a length scale ($k^{3/2}/\varepsilon$) by the expression:

$$\mu_t = \rho C_\mu \frac{k^2}{\varepsilon} \qquad (8.3)$$

and the velocity and length scales are predicted at each point in the flow via the solution of transport equations for k and ε:

$$\frac{\partial}{\partial x_i}\left(\rho u_i k\right) = \frac{\partial}{\partial x_i}\frac{\mu}{\sigma_k}\frac{\partial k}{\partial x_i} + G_k + G_b - \rho\varepsilon \qquad (8.4)$$

and

$$\frac{\partial}{\partial x_i}\left(\rho u_i \varepsilon\right) = \frac{\partial}{\partial x_i}\frac{\mu}{\sigma_\varepsilon}\frac{\partial \varepsilon}{\partial x_i} + C_1\frac{\varepsilon}{k}(G_k + (1-C_{3\varepsilon})G_b - C_2\rho\frac{\varepsilon^2}{k} \qquad (8.5)$$

Turbulence is generated according to G_k, where:

$$G_k = \mu_t\left(\frac{\partial u_j}{\partial x_i} + \frac{\partial u_i}{\partial x_j}\right)\frac{\partial u_j}{\partial x_i} \qquad (8.6)$$

and G_b is the generation due to buoyancy:

$$G_b = -g_i\frac{\mu_t}{\rho\sigma_h}\frac{\partial \rho}{\partial x_i} \qquad (8.7)$$

where σ_h is the turbulent Prandtl number, $\dfrac{\mu_t C_p}{k_t}$

and C_1, C_2, C_μ, σ_k and σ_ε are empirical constants, with values, 1.44, 1.92, 0.09, 1.0 and 1.3 respectively. The default value for $C_{3\varepsilon}$ is 1.0. This implies that the buoyancy effects go to zero in equation (8.5).

Woodburn and Britters (1996) used $C_{3\varepsilon}$ equal to 0.20 and showed that the inclusion of the modified buoyancy gave better predictions between the measured and predicted results. In Fletcher et al (1994), and Lea (1995), the values of $C_{3\varepsilon}$ were not reported. The present work set the value of $C_{\varepsilon 3}$ in the k-ε equations equal to 0.25. The decision to use this value will be discussed in Section 8.3.3.

(4) Energy Conservation

FLUENT solves the energy equation in the form of a transport equation for enthalpy, h. For steady state, the Convection of the Heat through local volume will be equal to the Diffusion of enthalpy minus the Diffusion of species with enthalpy minus Shear force, which gives the equation (8.8).

$$\frac{\partial}{\partial x_i}(\rho u_i h) = \frac{\partial}{\partial x_i}(k+k_t)\frac{\partial T}{\partial x_i} - \frac{\partial}{\partial x_i}\sum_j h_i J_{ji} + \frac{D_p}{Dt} - \tau_{ik}\frac{\partial u_i}{\partial x_k} + S_h \tag{8.8}$$

where,

k is the molecular conductivity; k_t is the effective conductivity due to turbulent transport; h_j is enthalpy of species j; J_{ji} is flux of species j in the ith direction and S_h is the source term. (includes heat of reaction, radiation, any exchange of heat, and any other volumetric sources).

Enthalpy is defined as the summation of the products mass fraction of species and the specific heat capacity of species at constant pressure, being described in equations (8.9) and (8.10):

$$h = \sum_j X_j h_j \tag{8.9}$$

where:

$$h_j = \int_{T_{ref}}^{T} c_{p,j} dT \qquad (8.10)$$

X_j is the mass fraction of species j ; $c_{p,j}$ is the specific heat capacity of species j at constant pressure.

This enthalpy term can be used to rewrite the heat flux term in equation (8.11):

$$k \frac{\partial T}{\partial x_i} = \frac{k}{c_p} \left(\frac{\partial h}{\partial x_i} - \sum_j h_j \frac{\partial X_j}{\partial x_i} \right) \qquad (8.11)$$

where c_p is the mixture heat capacity, $c_p = \Sigma_j X_j c_{pj}$.

Equation (8.11) then is substituted into equation (8.8) and the result is modified due to the compressible flow, by solving for the total enthalpy, h_o, defined as $h_o = h + v^2/2$, and the result is shown below equation (8.12).

$$\frac{\partial}{\partial x_i}(\rho u_i h_o) = \frac{\partial}{\partial x_i} \frac{k + k_t}{c_p} \left(\frac{\partial(h_o - v^2/2)}{\partial x_i} - \sum_j h_j \frac{\partial X_j}{\partial x_i} \right)$$

$$- \frac{\partial}{\partial x_i} \sum_j (h_j J_{jii}) - \frac{\partial}{\partial x_i}(\tau_{ik} u_k) + S_h \qquad (8.12)$$

(5) Combustion Models

In the combustion modelling, propane gas has been used as the fuel. The combustion was considered as stoichiometric reaction shown in equation (8.13).

$$C_3H_8 + 5CO_2 \Rightarrow 3CO_2 + 4H_2O \qquad (8.13)$$
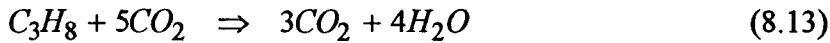
There are two alternative combustion models provided by FLUENT.

(a) Generalised Finite-Rate Formulation (FRF)

This model incorporates both Arrhenius expression and eddy-dissipation concept of Magnussen and Hjertager (1976). The reaction rates are computed from Arrhenius rate expressions (equation 8.14).

$$R_{i',k} = -v'_{i',k} M_{i'} T^{\beta_k} A_k \prod_{j'\,reac\tan ts} C_{j'}^{v_{j'k}} \exp\left(-E_k / RT\right) \qquad (8.14)$$

where $v'_{i',k}$ is the molar stoichiometric coefficient for species I' in reaction k (positive value for reactants, negative values for products); $M_{i'}$ is the molecular weight of species I' (kg/kmol); β_k is the temperature exponent (dimensionless); A_k is the pre-exponential factor (consistent unit); $C_{j'}$ is the molar concentration of each reactant species j' (kmol/m^3); $v_{j'k}$ is the exponent on the concentration of reactant j' in reaction k and E_k is the activation energy for the reaction (J/kmol).

The inputs required for equation (8.14) are as follow:

Physical constants

Species	Molecular Weight (M) (kg/kmol)	Formation Enthalpy (J/kmol)
C_3H_8	44.0	-1.0468×10^8
O_2	32.0	0
CO_2	44.0	-3.937×10^8
H_2O	18.0	-2.419×10^8
N_2	28.0	0

Reaction constants

Arrhenius constant (A_k)	1.8×10^{-5} kgm^{-2}s^{-1} atm^{-1}
Activation Energy (E_k)	1.8×10^{-12} J/kmol
Temperature exponent (β_k)	0.0
Rate exponent (C_3H_8)	1.0
Rate exponent (O_2)	1.0

The influence of turbulence on the reaction rate is taken into account by employing the Magnussen and Hjertager model (1976). In this model, the rate of reaction $R_{i',k}$ is given by the smallest (i.e. limiting value) of the two expressions in equations (8.15) and (8.16).

$$R_{i',k} = -v'_{i',k} M_{i'} A \rho \frac{\varepsilon}{k} \frac{m_R}{v'_{R,k} M_R} \tag{8.15}$$

$$R_{i',k} = -v'_{i',k} M_{i'} A B \rho \frac{\varepsilon}{k} \frac{m_R}{v'_{R,k} M_R} \tag{8.16}$$

where m_P represents the mass fraction of any product species, P; m_P represents the mass fraction of a particular reactant, R; R is the reactant species giving the smallest vales of $R_{i',k}$; A is an empirical constant equal to 4.0 and B is an empirical constant equal to 0.5.

(b) Mixture Fraction/ PDF Modelling Approach.

In this model, the individual concentrations for the species of interest are derived from the predicted mixture fraction distribution, $\bar{f}$. The reacting system is treated using either chemical equilibrium calculations or using infinitely fast chemistry (the flame sheet or mixed -is-burned approach). Physical properties of the chemical species and equilibrium data are obtained from a chemical database, eliminating the to define them. The mean mixture fraction is calculated using equation 8.17.

$$\frac{\partial}{\partial t}\left(\rho \bar{f}\right) + \frac{\partial}{\partial x_i}\left(\rho u_i \bar{f}\right) = \frac{\partial}{\partial x_i}\left(\frac{\mu_t}{\sigma_t}\frac{\partial \bar{f}}{\partial x_i}\right) + S_m \qquad (8.17)$$

The source term, Sm, is due solely to transfer of mass into the gas phase from liquid fuel droplets or reacting particles (e.g., coal). In all other cases there are no sources of *f*. In addition to solving for the mean mixture fraction, FLUENT solves a conservation equation for mixture fraction variance, f'^2.

$$\frac{\partial}{\partial t}\left(\rho \bar{f'^2}\right) + \frac{\partial}{\partial x_i}\left(\rho u_i \bar{f'^2}\right) = \frac{\partial}{\partial x_i}\left(\frac{\mu_t}{\sigma_t}\frac{\partial \bar{f'^2}}{\partial x_i}\right) + C_g \mu_t \left(\frac{\partial \bar{f'^2}}{\partial x_i}\right) - C_d \rho \frac{\varepsilon}{k}\bar{f'^2} \qquad (8.18)$$

where the constant σt, Cg and Cd take the value 0.7, 2.86 and 2.0, respectively. The mixture fraction variance is used in the closure model describing turbulence-chemistry interaction.

To model the combustion of propane in the PDF approach, the first stage was to create PDF file by using prePDF software. Initially, an Adiabatic case model with Stoichiometric Reaction was defined. Beta PDF was selected since it gave better prediction to the experimental results. The chemical species, C_3H_8, O_2, CO_2, H_2O and N_2 were then added to the case model (single step reaction). The composition and

operating conditions of the inlet fuel (C_3H_8) and oxidiser stream (O_2 and N_2) were then defined. The input file was then saved and adiabatic calculation was performed. The solution was then saved as the output file (PDF). The results of the adiabatic calculation were then examined in order to obtain insight into the system description that would be used for the non-adiabatic calculation. A look up table which consists of the temperature, density and species mole fractions were then generated and will be used to solve equations (8.17) and (8.18) in FLUENT.

8.2 CFD Simulations

Three dimensional simulations of the smoke flow in most of the model tunnels have been carried out in two stages. During the initial stage, the combustion was not modelled, the fire was represented by heat source. This involved only tunnels **B, C** and **E**. The main objective was to test parameters such as the k - ε model and the buoyancy modified term, grid analysis, boundary conditions and physical properties. In the second stage, the detailed modellings were carried out on tunnels **A, B, C. D** which have exactly the same height but different widths. To save the computational time, the flow was assumed to be symmetrical at the tunnel axis, hence only one-half of the cross-section was modelled.

The following sections discuss the detailed CFD simulations using combustion models.

8.2.1 Set Up of Computational Domain

The total simulated tunnel length was 8.1 metres with the exclusion of a downstream section of 3.0 m length. The longitudinal computational domain was divided into three segments. Segment 1 was the upstream section of length 5.0 m. Segment 2 was the burner section of length 0.1 m and segment 3 was the downstream section of length 3.0 m. The first plane of the longitudinal domain was set to be inlet of the ventilation flow and the last plane was set as the output of the smoke flow to the exhaust. The wall of the tunnel was set to be a solid which contains 1 cell.

A non uniform grids distribution was made to avoid a very large number of computational cells while maintaining a sufficient degree of accuracy in the solution. The spacing between the adjacent grid lines was set according to the recommended guidelines which should not change by more than 20 percent or 30 percent from one grid line to the next. The expansion factors were kept between 0.7 and 1.3 and the aspect ratio of the most cells are less than 5:1. The longitudinal and vertical grids were set at 102 and 28 cells, respectively. The half cross-sectional cells varying from 8, 14, 28 and 38, dependent on tunnel widths. The total cells for simulated models are, 22848, 39984, 79968 and 108528 for tunnels **A**, **B**, **C** and **D**, respectively. Figure 8.1 shows the longitudinal grid distribution for the tunnels. Figures 8.2 to 8.5 show the cross-sectional grids for each tunnel.

Some of the simplifications that were made:

(1) The circular burner was simulated as a square burner with the same burning area (0.008825 m^2).

(2) The ventilation flow has been modelled by setting the flow of air at the tunnel inlet uniformly through out the whole cross-sectional area.

(3) The tunnel wall was modelled as insulation wall therefore no heat loss was considered.

8.2.2 Boundary Conditions

Flow inlets boundary conditions was defined via velocity and temperature specifications. The velocity values are calculated from the known mass flow rate and the density.

Stream 1 : Air inlet

The inlet air velocity was first set according to the experimental value. The inlet temperature was set to 298K. The turbulence intensity for air stream was set between 5 percent to 10 percent as recommended by FLUENT. The characteristic length varies from 0.17, 0.25, 0.33 and 0.44 m for tunnels **A**, **B**, **C** and **D**, respectively.

Stream 2: Propane Inlet

Stream 2 was set to be 100 percent mole fraction of C_3H_8 at the temperature of 298K. The flow rate was converted from litre per min into the unit of m/s. The turbulent intensity was kept around 1 percent. The characteristic length was set to 0.006.

Calculation of propane velocity

1 mol of C_3H_8 gas occupy 22.4 litre (Himmelblau, 1982)

Consider density of C_3H_8 is 1.82 kg/m^3 at 298 K (PPDS)

Relative molecular weight = 44.0 kg/kmol

Thus 1 litre/min $= (1/22.4) \times 44$ g/min

$= 3.274 \times 10^{-5}$ kg/s

Volumetric flow rate $= \dfrac{\text{mass flowrate}}{\text{density}} = \dfrac{3.274 \times 10^{-5}}{1.82}$

$= 1.7988 \times 10^{-5}$ m^3/s

Velocity $= \dfrac{\text{volumetric flowrate}}{\text{burner area}}$

$= \dfrac{1.7988 \times 10^{-5}}{8.825 \times 10^{-3}}$

Velocity for 1 litre/min $= \dfrac{1.7988 \times 10^{-5}}{8.825 \times 10^{-3}}$ m/s

$= 20.38 \times 10^{-3}$ m/s

8.2.3 Physical Properties

In Finite Rate Formulation, the physical properties of each reactant and product (density, viscosity, heat capacity and thermal conductivity) were expressed in term of polynomial up to second order. The value for each coefficient are listed in Table E1 in Appendix E. However, in PDF approach, all the properties are obtained from the look-up tables generated by prePDF. Therefore no input is needed in FLUENT.

8.3 Simulation Procedures

The simulation cases and conditions are shown in Table 8.1. Only steady state combustion has been modelled. The radiation sub-model had not been included in the present work since previous CFD publications have shown although radiation effects are important in tunnel fire, it did not give the significant effects on the prediction of the smoke movement, especially, the extension of the backlayering flows. In addition, the combustion of propane in air was considered to be clean. The present works also avoided radiation modelling since it consumed a lot of computational time.

The solutions were solved by using First Order Discretization. Conservation of mass was obtained by using SIMPLER pressure correction algorithm. All convection terms were discretised using hybrid differencing for stability.

With the inclusion of body force and buoyancy term in standard k - ε turbulence model, it would be expected that there would be a fluctuating in the solution residuals which results to the difficulties for the solutions to converge. A good strategy was to set the underrelex factors at lower values in the initial stage to maintain the solution stability. The underrelax factors for all parameters during the simulations are summarised in Table 8.2.

The convergence typically reached after approximately 2000 iterations for tunnels **A** and **B** if the simulation was started from scratch. However, for tunnels **C** and **D**, the convergence result reached after more than 2000 iterations. It was observed that at higher ventilation velocity (no backlayering flow), the solutions were easy to converge. However, when the ventilation velocity was set to lower value, at which the backlayering propagating to the upstream, the solutions were very difficult to converge.

A final total of 39 cases have been modelled in the present study. Each case took approximately one day for the convergence by using SUN Workstation version 5.4

(after the initial range of critical ventilation velocity was found). The critical ventilation velocity was achieved when the backup contour of 298 K reaches the leading edge of the burner. The initial value of the ventilation velocity was set according to the experimental results. If the critical ventilation velocity was not reached, new simulations were performed by reducing the ventilation velocity within 0.005 m/s until the critical ventilation velocity reached.

8.3.1 Selection of the Combustion Models

To select the combustion model, 4 cases were modelled on tunnel **B** at HRRs 3.0 kW and 7.50 kW .

Case SR2 and SR3 (FRF) : Initially, the propane and air mixture were difficult to burn and maintain at the burner surface. As the calculation progressed, the flame shifted away from the burner to the downstream. This behaviour might be due to lack of mixing between propane and air at the burner region. In the simulations, the calculated propane velocity was in order of 10^{-3} m/s, whilst the velocity of the air was in the order of 0.3-0.6 m/s. As consequences, there might be a sudden change or sharp velocity gradient in the burner region. This problem was overcome by making a high density grid, particularly in the area just above the burner. The same number of grid was used vertically, but the compression ratio was increased at 1.5 times of the original value.

Case SR4 and SR5 (PDF): Unlike Finite Rate Formulation, the combustion has been successfully modelled without any modifications of the grid.

The critical ventilation velocities for SR2 and SR3 (FRF) were found to be 0.36 m/s and 0.40 m/s, respectively. Whilst, the critical ventilation velocities for SR4 and SR5 (PDF) were 0.40 m/s and 0.47 m/s, respectively. The measured values from the experiment were 0.48 m/s and 0.56 m/s, respectively.

The steady state temperature distributions at tunnel centreline for HRR 3.0 kW are shown in Figures 8.6a and 8.6b, respectively. Both figures show that the temperature distribution are almost identical for the two combustion models. The XY plots of the temperature profiles at various distances from the burner in Figure 8.7 also confirmed

the variations. Both models predict the same pattern of temperature profiles, except closed to the fire.

For further simulations, it has been decided that PDF approach should be used mainly for two main reasons. First, it predicts the critical ventilation velocity closed to the experimental results. Second, the simulations were more effective since the computing time was relatively shorter than Finite Rate. The availability of all the physical properties of the reactants and products in the computer databank give the additional advantage.

8.3.2 Grid Sensitivity Test

Solution in which truncation error or numerical diffusion are normally termed as grid independent. If the grid is refined until the solution no longer varies with additional grid refinement, then it can be said that a grid independent solution is achieved. Thus before further calculation, grid sensitivity tests have been made for the four tunnel models at 3.0 kW fire. For each tunnel, three grids have been setup, starting from the coarse grid. The total cells in the three grid setup are summarised in Table 8.3.

Figures 8.8 to 8.11 show the plot of velocity profiles for each tunnel at various distances for the burner for the three grids setup. It can be observed that the profiles for both grids 2 and 3 are quite similar. Thus, it can be concluded that grid 2 was adequate in the present study.

8.3.3 Effect of Inclusion/Exclusion Buoyancy Term

The inclusion of buoyancy term in the standard k-ε turbulence model is crucial in tunnel modelling as pointed out by Fletcher (1994), Woodburn and Britter (1996) and Lea(1995). The basic modifications reduce turbulent mixing in the presence of a stable density gradient by returning locally-lowered values of turbulent viscosity, and vice-versa for unstable density gradients (Lea, 1995). In the bulk flow, buoyancy forces disturb the simple picture of isotropic turbulence assumed by the k-ε model. Turbulent mixing in a

rising plume is enhanced by buoyancy whilst in a stable stratified ceiling layer it will be inhibited.

As stated in section 8.1, the present work used a value 0.25 for the modified buoyancy term in the standard k - ε turbulence model. This value was based on the optimisation performed on 5 cases using $C_{3\varepsilon}$ equal to 0, 0.25, 0.5, 0.75 and 1.0. When $C_{3\varepsilon}$ of 0.75 and 1.0 were used, the observed flame features were completely different from the experimental result. The majority of the plumes were confined just above tunnel floor and the plume extended longer to the downstream. The temperatures in the fire region were almost constant. However, when $C_{3\varepsilon}$ of 0, 0.25 and 0.5 were used, the plume started rising above tunnel floor, similar features obtained in the experiment.

With reference to Woodburn & Britter who used $C_{3\varepsilon}$ of 0.20, the present works decided to use the value of 0.25 for further simulations. Detailed optimisations on $C_{3\varepsilon}$ were not performed since it was time consuming and this study was also beyond the scope of the present work.

To investigate the effect of inclusion and exclusion of the buoyancy term, 6 more cases were modelled on tunnel **B**.

Cases SR6 and SR7 ($C3\varepsilon$ set to 0.25) : The critical ventilation velocities were found to be 0.50 m/s and 0.50 m/s.

Cases SR8, SR9, SR10 and SR11 ($C3\varepsilon$ set to 1.0) : The critical ventilation velocities for case SR8, SR9, SR10 and SR11 were 0.36 m/s, 0.420 m/s, 0.430 m/s and 0.440 m/s, respectively.

With the inclusion of the buoyancy term, the backlayering flows move further upstream from the fire source. The magnitude of the critical ventilation velocity increases at approximately between 10 to 12 percent when the buoyancy term was included in the standard k - ε turbulence model.

8.4 CFD Simulation Results and Discussions

The results of the computer modelling are held in storage arrays of very large size and represent complicated three dimensional distribution. A lot of effort have to be made to analyse and extract the data. Thus, vector plots, contour lines and profiles graph have been employed to interpret the results. Further comparison between experimental results also have been made.

8.4.1 Overall Flow

Comparison of the velocity profiles predicted by CFD and experimental data shown in Figure 8.12 showed that the CFD simulations have modelled the velocity field very well. The example of the velocity vector field prediction at symmetrical plane in tunnel **B** at 3.0 kW fire is shown in Figure 8.13. The length and the size of the arrow head indicate the magnitude of the velocity. As would be expected, once the air reached the fire, the velocities were increased to the maximum values. The maximum velocity vector was in the order of 1.5 m/s. Above the burner, it can be seen the vector directed opposite to the ventilation flow. This represents the movement of backlayering flow.

The combined horizontal velocity profiles and temperature contours in tunnel **B** at 3.0 kW fire shown in Figure 8.14 showed that the upstream flow inside the tunnel was fully developed. Upon reaching the fire, the velocity profiles changes in the shape since the flame has raised the velocity magnitude. The present of the backlayering flow can be seen by the negative profiles, directed to the left, just below tunnel ceiling.

8.4.2 Fire Plume

The examples of the predicted fire plume distributions inside each tunnel at 3.0 kW and 15.0 kW fire at the symmetrical plane are shown in Figures 8.15 to 8.18. With the interaction between tunnel geometry and the ventilation flow, the fire plume rises above the tunnel floor and deflects at certain angle from the vertical. The sizes and the shapes of the fire plumes can be clearly seen.

Comparisons of the centreline temperature distributions at HRR 3.0 kW and 15.0 kW in both tunnels **B** and **D** within the fire region shown in Figures 8.19 to 8.22, indicate that the CFD simulations have not produced matched temperature field for the fires. CFD predicted much higher temperature in the flame area. The maximum temperature reached 2200 K, which was too high for propane and air burner combustion. This is caused by the combustion models employed by the FLUENT.

The turbulent combustion models are based on fast chemistry concepts, which overestimates the reaction rates. Therefore the temperature is over predicted in the flame area. This problem is well known by the CFD simulation community. Both the scientists and CFD commercial users have pointed out the needs of better turbulence models. However, this is not the scope of the present study. Therefore this problem will not be discussed further.

Another limitation of the combustion models is that the combustion is directly determined by the present of the fuel, therefore the CFD simulation can only predict continuous flame. The intermittent flames existing in the real fire plumes could not be predicted by the CFD simulations. Although the combustion model can not predict the intermittent flame area directly, the CFD simulations have predicted good flow field for the tunnel flow, therefore the discussion of the fire plume distribution will be based on the velocity distribution from the CFD simulations using the definition given by McCaffrey. By the definitions, the persistent flame has the accelerating velocity, the intermittent flame has a near constant flow velocity and finally the buoyant plume has the decreases in flow velocity.

Figure 8.23 shows the temperature contours at the symmetrical plane for 3.0 kW fire at the critical ventilation velocity in tunnel **B**, being divided into several slices starting from the burner centreline. The velocity profiles for slices B to G are shown in Figure 8.24.

There are three distinguished regions that can be seen. Beyond 150 mm above tunnel floor is the backlayering region. The constant velocity approximately between 75 mm to 150 mm corresponds to the region between the backlayering flow and the fire plume. Finally, below 75 mm is the region of the fire plume. It can be seen that the maximum velocity increases from slices B to E, up to 1.25 m/s. The maximum velocity remains approximately the same value until slice F. It then decreases slightly in slice G. Thus according to the definition, the persistent regime exist up to slice E. Between slice E and F, the regime is associated with the intermittent regime. Beyond this region is associated to the buoyant smoke flow with decreasing velocity.

Figure 8.25 shows the temperature contours at the symmetrical plane for 7.50 kW fire also at the critical ventilation velocity. The velocity profiles for the slices are shown in Figure 8.26. Similarly, starting from the burner centreline, the maximum velocity increases up to 2.0 m/s from slices A to F. The maximum velocity then decreases up to 1.6 m/s in slice G and remains at approximately 1.5 m/s in slice H. It then further decreases to approximately 1.0 m/s in slice I. Finally, Figure 8.27 shows the temperature contours for 15.0 kW fire at the critical ventilation velocity. The velocity profiles shown in Figure 8.28 indicate that the maximum velocity increases up to slice H, approximately 2.25 m/s. It then decreases to approximately 2.0 m/s in slice I and remains approximately the same at 1.5 m/s until slice K, suggesting the intermittent regime.

To conclude, although much higher temperature for the fire plume have been predicted, the flow patterns have shown that McCaffrey's fire plume distribution can be applied. To avoid the problem caused by the combustion models, the velocity profiles were compared with the temperature contours, new temperature values were proposed to define the flame regimes. The intermittent flame regime had a temperature of 1100 - 1500 K. The persistent flame had a temperature of higher than 1500 K.

The fire plume will be discussed below in the aspects of flame height, flame deflection angles, air entrainment and acceleration.

(1) Flame Height (FH) and Flame Width

Based on the new temperature boundary for each regime as being defined in the previous section, the flame height in each tunnel was measured. The results showed that for a small fire (3.0 kW), the intermittent flame was approximately one third of the height of the tunnel. Further increased the HRR to 7.50 kW, the intermittent flame was approximately three quarter of the height of the tunnel. Finally at higher HRR (15.0 kW), the intermittent flame already reached tunnel ceiling.

The CFD results also showed that the persistent flame never reached the ceiling at critical condition even at higher HRR as shown in Figure 8.29 for 22.50 kW fire. The persistent flame (>1500 K) only elongated further downstream. The variations of the flame heights predicted by CFD were almost similar to the experimental results, previously discussed in Section 7.1.

The cross-sectional temperature contours in each tunnel at slice (I = 65), 100 mm downstream from the burner at 3.0 kW fire are shown in Figures 8.30 to 8.33. The width of the fire plume can be clearly seen. The flame in tunnel **A** is nearly reached the tunnel wall whereas the flame in tunnel **B** is approximately one third of the tunnel width. However, the flame in both tunnels **C** and **D** are confined near the centreline. The flame geometries are almost similar to the experimental results shown in Figures 6.7 and 6.12 for tunnels **B** and **D**, respectively.

(2) Deflection Angle (α)

The fire plumes deflection angles in Figures 8.15 to 8.18 have been measured. The comparisons between the measured and predicted fire plume tilt angles from the vertical are shown in Table 8.4. Similar to the experimental results, CFD predicted the increase

of fire plume tilt angles with the HRRs. In addition, CFD also predicted that the fire plume tilt angle decreases with the increase of tunnel aspect ratio.

It can be observed in Table 8.4 that the plume in tunnel **A** has the highest deflection angle from the vertical. In contrast, the plume in tunnel **D** has the smallest deflection angle from the vertical. The deflection angles vary from 75° to 56° in tunnel **A** to tunnel **D** at 3.0 kW. The deflection angles at 15.0 kW fire vary from 87° to 60°. The overall comparison shows that at specific tunnel and HRR, the predicted plume tilts angle was slightly lesser than the experimental results.

(3) Air Entrainment and Flow Acceleration

It has been pointed earlier in Chapter 7, the mechanisms for the behaviour of the plume distribution are due to the interaction of the fire plume with the ventilation flow and the interaction of the fire plume with the tunnel walls. These mechanisms are reflected in the behaviour of air entrainment and local acceleration of the air around the fire plume. The illustration of the air entrainment in the fire plume for each tunnel are shown in Figures 8.34 to 8.37. The general flow patterns in the four tunnels show that the fire induced the air from the tunnel floor, moving toward the fire plume. The fresh air from the top and side is entrained into the fire.

The effect of tunnel width on the behaviour of the air entrainment can also clearly seen. It is shown in Figure 8.34 that since there is limited spaces and opportunity for the fire plume to entrain the air from the sides in tunnel **A**, most of the air entrainment takes place in the upwind. The different rates of the entrainment on the upwind and downwind sides of the plume leads to a pressure drop to which the plume responds. As a results, this could create a pressure gradient across the plume which tilts it towards the tunnel floor.

As the tunnel becomes wider, there is opportunity for the entrainment from the sides. The results for tunnel **B** as shown in Figure 8.35 clearly show that the air is entrained

from the side. As a result, it can be observed that the magnitude of the velocity vector especially at tunnel centreline increases up to 0.769 m/s. A similar situation occurred in tunnel **C** shown in Figure 8.36 where the plume is getting higher and the maximum magnitude of the velocity vectors further increased to 0.785 m/s. Finally, it is shown in Figure 8.37 that further increased in tunnel width, the interaction between the tunnel walls with the fire plume becomes less significant. The fire plume even inclined at higher angle from the floor. It can be observed that the magnitude of the maximum velocity vector increased up to 1.03 m/s.

Figures 8.38 to 8.39 show the contours of the pressure drop relative to absolute pressure in both tunnels **A** and **D** at 7.50 kW fire. It can be observed in tunnel **A** that the contours indicating maximum pressure drop are confined just below tunnel ceiling and further extend to the downstream. Similarly, the contours representing the lowest pressure drop just above tunnel floor further extend to the downstream. However, the distribution of the pressure contours in tunnel **D** shown in Figure 8.39 are slightly different. It can be seen that the contours, representing the highest pressure are shorter just below tunnel ceiling. In addition, the pressure downstream from the burner is relatively higher.

The flow acceleration in the near flame area was clearly shown in the LDV measurements. Figure 8.40 shows the comparison between the velocity profiles measured by LDV and predicted by the CFD in tunnel **B**. The CFD results were in a good agreement with the experimental results.

8.4.3 Backlayering

The examples of the interactions between ventilation flow and the backlayering flows are shown in Figure 8.41 at 7.50 kW fire at three ventilation velocities in tunnel **B**. In Figure 8.41(a), the ventilation flow was set to 0.44 m/s. At this condition, the backlayering flows occurred and travelled upstream against the ventilation current at approximately 2 tunnel heights. Figure 8.41(b) shows that at critical condition (0.47

m/s), the backlayering flows were suppressed and become stagnant at the leading edge of the burner. Further increased in the ventilation velocity as shown in Figure 8.41(c) resulted that the flame further deflected to downstream, releasing the majority of heat in the downstream and the backlayering flow disappeared completely. The backlayering flows were found to be very sensitive to the ventilation flow. However, the details of sensitivity of the backlayering flow towards the ventilation velocity has not been studied since this parameter was not the primary concern in the present study.

The comparison between CFD and experimental results in Figure 8.12 also show that CFD predicts matched flow field in the backlayering flow. The velocity results in Figure 4.40 further justify the agreement in the flow pattern. It is shown that the thickness of the backlayering flow is almost constant regardless of the HRRs.

The backlayering flow was also observed to fill the whole tunnel width at the top part of the tunnel, similar to the experimental observation. This behaviour can be seen in Figures 8.42 to 8.45 in each tunnel when the backlayering flow was allowed to travel up to 2 tunnel heights upstream.

8.4.4 Downstream Smoke Flow

The comparisons between the measured and predicted temperature distributions in the downstream region are shown in Figures 8.46 to 8.49 for 3.0 kW and 15.0 kW fires in both tunnels **B** and **D**. The results show that in tunnel **B**, the smoke fill most of the tunnel. However, in tunnel **D**, the downstream smoke only fill half of the tunnel.

8.4.5 Critical Ventilation Velocity

The predicted critical ventilation velocities for each tunnel at HRRs between 3.0 kW to 43.5 kW are shown in Table 8.5. The plot of the predicted and measured critical ventilation velocity against the HRRs for the four tunnels is shown in Figure 8.50.

The most important finding was that CFD predicts the same patterns of the critical ventilation velocity to the experimental results for the four tunnels. However, the predicted values from CFD lower by approximately 15 to 20 percent.

One important outcome of these results is that the near independent of the critical ventilation velocity on fire output at higher HRRs were obtained in all tunnels in CFD simulations. The behaviour was predicted to occur in tunnels **A** and **B** at HRRs 7.50 kW and 15.0 kW, respectively, consistent with the experimental results. The near independent of critical velocity on HRRs were also predicted to occur in tunnels **C** and **D** at HRRs at 30.0 kW and 45.0 kW, respectively.

The detailed study in the velocity profiles suggested that even though the HRR was increased, the region at approximately beyond 125 mm above tunnel floor has the similar conditions. The velocity profiles were almost the same. This behaviour can be seen in Figure 8.51 where the centreline velocity profiles for three HRRs (7.50 kW, 15.0 kW and 22.50 kW) at various distances from the burner in tunnel **B** are compared. Starting from Figure 8.51 (e), a striking feature that can be observed is that the magnitude of the velocities above 125 mm from tunnel floor are quite similar, for both 15.0 kW and 22.50 kW fires. Both 15.0 kW and 22.50 kW fires have the same critical ventilation velocity, 0.50 m/s.

Examination on the flame height showed that for 15.0 kW and 22.50 kW fires, the region below the tunnel ceiling was dominated by the intermittent flame. Due to its behaviour of the near constant velocity, it would be expected that the critical ventilation velocity

would be nearly constant. Thus, it showed that there is a strong link between the predicted critical ventilation velocity with fire plume distribution.

8.5 Summary of the Conclusions

The three dimensional simulations have been successfully performed. The behaviour of the backlayering, fire plume distribution and downstream smoke flow were correctly mimicked. The principal conclusions that can be made are as follows:

- CFD simulations predicted velocity field matching with experimental measurement. However higher temperatures were especially in the fire plume due to the limitation of the combustion models.

- Detailed investigations on the velocity profiles in the fire plume distribution suggested that McCaffreys' fire plume theory could be extended in CFD. The behaviour of the three regimes existing in the predicted fire plume were found. However, since the predicted temperature distributions were found to be much higher, the present work proposed new temperature values to define the flame regime in CFD simulated results. The intermittent flame regime had a temperature of 1100 - 1500 K. The persistent flame had a temperature of higher than 1500 K.

- The results of predicted flame heights showed that for 3.0 kW fire, the flame was approximately one third of the height of the tunnel. At higher HRR 7.50 kW, the flame was nearly reached the ceiling whilst at 15.0 kW, the intermittent flame was definitely reached the ceiling. The CFD results showed that the persistent flame never reached the ceiling even at higher at the critical ventilation velocity. This further confirmed the findings from the experiment.

- CFD predicted the same variations of the flame tilt angles to the measured in the experiment. The tilt angle decreases with the increase of the tunnel width and increases with the increase of the HRR in the same tunnel. The overall comparison shows that at specific tunnel and HRR, the predicted plume tilts angle was slightly lesser than the experimental results.

- The mechanism for the distribution of the fire plume has been further investigated. To some extent CFD further confirmed that the fire plume air entrainment plays significant roles for the distribution of the fire plume such as the large tilt angle from the vertical. In addition, the local obstruction of the oncoming air to the fire also determine the fire plume distribution.

- The presence of the backlayering flow were correctly mimicked by the CFD. Similar to the experimental observation, the backlayering flow was sensitive to the ventilation flow. The backlayering flow also was observed to fill the whole tunnel width at the top part of the tunnel.

- Further comparison between the backlayering velocity profiles from LDV showed that the flow patterns were correct but the predicted values were slightly lower. One of the most important finding was that both results showed that the velocity profiles in the backlayering flow were similar regardless of HRRs.

- The most important finding from the present works was that CFD predicted the same pattern of the variations of the critical ventilation velocity in the four tunnels with respect to tunnel cross-sectional geometries and HRRs. The present work found that the predicted critical ventilation velocity were lower between 15 to 20 percent. This indicates that CFD has the ability to predict the same flow patterns but lower value in the critical velocity. This suggests that further works are required to validate the data, if the CFD is used in design the ventilation system for tunnels.

- Another important outcome of these results is that the near-independence of critical ventilation velocity on fire heat output at higher HRR were obtained in all tunnels in CFD simulations.

- Finally, detailed investigations in the predicted critical ventilation velocity also show that there is a strong link between the critical ventilation velocity with the fire plume distribution. For a small fire, the critical ventilation velocity was found strongly affected by the HRR. However, once the intermittent flame reached the ceiling, the critical ventilation velocity started becomes insensitive to the HRR. This further confirmed the finding from the experiments.

	Longitudinal Grid	Aug 10 1999
	Grid (101 X 27 X 9)	Fluent 4.51
	Slice: K=9	Fluent Inc.
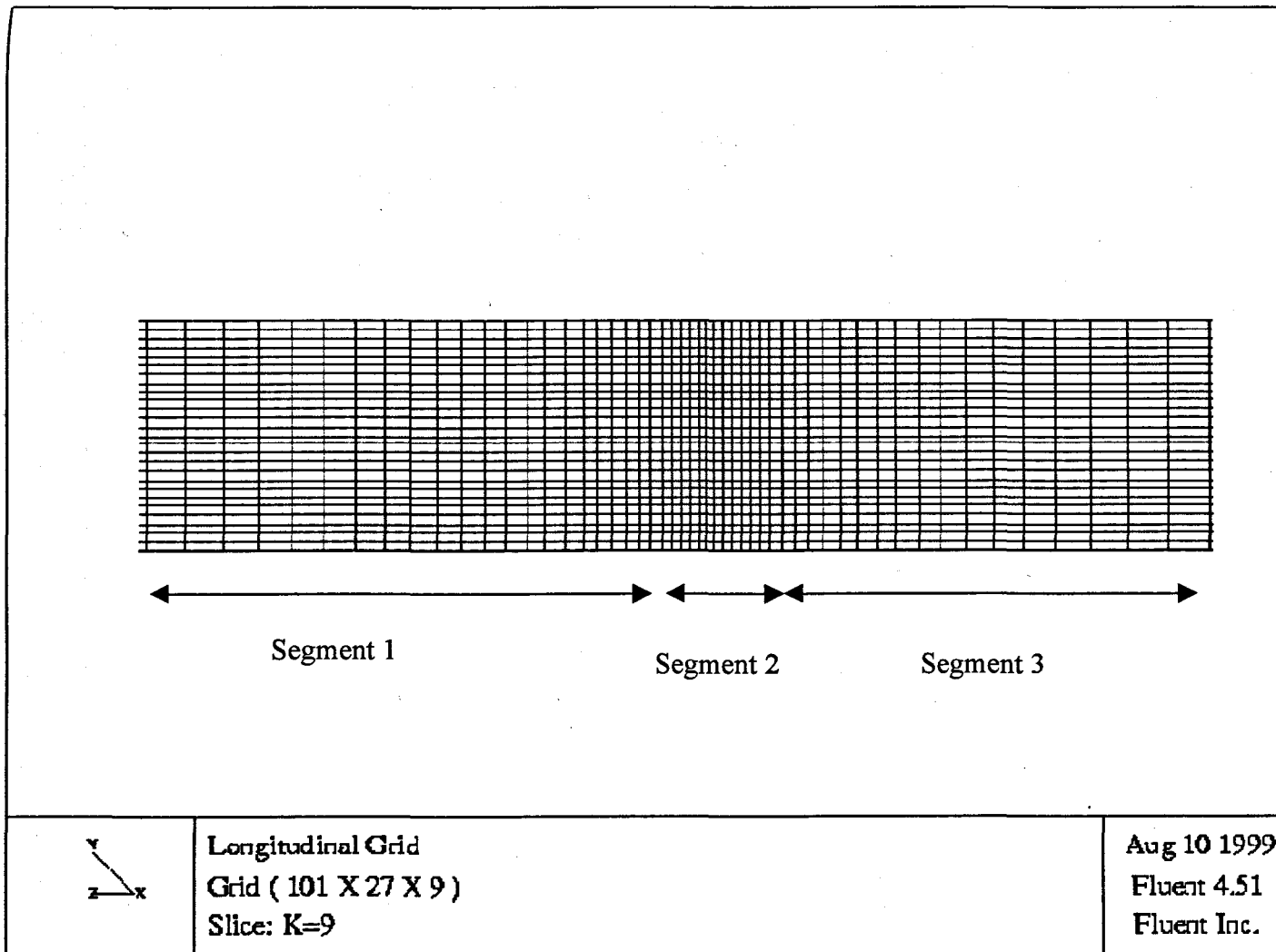
Figure 8.1: Longitudinal grid distributions

CL
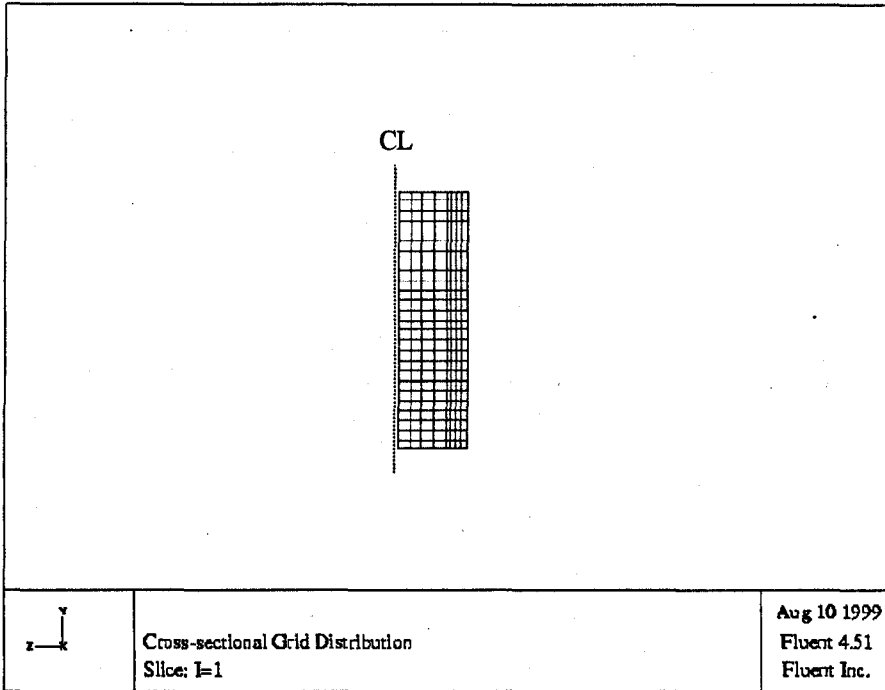
Figure 8.2 : Cross-sectional grid distribution in tunnel A

CL
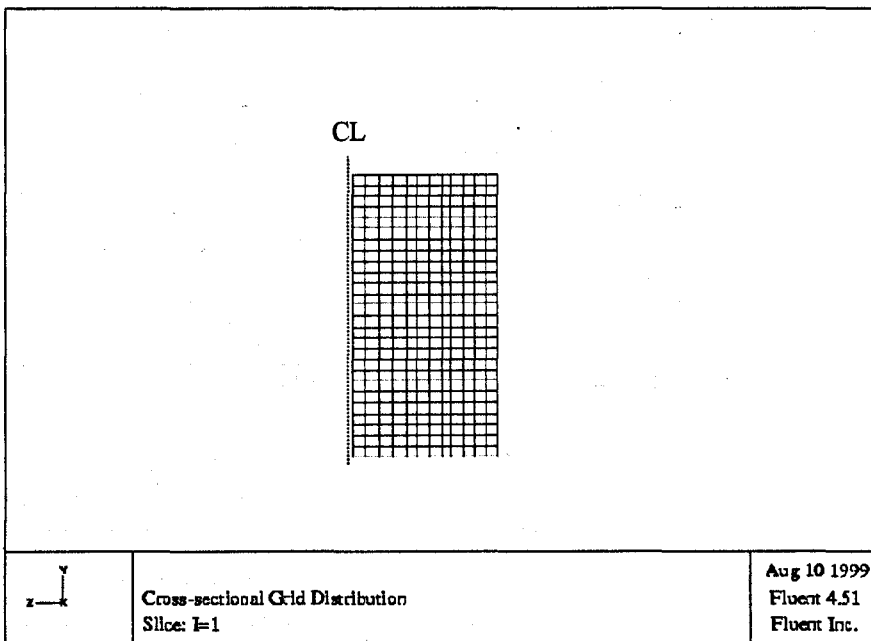
Figure 8.3: Cross-sectional grid distributions in tunnel B
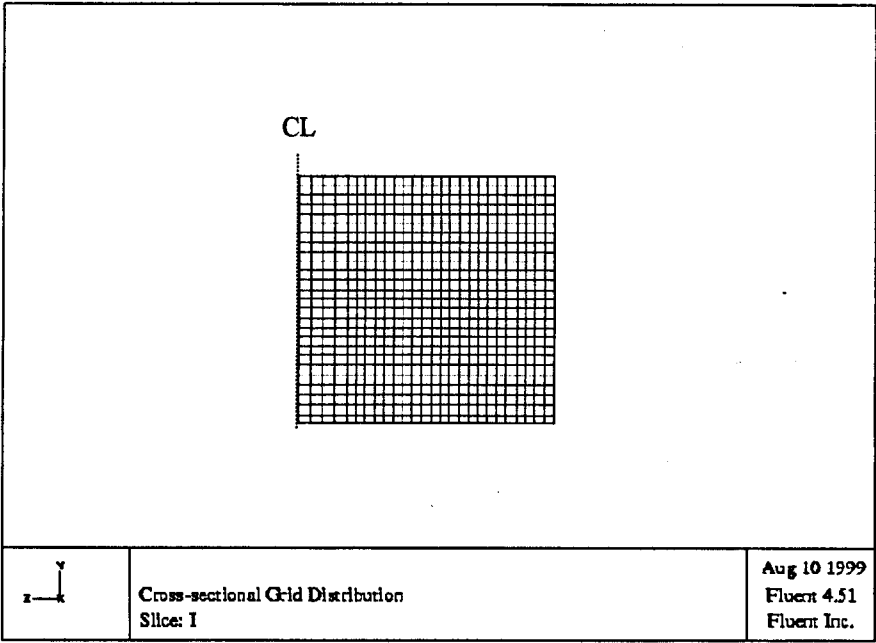
Figure 8.4 : Cross-sectional grid distribution in tunnel C
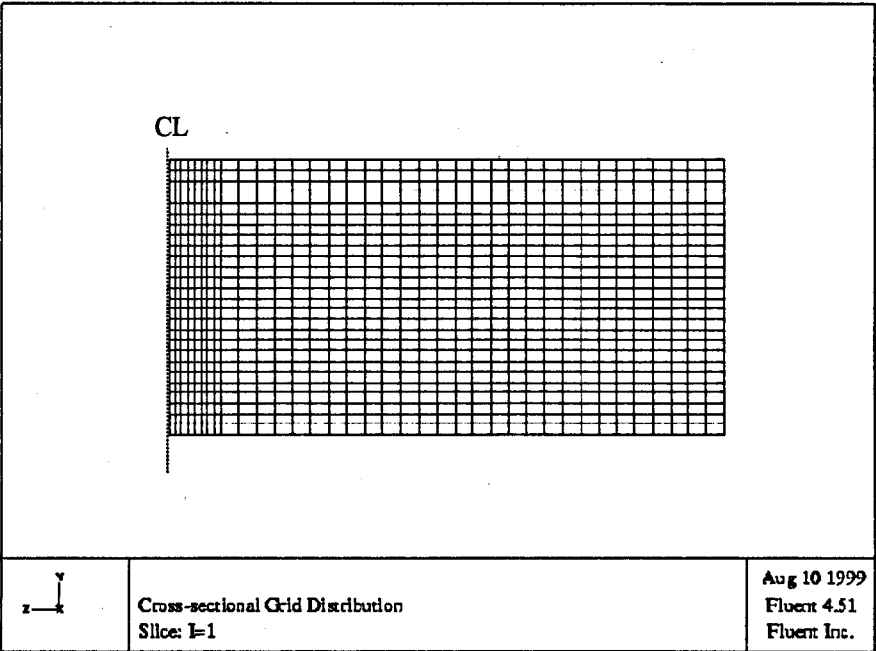
Figure 8.5: Cross-sectional grid distributions in tunnel D

(a) FRF

| | Tunnel B [Q = 3.0 kW, V = 0.36 m/s]
Temperature (K)
Lmax = 2.073E+03   Lmin = 2.980E+02 | Feb 03 1999
Fluent 4.51
Fluent Inc. |

(b) PDF

| | Tunnel B [Q = 3.0 kW, V = 0.40 m/s]
Temperature (K)
Lmax = 2.196E+03   Lmin = 2.985E+02 | Feb 03 1999
Fluent 4.51
Fluent Inc. |
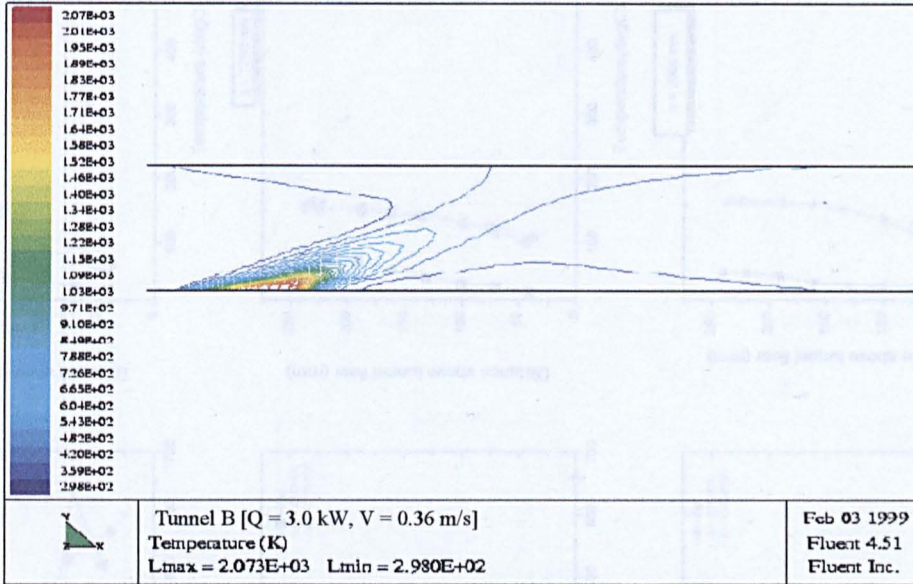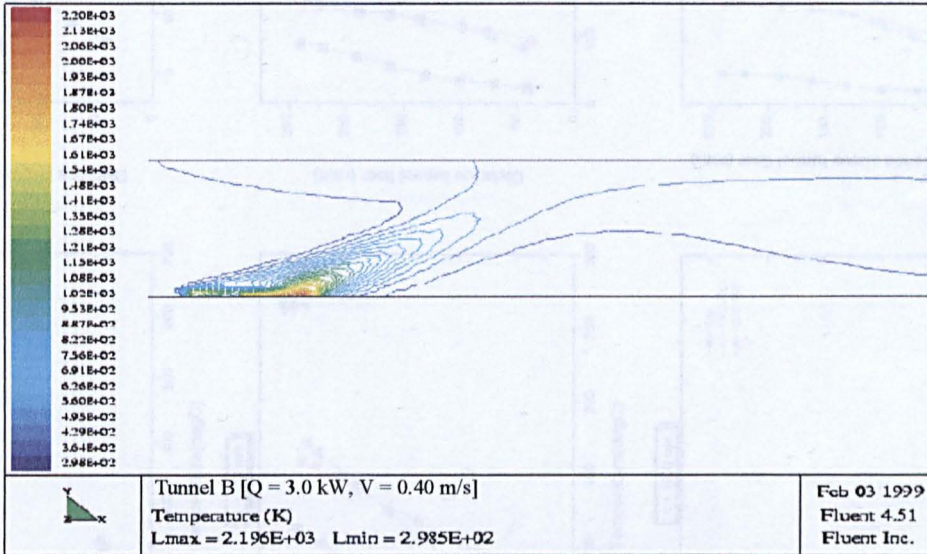
Figure 8.6: Temperature distribution at the symmetrical plane in tunnel B at 3.0 kW
Investigation of combustion models

194
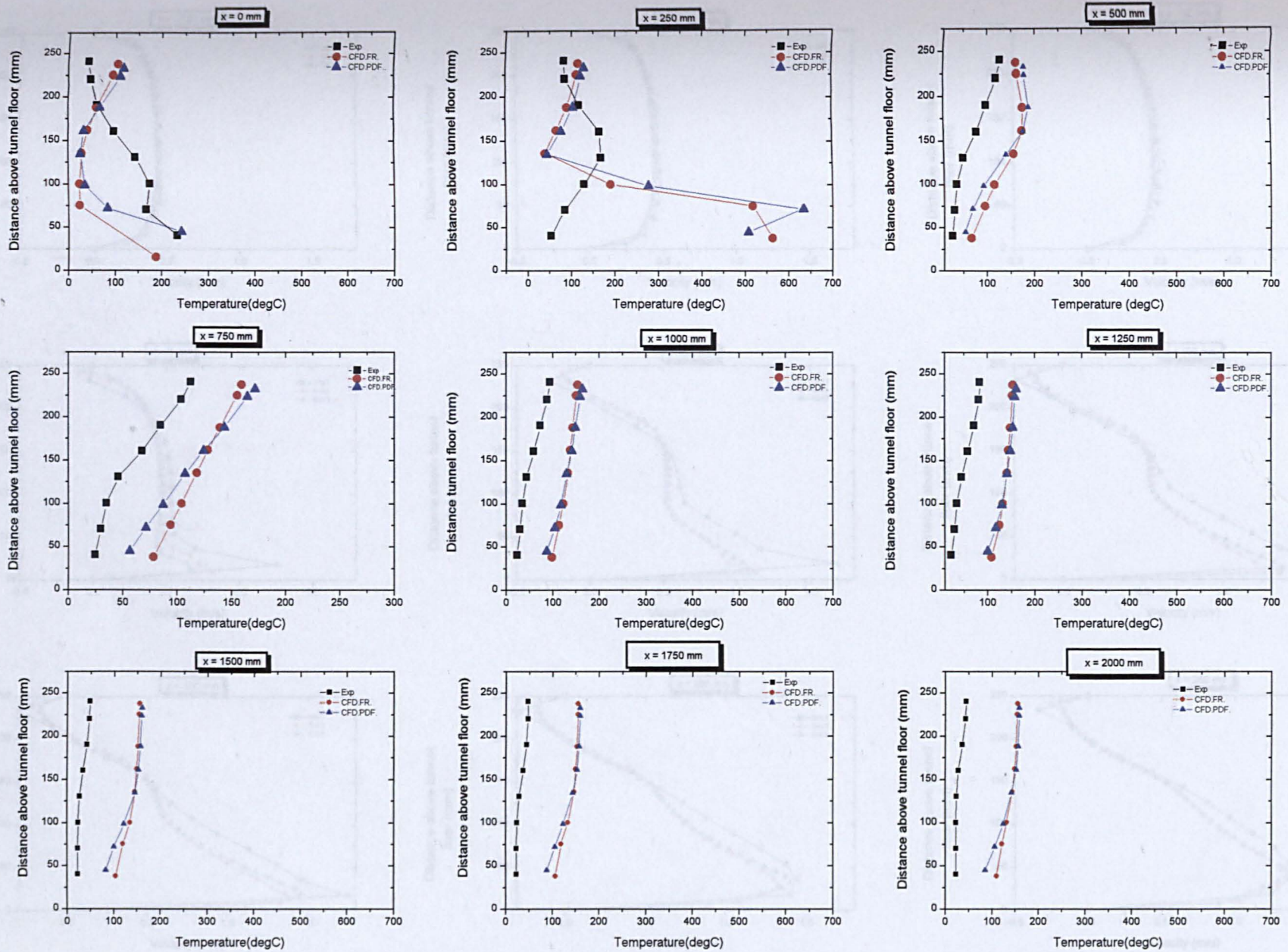
Figure 8.7: Comparison of temperature distribution at symmetrical plane between CFD and experimental in tunnel B at 3.0 kW
(Vexp = 0.48 m/s, VCFD(FR) = 0.36 m/s, VCFD(PDF) = 0.40 m/s)
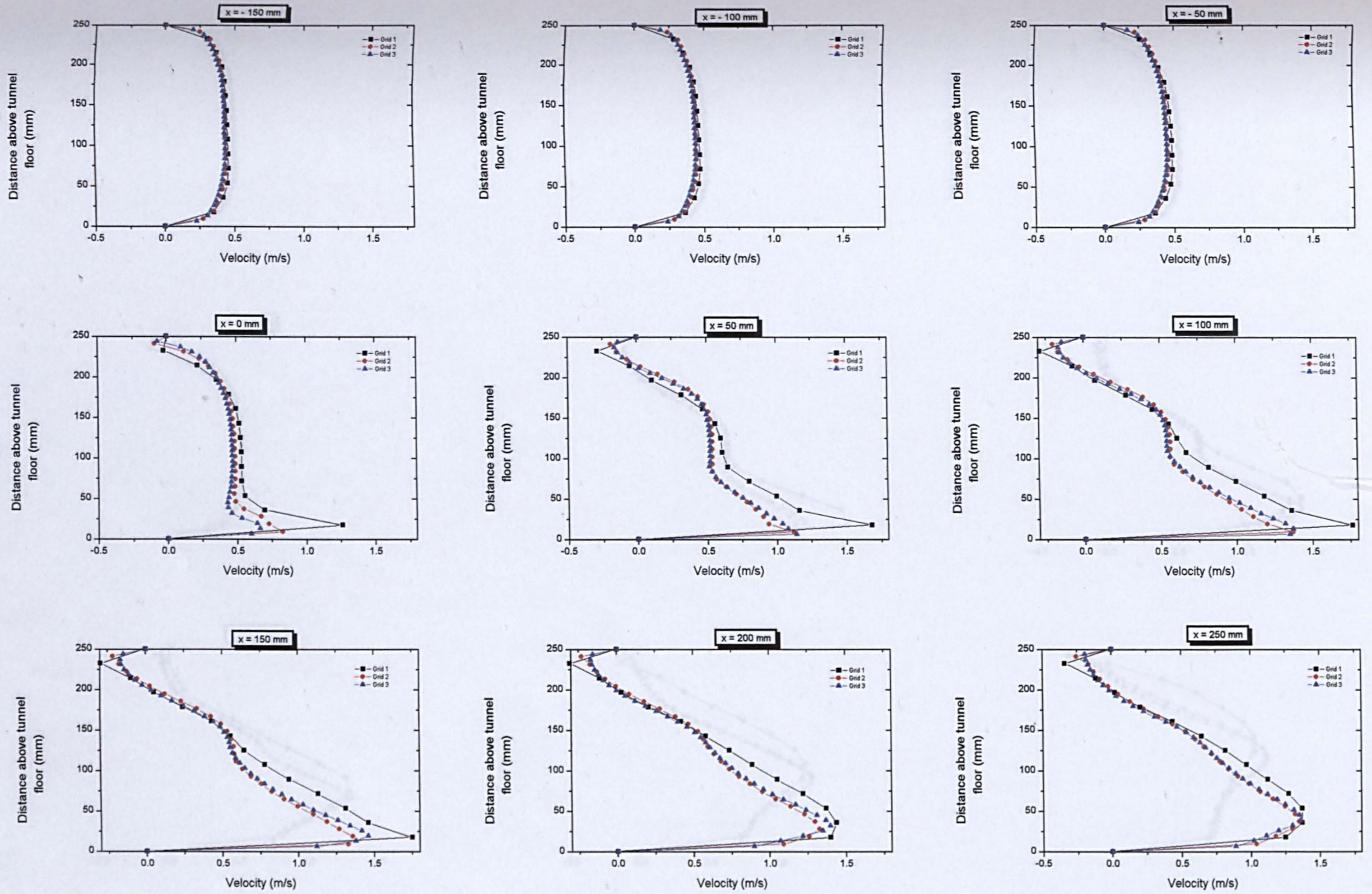
Figure 8.8 : Comparison of velocity profiles for various grid setups in tunnel A at HRR 3.0 kW at critical conditions
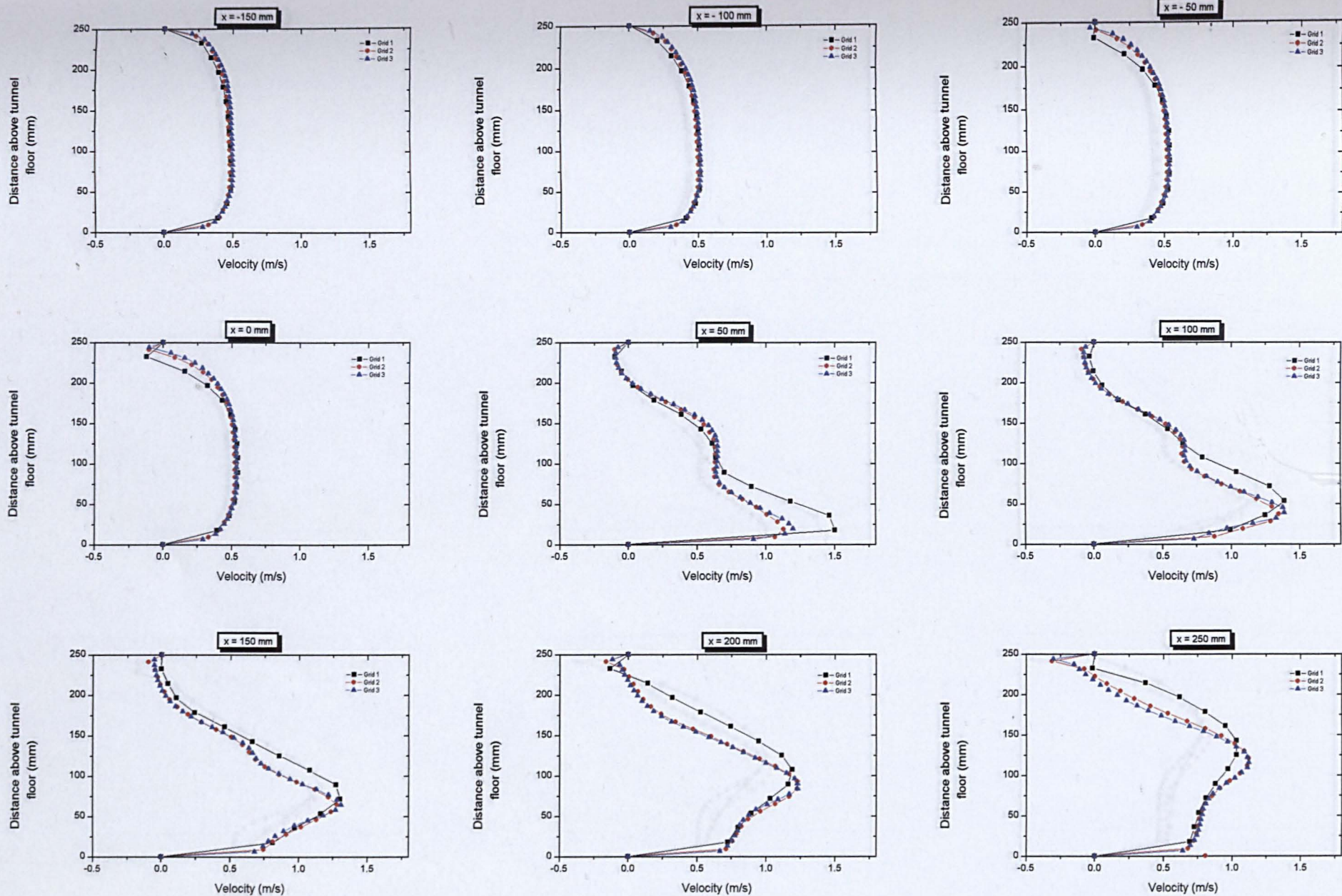
Figure 8.9 : Comparison of velocity profiles for various grid setups in tunnel B at HRR 3.0 kW at critical conditions
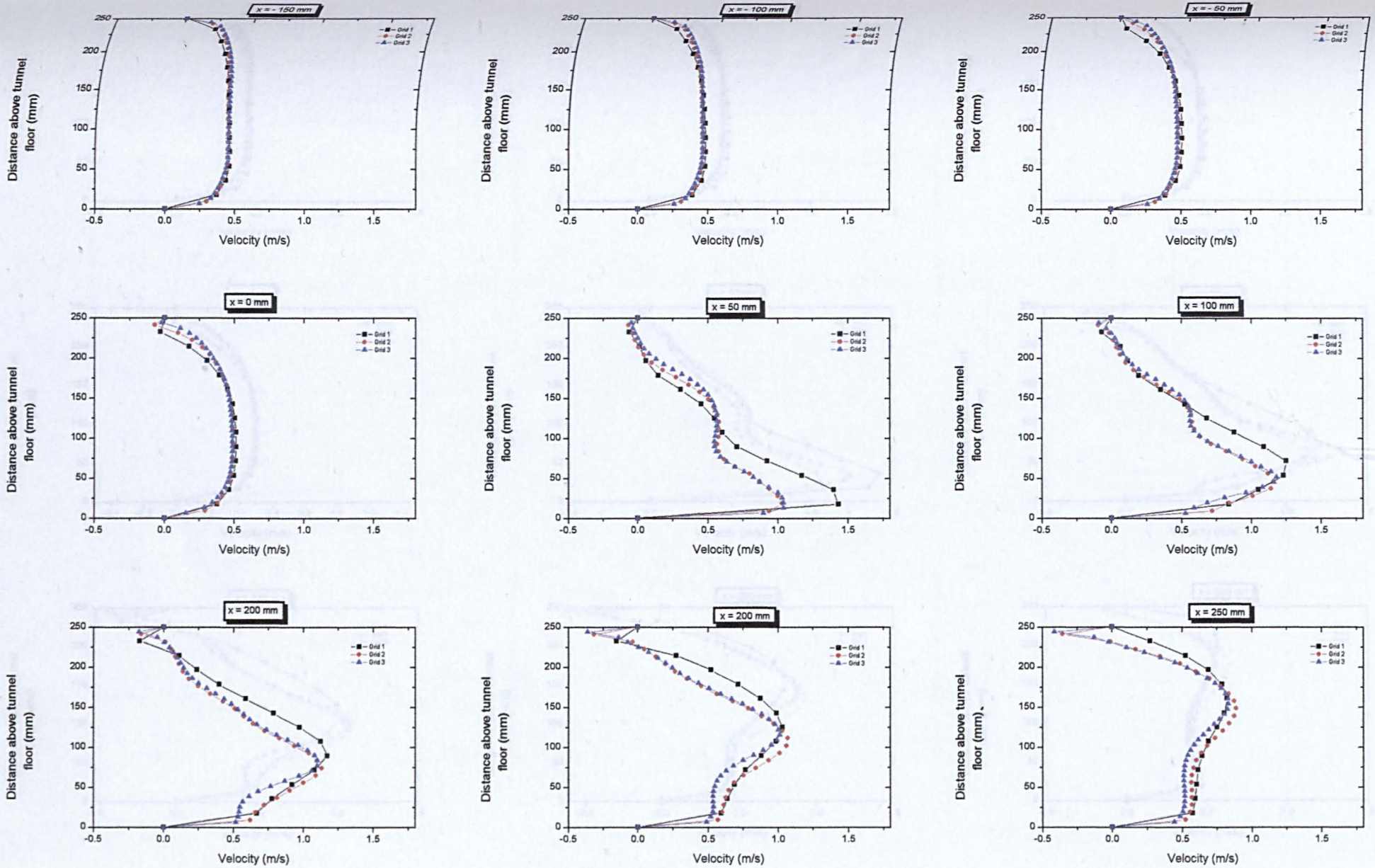
Figure 8.10 : Comparison of velocity profiles for various grid setups in tunnel C at HRR 3.0 kW at critical conditions

Figure 8.11: Comparison of velocity profiles for various grid setups in tunnel D at HRR 3.0 kW at critical conditions
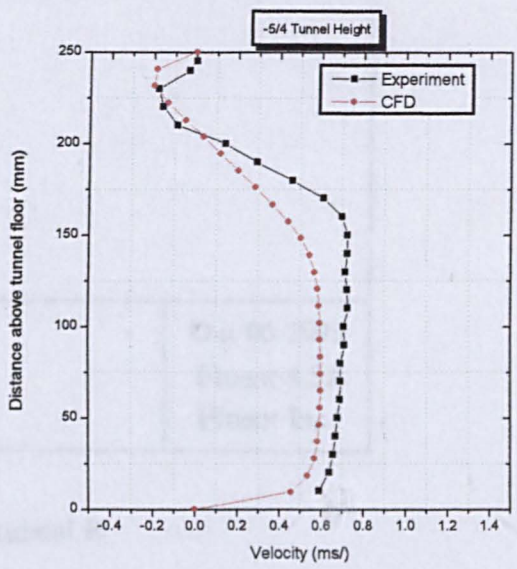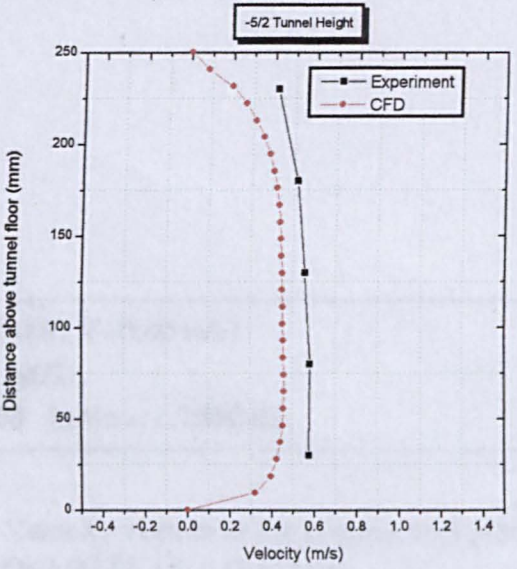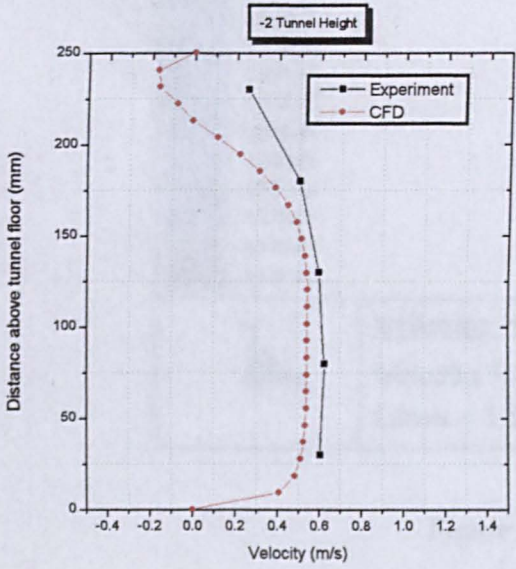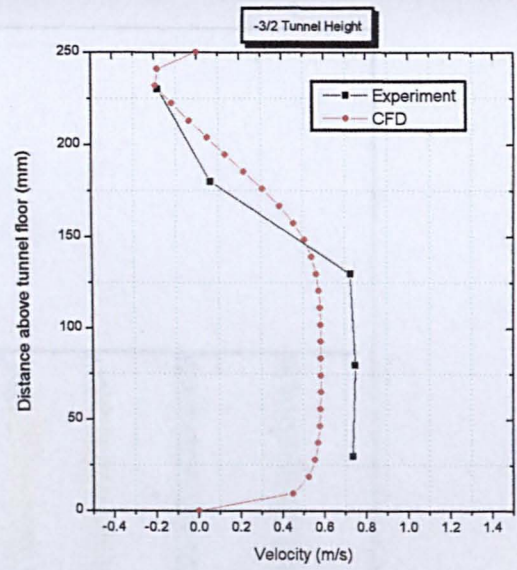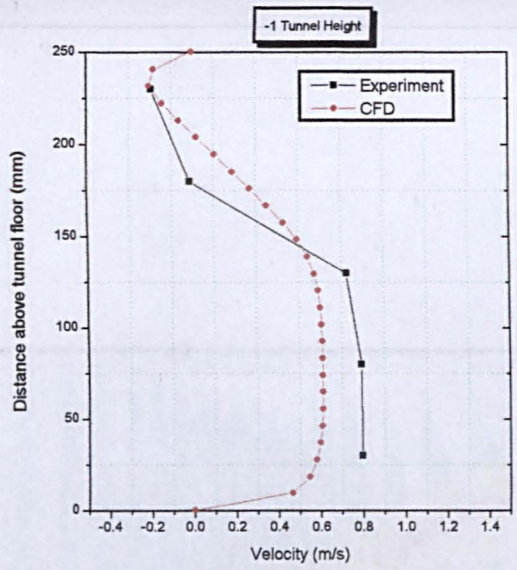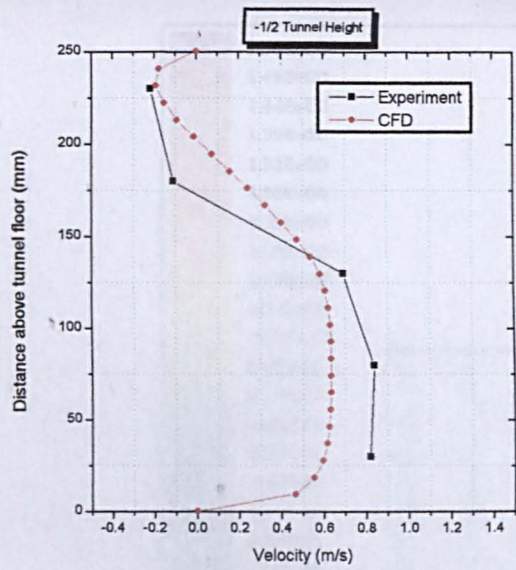
Figure 8.12: Comparison of velocity profiles between measured and predicted in tunnel B at 3.0 kW when backlayering was controlled at 2.25 tunnel heights (V(exp) = 0.47 m/s, V(CFD) = 0.37 m/s)
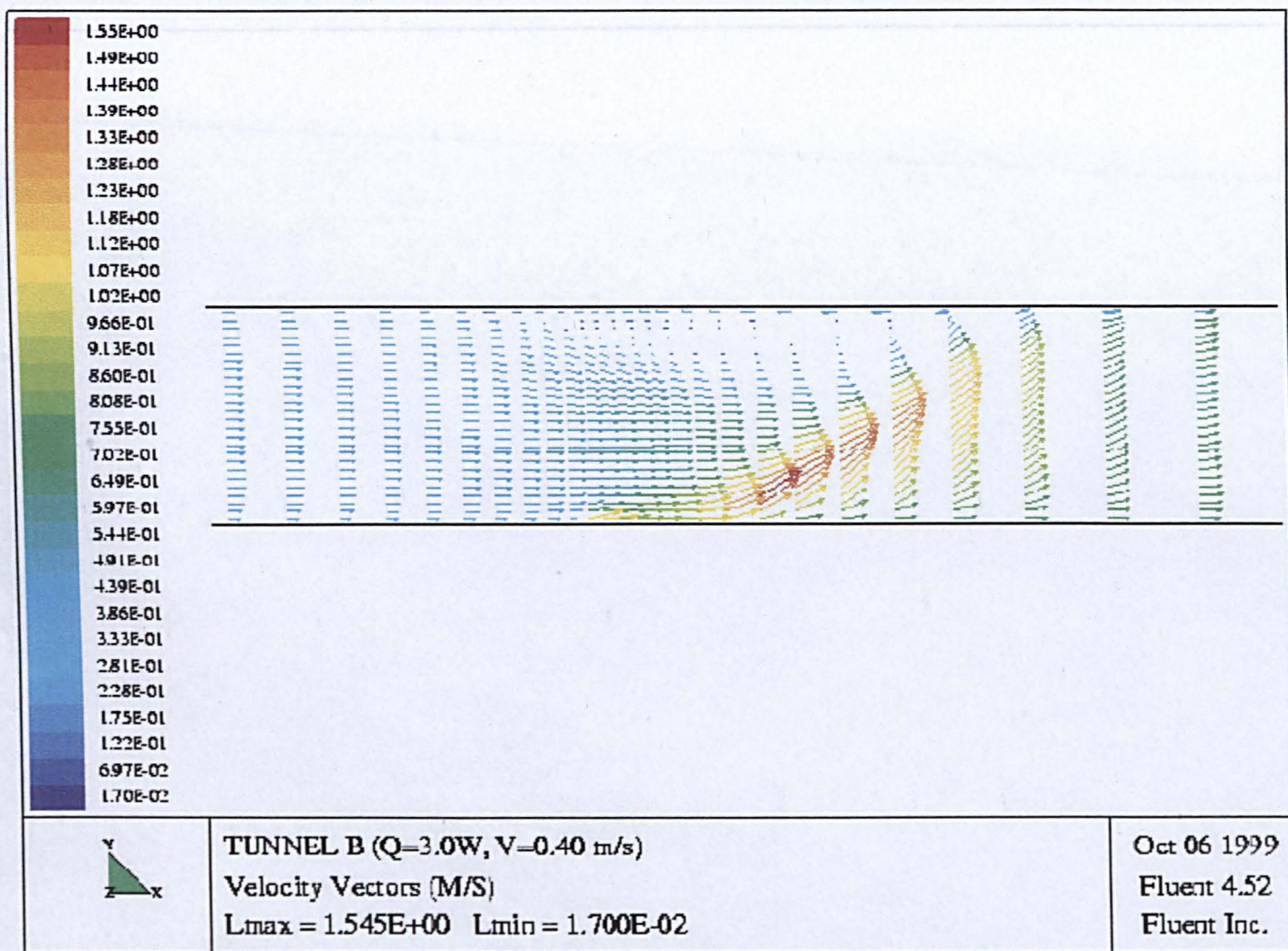
Figure 8.13 : Velocity vectors at the symmetrical plane in tunnel B
(Q=3.0 kW, Uc = 0.40 m/s)

| | Velocity profiles and temperature contours | Oct 25 1999
Fluent 4.52
Fluent Inc. |
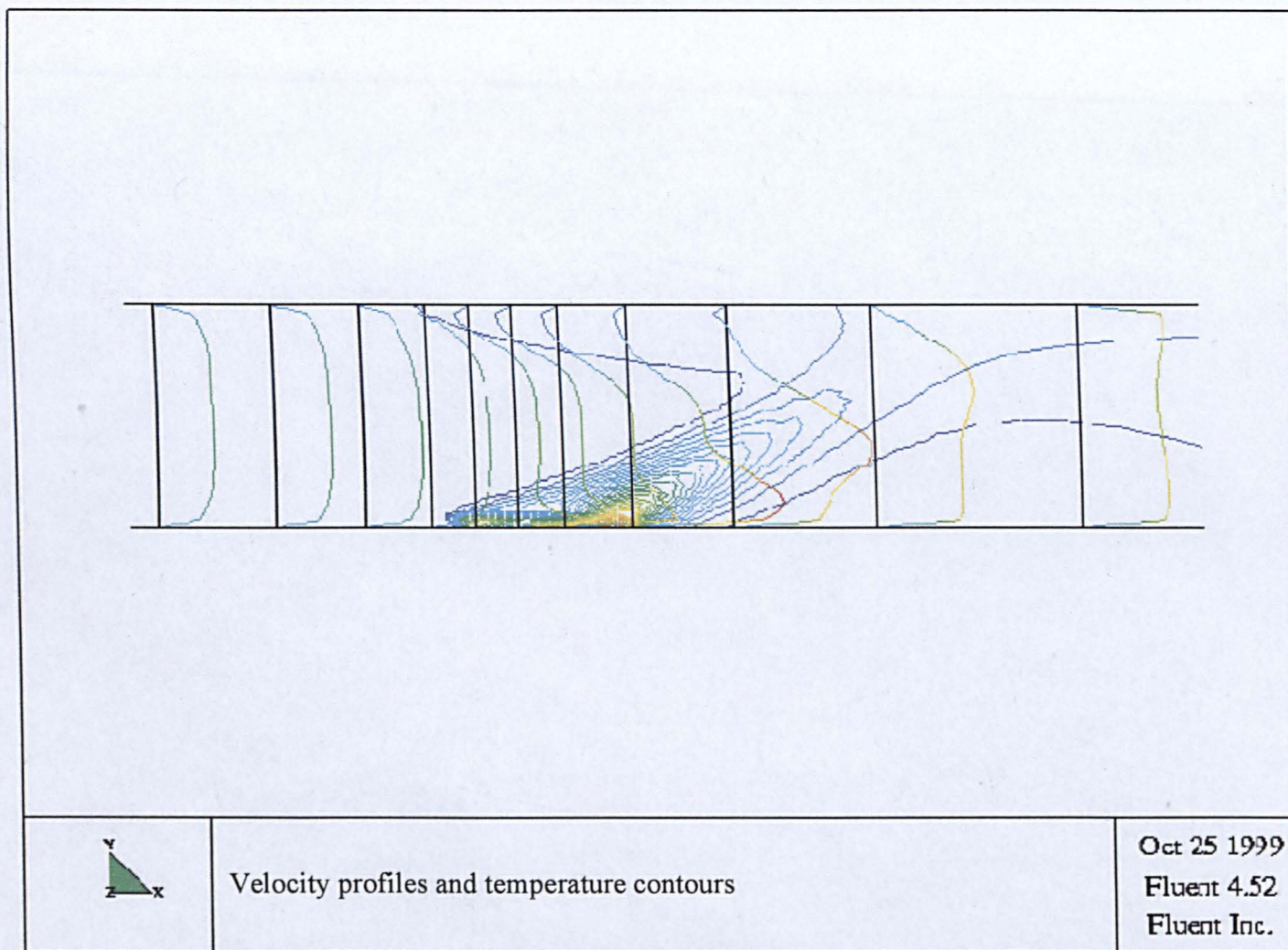
Figure 8.14 : Velocity profiles and temperature contours at the symmetrical plane in tunnel B
[Q = 3.0 kW, Uc = 0.40 m/s]

(a) Q = 3.0 kW (Uc = 0.36 m/s)

Tunnel A[Q = 3.0 kW, Uc = 0.36 m/s] Temperature (K) Lmax = 2.236E+03 Lmin = 2.981E+02	Mar 17 1999 Fluent 4.51 Fluent Inc.

(b) Q = 15.0 kW (Uc = 0.365 m/s)

Tunnel A [Q= 15.0 kW, Uc = 0.365 m/s] Temperature (K) Lmax = 2.271E+03 Lmin = 2.980E+02	Mar 17 1999 Fluent 4.51 Fluent Inc.
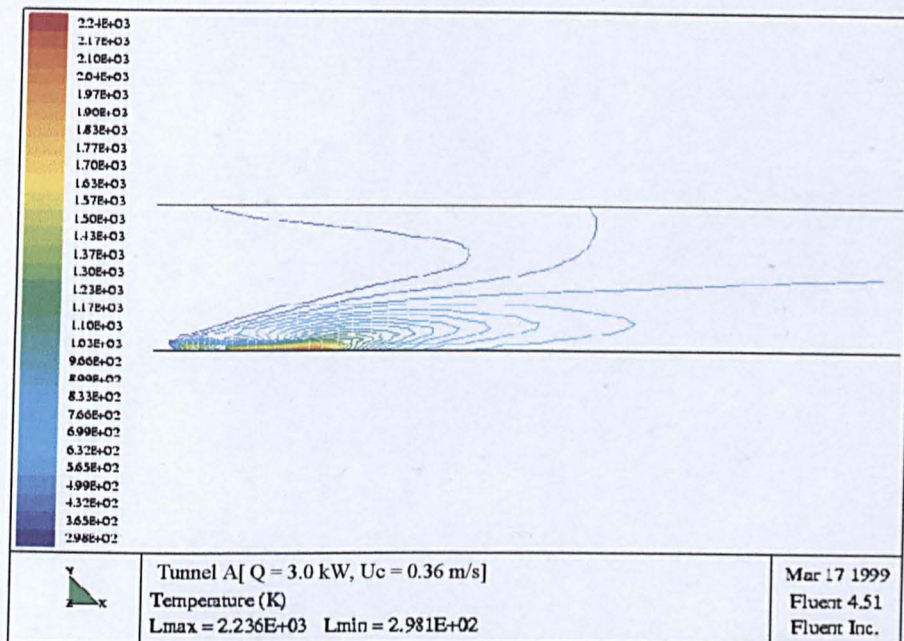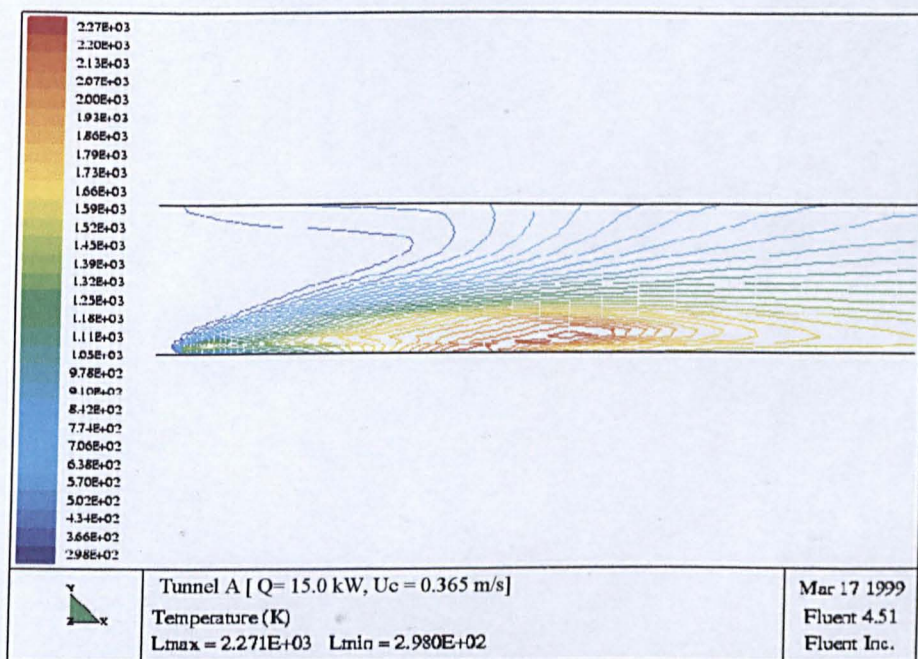
Figure 8. 15 : Temperature distribution at the symmetrical plane in tunnel A
at critical ventilation conditions

(a) Q = 3.0 kW(Uc = 0.40 m/s)

Tunnel B [Q = 3.0 kW, V = 0.40 m/s]	Feb 03 1999
Temperature (K)	Fluent 4.51
Lmax = 2.196E+03 Lmin = 2.985E+02	Fluent Inc.

(b) Q = 15.0 kW (Uc = 0.50 m/s)

Tunnel B [Q = 15.0 kW, V = 0.40 m/s]	Mar 17 1999
Temperature (K)	Fluent 4.51
Lmax = 2.103E+03 Lmin = 2.980E+02	Fluent Inc.
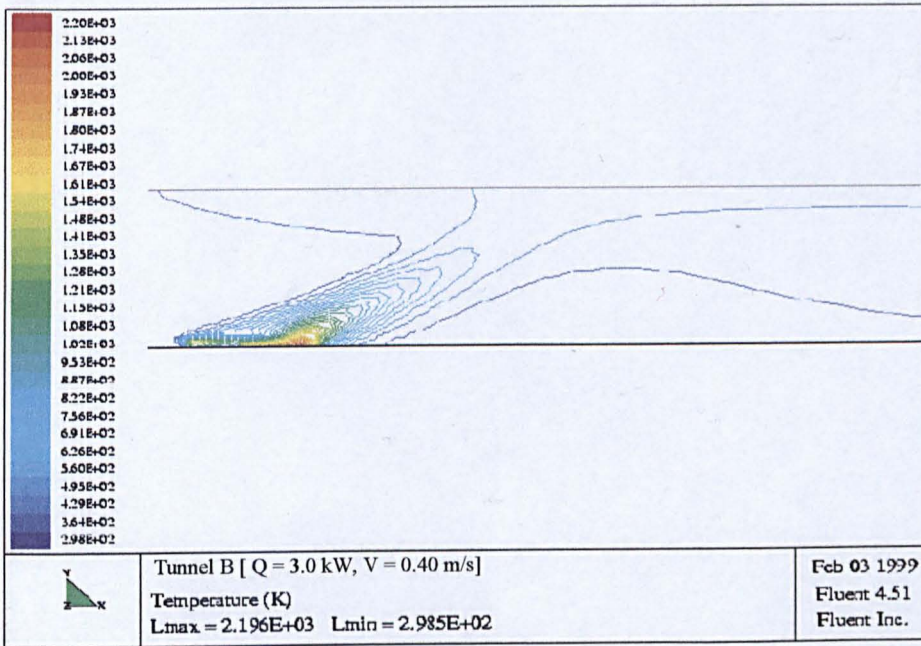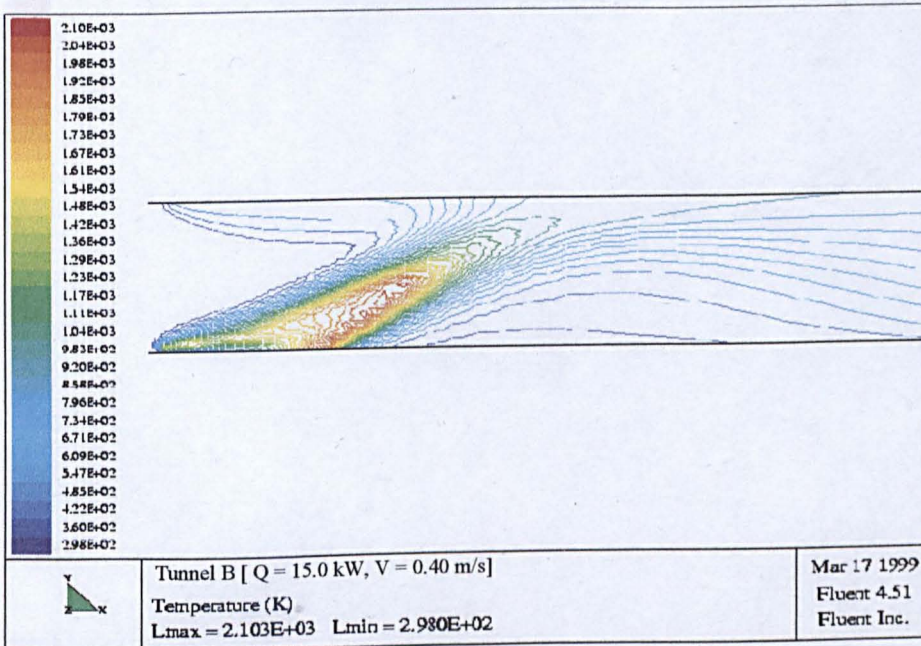
Figure 8.16 : Temperature distribution at the symmetrical plane in tunnel B
at critical ventilation conditions
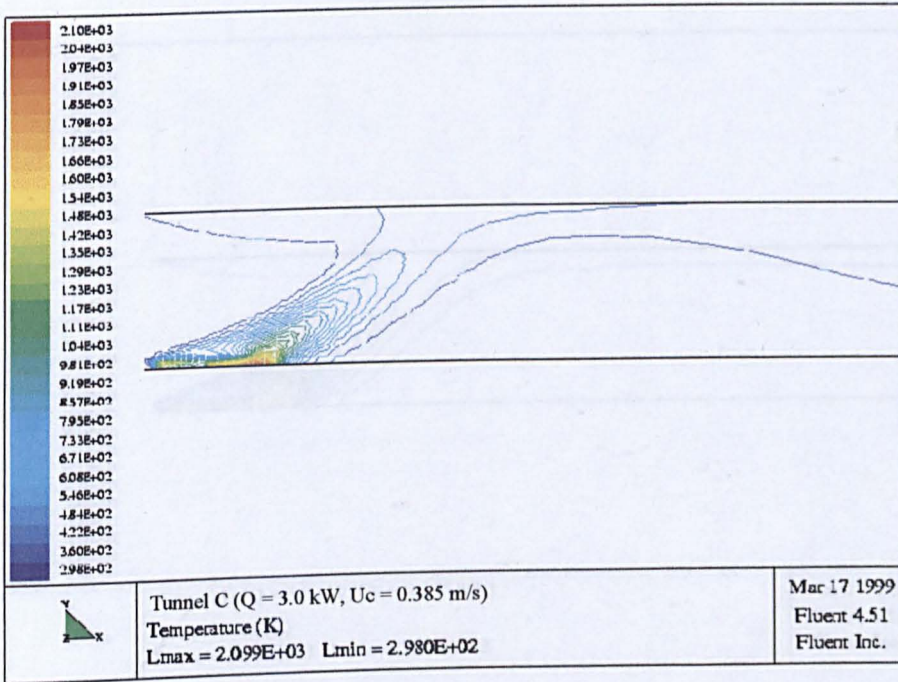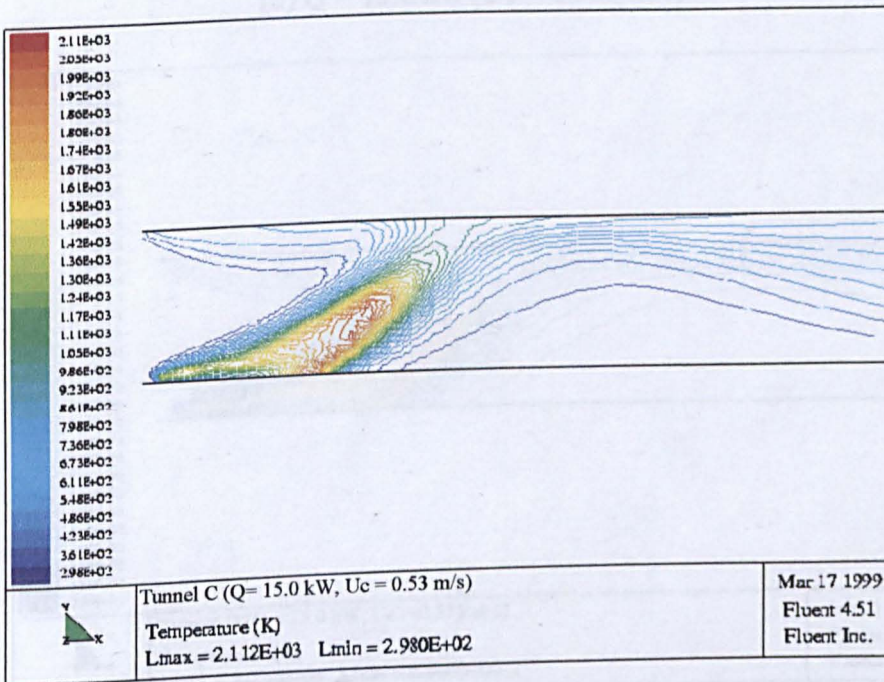
(a) Q = 3.0 kW(Uc = 0.385 m/s)

Tunnel C (Q = 3.0 kW, Uc = 0.385 m/s)
Temperature (K)
Lmax = 2.099E+03   Lmin = 2.980E+02

Mar 17 1999
Fluent 4.51
Fluent Inc.

(b) Q = 15.0 kW(Uc = 0.53 m/s)

Tunnel C (Q= 15.0 kW, Uc = 0.53 m/s)
Temperature (K)
Lmax = 2.112E+03   Lmin = 2.980E+02

Mar 17 1999
Fluent 4.51
Fluent Inc.

Figure 8.17 : Temperature distribution at the symmetrical plane in tunnel C at critical ventilation conditions

(a) Q = 3.0 kW(Uc = 0.385 m/s)

Tunnel C (Q = 3.0 kW, Uc = 0.385 m/s)	Mar 17 1999
Temperature (K)	Fluent 4.51
Lmax = 2.099E+03 Lmin = 2.980E+02	Fluent Inc.

(b) Q = 15.0 kW(Uc = 0.53 m/s)

Tunnel C (Q= 15.0 kW, Uc = 0.53 m/s)	Mar 17 1999
Temperature (K)	Fluent 4.51
Lmax = 2.112E+03 Lmin = 2.980E+02	Fluent Inc.

Figure 8.17 :Temperature distribution at the symmetrical plane in tunnel C
at critical ventilation conditions

Tunnel D (Q = 3.0 kW, Uc = 0.375 m/s)

Temperature (K)

Lmax = 2.212E+03   Lmin = 2.982E+02

Mar 17 1999

Fluent 4.51

Fluent Inc.

(b) Q = 15.0 kW(Uc = 0.535 m/s)

Tunnel D (Q = 15.0 kW, Uc = 0.535 m/s)

Temperature (K)

Lmax = 2.052E+03   Lmin = 2.980E+02

Jun 23 1999

Fluent 4.51

Fluent Inc.
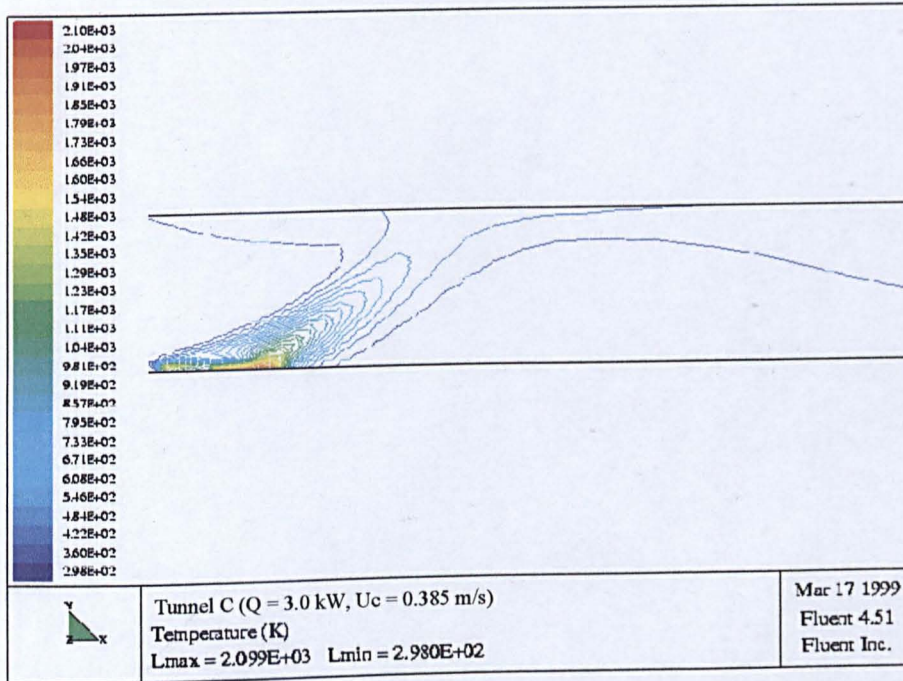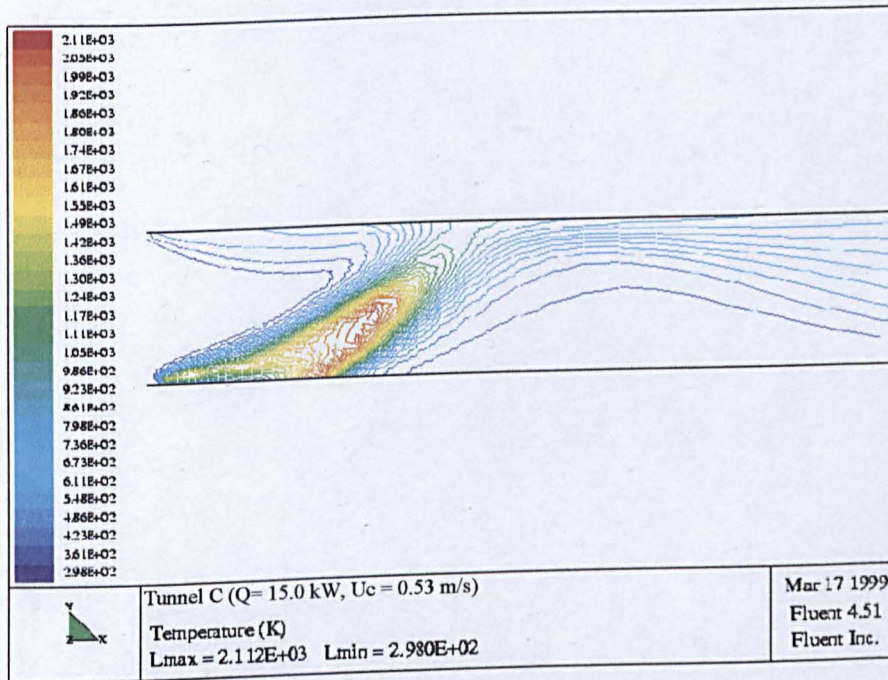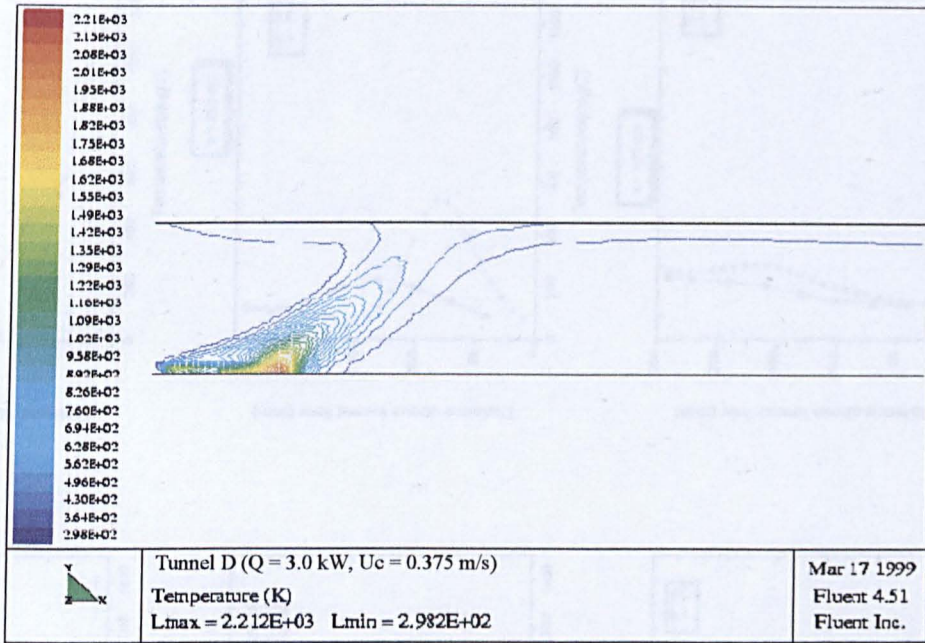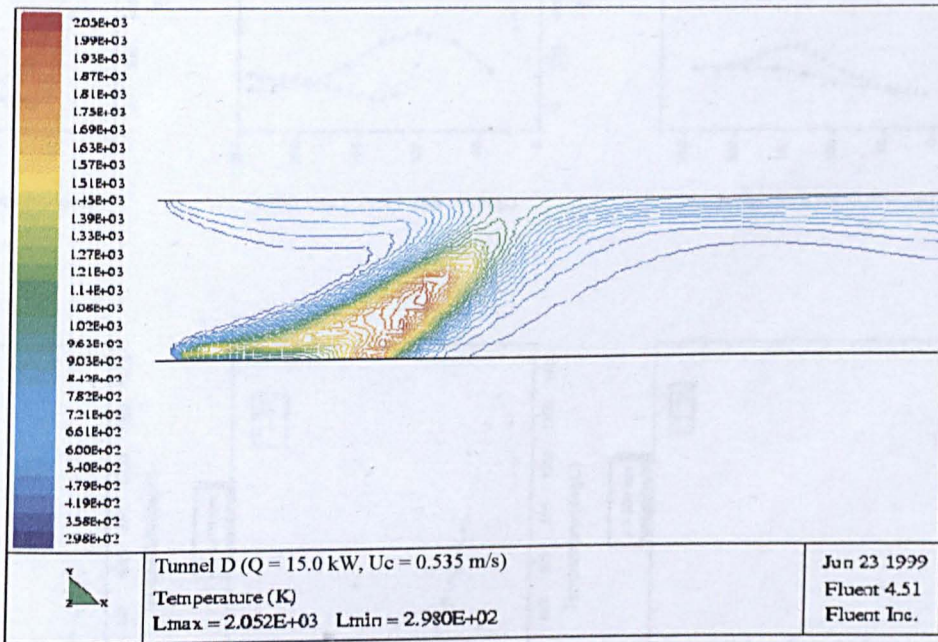
Figure 8.18 : Temperature distribution at symmetrical plane in tunnel D
at critical ventilation conditions
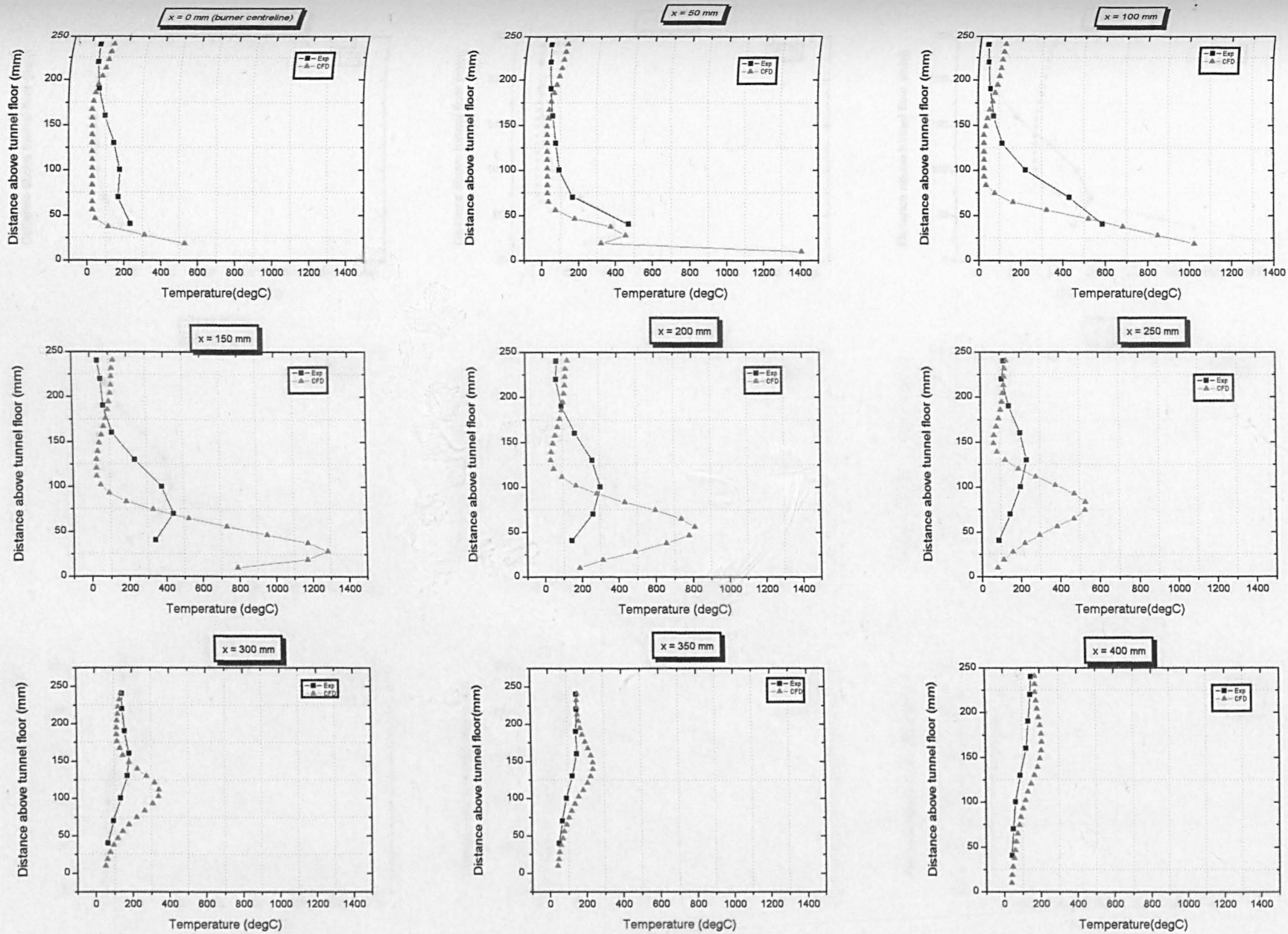
Figure 8.19 : Comparison of temperature distribution at the symmetrical in the fire region in tunnel B at various distances downstream from the burner at 3.0 kW [Uc(exp) = 0.48 m/s, Uc(CFD) = 0.40 m/s]
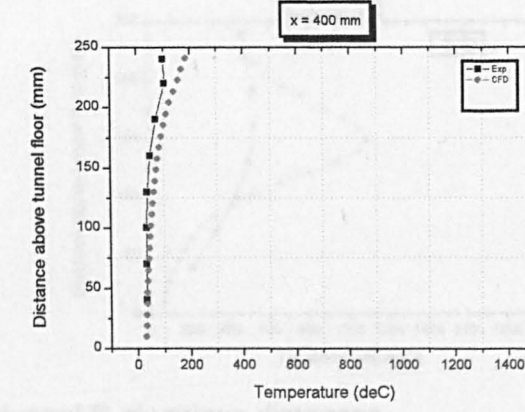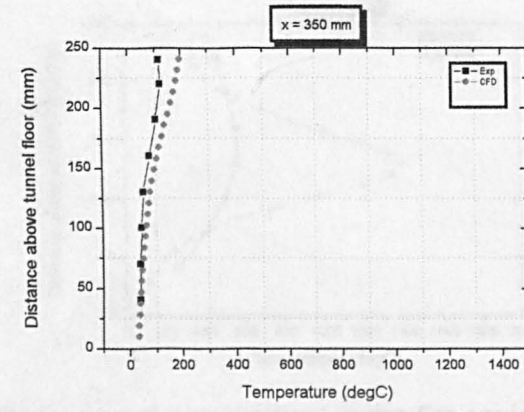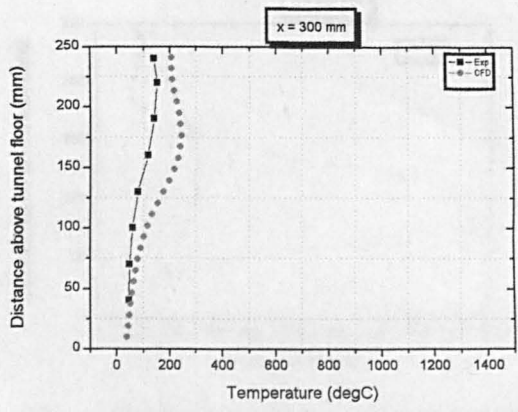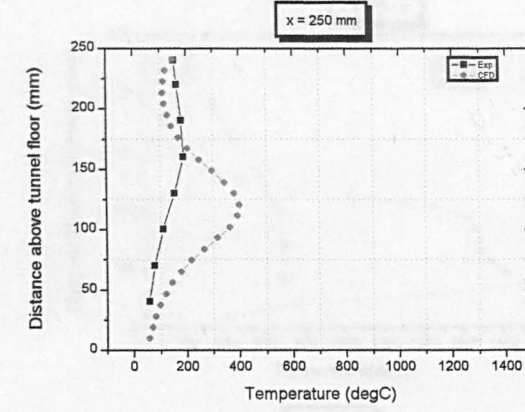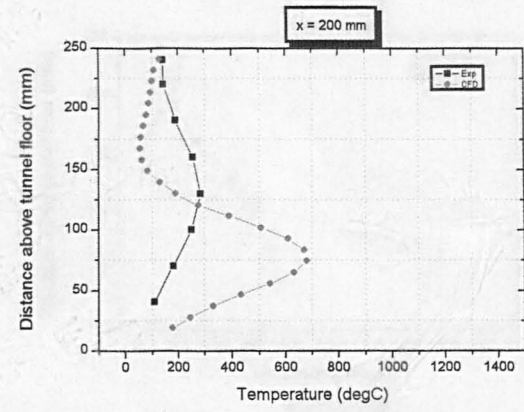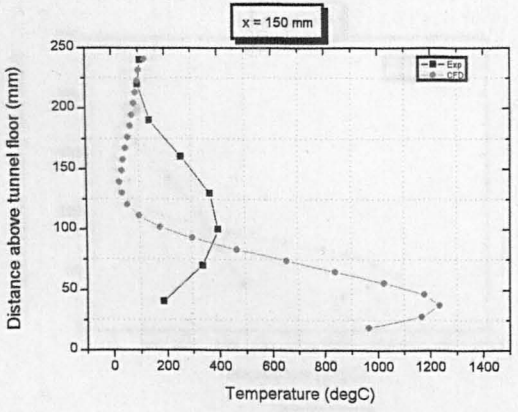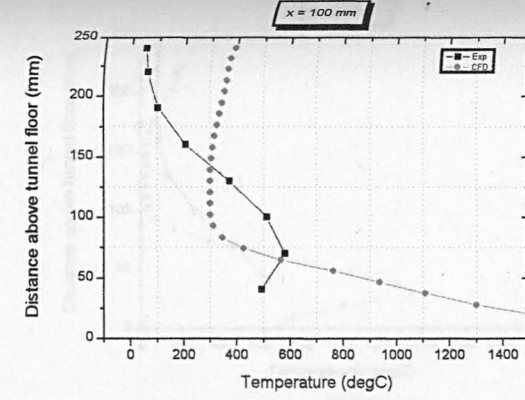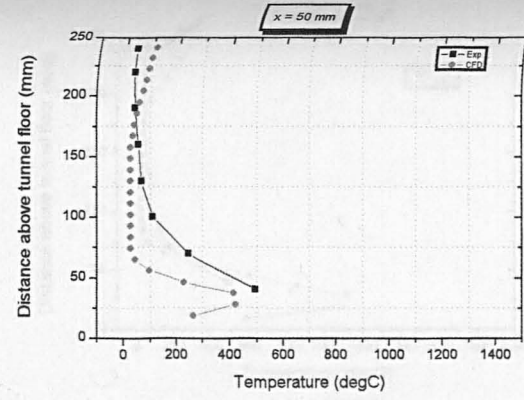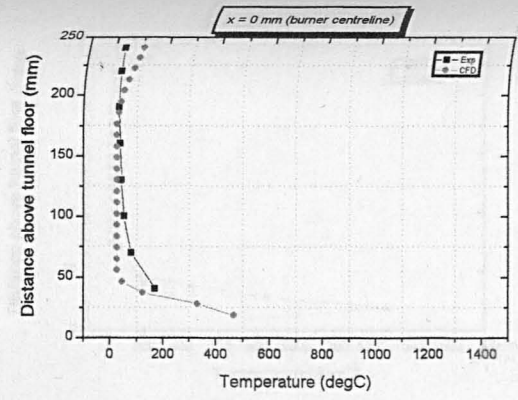
Figure 8.20 : Comparison of temperature distribution at symmetrical in the fire region in tunnel D in the fire region at various distances downstream from theburner at 3.0 kW [Uc(exp) = 0.40 m/s, Uc(CFD) = 0.375 m/s]
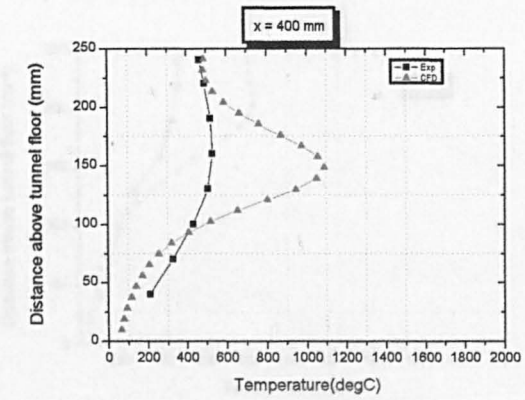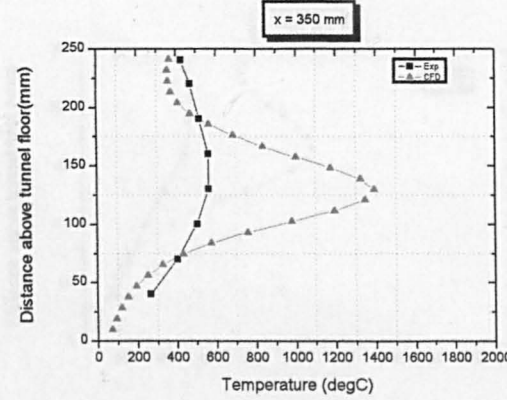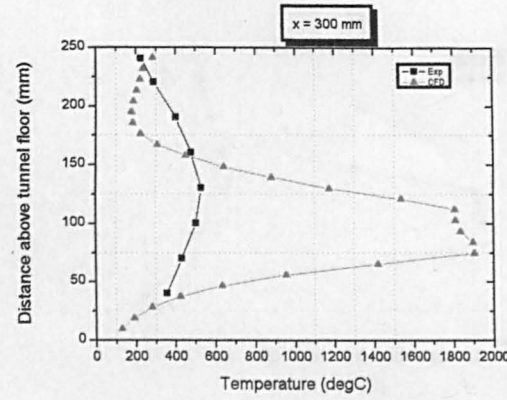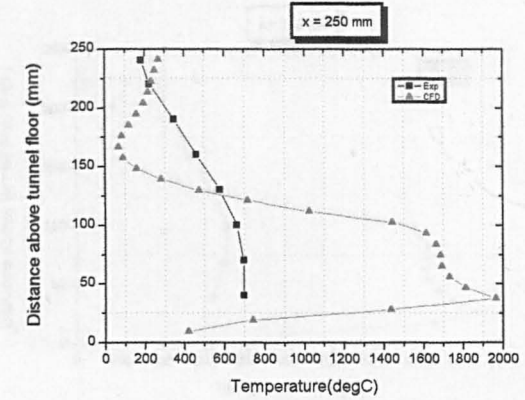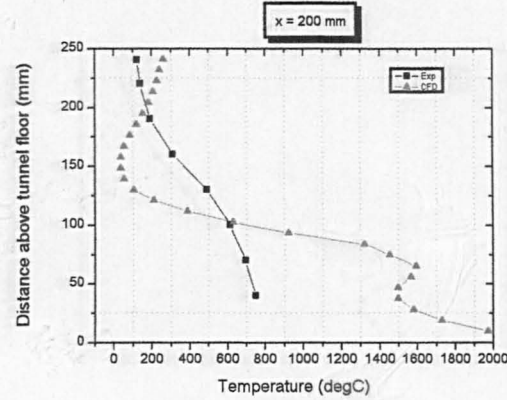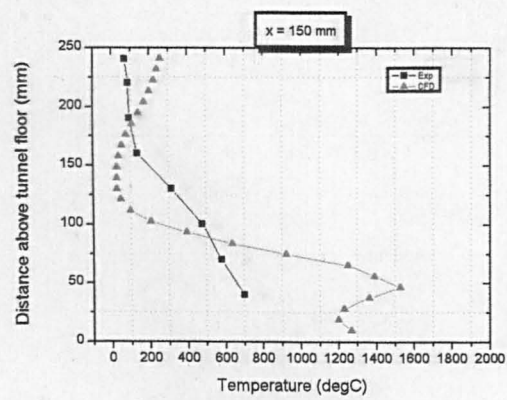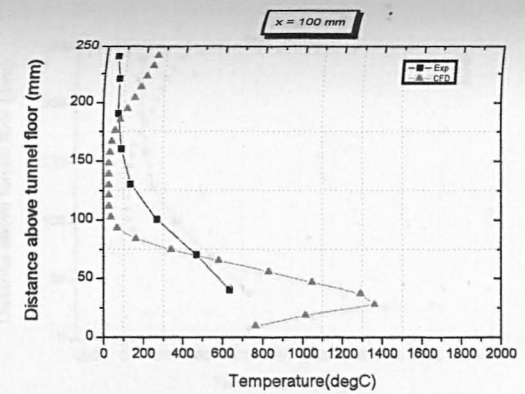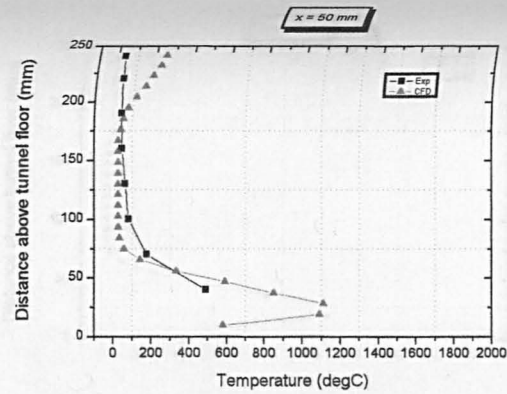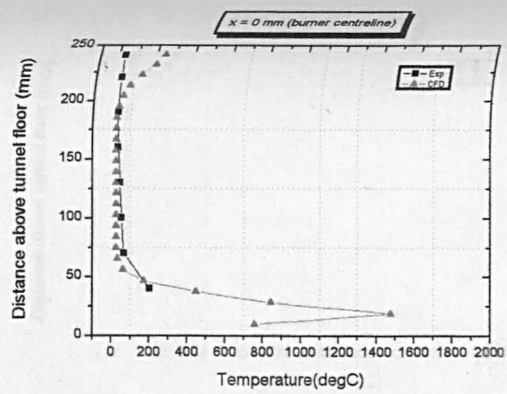
Figure 8.21: Comparison of temperature distribution at symmetrical in the fire region in tunnel B at various distances downstream from the burner at 15.0 kW [Uc(exp) = 0.60 m/s, Uc(CFD) = 0.50 m/s]
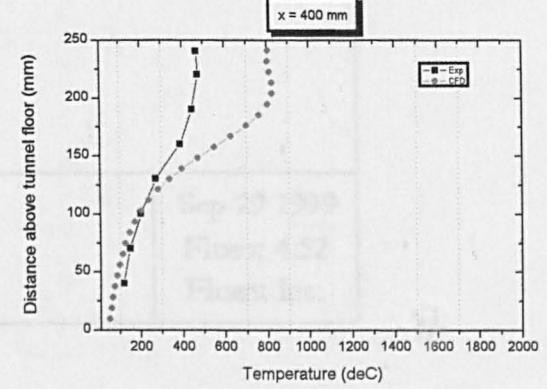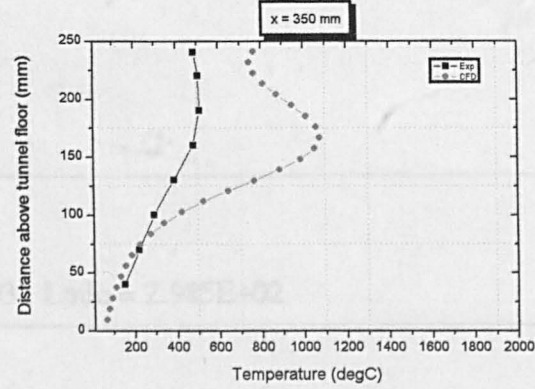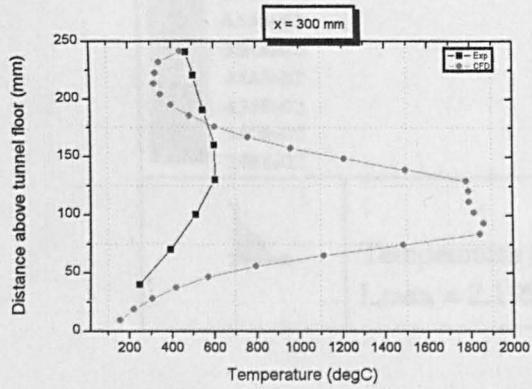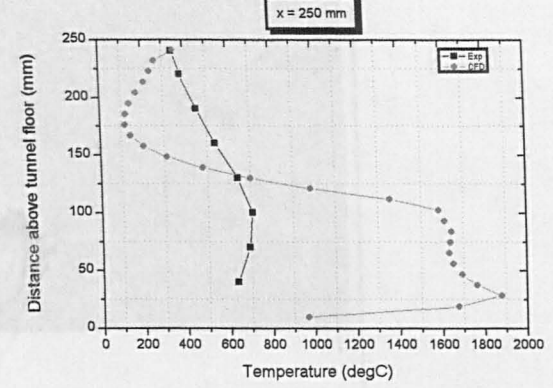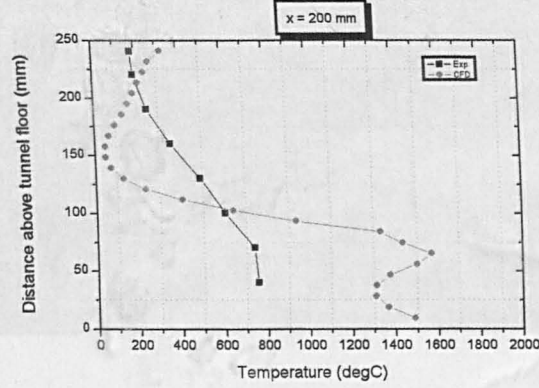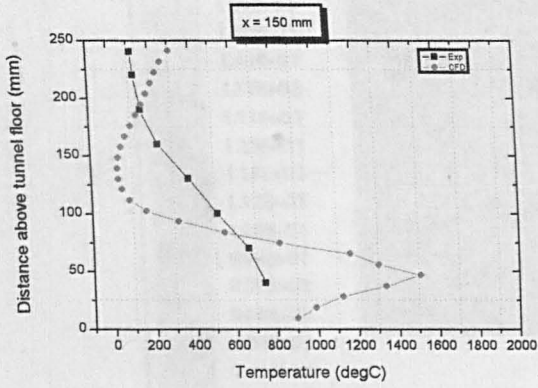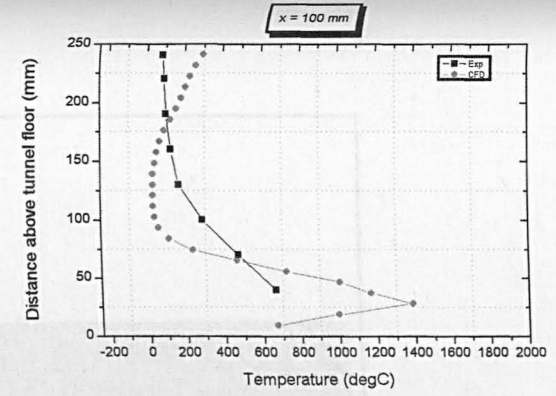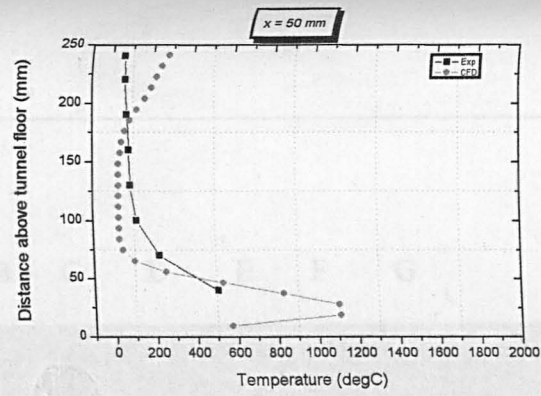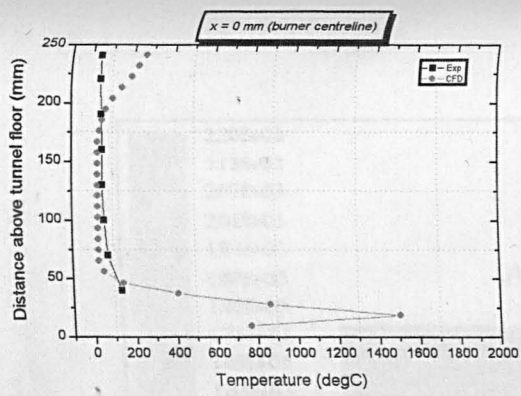
Figure 8.22: Comparison of temperature distribution at the symmetrical in the fire region in tunnel D at various distances from the burner at 15.0 kW[Uc(exp) = 0.59 m/s, Uc(CFD) = 0.535 m/s]
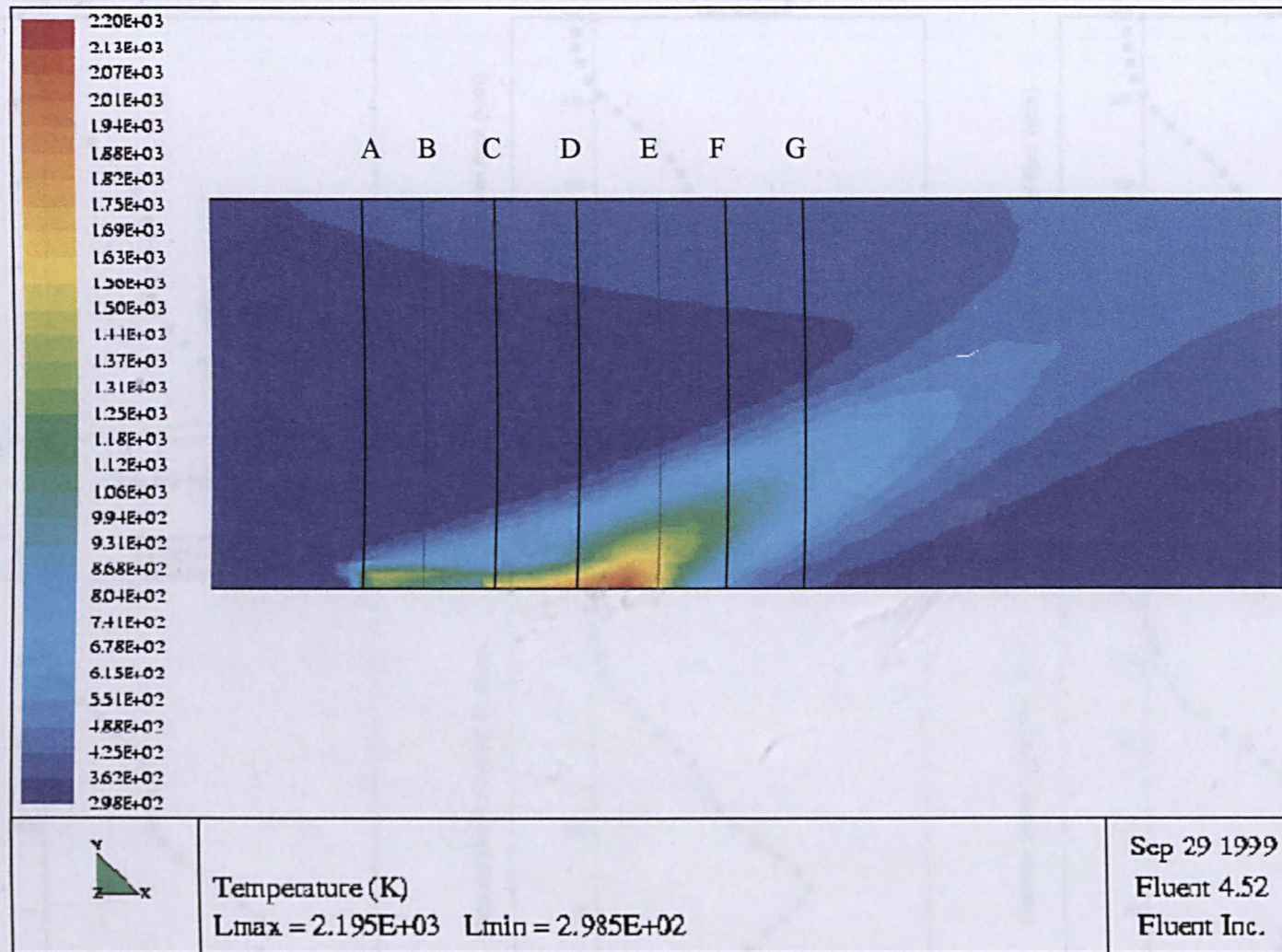
Figure 8.23: Temperature distribution at the symmetrical plane in tunnel B (Q = 3.0 kW, Uc = 0.40 m/s)
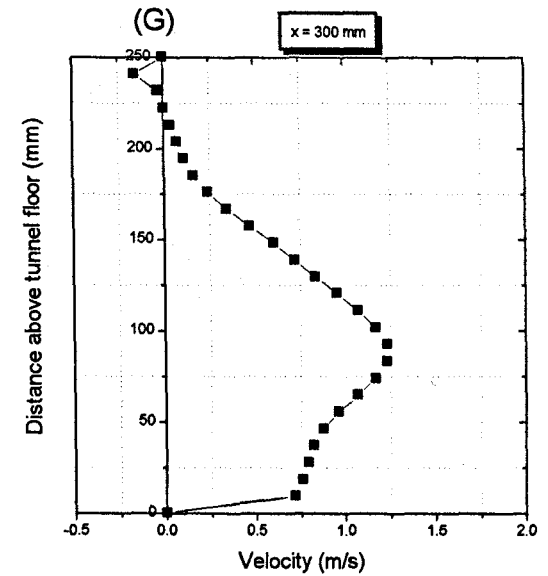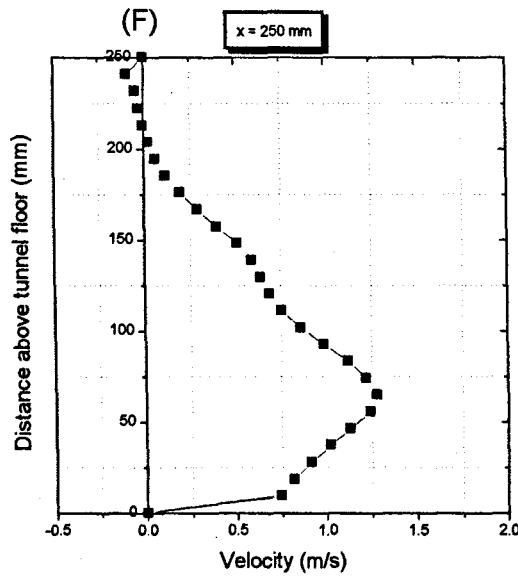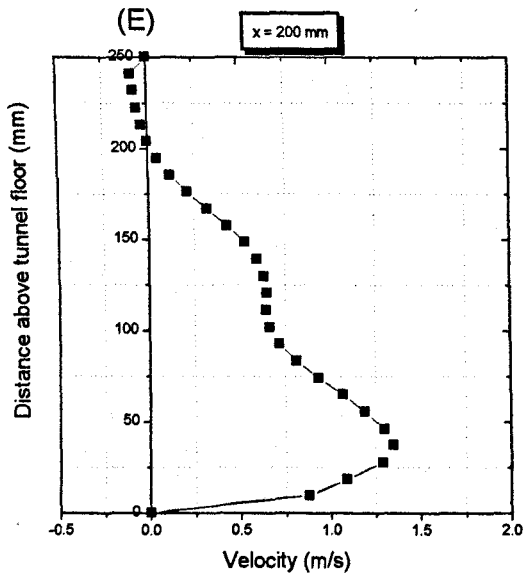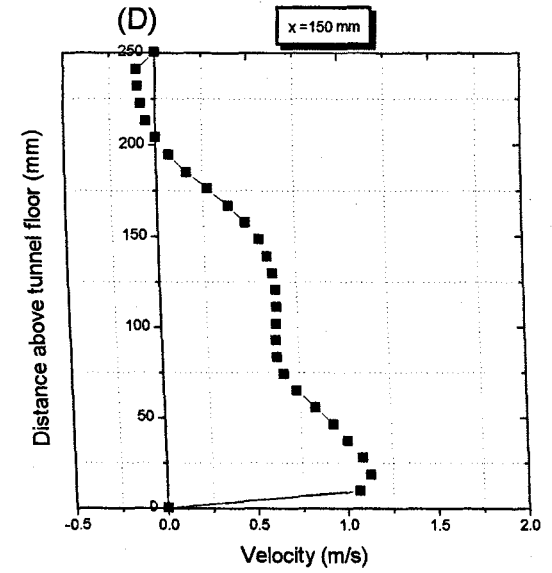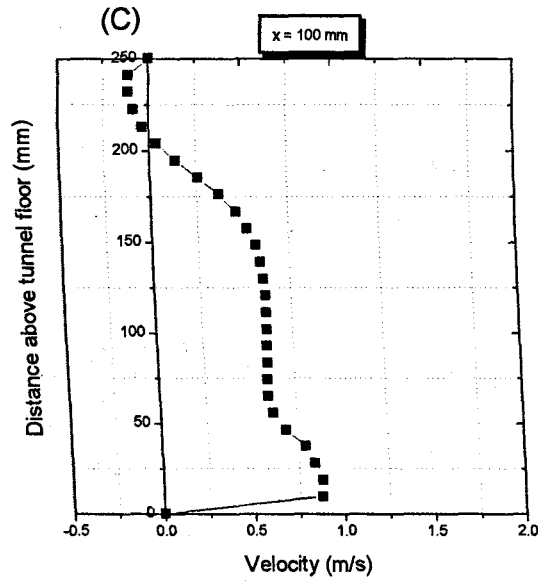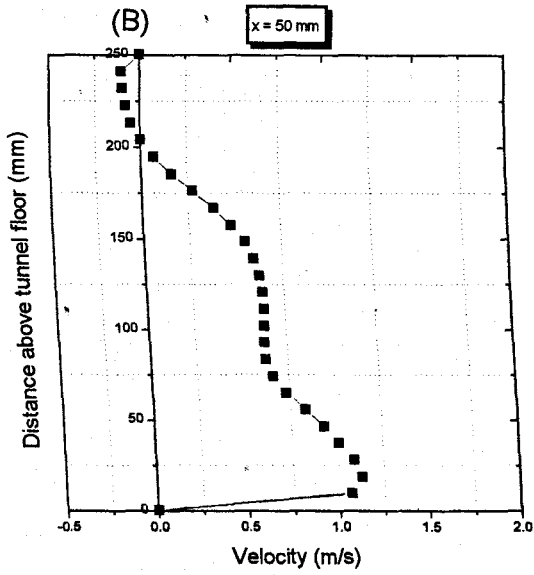
Figure 8.24 : Velocity profiles at the symmetrical plane in tunnel B at various distances from the burner (Q = 3.0 kW, Uc = 0.40 m/s)
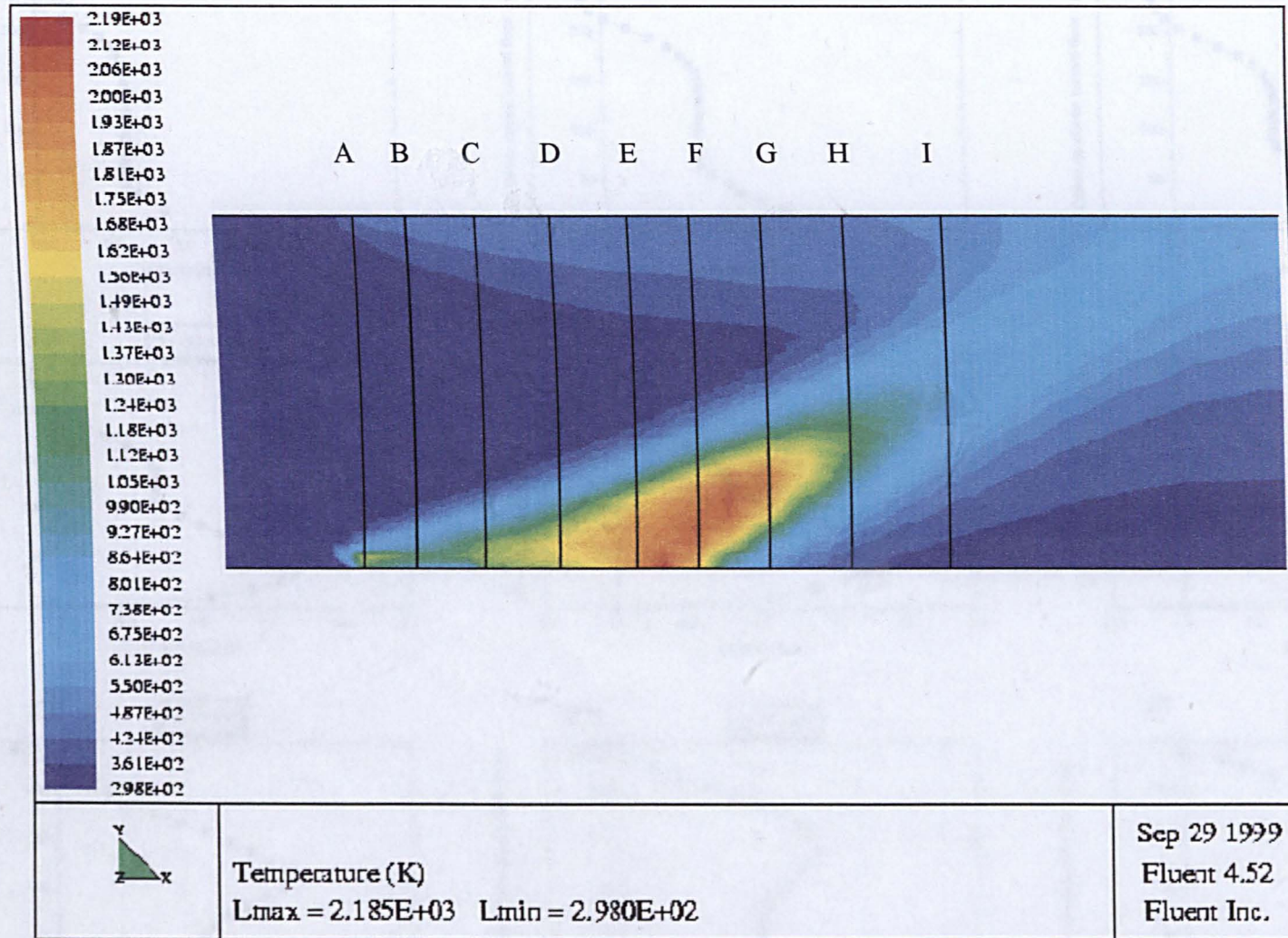
Figure 8.25: Temperature distribution at the symmetrical plane in tunnel B (Q = 7.50 kW, Uc = 0.47 m/s)
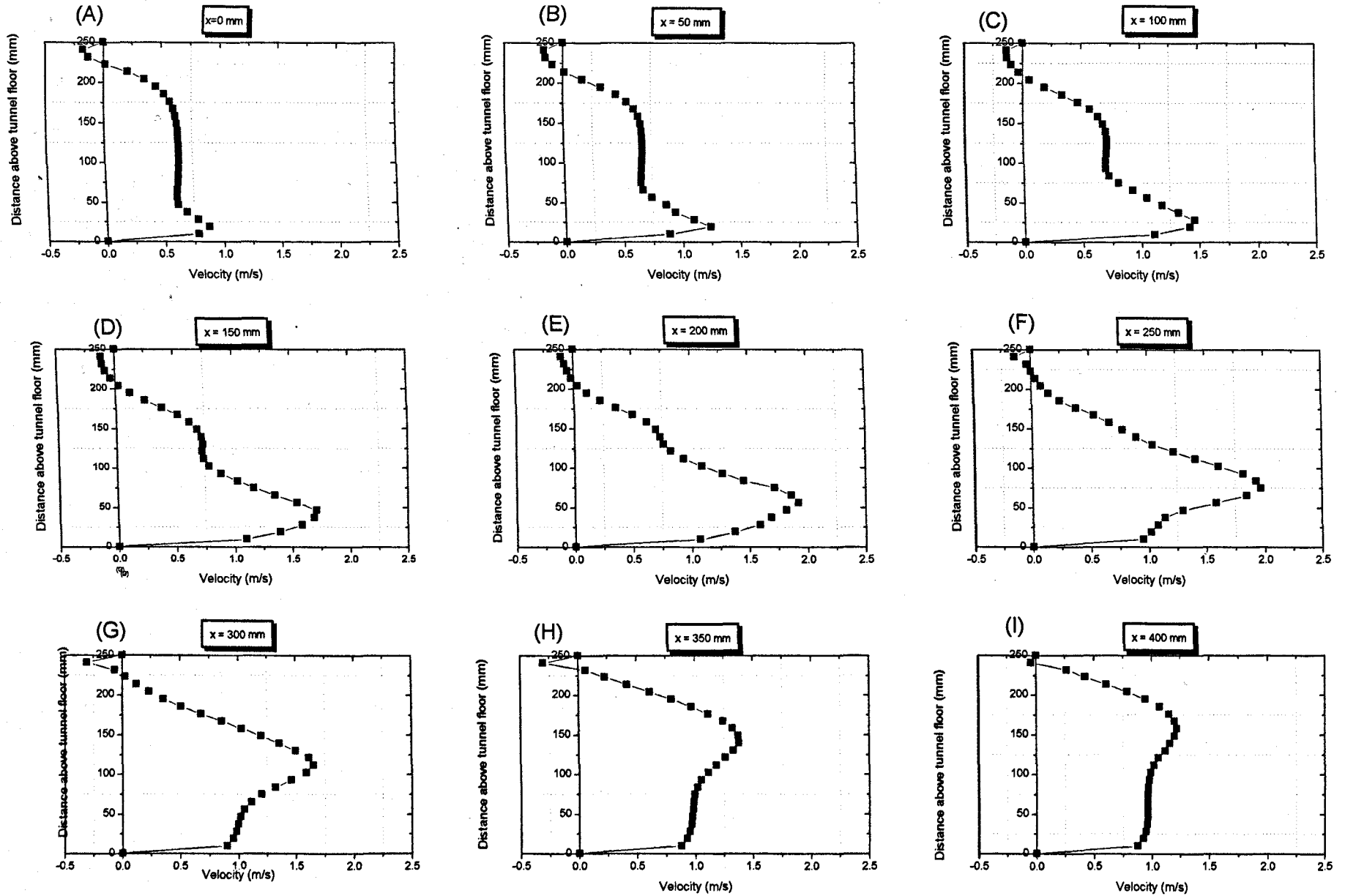
Figure 8.26 :Velocity profiles at the symmetrical plane in tunnel B at various distances from burner (Q = 7.50 kW, Uc = 0.47 m/s)
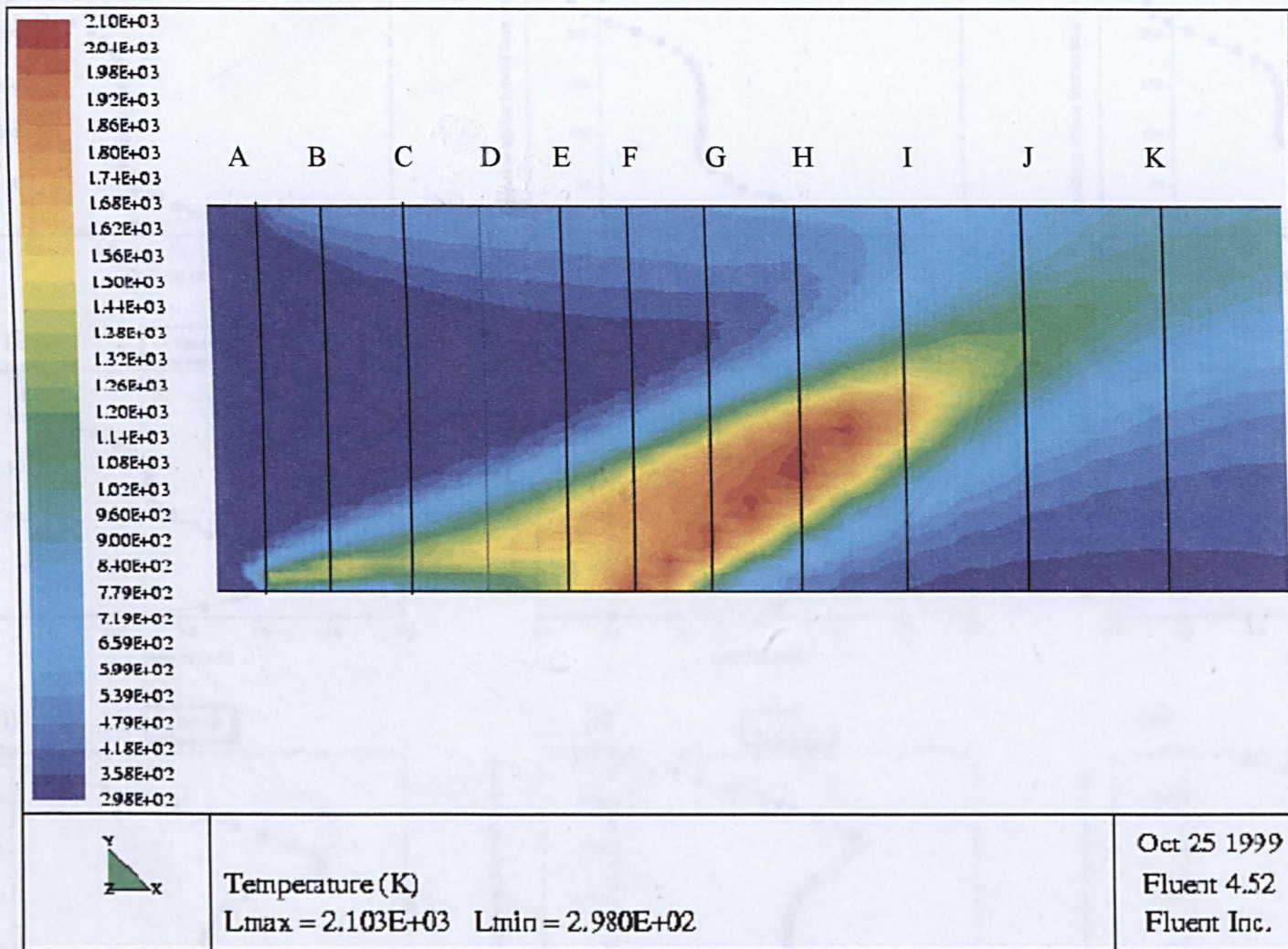
Figure 8.27: Temperature distribution at the symmetrical plane in tunnel B (Q = 15.0 kW, Uc = 0.50 m/s)
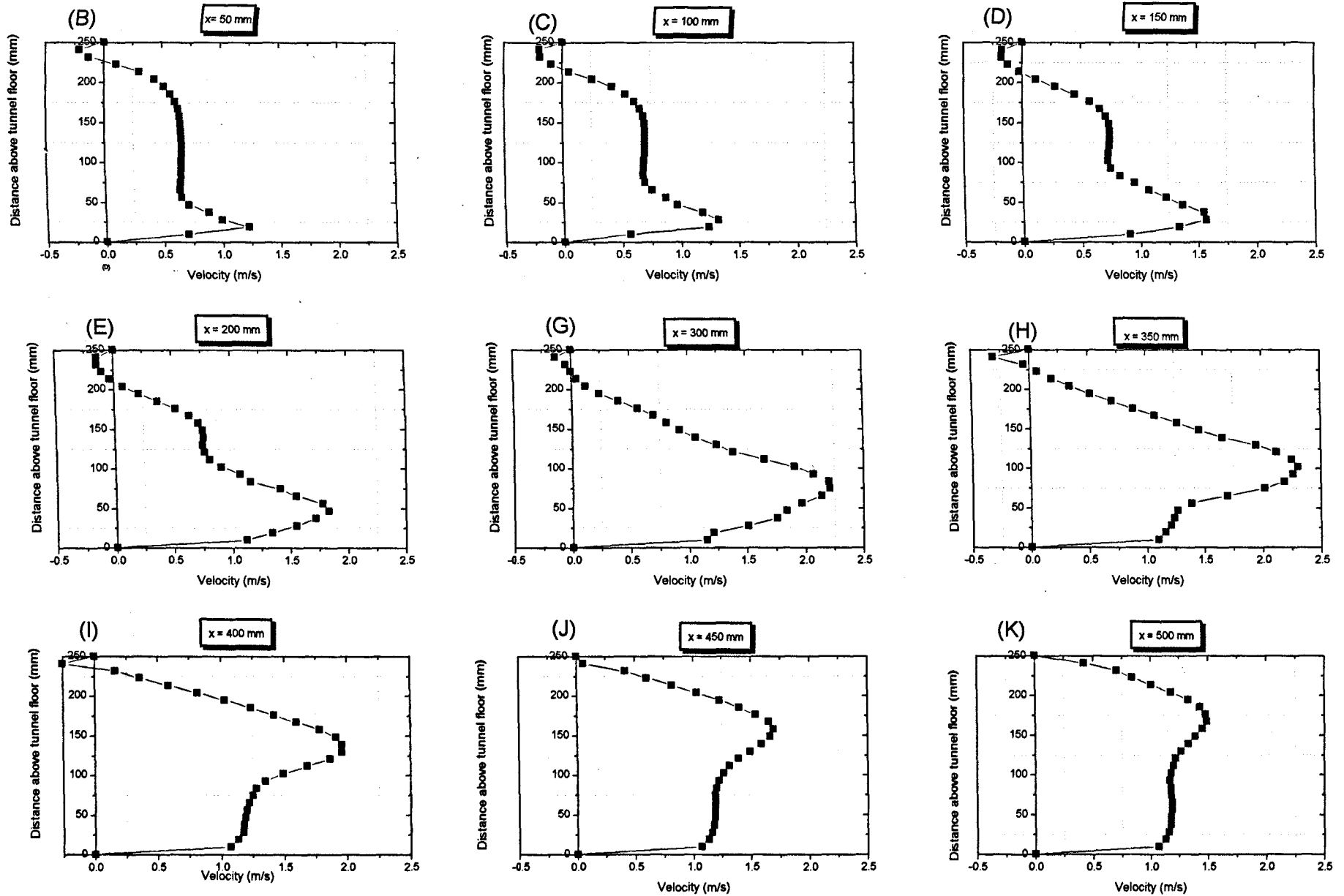
Figure 8.28 : Velocity profiles at the symmetrical plane in tunnel B at various distances from burner (Q = 15.0kW, Uc = 0.50 m/s)

216
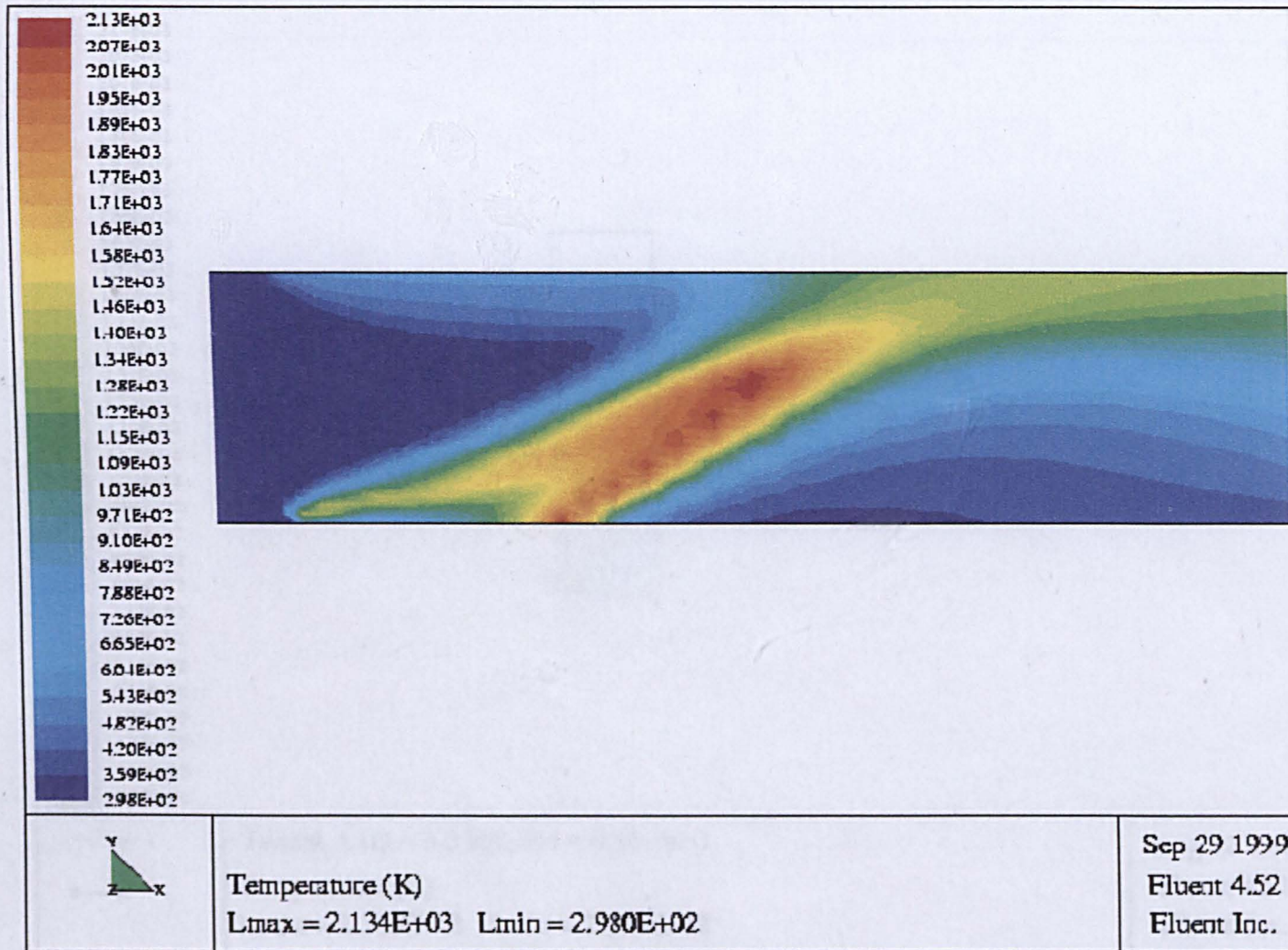
Figure 8. 29 : Temperature distribution at the symmetrical plane in tunnel B (Q = 22.50 kW, Uc = 0.50 m/s)

2.14E+03	
2.07E+03	
2.01E+03	
1.95E+03	
1.88E+03	
1.82E+03	
1.76E+03	
1.69E+03	
1.63E+03	
1.57E+03	
1.50E+03	
1.44E+03	
1.38E+03	
1.31E+03	
1.25E+03	
1.19E+03	
1.12E+03	
1.06E+03	
9.96E+02	
9.33E+02	
8.70E+02	
8.06E+02	
7.43E+02	
6.80E+02	
6.16E+02	
5.53E+02	
4.90E+02	
4.27E+02	
3.63E+02	
3.00E+02	

Y
z — x

Tunnel A (Q = 3.0 kW, Uc = 0.36 m/s)

Temperature (K)

Lmax = 2.135E+03   Lmin = 2.999E+02

Aug 12 1999
Fluent 4.51
Fluent Inc.
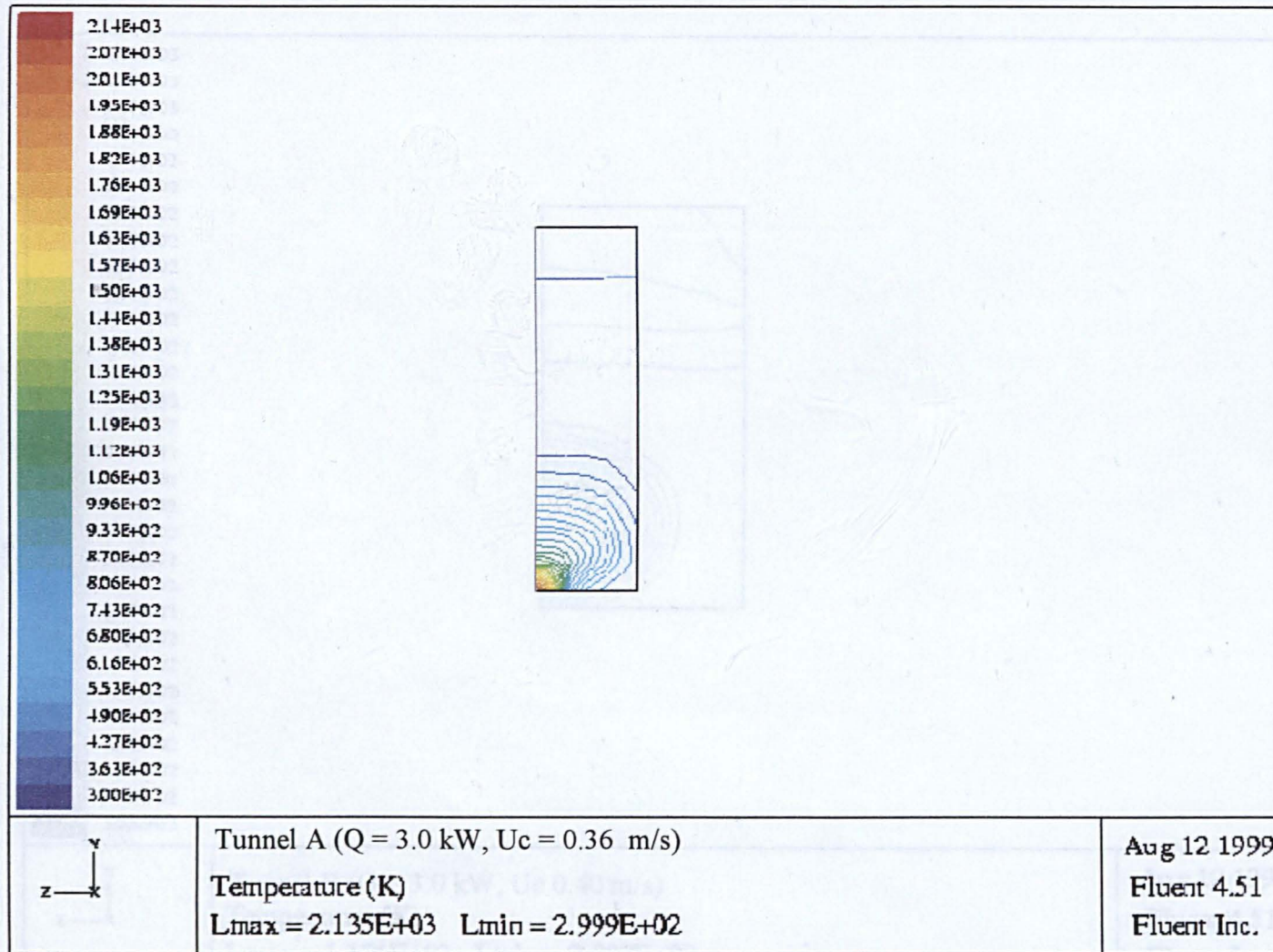
Figure 8.30 : Cross-sectional temperature distribution in tunnel A at 100 mm downstream from
the burner (Q = 3.0 kW, Uc = 0.36 m/s)

1.13E+03	
1.10E+03	
1.07E+03	
1.04E+03	
1.01E+03	
9.83E+02	
9.55E+02	
9.26E+02	
8.98E+02	
8.69E+02	
8.41E+02	
8.12E+02	
7.84E+02	
7.55E+02	
7.27E+02	
6.98E+02	
6.70E+02	
6.41E+02	
6.13E+02	
5.85E+02	
5.56E+02	
5.28E+02	
4.99E+02	
4.71E+02	
4.42E+02	
4.14E+02	
3.85E+02	
3.57E+02	
3.28E+02	
3.00E+02	

Tunnel B (Q = 3.0 kW, Uc 0.40 m/s)
Temperature (K)
Lmax = 1.126E+03   Lmin = 2.997E+02

Aug 12 1999
Fluent 4.51
Fluent Inc.
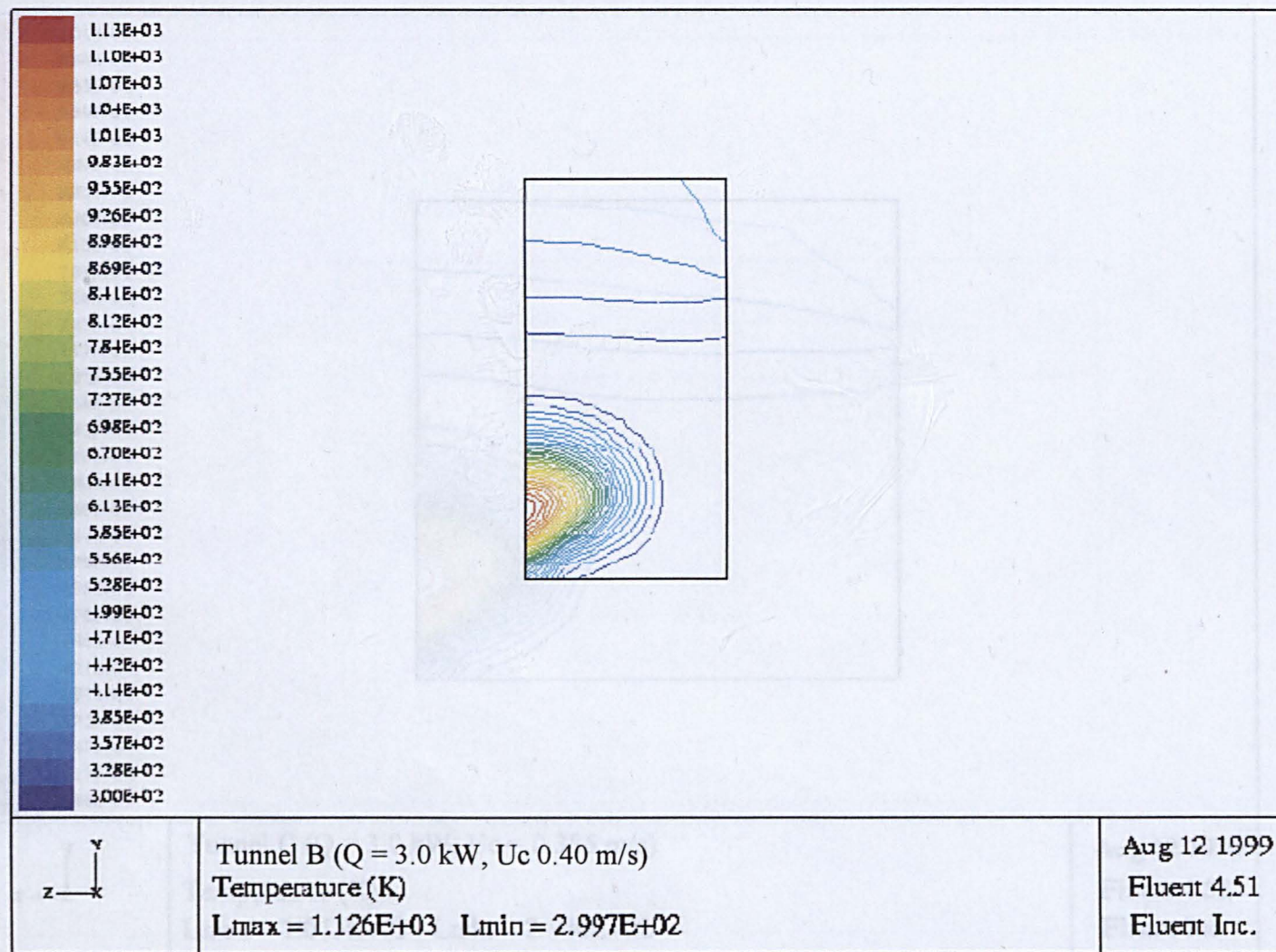
Figure 8.31: Cross-sectional temperature distribution in tunnel B at 100 mm downstream from the burner (Q = 3.0 kW, Uc = 0.40 m/s)
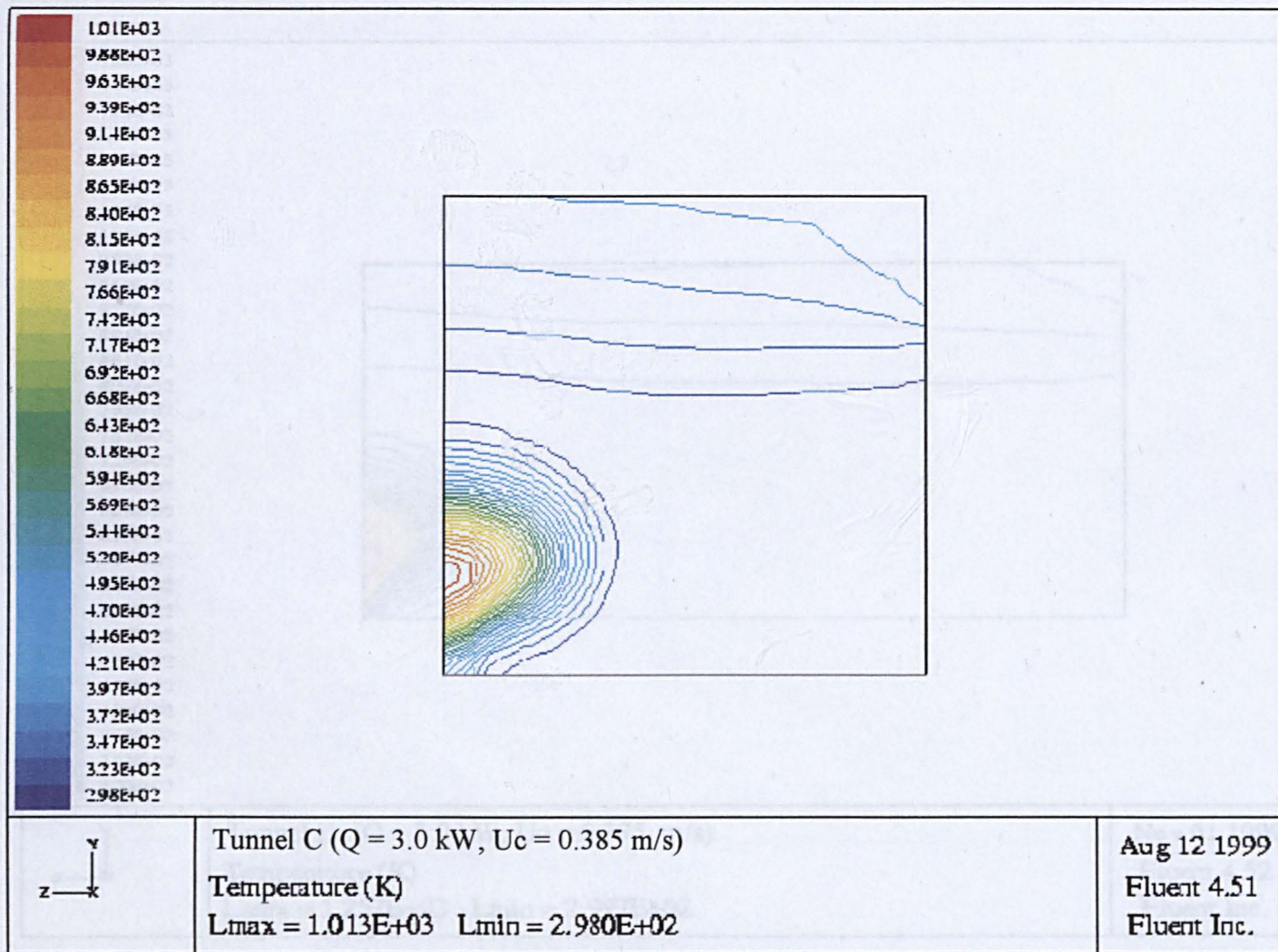
Figure 8.32 :Cross-sectional temperature distribution in tunnel C at 100 mm downstream from the burner (Q = 3.0 kW, Uc = 0.385 m/s)

3.77E-01	
3.64E-01	
3.51E-01	
3.38E-01	
3.25E-01	
3.12E-01	
2.99E-01	
2.87E-01	
2.74E-01	
2.61E-01	
2.48E-01	
2.35E-01	
2.22E-01	
2.09E-01	
1.97E-01	
1.84E-01	
1.71E-01	
1.58E-01	
1.45E-01	
1.32E-01	
1.20E-01	
1.07E-01	
9.38E-02	
8.09E-02	
6.81E-02	
5.52E-02	
4.24E-02	
2.95E-02	
1.67E-02	
3.81E-03	

Tunnel A (Q = 3.0 kW, Uc = 0.36 m/s)

Velocity Vectors (M/S)

Lmax = 3.766E-01   Lmin = 3.809E-03

Aug 12 1999

Fluent 4.51

Fluent Inc.
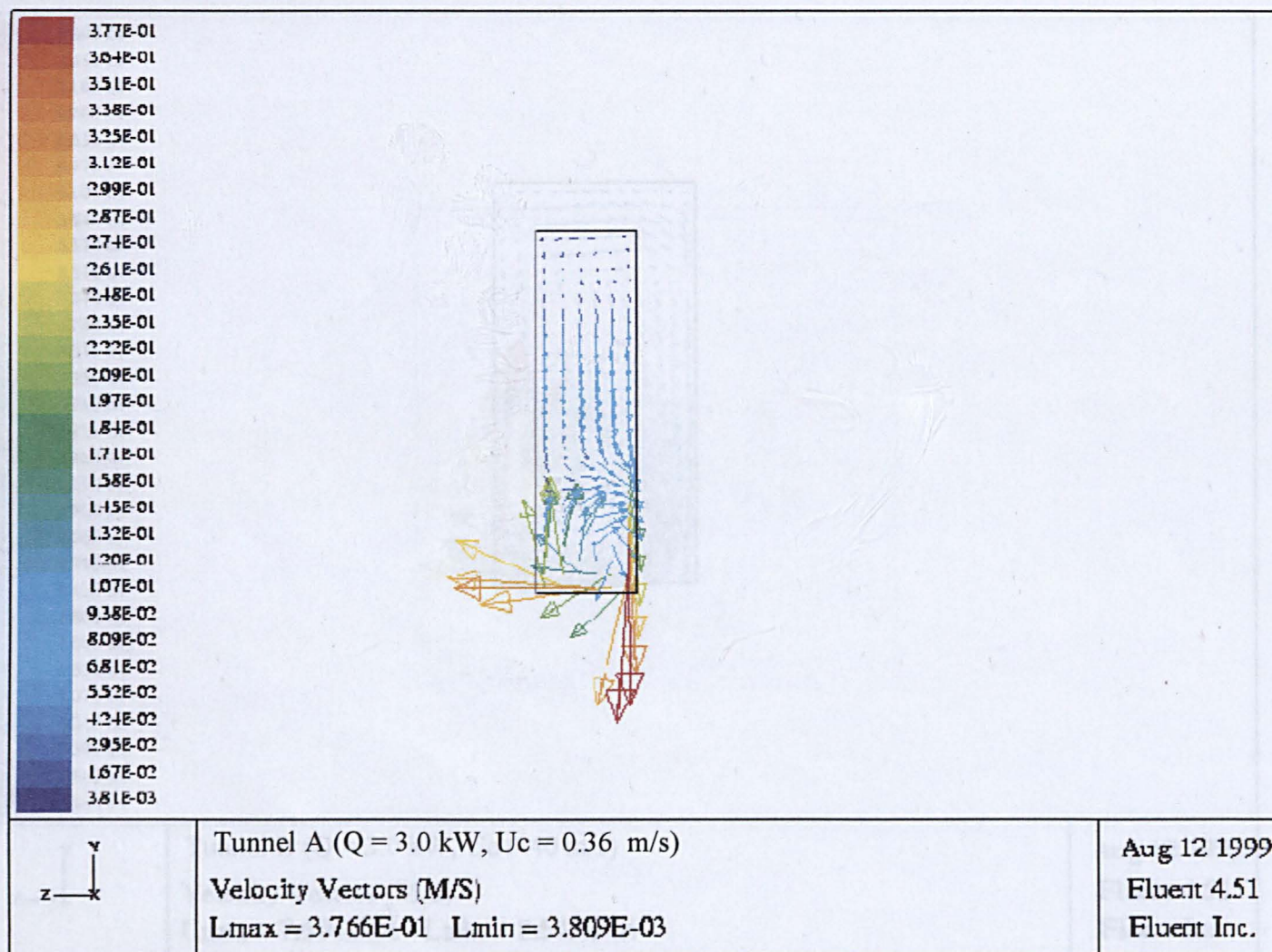
Figure 8.34 : Cross-sectional velocity vectors in tunnel A at 100 mm downstream from
the burner (Q = 3.0 kW, Uc = 0.36 m/s)

7.69E-01	
7.43E-01	
7.16E-01	
6.90E-01	
6.63E-01	
6.37E-01	
6.10E-01	
5.84E-01	
5.57E-01	
5.31E-01	
5.04E-01	
4.78E-01	
4.51E-01	
4.25E-01	
3.98E-01	
3.72E-01	
3.45E-01	
3.19E-01	
2.92E-01	
2.66E-01	
2.39E-01	
2.13E-01	
1.86E-01	
1.60E-01	
1.33E-01	
1.07E-01	
8.04E-02	
5.39E-02	
2.74E-02	
8.54E-04	

Tunnel B (Q = 3.0 kW, Uc 0.40 m/s)

Velocity Vectors (M/S)

Lmax = 7.694E-01   Lmin = 8.543E-04

Aug 12 1999
Fluent 4.51
Fluent Inc.
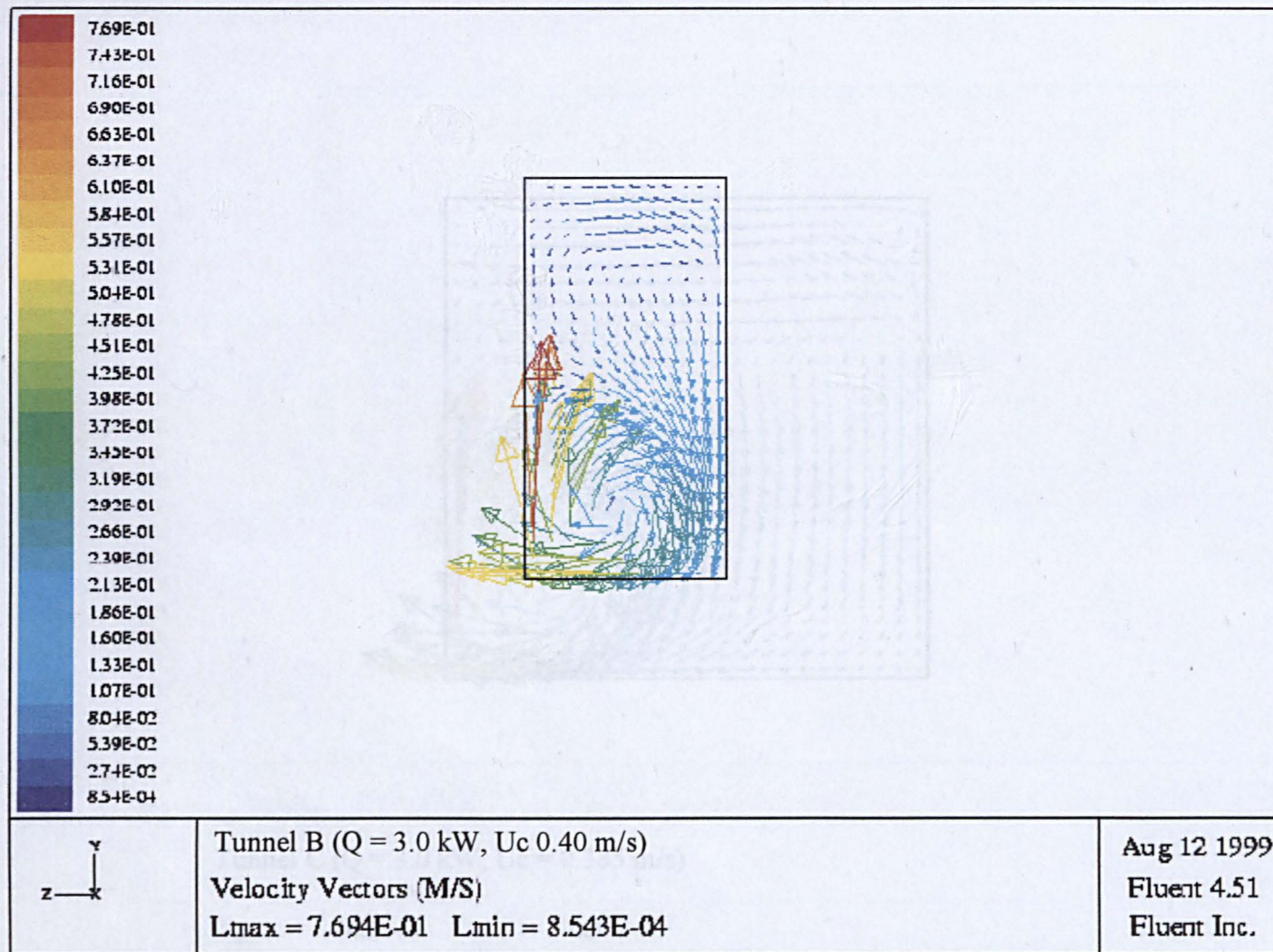
Figure 8.35 : Cross-sectional velocity vectors in tunnel B at 100 mm downstream from
the burner (Q = 3.0 kW, Uc = 0.40 m/s)
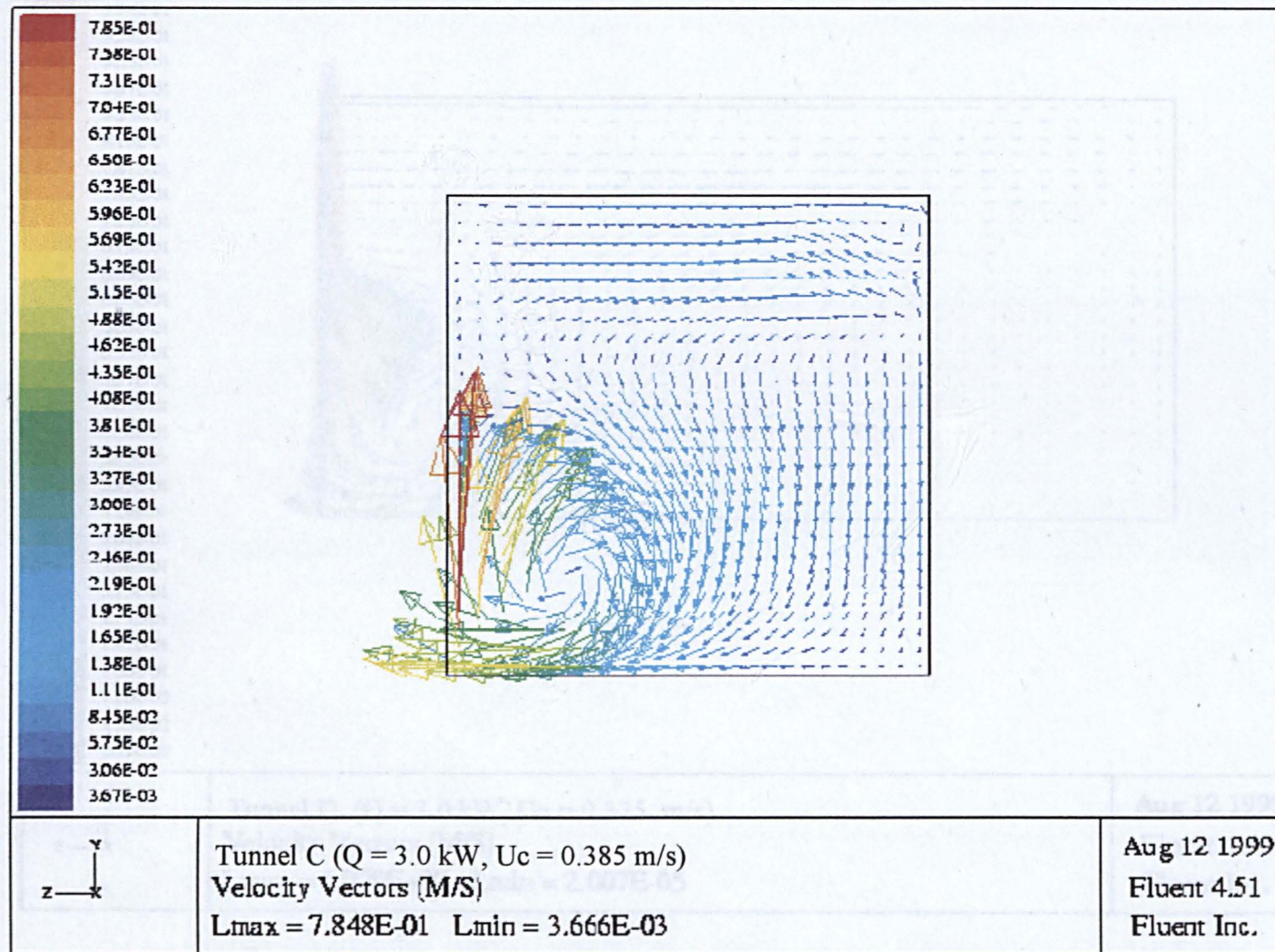
Figure 8.36 : Cross-sectional velocity vectors in tunnel C at 100 mm downstream from the burner (Q = 3.0 kW, Uc = 0.385 m/s)

The color scale (left side) reads from top to bottom:

7.85E-01
7.58E-01
7.31E-01
7.04E-01
6.77E-01
6.50E-01
6.23E-01
5.96E-01
5.69E-01
5.42E-01
5.15E-01
4.88E-01
4.62E-01
4.35E-01
4.08E-01
3.81E-01
3.54E-01
3.27E-01
3.00E-01
2.73E-01
2.46E-01
2.19E-01
1.92E-01
1.65E-01
1.38E-01
1.11E-01
8.45E-02
5.75E-02
3.06E-02
3.67E-03

Tunnel C (Q = 3.0 kW, Uc = 0.385 m/s)
Velocity Vectors (M/S)
Lmax = 7.848E-01   Lmin = 3.666E-03

Aug 12 1999
Fluent 4.51
Fluent Inc.

Color scale (left):

```
1.03E+00
9.94E-01
9.58E-01
9.23E-01
8.87E-01
8.52E-01
8.16E-01
7.81E-01
7.45E-01
7.10E-01
6.74E-01
6.39E-01
6.03E-01
5.68E-01
5.32E-01
4.97E-01
4.61E-01
4.26E-01
3.90E-01
3.55E-01
3.19E-01
2.84E-01
2.48E-01
2.13E-01
1.77E-01
1.42E-01
1.06E-01
7.10E-02
3.55E-02
2.01E-05
```

Tunnel D (Q = 3.0 kW, Uc = 0.375 m/s)
Velocity Vectors (M/S)
Lmax = 1.029E+00   Lmin = 2.007E-05

Aug 12 1999
Fluent 4.51
Fluent Inc.

Figure 8.37 : Cross-sectional velocity vectors in tunnel D at 100 mm downstream from the burner (Q = 3.0 kW, Uc = 0.375 m/s)

| 5.12E-01 |
| 4.46E-01 |
| 3.81E-01 |
| 3.15E-01 |
| 2.50E-01 |
| 1.84E-01 |
| 1.19E-01 |
| 5.33E-02 |
| -1.22E-02 |
| -7.77E-02 |
| -1.43E-01 |
| -2.09E-01 |
| -2.74E-01 |
| -3.40E-01 |
| -4.05E-01 |
| -4.71E-01 |
| -5.36E-01 |
| -6.02E-01 |
| -6.67E-01 |
| -7.33E-01 |
| -7.98E-01 |
| -8.64E-01 |
| -9.29E-01 |
| -9.95E-01 |
| -1.06E+00 |
| -1.13E+00 |
| -1.19E+00 |
| -1.26E+00 |
| -1.32E+00 |
| -1.39E+00 |
| -1.45E+00 |

Fire Plume Region

Total Pressure (Pa)
Lmax = 5.117E-01   Lmin = -1.453E+00

Nov 03 1999
Fluent 4.52
Fluent Inc.
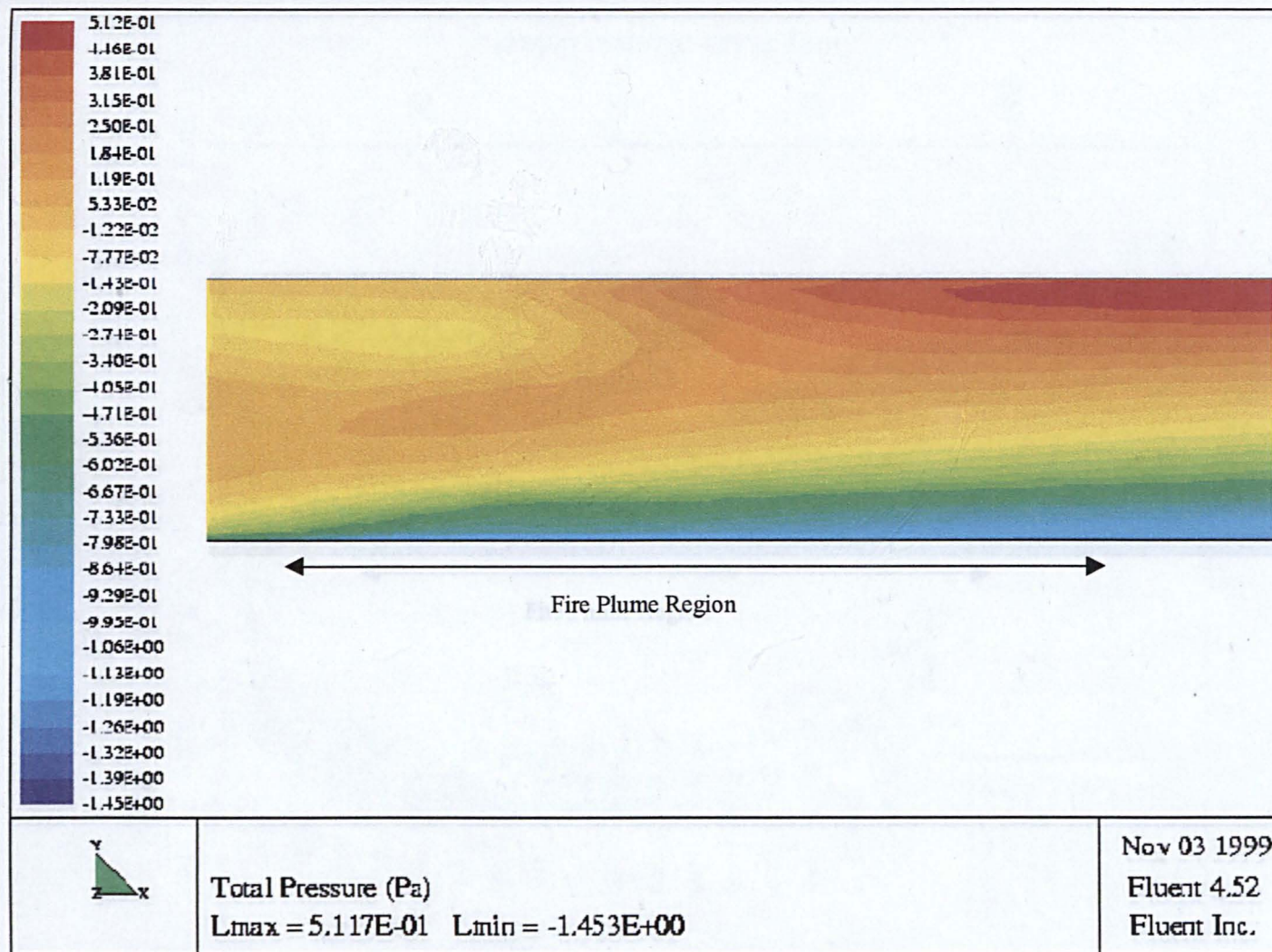
Figure 8. 38: Pressure contours at the symmetrical plane in tunnel A at 7.50 kW at critical condition
Uc = 0.375 m/s
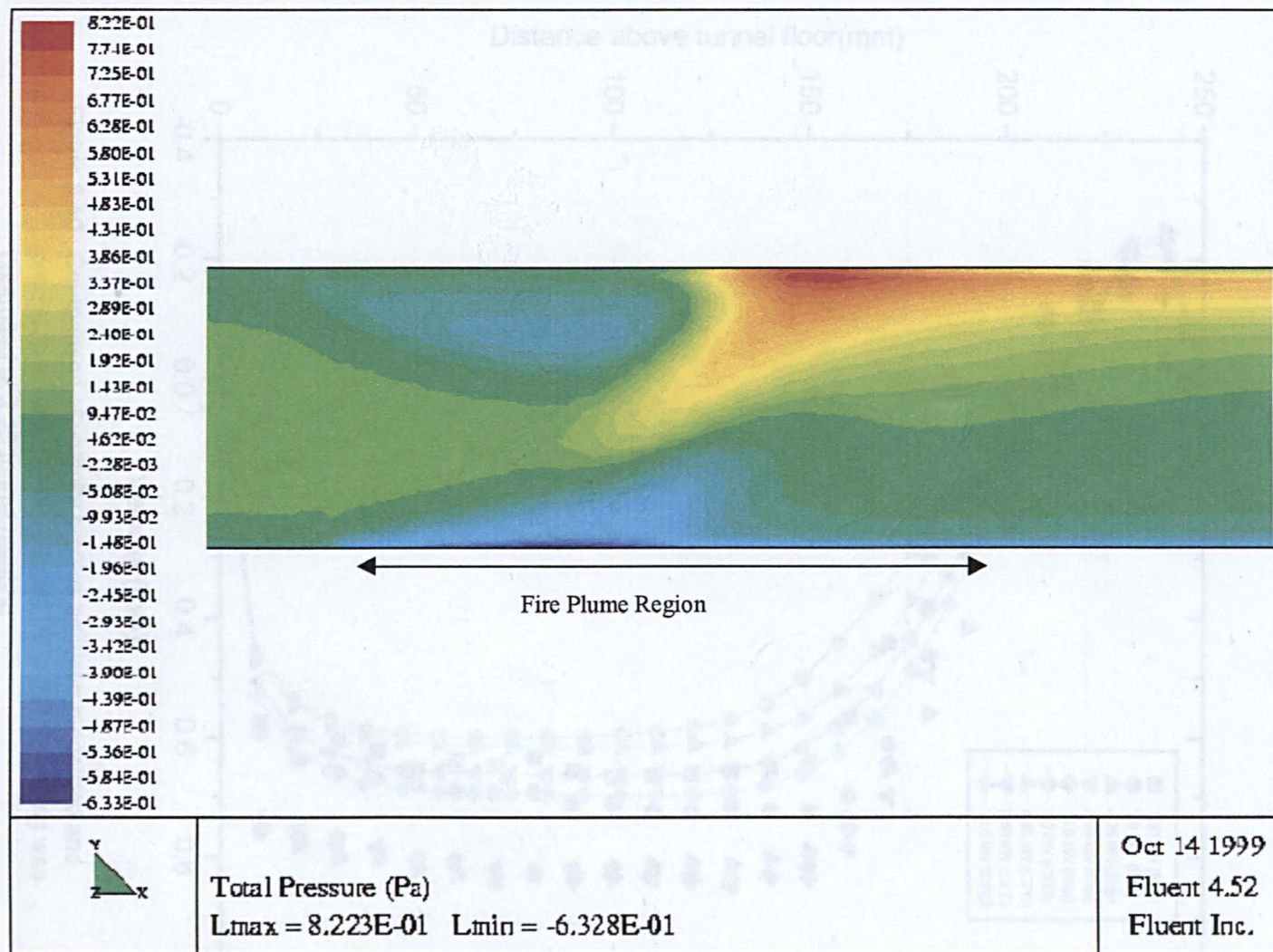
Figure 8. 39: Pressure contours at the symmetrical plane in tunnel D at 7.50 kW at critical condition
Uc = 0.46 m/s
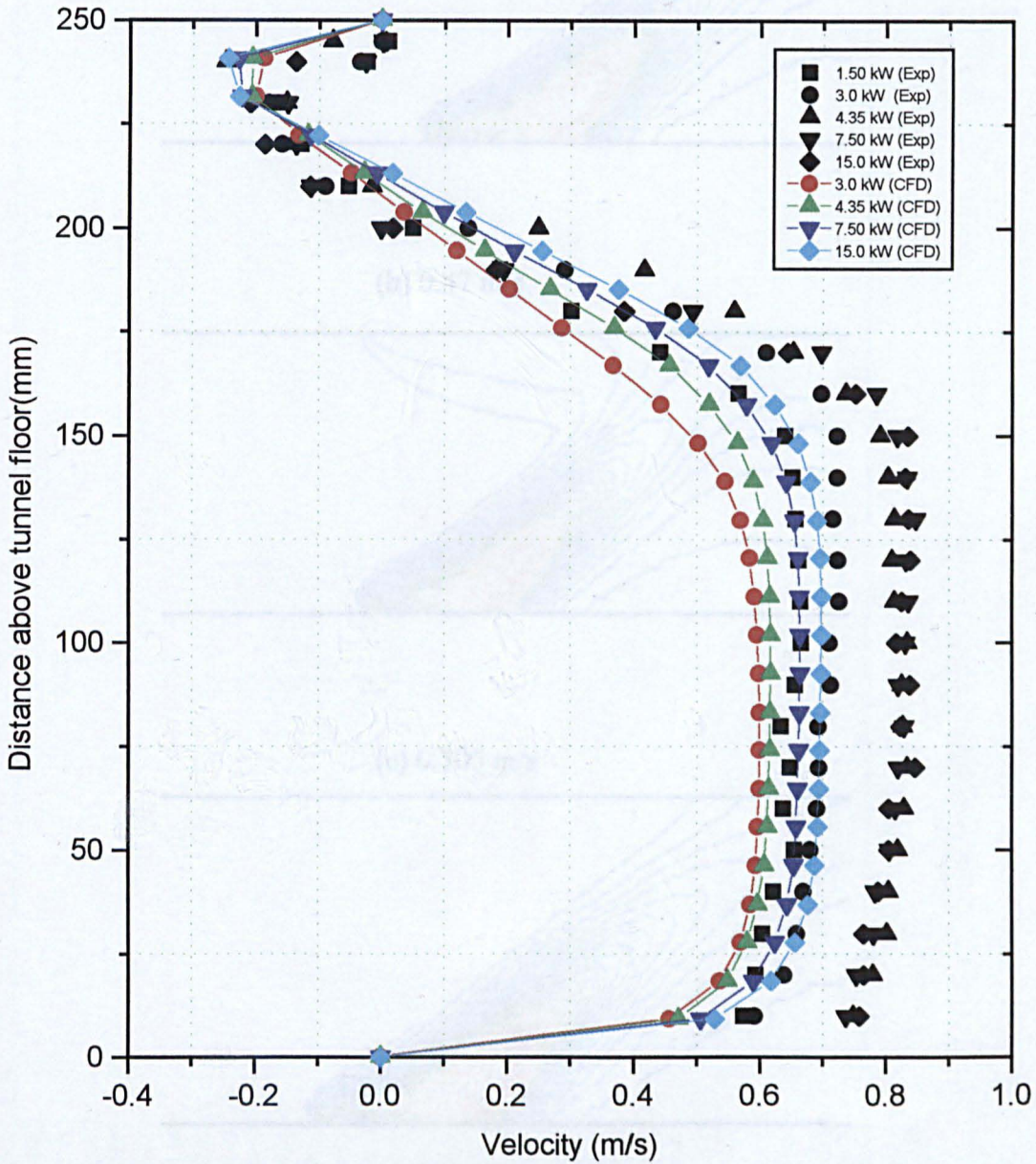
Figure 8.40 : Comparison of velocity profiles between measured and predicted in tunnel B at various HRRs (Backlayering was controlled at 2.25 tunnel heights)

(a) V = 0.44 m/s
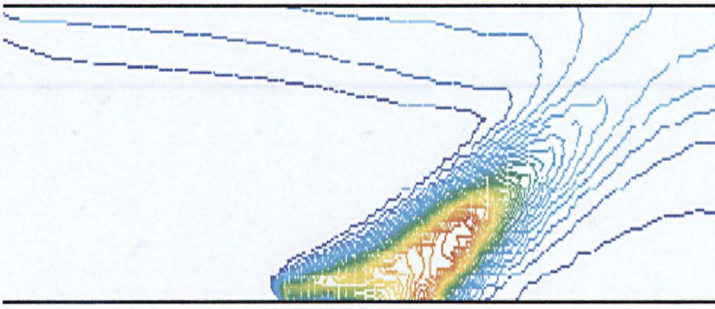
(b) 0.47 m/s
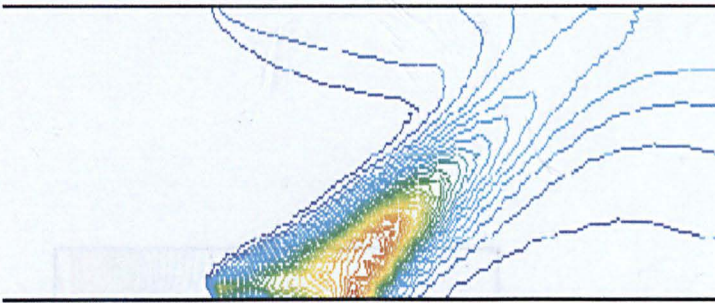
(c) 0.705 m/s
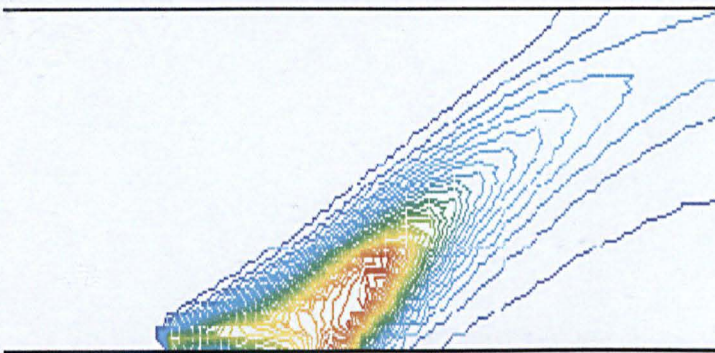
Figure 8. 41 :Temperature distributions at the symmetrical plane in tunnel B at 7.50 kW.
Effects of ventilation velocities

Color scale (top to bottom):
4.83E+02
4.77E+02
4.70E+02
4.64E+02
4.58E+02
4.51E+02
4.45E+02
4.39E+02
4.32E+02
4.26E+02
4.20E+02
4.13E+02
4.07E+02
4.01E+02
3.95E+02
3.88E+02
3.82E+02
3.76E+02
3.69E+02
3.63E+02
3.57E+02
3.50E+02
3.44E+02
3.38E+02
3.31E+02
3.25E+02
3.19E+02
3.13E+02
3.06E+02
3.00E+02

Tunnel A
Cross-sectional temperature distribution

Oct 14 1999
Fluent 4.52
Fluent Inc.
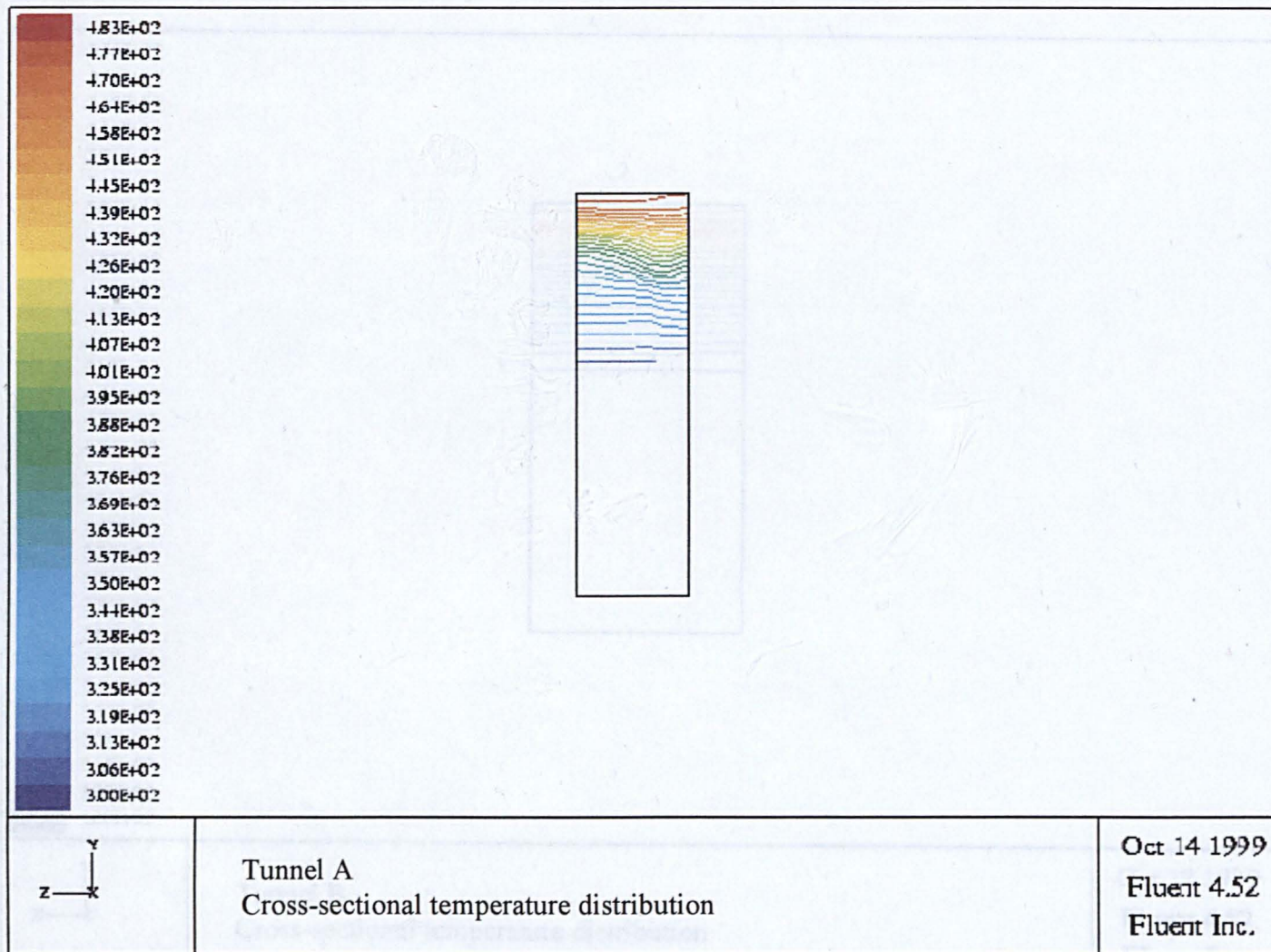
Figure 8.42 : Cross-sectional temperature distribution in tunnel A at 100 mm upstream from the burner (Q = 3.0 kW, backlayering was controlled at 2 tunnel heights upstream)

5.56E+02	
5.47E+02	
5.39E+02	
5.30E+02	
5.21E+02	
5.12E+02	
5.03E+02	
4.94E+02	
4.85E+02	
4.77E+02	
4.68E+02	
4.59E+02	
4.50E+02	
4.41E+02	
4.32E+02	
4.24E+02	
4.15E+02	
4.06E+02	
3.97E+02	
3.88E+02	
3.79E+02	
3.71E+02	
3.62E+02	
3.53E+02	
3.44E+02	
3.35E+02	
3.26E+02	
3.18E+02	
3.09E+02	
3.00E+02	

Tunnel B
Cross-sectional temperature distribution

Oct 12 1999
Fluent 4.52
Fluent Inc.
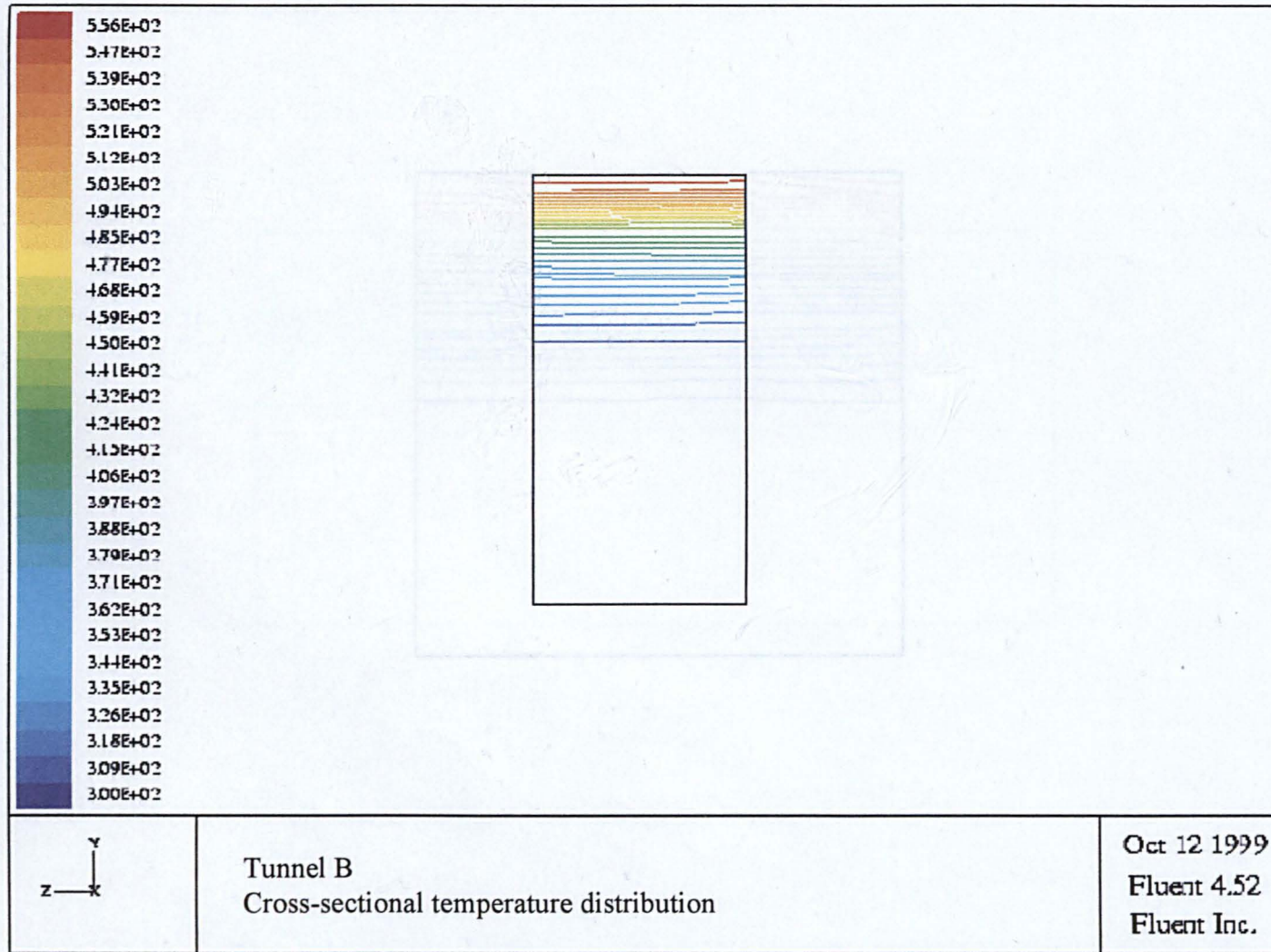
Figure 8.43 : Cross-sectional temperature distribution in tunnel B at 100 mm upstream from
the burner(Q = 3.0 kW, backlayering was controlled at 2 tunnel heights upstream)

Legend (temperature values):

5.01E+02
4.94E+02
4.87E+02
4.81E+02
4.74E+02
4.67E+02
4.60E+02
4.53E+02
4.46E+02
4.39E+02
4.32E+02
4.25E+02
4.18E+02
4.11E+02
4.04E+02
3.97E+02
3.90E+02
3.83E+02
3.76E+02
3.69E+02
3.62E+02
3.56E+02
3.49E+02
3.42E+02
3.35E+02
3.28E+02
3.21E+02
3.14E+02
3.07E+02
3.00E+02

Tunnel C
Cross-sectional temperature distribution

Oct 13 1999
Fluent 4.52
Fluent Inc.
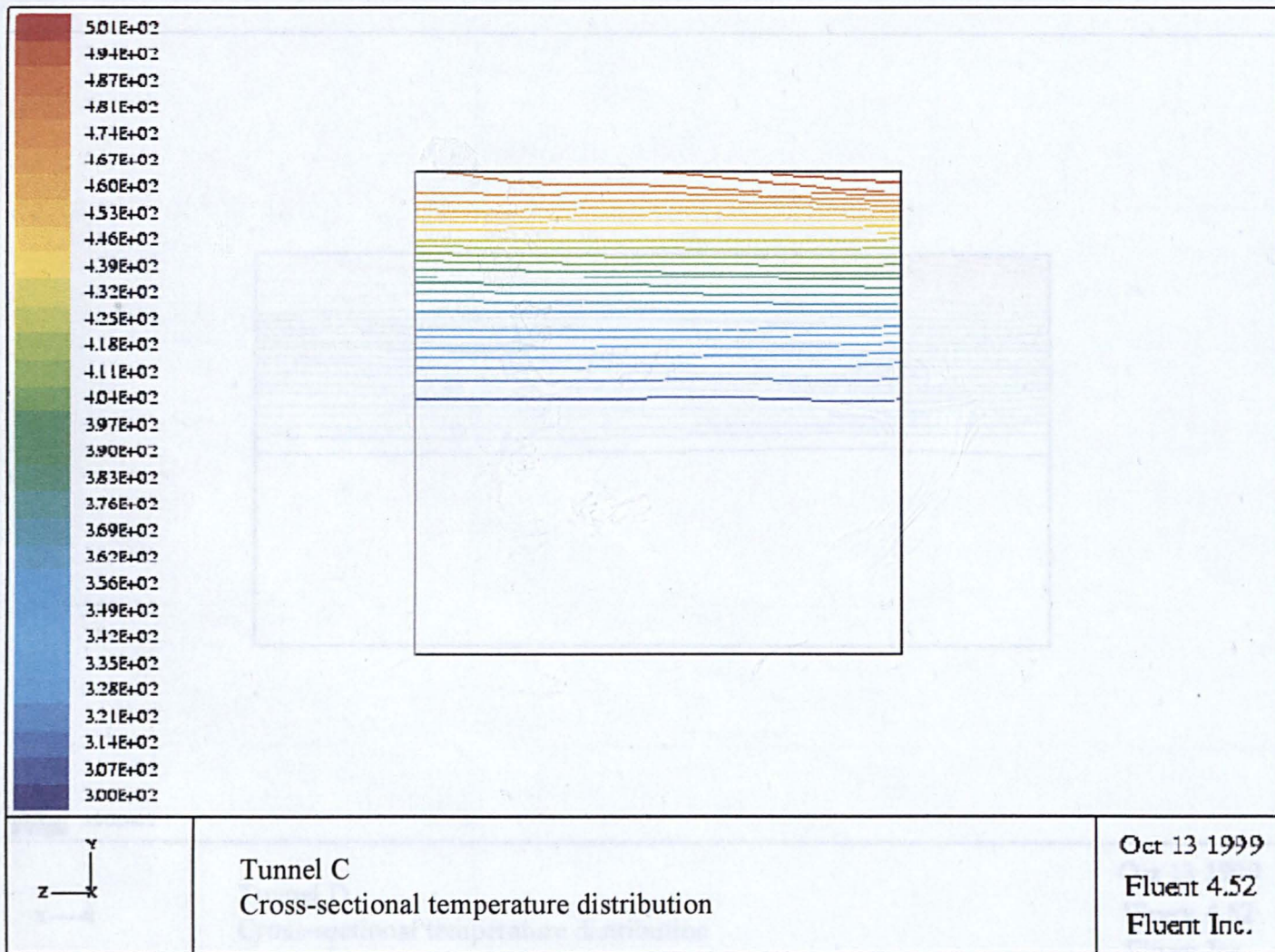
Figure 8.44 : Cross-sectional temperature distribution in tunnel C at 100 mm upstream from the burner (Q = 3.0 kW, backlayering was controlled at 2 tunnel heights upstream)
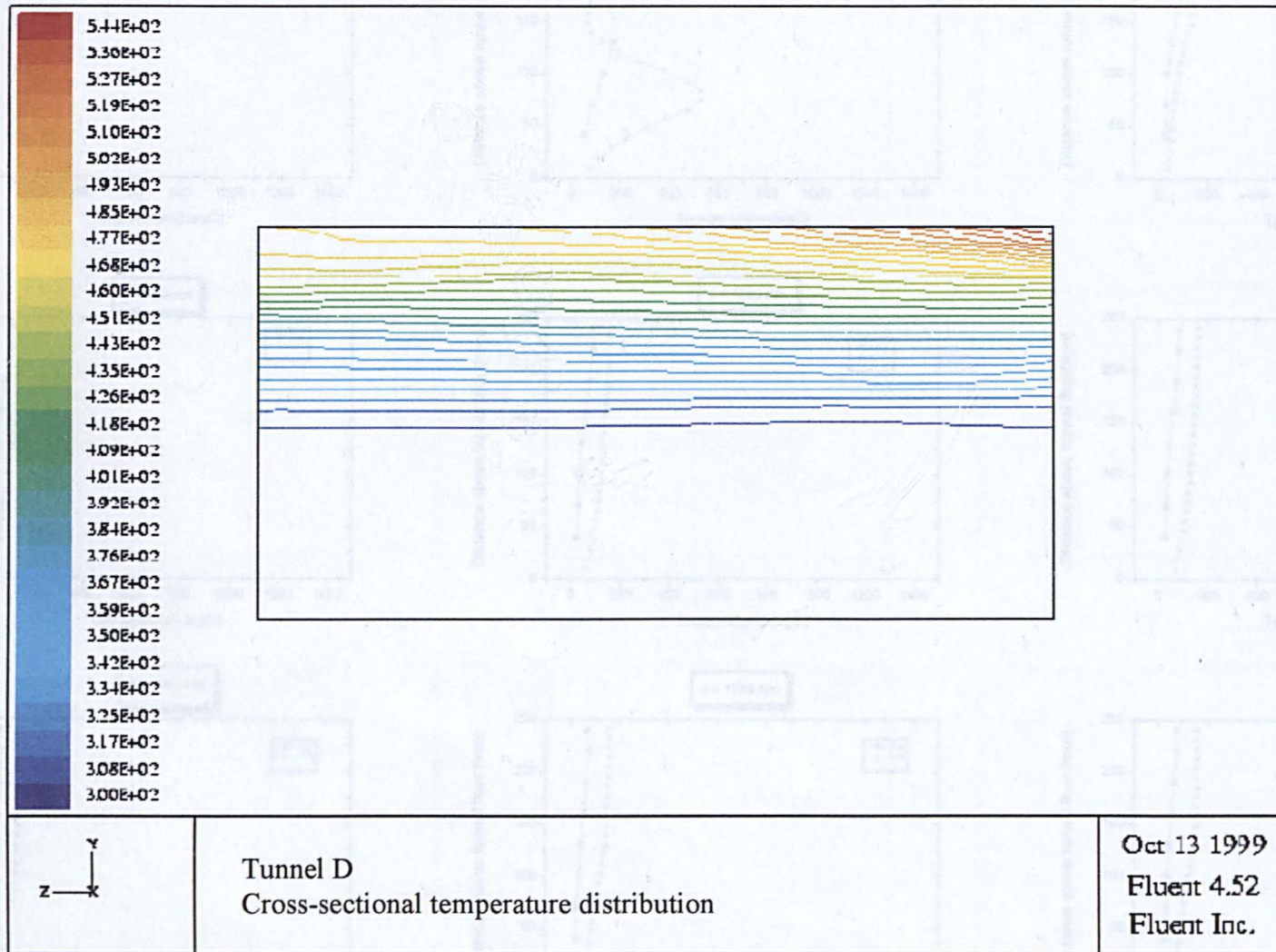
Figure 8.45 : Cross-sectional temperature distribution in tunnel D at 100 mm upstream from
the burner (Q = 3.0 kW, backlayering was controlled at 2 tunnel height upstream)
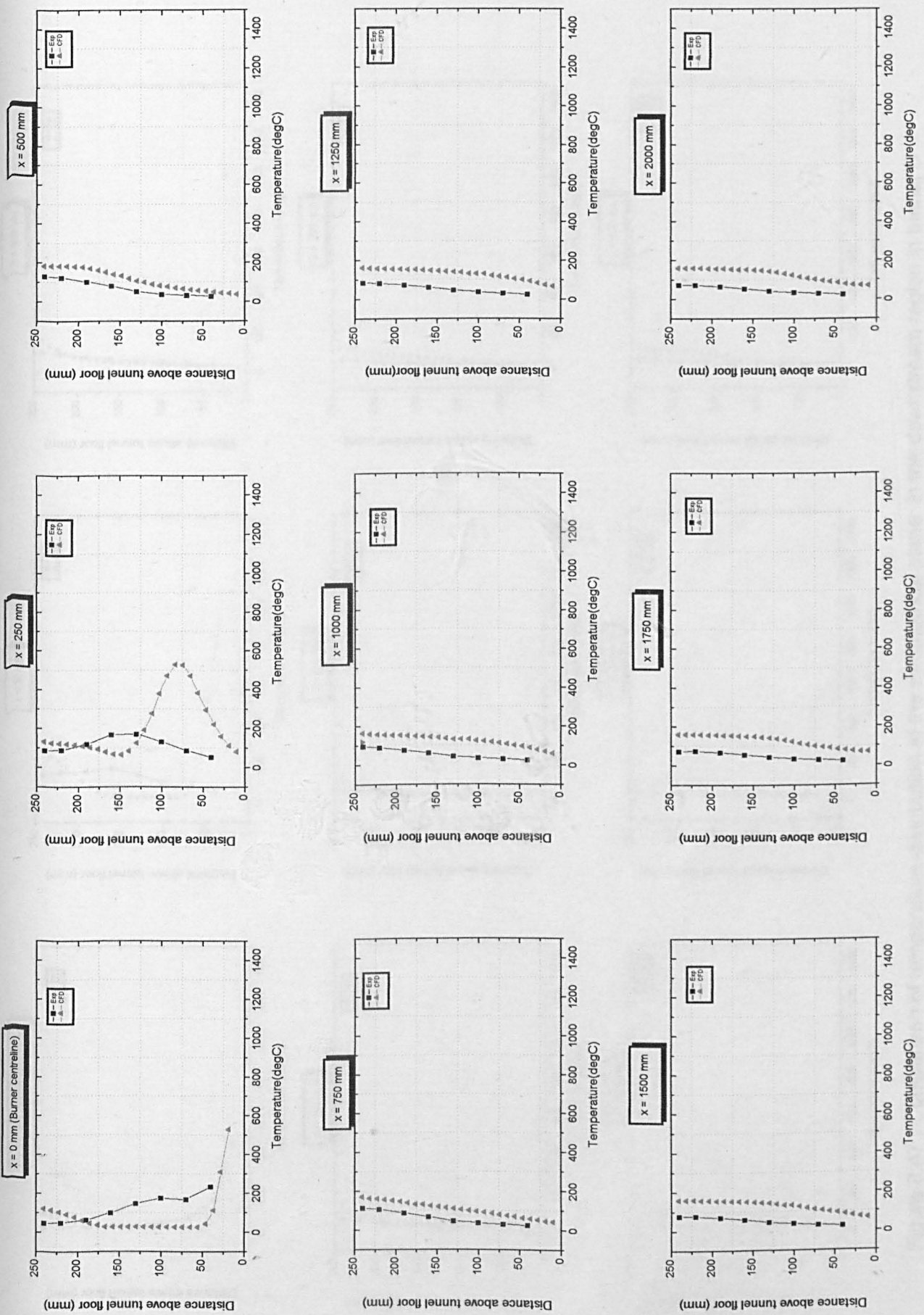
Figure 8.46 : Comparison of temperature distribution at the symmetrical plane in the downstream region in tunnel B at various distances from the burner at 3.0 kW [Uc(exp) = 0.48 m/s, Uc(CFD) = 0.40 m/s]
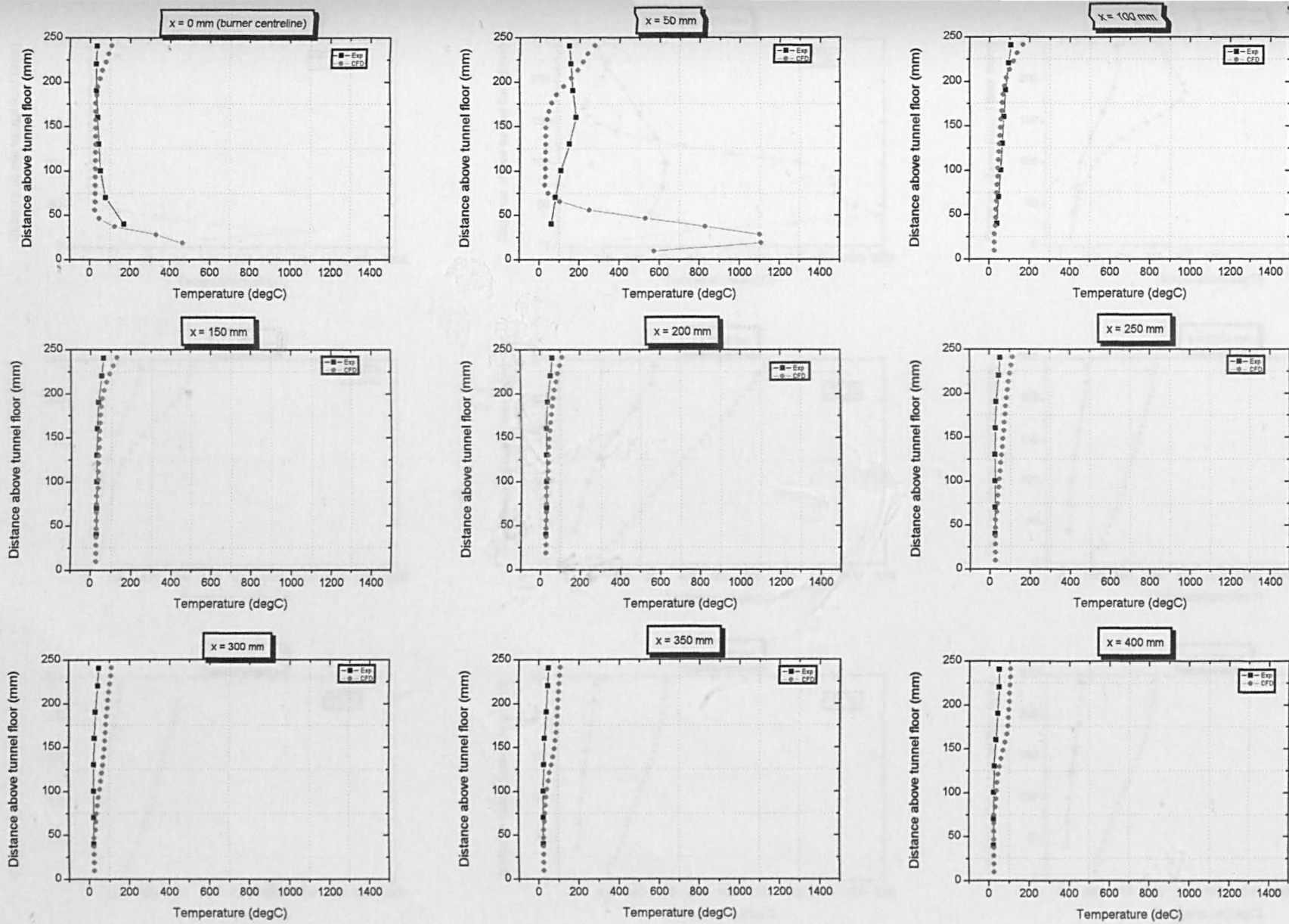
Figure 8.47 : Comparison of temperature distribution at the symmetrical plane in the downstream region in tunnel D
at various distances from the burner at 3.0 kW[Uc(exp) = 0.40 m/s, Uc(CFD) = 0.375 m/s]
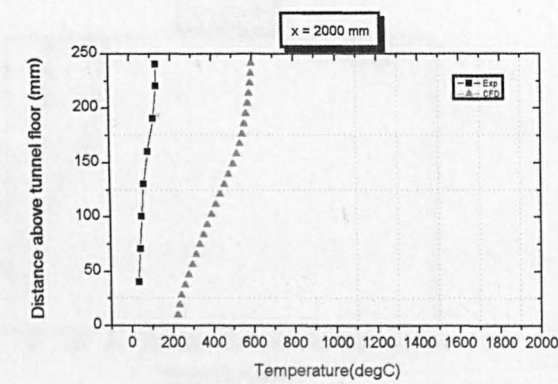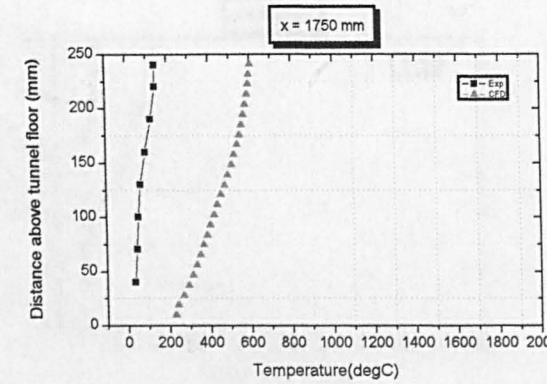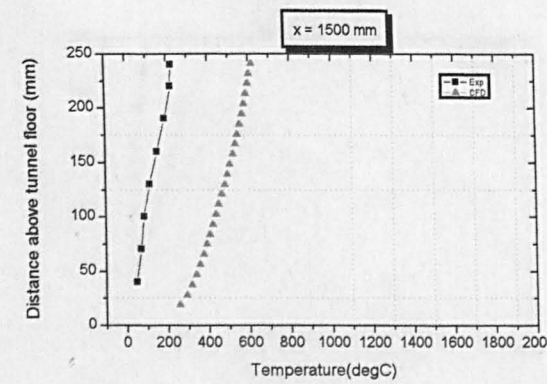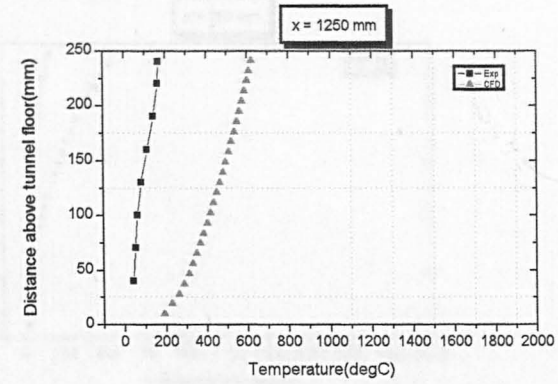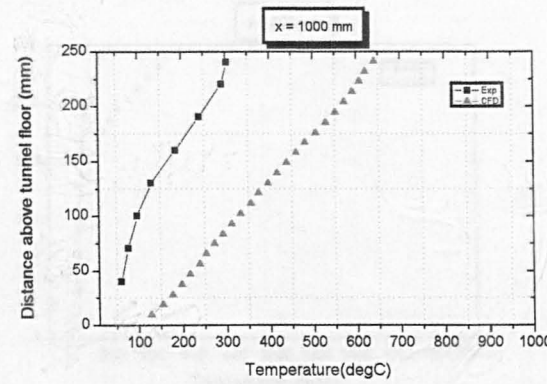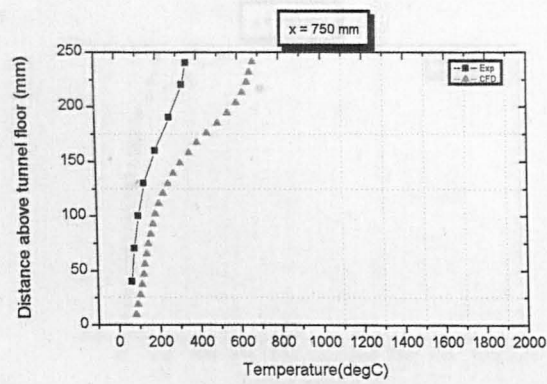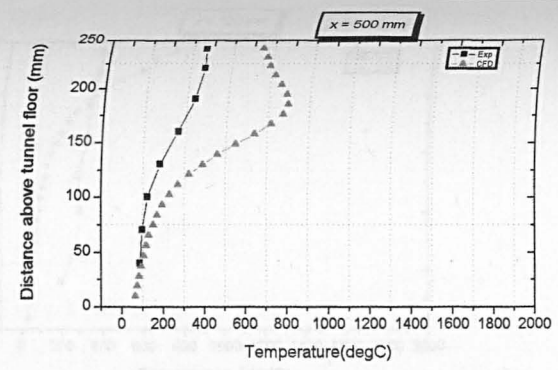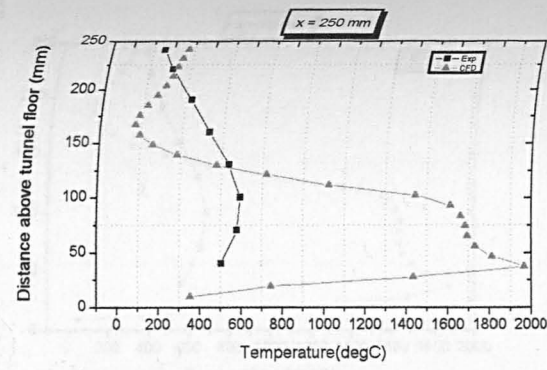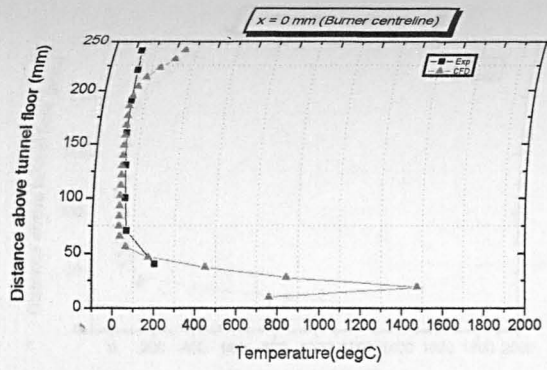
Figure 8.48 : Comparison of temperature distributions at the symmetrical in the downstream region in tunnel B at various distances from the burner at 15.0 kW [U(exp) = 0.60 m/s, U(CFD) = 0.50 m/s]
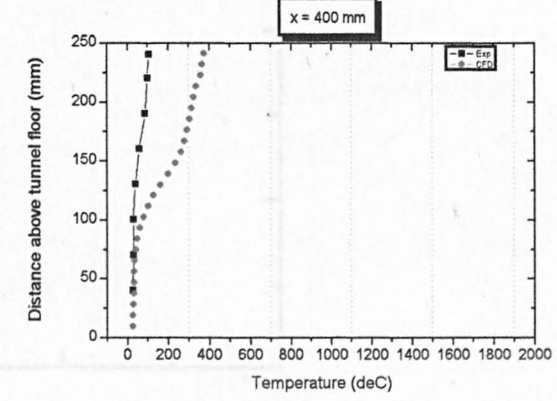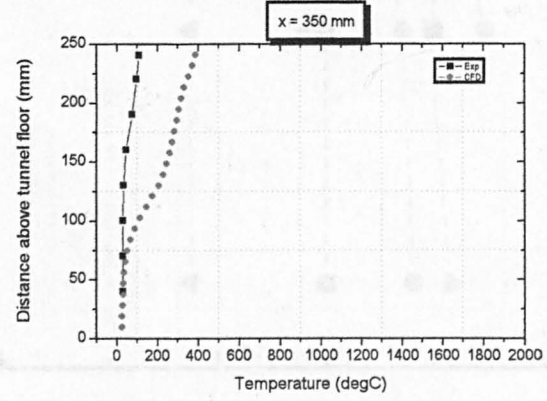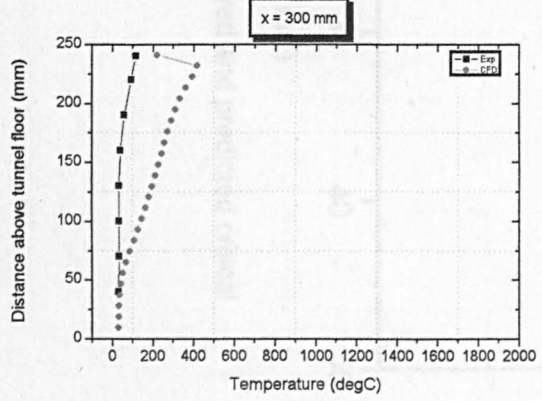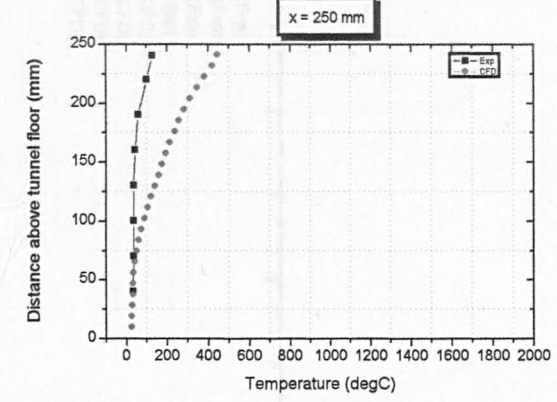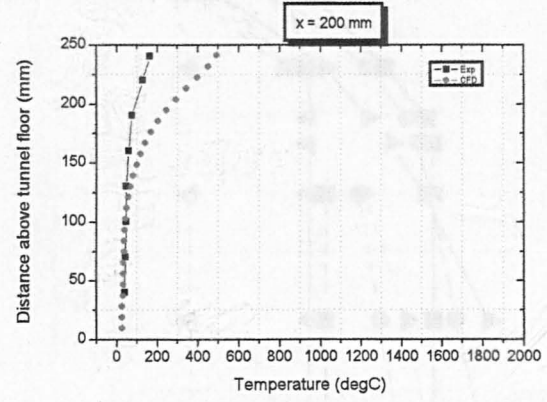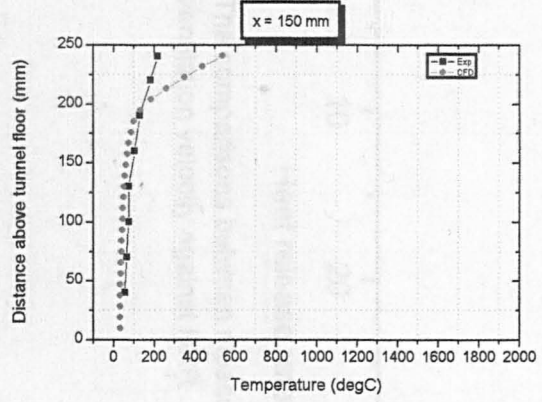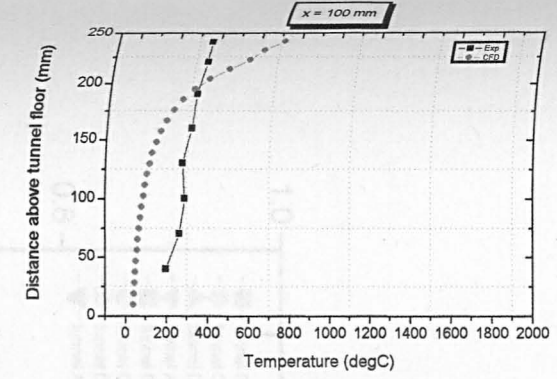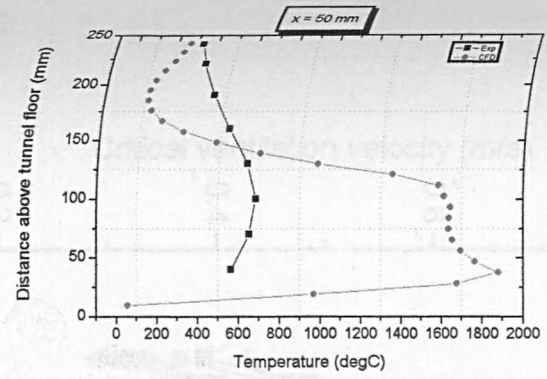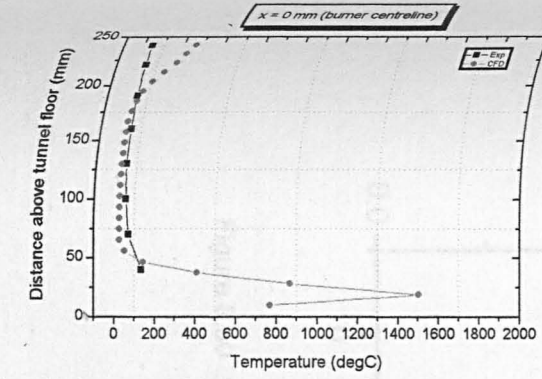
Figure 8.49 : Comparison of temperature distribution at the symmetrical plane in the downstream in tunnel D
at various distances from the burner at 15.0 kW[Uc(exp) = 0.59 m/s, Uc(CFD) = 0.536 m/s]
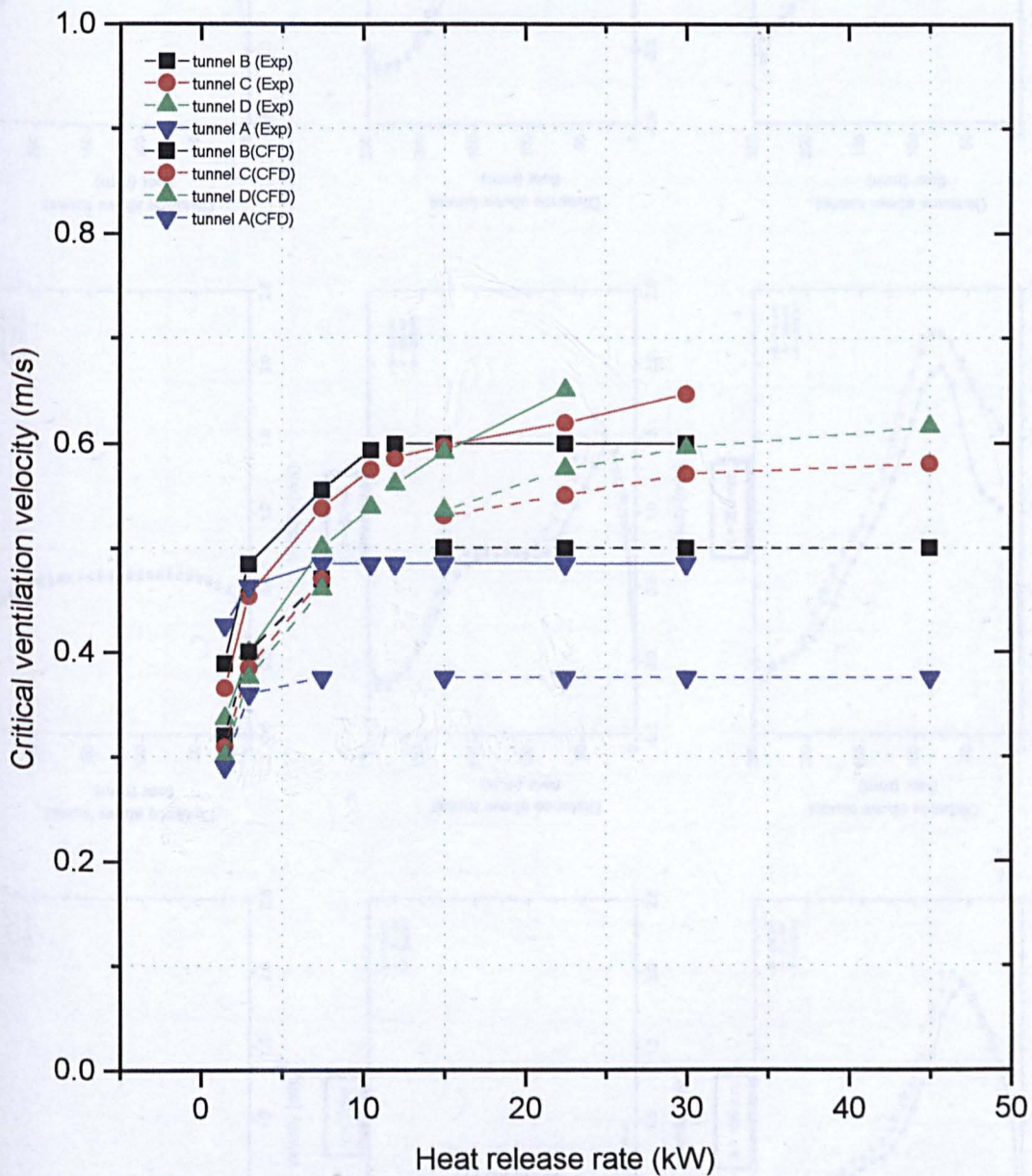
Figure 8.50 : The comparisons between measured and predicted critical
ventilation velocity against HRR

Figure 8.51: Comparison of velocity profiles at the symmetrical plane at various distances from the burner in tunnel B at 7.50 kW, 15.0 kW and 22.50 kW at critical ventilation velocities [Uc(7.50kW) = 0.47 m/s, Uc(15.0 kW) = 0.50 m/s, Uc(22.50 kW) = 0.50 m/s]

Table 8.1 : Simulated cases, conditions and objectives

Case	Tunnel	Q (kW)	GS	CM	TM	CV	BL
NR(1)a,b,c	A	3.0	✓				
NR(2)	A	3.0				✓	
NR(3)	A	7.50				✓	✓
NR(4)	A	15.0			✓	✓	
NR(5)	A	22.50				✓	
NR(6)	A	0.705				✓	
SR(1)a,b,c	B	3.0	✓				
SR(2)	B	3.0		✓		✓	
SR(3)	B	7.50		✓		✓	
SR(4)	B	3.0		✓	✓	✓	
SR(5)	B	7.50		✓	✓	✓	✓
SR(6)	B	15.0			✓	✓	
SR(7)	B	22.50			✓	✓	
SR(8)	B	3.0			✓	✓	
SR(9)	B	7.50			✓	✓	
SR (10)	B	15.0				✓	
SR(11)	B	22.50					
MR(1)a,b,c	C	3.0	✓				
MR(2)	C	3.0				✓	
MR(3)	C	7.50				✓	✓
MR(4)	C	15.0				✓	
MR(5)	C	22.50				✓	
MR(6)	C	30.0				✓	
MR(7)	C	43.5				✓	
WR(1),a,b,c	D	3.0	✓				
WR(2)	D	3.0				✓	
WR(3)	D	7.50				✓	✓
WR(4)	D	15.0				✓	
WR(5)	D	22.30				✓	
WR(6)	D	30.0				✓	
WR(7)	D	43.5				✓	

Keynotes: GS - Grid sensitivity, CM - Combustion model, TM - Turbulence model, CV-Critical ventilation, BL - Backlayering , a - Grid 1, b-Grid 2, c-Grid 3

Table 8.2 : Values of underrelax factors

Parameters	Underrelax Factor
Velocity	0.35
Pressure	0.40
Turbulence Kinetic	0.30
Turbulence Dissipation	0.30
Viscosity	0.30
Buoyancy	0.30
Temperature	0.60
Enthalpy	0.65
F-Mean	0.6
F-Variance	0.6

Table 8.3: Total number of computational cells

Tunnel	Grid 1	Grid 2	Grid 3
A	12240	22848	57120
B	12240	39984	81600
C	22950	79968	155040
D	30600	108528	209304

Table 8.4: Predicted fire plume tilt angles

Heat releas rate (kW)	Tunnel A		Tunnel B		Tunnel D	
	Measured	Predicted	Measured	Predicted	Measured	Predicted
3.0	75°	75°	70°	65°	60°	56°
15.0	79°	87°	73°	65°	70°	60°

Table 8.5 : The calculated result for the critical ventilation velocity

Heat Release Rate (kW)	Tunnel A	Tunnel B	Tunnel C	Tunnel D
3.0	0.360	0.400	0.385	0.375
7.50	0.375	0.470	0.470	0.460
15.0	0.360	0.500	0.530	0.535
22.5	0.355	0.500	0.550	0.575
30.0	0.355	0.500	0.570	0.595
45.0	0.355	0.500	0.580	0.615

Chapter 9

Dimensionless Analysis

This chapter discusses the proposed dimensionless analysis for HRR and the critical ventilation velocity. The main objectives are to find a scaling criterion for the experimental results obtained in small scale tunnels to be extended to larger scale tunnels and to find a simple way to co-ordinate all experimental results.

The two objectives are aimed due to two main limitations of the old dimensionless analysis methods. The first one is that buoyant force in the backlayering was considered as a function of tunnel height. Therefore the effect of the cross-sectional geometry is not considered. The second one is that the existing methods cannot co-ordinate the experimental results into simple forms.

To include the effect of the cross-sectional geometry in the variation of the critical ventilation velocity, the present work proposed to use the hydraulic tunnel height to replace the tunnel height as the characteristic length in the dimensionless analysis. The hydraulic tunnel height is defined as the ratio of 4 times the cross-sectional area to the tunnel wetted perimeter. This suggestion are based on two findings:

- The backlayering adopts the shape of the tunnel. The backlayering occupies approximately top half of the tunnel.

- The experimental and CFD studies showed that the critical ventilation velocity is determined by the interaction of the fire with the tunnel walls and the fresh ventilation flow. Therefore flow behaviours should be studied in three dimensions. The buoyant force in the backlayering is contributed by the whole fire plume. This problem can not be treated as a fire plume impinging the ceiling, in which the flow can be treated as two-dimensional problems. This was how the previous researchers

treated the tunnel fire problems. However, examination on the flow and temperature distribution at the symmetrical plane, the tunnel fire at critical conditions can be simplified as a one dimensional problem with the three regimes as duct flow. This will be examined in the dimensional analysis.

9.1 Dimensionless Heat Release Rate & Critical Ventilation Velocity Based on Hydraulic Tunnel Height

To differentiate the mean hydraulic tunnel height with the tunnel height, in the present work, the hydraulic tunnel height was defined as $\overline{H}$. Thus, the dimensionless critical ventilation velocity and dimensionless HRR becomes:

$$V'' = \frac{V}{\sqrt{g\overline{H}}} \quad \text{and} \quad Q'' = \frac{Q}{\rho_0 C_p T_0 \sqrt{g\overline{H}^5}}.$$

where ρ_0 is ambient air density, C_p is heat capacity of the flow and T_0 is ambient temperature. The value for each parameter is similar to Section 7.4.2.

The calculated hydraulic tunnel heights for the tunnels **A, B, C, D** and **E** are 117 mm, 250 mm, 333 mm, 444 mm and 238 mm, respectively. The calculated values of V'' and Q'' are shown in the Tables 9.1 and Table 9.2. The plot of V'' against Q'' using the hydraulic tunnel height is shown in Figure 9.1

It is clearly seen in Figure 9.1 that after using the $\overline{H}$, all experimental results can be correlated into a single form. This suggests that a new correlation for predicting the critical ventilation velocity for tunnels having the same height but different widths can be derived. The results also show that V'' value becomes independent on the Q'', approaching 0.4, when the Q'' is greater than approximately 0.2.

Based on the new characteristic length $\overline{H}$, the present work proposed a simple one dimensional correlation to predict the critical ventilation velocity for tunnel having the same height but different cross-sectional geometries. The suggested equations are:

$$V'' = 0.40 \, [0.20]^{-1/3} \, [Q'']^{1/3} \quad \text{for } Q'' < 0.20 \qquad (9.1)$$

$$V'' = 0.40 \qquad\qquad\qquad \text{for } Q'' > 0.20 \qquad (9.1a)$$

In the derivations, there are two main considerations that have been emphasised. First, the curve must follow the one third power of the dimensionless HRR. This value is represented by the slope of the points which exhibit the straight line. Second, the value of $V''max$ must be set equal to 0.40. By using these two restrictions, the value of $Q''max$ which fit the curve is 0.20.

The above equations suggest that the critical ventilation velocity for tunnels having the same height but different widths increases with the HRR to the power of 1/3 up to Q'' equal to 0.20. Beyond this value, the critical ventilation velocity is weakly dependent on HRR and becomes constant at V'' equal to 0.40.

Figure 9.2 shows the comparison between the measured and predicted critical ventilation velocity expressed in the new dimensionless forms. It can be observed that both results follows the same pattern. There are two distinguished regions that can be seen, V'' increases with Q'' and the near independent of V'' on Q''. Although the predicted critical ventilation velocities are slightly lower, the most important finding is that both results show V'' is increasing with Q'' up to Q'' between 0.2 to 0.30. Beyond Q'' between 0.20 to 0.30, the value of V'' has become nearly constant.

In addition to the present results, Figure 9.2 also shows several published results especially from Lea (1995) and Chow (1988) and Kawabata et al (1991). It can be seen

that there was a good agreement in the pattern of the variations. However, the previous values were slightly lower than the present results. The difference arises due to several reasons such as the type of the combustion models used and the nature of the fire, whether being generated by the combustion model or represented by heat source. In addition, the fuel type should also be taken into consideration.

9.2 Comparison of the Result Obtained in This Work with Results from Larger Scale Tests

The only limitation of the present results is that the critical results were obtained from small scale tunnel models. As being discussed in Chapter 3, extrapolating the small scale results to larger scale is still remain risky. In the present work, the experimental data were further compared with small and large scales data, gathered from the literature.

One of the problems that has been encountered in this section was that the reported values of the critical velocities with HRRs limited to only one or two data. As a result, it would be expected that there will be some difficulties to predict the variation of the critical ventilation velocity. Among the established data, only the results Bettis et al (1993,1994), Gonzalez (1988), Heselden (1978), PIARC and World Associations to some extend reported more than one data.

The dimensionless HRR and dimensionless critical velocities were calculated using the same parameters as in Section 7.4.2. However the values of the hydraulic tunnel height $\overline{H}$ and the initial ambient temperatures varied with authors. The initial ambient temperature were between 288 K to 300 K. The comparisons were divided into 3 sections; the real experimental results (blue in colour), predicted results based on larger scales (red in colour) and the values obtained from guideline (green in colour).

The calculated values of V'' and Q'' are shown in Table 9.3 and Table 9.3a. It is shown in Figure 9.3 that although the critical data are scattered, especially at higher HRRs, the

present results show a good agreement. Comparing with the real large scale experiments (blue colour), it can be observed that the present data correlate very well with the Gallery, Memorial and Eureka results. Most of the Gallery data fit the present results in the region where V'' increases with Q''. A similar pattern is seen for the most recent data from the Memorial test of 10 MW fire ($V'' = 0.287$, $Q'' = 0.051$).

Comparing with the critical data at higher HRRs, it can be seen that the present results also fit with the Memorial and Eureka data for 100 MW fires which are also the most recent and accurate results. The results from Memorial ($V'' = 0.344$, $Q'' = 0.513$) and Eureka ($V'' = 0.364$, $Q'' = 0.964$; $V'' = 0.34$, $Q'' = 1.32$) indicates that they lies in the region where V'' independent of Q'', consistent with the present results of V''max equal to 0.40.

Comparing with the predicted and guideline results (red and green), it can be observed that there are no strong disagreement when V'' value less that 0.40. However, above this value, the critical ventilation velocity can be regarded as over predicted.

9.3   Conclusions

New dimensionless analysis techniques were proposed. The hydraulic tunnel height was used to replace the tunnel height as the characteristic length. The new data analysis showed that the results from the five tunnels were well co-ordinated and followed the same pattern. The dimensionless critical velocity becomes independent on the dimensionless HRR, approaching 0.4 when the dimensionless HRR greater than 0.2. Correlations to predict the critical ventilation velocity based on dimensionless HRR and dimensionless critical velocity have been derived based on the five tunnels.

The present small scale results have been compared with the measured and predicted results from larger scale tunnels and the predicted from CFD. The comparisons showed that the present results were in a good agreement with the larger scale results. Therefore

the present results can be used for prediction of the critical ventilation velocity for large scale tunnel in any cross-sectional geometry.
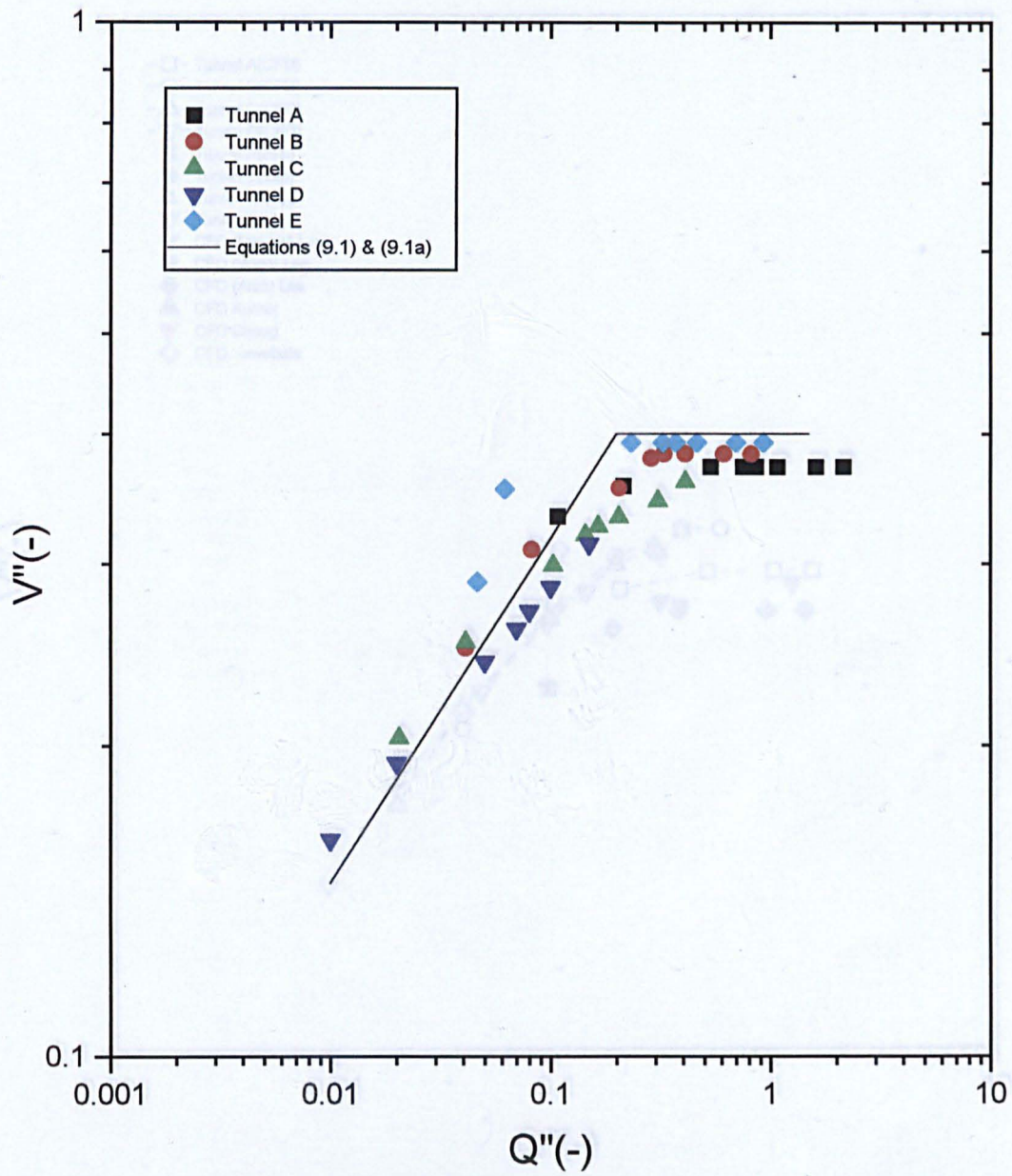
Figure 9.1: Plot of dimensionless critical velocity against dimensionless heat release rate
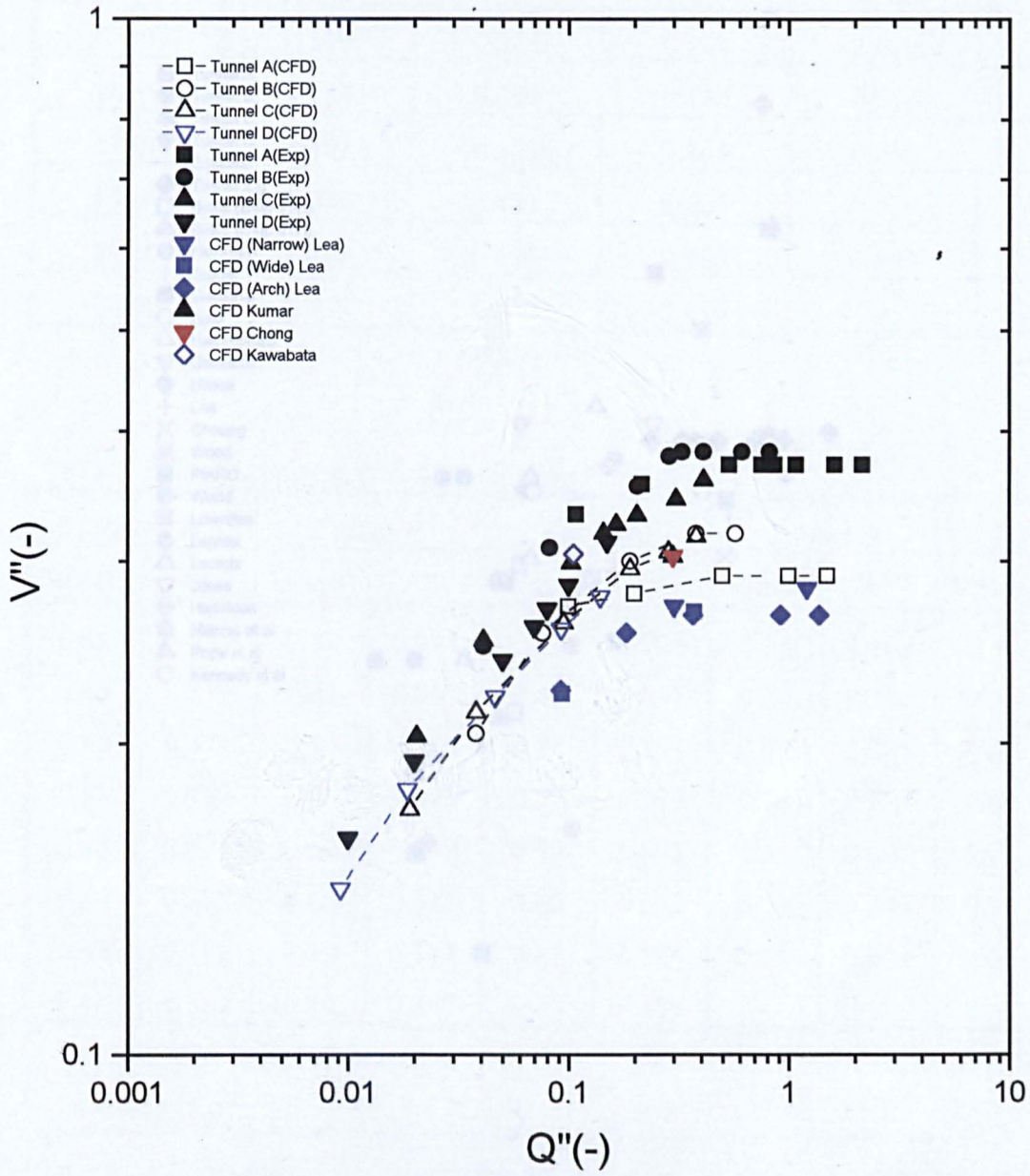
Figure 9.2: Comparison between measured and predcited dimensionless
critical velocity against heat release rate

Figure 9.3: Comparison of dimensionless critical velocity
against dimensionless heat release rate

Table 9.1: Dimensionless heat release rate (Q")

Q (kW)	Tunnel A Q"	Tunnel B Q"	Tunnel C Q"	Tunnel D Q"	Tunnel E Q"
1.50	0.108	0.041	0.021	0.010	0.046
3.00	0.216	0.082	0.041	0.020	0.0.93
7.50	0.539	0.205	0.103	0.050	0.232
10.50	0.754	0.288	0.144	0.070	0.325
12.00	0.862	0.329	0.164	0.080	0.372
15.00	1.078	0.411	0.205	0.100	0.465
22.50	1.616	0.616	0.308	0.150	0.670
30.00	2.155	0.822	0.410	-	0.929

Table 9.2: Dimensionless critical ventilation velocity (V")

Tunnel A V(m/s)	V"	Tunnel B V(m/s)	V"	Tunnel C V(m/s)	V"	Tunnel D V(m/s)	V"	Tunnel E V(m/s)	V"
0.43	0.333	0.39	0.248	0.37	0.203	0.34	0.162	0.44	0.288
0.46	0.356	0.48	0.309	0.45	0.251	0.40	0.192	0.54	0.353
0.48	0.372	0.56	0.354	0.54	0.298	0.50	0.241	0.60	0.393
0.48	0.372	0.59	0.379	0.57	0.319	0.54	0.259	0.60	0.393
0.48	0.372	0.60	0.382	0.59	0.325	0.56	0.270	0.60	0.393
0.48	0.372	0.60	0.382	0.60	0.332	0.59	0.284	0.60	0.393
0.48	0.372	0.60	0.382	0.62	0.344	0.65	0.313	0.60	0.393
0.48	0.372	0.60	0.382	0.65	0.359	-	-	0.60	0.393

$$Q'' = \frac{Q}{\rho_0 T_0 C_p g^{\frac{1}{2}} H^{\frac{5}{2}}} \qquad V'' = \frac{U_c}{\sqrt{gH}}$$

Table 9.3: Dimensionless heat release rate and dimensionless critical velocity for various tunnels

Authors	Tunnel Geometry			Q	V	Q″	V″
	Height	Width	H(TH)	(kW)	(m/s)	(-)	(-)
Oka et al	0.274	0.244	0.238	1.50	0.463	0.045	0.303
				3.00	0.570	0.090	0.373
				7.50	0.621	0.225	0.406
				10.50	0.621	0.314	0.406
				12.00	0.621	0.359	0.406
				15.00	0.621	0.449	0.406
				22.50	0.621	0.634	0.406
				30.00	0.621	0.898	0.406
Bettis et al (< 3TH)	2.44	2.74	2.38	204	0.908	0.019	0.188
				606	1.438	0.056	0.298
				1040	1.363	0.096	0.282
				1290	1.400	0.119	0.290
				570	1.037	0.052	0.215
				1230	1.387	0.113	0.287
				204	0.757	0.019	0.157
Bettis et al (> 5TH)				204	0.757	0.019	0.157
				953	1.302	0.088	0.269
				490	1.022	0.045	0.212
Fiezlmayr	4.0	5.0	4.4	14500	2.0	0.298	0.303
Jagger	2.44	2.74	2.38	5400	1.6	0.497	0.327
Memorial	7.86	7.6	7.75	10000	2.5	0.051	0.287
				100000	3.0	0.513	0.344
Apte et al	2.4	5.4	3.32	1650	2.0	0.068	0.350
Haack	4.8-6.5	5-11.6	5.0	100000	2.8	1.521	0.340
Haack	4.8-6.5	5-11.6	6.0	100000	2.8	0.964	0.365
Hammerfast	5.0	6.6	5.68	100000	2.8	1.067	0.375
Gonzalez	6.6	6.4	6.49	5000	1.6	0.040	0.201
				20000	2.32	0.158	0.291
				100000	3.17	0.792	0.397
Chow et al	4.0	5.0	4.4	14500	2.5	0.304	0.381

Table 9.3a: Dimensionless heat release rate and dimensionless critical velocity for various tunnels

Authors	Tunnel Geometry			Q	V	Q"	V"
	Height	Width	H(TH)	(kW)	(m/s)	(-)	(-)
Lacroix			7.0	2000 - 3000	2	0.0131 - 0.0196	0.241
			7.0	3000 - 5000	3	0.0196 - 0.0327	0.362
Lacroix			7.0	5000	2.0	0.0327	0.241
				10000	2.5 - 3.0	0.0656	0.302 - 0.362
				20000	3.5 - 4.0	0.1311	0.422 - 0.483
Wood, D	6.6	6.4	6.49	50000	4	0.396	0.501
Haselden	5.0	10.0	6.66	3000	1.3	0.022	0.161
				20000	3.0	0.149	0.371
				100000	6.7	0.745	0.828
Lea	6.6	6.4	6.49	20000	2.4	0.158	0.301
				100000	3.2	0.792	0.401
Kennedy	6.6	6.4	6.49	50000	2.8	0.399	0.351
Lowndes			7.89	50000	5.0	0.245	0.568
Pope et al			6.4	100000	5.0	0.826	0.631
Mizuno			11.2	500000	2 -3	0.102	0.1908 - 0.2862
Jones			5.53	50000	3.0	0.059	0.4073
18 World	6.6	6.4	6.49	5000	1-2	0.0399	0.125 - 0.251
				20000	2-3	0.160	0.251- 0.376
				100000	5-8	0.798	0.627 - 1.002

Chapter 10

Conclusions and Suggestions for Future Work

Finally this chapter briefly concludes the overall conclusions in the present study. The detailed conclusions related to the present study have been previously outlined at the end of each chapter in this thesis.

10.1 Conclusions

The bulk of the present works concerns with the critical ventilation velocity. An extensive experimental programmes were carried out to measure the critical ventilation velocity for five model tunnels. Measurements of the velocity and temperature distribution in the tunnels were made. Three dimensional CFD modellings were also carried out to verify the experimental results. Following are the summary of the principal conclusions:

- The critical ventilation velocity has been reviewed in relation with two main parameters: a) tunnel aspect ratio, and b) fire power

- The critical ventilation velocity did vary for tunnels which have the same height but different widths.

- The critical ventilation velocity strongly depends on the one third of the power of the HRR at lower HRRs. However, it is becoming independent on the HRR at higher HRRs.

- The variations of critical ventilation velocity have been related to the distribution of the fire plume inside the tunnels. McCaffrey (1979) fire plume theory has been extended and used in analysing the variations of the critical ventilation velocity.

- The behaviour of the air entrainment near the fire and the flow acceleration approach the fire have been identified as the mechanisms for the distribution of the fire plume inside the tunnels.

- CFD simulations have successfully supported the experimental results in: a) flow behaviour, b) identifying the mechanisms of the distribution of the fire plume inside the tunnel , c) behaviour of the backlayering and finally prediction of the variations of the critical ventilation velocity.

- New characteristic length for buoyant flow which is the hydraulic tunnel height has been used to replace the tunnel height in the dimensionless analysis of the critical ventilation velocity and the HRR. The experimental results have been correlated into a simple form when the hydraulic tunnel height was used.

- The scaling problems have been resolved by comparing the present results with the large scale experimental data. The results showed that there was a good agreement. Thus, the present results can be used with high degree of confidence for the reference to design the tunnel ventilation velocity.

10.2   Suggestions for Future Works

Much of works in the experimental investigations are still required in the tunnel fire studies. Thus in future, the present work can be extended to further investigate

- The effect of the tunnel slopes on the critical ventilation velocity for the set of tunnels which have the same height but different cross-sectional geometries.

- In the present work, the critical ventilation velocity were measured based on the fire at tunnel axis. In the real situation, for example petrol spillage, most of the fuel will be in the drain. Thus, it is necessary to further investigate the critical ventilation for the fire being placed other than at tunnel axis.

- The present experimental setup also can be used to investigate the effect of the blockage inside the tunnel.

- The present work found that the fire plume could affect the critical ventilation inside the tunnel. The behaviour of the independent of the critical ventilation velocity on the HRR should be further investigated. The outcome from the LDV measurements showed that the backlayering flow was almost constant regardless on heat release rate. Thus, the behaviour of independent of the critical ventilation velocity on the heat release rate should be further focused on the flame itself. Therefore in future, new techniques such as the real thermal image or using advanced method to capture the fire plume are required.

- The most recent technology to study tunnel fires is using Computational Fluids Dynamics. It should be bear in mind that CFD technique is a new approach. In the present works, the CFD that have been performed were based on simple approach. However, the results were promising since CFD were capable to predict the same variation of the critical ventilation velocity compared to the experimental result. The percentage different obtained in the present work was up to 20 percent. Therefore in future, it is necessary to optimise the CFD codes especially the study on the flow behaviour. The buoyancy related term for example should be further optimised in future in order to find the desired value for tunnel fire. In general, further investigation and validation of computer code are necessary. It has been pointed earlier that the combustion models are not matured enough to represent the fire.

References

Allen, J. T. Bettis, R.J., Jagger, S.F. (1999) "LDA Measurements of the Air Movement in Tunnel Fire", the Health and Safety Laboratory Report, (to be completed), Health and Safety Executive, U.K.

Apte, V.B, Green, A. R and Kent, J.H, (1991) "Pool Fire Plume Flow in a Large-Scale Wind Tunnel", Fire Safety Science- Proceeding of the 3rd International Symposium, Edinburgh, Scotland, pp 907-918

Atkinson, G.T. & Wu, Y., (1996)" Smoke Control in Sloping Tunnels", Fire Safety Journal, 27, pp 335-322.

Bakar, M.Z, Wu, Y., Atkinson, G. T. and Jagger, S., (1999), "A Study of the Effect of Tunnel Aspect Ratio on the Critical Ventilation Velocity in Tunnel Fires", to be submitted to Journal of Fire Safety.

Bakke, P. and Leach, S. J., (1960) "Methane Roof Layers", Safety in Mines Research Establishment, Research Report No. 195, Sheffield.

Beard, A. N, Drysdale,D. D., (1995) "A Non-Linear Model of Major Fire Spread in a Tunnel", Fire Safety Journal, Vol 24, pp 333-357.

Bechtel/Parsons Brinckerhoff, (1995) "Memorial Tunnel Fire Ventilation Test Program, Comprehensive Test Report", prepared for Massachusetts Highway Department.

Bennardo. V, et al, (1997) "Physical Modelling and Numerical Simulation of Fire Events in Road Tunnels", 9th International Conference on Aerodynamics and Ventilation of Vehicle Tunnels, Aosta Valley, Italy, pp 649-668.

Bettis, R.J., Jagger, S.F. & Wu,Y., (1993) "Interim Validation of Tunnel Fire Consequence Models; Summary of Phase 2 Tests", the Health and Safety Laboratory Report IR/L/FR/93/11, Health and Safety Executive, U.K.

Bettis, R.J., Jagger, S.F., Macmillan, A.J.R. & Hambleton, R.T., (1994) "Interim Validation of Tunnel Fire Consequence Models; Summary of Phase 1 Tests", the Health and Safety Laboratory Report IR/L/FR/94/2, Health and Safety Executive, U.K.

Bettis, R, (1995) "Controlling Smoke in Tunnel Fires", Fire Prevention, Vol 280, pp 19-22.

Berner, M. A., (1992), " Safety Considerations in Ventilating and Cooling Long Railway Tunnels", 23rd - 25th November, Proc of First International Conference on safety in Road and Rail Tunnels, Basle, Switzerland, pp 641-648.

Brandies, J and Bergmann, D., (1983) "A Numerical Study of Tunnel Fires", Combustion Science and Technology, Vol 35, pp 133-155.

Britter, R.E. and Linden, P.F., (1980) "The Motion of a Gravity Current Travelling Down an Incline", J. Fluid Mechanic, Vol. 99, pp 531.

BS1042 : Section 1.1: (1989) " Measurement of Fluid Flow in Closed Conduit"

Chaiken, R.F., Singer, J. M and Lee, C. K, (1979), "Model Coal Tunnel Fire in Ventilation Flow", US Bureau of Mines, Report of Investigations 8355.

Chow, W.K. and Leung, W. M., (1988), " Application of Field Model to Tunnel Fire Services Design", 27th-29th September, Proc of 6th International Symposium on the Aerodynamics and Ventilation of Vehicle Tunnels, Durham, England, pp 495-514.

Cox, G. and Kumar, S., (1987), "A Numerical Model of Fire in Road Tunnels", March, Tunnels and Tunnelling, pp 55-60.

Danziger, N.H, and Kennedy,W.D., (1982) "Longitudinal Ventilation Analysis for the Glenwood Canyon Tunnels", Proc of the 4th Int. Symp. Aerodynamics and Ventilation of Vehicle Tunnels, pp 169-186.

Danziger, N.H. and Kennedy, W. D., (1982), "Longitudinal Ventilation Analysis for the Glenwood Canyon tunnels", 23rd-25th March, Proc. of 4th International Symposium on the Aerodynamics and Ventilation of Vehicle Tunnels, York, England, pp 169-186.

Drysdale, D, "An Introduction to Fire Dynamics", Wiley, 1985.

Ellison, T. H., and Turner, J. S, (1959) "Turbulent Entrainment in Stratified Flows", Journal of Fluid Mechanics, Vol 6, pp 423- 448.

Emori, R. I and Saito, K, (1983), "A Study of Scaling Laws in Pool and Crib Fires", Combustion Science and Technology, Vol 31, pp 217-231.

Feizlmayr, A.H, (1976), "Research in Austria on Tunnel Fire", 2nd Int. Symp. on the Aerodynamics and Ventilation of Vehicle Tunnels, 23rd-25th March, Cambridge, England, pp (J2 - 19) - (J2 - 40).

Fletcher, D. F, Kent, J. H., Apte, V. P. and Green, A. R., (1994), "Numerical Simulations of Smoke Movement from a Pool Fire in a Ventilated Tunnel", Fire Safety Journal, Vol 23, No. 3, pp 305-325.

Fire Protection Engineering Handbook (1995), National Fire Protection Association, Quincy, Massachusetts.

Gaffney, P. and Kynaston, R., (1992), "Smoke Control System of the Hong Kong Mass Transit Railway", 23rd - 25th November, Proc of First International Conference on Safety in Road and Rail Tunnels, Basle, Switzerland, pp 79-93.

Grant, G.B, Vardy, A.E and Davies, P.A, (1988), "Thermally Stratified Forced Ventilation in Tunnels", 27th-29th September, Proc of 6th International Symposium on the Aerodynamics and Ventilation of Vehicle Tunnels, Durham, England, pp 527-547.

Haack, A., (1995), "Modelling Fire at Large Scale: Lessons from the EUREKA fire tests", One Day Seminar, Physical and Numerical Modelling of Fires in Tunnels", Friday 7 April, Granada, Spain.

Haack, A., (1992), "Fire Protection in Traffic Tunnels-Initial Recognitions From Large Scale Tests", 23rd - 25th November, Proc of First International Conference on Safety in Road and Rail Tunnels, Basle, Switzerland, pp 349-361.

Haerter,A, (1965) "Fire Test in The Ofnegg-Tunnel in 1965", pg 195-204

Heselden A.J.M, (1978), "Studies of Fire and Smoke Behaviour Relevant to Tunnels ", Building Research Establishment, CP66/ 1978, pp 1-14.

Heselden, A. J. M and Hinkley, P. L, (1970), "Smoke Travel in Shopping Malls; Experiment in Co-operation with Glasgow Fire Brigade - Part 1", Fire. Research Note, No. 832, July.

Hinkley, P. L, (1970) "The Flow of Hot Gases Along an Enclosed Shopping Mall. A Tentative Theory", March, Fire Research Note No. 807

Himmelblau, D. M, (1982), "Basic Principles and Calculations in Chemical Engineering", Prentice Hall publication.

Hwang, C. C., Chaiken, R.F., Singer, J. M. and Chi, D. N. H., (1976), "Reverse Stratified Flow in Duct Fires: A Two-Dimensional Model Approach", Proc. of 16th International Symposium on Combustion, MIT, Cambridge, Mass. pp 1385-1395.

Hwang, C. C. and Chaiken, R. F., (1978), "Effect of Duct Fire on the Ventilation Air Velocity", US Bureau of Mines, Report of Investigations 8311.

Hwang, C.C and Wargo, J.D, (1986), " Experimentally Study of Thermally Generated Reverse Stratified Layers in a Fire Tunnel", Combustion and Flame, 66, 171-180.

Jones, R.L., Evans, K., Marshall, J. G., Allchin, L. and Hobson, A. P.H., (1988) "Operational Control, Emergency Procedures, Ventilation and Transportation of Dangerous Goods at British Toll Tunnels", 27th-29th September, Proc of 6th International Symposium on the Aerodynamics and Ventilation of Vehicle Tunnels, Durham, England, pp 463-479.

Kawabata, H., Ohashi, H. and Kato, Y., (1991), "Numerical Simulation of Fire Fume Propagation Along the Ceiling of a Down-grade Tunnel", Proc of 7th International Symposium on the Aerodynamics and Ventilation of Vehicle Tunnels, Brighton, England, pp 319-335.

Kennedy, W. D., (1997), "The Influence of the Memorial Tunnel Fire Tests on Transit Tunnel Fire Emergency Ventilation Analysis", Parsons Brinckerhoff Quade and Douglas, Inc. A report for 1997 Rapid Transit Conference, Ventilation of Transit Tunnels and Underground Stations, Washington, D.C.

Kennedy, W.D. and Patel, S.J., (1988), "The Mount Lebanon Tunnel Ventilation System", 27th-29th September, Pro of 6th International Symposium on the Aerodynamics and Ventilation of Vehicle Tunnels, Durham, England, pp 235-244.

Kwack, E.Y, Bankston, C.P, Shakkottai, P. and Back, L.H, (1990), "On the Reverse Flow Ceiling Jet in Pool Fire-Ventilation Crossflow Interactions in a Simulated Aircraft Cabin Interior, Heat and Mass Transfer in fires", ASME Thermophysics and Heat Transfer Conference, 1990, Vol. 141, pp. 101-108.

Lacroix, D., (1995) "Modelling Tunnel Fires at Medium and Small Scale: Capabilities and Limitations", Seminar on Physical and Numerical Modelling of fires in Tunnels, Granada, Spain, April.

Lacroix, D., (1997), "New French Recommendations for Fire Ventilation in Road Tunnel", 9th Int Conference on Aerodynamics and Ventilation of Vehicle Tunnels, Italy, pp103-123.

Launder, B. E. and Spalding, D. B., (1974), "The Numerical Computation of Turbulent Flows", J. for Computer Methods in Applied Mechanics and Engineering, Vol. 3. pp 269 - 289.

Lee, C. K., Chaiken, R.F., Singer, J. M., (1979a), "Interaction Between Duct Fires And Ventilation Flow: An Experimental Study", Combustion Science and Technology, Vol 20, pp 59-72.

Lee, C. K., Hwang, C.C., Singer, J. M. and Chaiken, R. F., (1979b), "Influence of Passageway Fires on Ventilation Flow", 4th - 8th November, Proc of Second International Mine Ventilation Congress, Reno, Nevada, pp 448 - 454.

Lea,C.J, Bettis, R.J and Jagger, S.F, (1994), "A Review of Available Data and Models for Tunnel Fires", Health and Safety Laboratory Report IR/L/FR/94/12, the Health and Safety Executive, U.K.

Lea, C. J., (1993), "A Review of Ventilation of Tunnels in the Event of Fire, With Particular Reference to the Channel Tunnel", Health and Safety Executive, Report IR/L/FR/93/05, April.

Lea C.J, (1995), "CFD Modelling of the Control of Smoke Movement from Tunnel Fires Using Longitudinal Ventilation", Health and safety Executive, Report IR/L/FR/94/10, April.

Lea, C.J, Jones, I.P and Owens, M, (1997), "Computational Fluid Dynamics Modelling of Fire on a One-third Scale Model of a Channel Tunnel Heavy Goods Vehicle Shuttle", 9th Int Conference on Aerodynamics and Ventilation of Vehicle Tunnels, Italy, pp 681- 689.

Liew, S. K., Hall, R. C. and Deaves, D, M., (1988), "Smoke Control - Problem and Solutions", INTERFLAM, pp 164-171.

Ljuboja, M. and Rodi, W., (1980), "Calculation of Turbulent Wall Jets with an Algebraic Reynolds Stress Models", J. of Fluids Engineering, Trans. of ASME.

Ljuboja, M. and Rodi, W., (1981)"Prediction of Horizontal and Vertical Turbulent Buoyant Wall Jets", J. of Heat Transfer, Trans. of ASME.

Lowndes,J.F.L. and Pursall, B.R., (1988), "Ventilation Design Considerations for the Proposed Route - 5 Tunnels in Hong Kong", 6th Int Symp. on the Aerodynamics and Ventilation of Vehicle Tunnels, 27-29 September, Durham, U.K, pp 409-426.

McCaffrey, B. J., (1979) "Purely Buoyant Diffusion Flames: Some Experimental Results", NBSIR, 79-1910.

Magnussen, B. F. and Hjertager, B. H., (1976), "On Mathematical Modelling of Turbulent Combustion with Special Emphasis on Soot Formation and Combustion", Proc. of 16th Int. Symp. on Combustion, The Combustion Institute, pp. 719 - 729.

Malhotra, H.J., (1992), "Vehicle Fire Experiments For the Channel Tunnel Transport System", 23rd - 25th November, Proc of First International Conference on Safety in Road and Rail Tunnels, Basle, Switzerland, pp 405-421.

Malhotra, H. J., (1995), "Goods Vehicle Fire Test in A Tunnel", 2nd Int Conference on Safety in Road and rail Tunnels, pp 237-244, Organised by University of Dundee and Independent Technical Conferences Ltd.

Mizuno, A., and Ichikawa, A., (1991), "The Emergency Control of Ventilation for the Trans-Tokyo Bay Tunnel", Proc of 7th International Symposium on the Aerodynamics and Ventilation of Vehicle Tunnels, Brighton, England, pp 365-384.

Mizuno, A. and Icikawa, A., (1992), "Experimental Studies on Emergency Ventilation System for Trans-Tokyo Bay Road Tunnel", 23rd - 25th November, Proc of First International Conference on safety in Road and Rail Tunnels, Basle, Switzerland, pp 571-585.

Newman, S. J., and Tewarson, A., (1983), "Flame Propagation in Ducts", Combustion and Flame, Vol 51, pp 347-355.

Newman, S. J., (1984), "Experimental Evaluation of Fire-Induced Stratification", Combustion and Flame, Vol 57, pp 33-39.

Oka, Y. and Atkinson, G.T, (1995), "Control of Smoke Flow in Tunnel Fires", Fire Safety Journal, Vol 25, pp 305-322.

Parsons Brinkerhoff Quade & Douglas, Inc., (1980), "Subway Environmental Design Handbook Volume II Subway Environment Simulation (SES) Computer Program Version 3 Part 1: User's Manual, prepared in draft for the U.S. Department of Transportation", October.

Permanent International Association of Road Congresses, (1987), "Technical Committee Report No. 5: Road Tunnels", 13th-19th September, XVIIIth World Road Congress, Brussels, pp 68-74.

Pope, C.W., Johnson, T. and Broomhead, S.F., (1988), "Aerodynamics and thermal design for the Great Belt tunnel", 27th-29th September, Proc of 6th International Symposium on the Aerodynamics and Ventilation of Vehicle Tunnels, Durham, England, pp 245-2724.

Quintiere, J. G., (1989), "Scaling Applications in Fire Research", Fire Safety Journal, Vol 15, pp 3-29.

Ris, D., (1970), "Duct Fires", Combustion and Science Technology, Vol 2, pp 239-258.

Rhodes, N., (1995), "CFD Modelling of Fire and Smoke Movement, One Day Seminar, Physical and Numerical Modelling of Fires in Tunnels", Friday 7 April, Granada, Spain.

Thomas, P.H, (1968), "The Movement of Smoke in Horizontal Passages Against an Air Flow", Fire Research Station, Note No. 723, Fire Research Station, U.K, Sept.

Tuovinen, H and Holmstedt, G, (1996), "Sensitivity Calculations of Tunnel Fires Using CFD", Fire Technology Second Quater, pp 99-119.

Van De Leur, (1989), "Numerical Study of the Stratified Smoke Flow in a Corridor: Full Scale Calculations", Fire Safety Journal, Vol 14, pp 287-302.

Vantelon,J.P, Guelzim, A and Quach, D., (1991), "Investigation of Fire-Induced Smoke Movement in Tunnels and Stations: An application to the Paris Metro ", Proceedings 3rd International Symp. Fire Safety Science, pp 907-918.

World Road Association ,PIARC, (1987), Committee on Road Tunnels, Report to the XVIIIth World Road Congress, Brussels, 13-19 Sept, pp 67-78.

Wood, D., (1993), "Matching Tunnel Ventilation to Traffic Density", Professional Engineering, May, pp 29-30.

Woodburn, P.J. and Britter, R.E, (1996), "CFD Simulation of a Tunnel Fire - Part 1", Fire Safety Journal, Vol 26, pp 35-62.

Woodburn, P.J and Britter, R.E, (1996), "CFD Simulation of a Tunnel Fire - Part 2", Fire Safety Journal, Vol 26, pp 63-.90

Xue,H., Hihara, E. and Saito,T, (1993), "Turbulence Model of Fire-Induced Air Flow in a Ventilated Tunnel", International Journal Heat Mass Transfer, Vol 36, No 7, pp 1739 - 1748.

Wu, Y., Bakar, M.Z, Atkinson, G. T. and Jagger, S., (1997), "A Study of the Effect of Tunnel Aspect Ratio on Control of Smoke Flow", 9th International Conference on Aerodynamics and Ventilation of Vehicle Tunnels, Aosta Valley, Italy, pp 573 - 587.

Appendix A

Safety Rules and Risk Assessment

These rules must be read in conjunction with HSL and Section Safety Rules and must be complied with at all times.

Safety Rules

- Effective fume extraction must be continued throughout the tests.

- A carbon dioxide fire extinguisher should be immediately available at the air inlet end of the tunnel.

- Ancillary equipment should not be obstruct access to any fire exits.

- All fuel gas piping should be checked for leaks and gas supplies should be turned off at the cylinder before the laboratory is vacated.

- Large gas cylinders should be stored outside

Risk Assessment

- Propane gas is used to create the fires in the stainless steel section of the tunnel. Any uncontrolled release of propane and the resulting ignition is obviously a hazard. The consequences of such an event could result in damage to the tunnel and surrounding laboratory and possible injury to near by personal. However this event is unlikely to occur as all gas piping is checked periodically and gas cylinders are closed when the laboratory is unoccupied.

- Butane gas is used to create a pilot flame in order to ignite the propane gas. The butane gas is stored in a gas cylinder on the trolley and is placed outside when not in use. The hazards and consequences of the butane gas are as above and the same precautions are adopted to remove the risk.

- The fumes from the burnt propane may cause a hazard to near by personnel if not dealt with correctly. However an extraction system is in place throughout any tests and the fumes are fed directly into the system.

Appendix B

Calculated Velocity Data for Each Tunnel

Table B1 : Velocity data for tunnel A

Ave. vel in pipe (m/s)	Reynold No (-)	Discharge Coeff (-)	Calculated Differential Press (Pa)	Manometer Differential Press (kPa)	Vel in tunnel m/s (136x250)
0.10	625.0	0.91	0.02	0.00	0.02
0.15	937.5	0.83	0.06	0.00	0.04
0.20	1250.0	0.78	0.13	0.00	0.05
0.25	1562.5	0.75	0.21	0.00	0.06
0.30	1875.0	0.73	0.32	0.01	0.07
0.35	2187.5	0.72	0.46	0.01	0.08
0.40	2500.0	0.71	0.62	0.01	0.10
0.45	2812.5	0.70	0.80	0.02	0.11
0.50	3125.0	0.69	1.01	0.02	0.12
0.55	3437.5	0.69	1.25	0.02	0.13
0.60	3750.0	0.68	1.51	0.03	0.14
0.65	4062.5	0.68	1.79	0.04	0.16
0.70	4375.0	0.67	2.11	0.04	0.17
0.75	4687.5	0.67	2.44	0.05	0.18
0.80	5000.0	0.66	2.81	0.06	0.19
0.85	5312.5	0.66	3.20	0.06	0.20
0.90	5625.0	0.66	3.61	0.07	0.21
0.95	5937.5	0.66	4.06	0.08	0.23
1.00	6250.0	0.65	4.52	0.09	0.24
1.05	6562.5	0.65	5.02	0.10	0.25
1.10	6875.0	0.65	5.54	0.11	0.26
1.15	7187.5	0.65	6.08	0.12	0.27
1.20	7500.0	0.65	6.66	0.13	0.29
1.25	7812.5	0.65	7.25	0.15	0.30
1.30	8125.0	0.64	7.88	0.16	0.31
1.35	8437.5	0.64	8.53	0.17	0.32
1.40	8750.0	0.64	9.21	0.18	0.33
1.45	9062.5	0.64	9.91	0.20	0.35
1.50	9375.0	0.64	10.64	0.21	0.36
1.55	9687.5	0.64	11.40	0.23	0.37
1.60	10000.0	0.64	12.18	0.24	0.38
1.65	10312.5	0.64	12.99	0.26	0.39
1.70	10625.0	0.64	13.82	0.28	0.41
1.75	10937.5	0.64	14.68	0.29	0.42
1.80	11250.0	0.63	15.57	0.31	0.43
1.85	11562.5	0.63	16.49	0.33	0.44
1.90	11875.0	0.63	17.43	0.35	0.45
1.95	12187.5	0.63	18.39	0.37	0.47
2.00	12500.0	0.63	19.39	0.39	0.48
2.05	12812.5	0.63	20.41	0.41	0.49
2.10	13125.0	0.63	21.45	0.43	0.50
2.15	13437.5	0.63	22.53	0.45	0.51
2.20	13750.0	0.63	23.63	0.47	0.53
2.25	14062.5	0.63	24.75	0.50	0.54
2.30	14375.0	0.63	25.91	0.52	0.55
2.35	14687.5	0.63	27.08	0.54	0.56
2.40	15000.0	0.63	28.29	0.57	0.57
2.45	15312.5	0.63	29.52	0.59	0.58
2.50	15625.0	0.63	30.78	0.62	0.60
2.55	15937.5	0.63	32.07	0.64	0.61
2.60	16250.0	0.63	33.38	0.67	0.62
2.65	16562.5	0.63	34.72	0.69	0.63
2.70	16875.0	0.63	36.08	0.72	0.64
2.75	17187.5	0.63	37.47	0.75	0.66
2.80	17500.0	0.62	38.89	0.78	0.67
3.00	18750.0	0.62	44.83	0.90	0.72

Table B2 : Velocity data for tunnel B

Ave. Vel in pipe (m/s)	Reynold No (-)	Discharge Coeff (-)	Calculated Differential Press (Pa)	Manometer Differential Press (kPa)	Vel in tunnel m/s (250x250)
0.40	2500.0	0.71	0.62	0.01	0.05
0.50	3125.0	0.69	1.01	0.02	0.06
0.60	3750.0	0.68	1.51	0.03	0.08
0.70	4375.0	0.67	2.11	0.04	0.09
0.80	5000.0	0.66	2.81	0.06	0.10
0.90	5625.0	0.66	3.61	0.07	0.12
1.00	6250.0	0.65	4.52	0.09	0.13
1.10	6875.0	0.65	5.54	0.11	0.14
1.20	7500.0	0.65	6.66	0.13	0.16
1.30	8125.0	0.64	7.88	0.16	0.17
1.40	8750.0	0.64	9.21	0.18	0.18
1.50	9375.0	0.64	10.64	0.21	0.19
1.60	10000.0	0.64	12.18	0.24	0.21
1.70	10625.0	0.64	13.82	0.28	0.22
1.80	11250.0	0.63	15.57	0.31	0.23
1.90	11875.0	0.63	17.43	0.35	0.25
2.00	12500.0	0.63	19.39	0.39	0.26
2.10	13125.0	0.63	21.45	0.43	0.27
2.20	13750.0	0.63	23.63	0.47	0.29
2.30	14375.0	0.63	25.91	0.52	0.30
2.40	15000.0	0.63	28.29	0.57	0.31
2.50	15625.0	0.63	30.78	0.62	0.32
2.60	16250.0	0.63	33.38	0.67	0.34
2.70	16875.0	0.63	36.08	0.72	0.35
2.80	17500.0	0.62	38.89	0.78	0.36
2.90	18125.0	0.62	41.81	0.84	0.38
3.00	18750.0	0.62	44.83	0.90	0.39
3.10	19375.0	0.62	47.96	0.96	0.40
3.20	20000.0	0.62	51.19	1.02	0.42
3.30	20625.0	0.62	54.53	1.09	0.43
3.40	21250.0	0.62	57.98	1.16	0.44
3.50	21875.0	0.62	61.53	1.23	0.45
3.60	22500.0	0.62	65.19	1.30	0.47
3.70	23125.0	0.62	68.96	1.38	0.48
3.80	23750.0	0.62	72.83	1.46	0.49
3.90	24375.0	0.62	76.81	1.54	0.51
4.00	25000.0	0.62	80.90	1.62	0.52
4.10	25625.0	0.62	85.09	1.70	0.53
4.20	26250.0	0.62	89.39	1.79	0.55
4.30	26875.0	0.62	93.80	1.88	0.56
4.40	27500.0	0.62	98.31	1.97	0.57
4.50	28125.0	0.62	102.93	2.06	0.58
4.60	28750.0	0.62	107.66	2.15	0.60
4.70	29375.0	0.62	112.49	2.25	0.61
4.80	30000.0	0.62	117.43	2.35	0.62
4.90	30625.0	0.62	122.48	2.45	0.64
5.00	31250.0	0.62	127.64	2.55	0.65
5.10	31875.0	0.62	132.90	2.66	0.66
5.20	32500.0	0.62	138.26	2.77	0.68
5.30	33125.0	0.62	143.74	2.87	0.69
5.40	33750.0	0.61	149.32	2.99	0.70
5.50	34375.0	0.61	155.01	3.10	0.71
5.60	35000.0	0.61	160.80	3.22	0.73
5.70	35625.0	0.61	166.71	3.33	0.74
5.80	36250.0	0.61	172.71	3.45	0.75
5.90	36875.0	0.61	178.83	3.58	0.77
6.00	37500.0	0.61	185.05	3.70	0.78

Table B3 : Velocity data for tunnel C

Ave. Vel in pipe (m/s)	Reynold No (-)	Discharge Coeff (-)	Calculated Differential Press (Pa)	Manometer Differential Press (kPa)	Vel in tunnel m/s (500x250)
1.0	6250.0	0.65	4.52	0.02	0.06
1.1	6875.0	0.65	5.54	0.03	0.07
1.2	7500.0	0.65	6.66	0.03	0.08
1.3	8125.0	0.64	7.88	0.04	0.08
1.4	8750.0	0.64	9.21	0.05	0.09
1.5	9375.0	0.64	10.64	0.05	0.10
1.6	10000.0	0.64	12.18	0.06	0.10
1.7	10625.0	0.64	13.82	0.07	0.11
1.8	11250.0	0.63	15.57	0.08	0.12
1.9	11875.0	0.63	17.43	0.09	0.12
2.0	12500.0	0.63	19.39	0.10	0.13
2.1	13125.0	0.63	21.45	0.11	0.14
2.2	13750.0	0.63	23.63	0.12	0.14
2.3	14375.0	0.63	25.91	0.13	0.15
2.4	15000.0	0.63	28.29	0.14	0.16
2.5	15625.0	0.63	30.78	0.15	0.16
2.6	16250.0	0.63	33.38	0.17	0.17
2.7	16875.0	0.63	36.08	0.18	0.18
2.8	17500.0	0.62	38.89	0.19	0.18
2.9	18125.0	0.62	41.81	0.21	0.19
3.0	18750.0	0.62	44.83	0.22	0.19
3.1	19375.0	0.62	47.96	0.24	0.20
3.2	20000.0	0.62	51.19	0.26	0.21
3.3	20625.0	0.62	54.53	0.27	0.21
3.4	21250.0	0.62	57.98	0.29	0.22
3.5	21875.0	0.62	61.53	0.31	0.23
3.6	22500.0	0.62	65.19	0.33	0.23
3.7	23125.0	0.62	68.96	0.34	0.24
3.8	23750.0	0.62	72.83	0.36	0.25
3.9	24375.0	0.62	76.81	0.38	0.25
4.0	25000.0	0.62	80.90	0.40	0.26
4.1	25625.0	0.62	85.09	0.43	0.27
4.2	26250.0	0.62	89.39	0.45	0.27
4.3	26875.0	0.62	93.80	0.47	0.28
4.4	27500.0	0.62	98.31	0.49	0.29
4.5	28125.0	0.62	102.93	0.51	0.29
4.6	28750.0	0.62	107.66	0.54	0.30
4.7	29375.0	0.62	112.49	0.56	0.31
4.8	30000.0	0.62	117.43	0.59	0.31
4.9	30625.0	0.62	122.48	0.61	0.32
5.0	31250.0	0.62	127.64	0.64	0.32
5.1	31875.0	0.62	132.90	0.66	0.33
5.2	32500.0	0.62	138.26	0.69	0.34
5.3	33125.0	0.62	143.74	0.72	0.34
5.4	33750.0	0.61	149.32	0.75	0.35
5.5	34375.0	0.61	155.01	0.78	0.36
5.6	35000.0	0.61	160.80	0.80	0.36
5.7	35625.0	0.61	166.71	0.83	0.37
5.8	36250.0	0.61	172.71	0.86	0.38
5.9	36875.0	0.61	178.83	0.89	0.38
6.0	37500.0	0.61	185.05	0.93	0.39
6.1	38125.0	0.61	191.38	0.96	0.40

Table B3   .continue

6.2	38750.0	0.61	197.82	0.99	0.40
6.3	39375.0	0.61	204.36	1.02	0.41
6.4	40000.0	0.61	211.01	1.06	0.42
6.5	40625.0	0.61	217.77	1.09	0.42
6.6	41250.0	0.61	224.64	1.12	0.43
6.7	41875.0	0.61	231.61	1.16	0.43
6.8	42500.0	0.61	238.69	1.19	0.44
6.9	43125.0	0.61	245.87	1.23	0.45
7.0	43750.0	0.61	253.16	1.27	0.45
7.1	44375.0	0.61	260.56	1.30	0.46
7.2	45000.0	0.61	268.07	1.34	0.47
7.3	45625.0	0.61	275.68	1.38	0.47
7.4	46250.0	0.61	283.40	1.42	0.48
7.5	46875.0	0.61	291.23	1.46	0.49
7.6	47500.0	0.61	299.17	1.50	0.49
7.7	48125.0	0.61	307.21	1.54	0.50
7.8	48750.0	0.61	315.36	1.58	0.51
7.9	49375.0	0.61	323.61	1.62	0.51
8.0	50000.0	0.61	331.98	1.66	0.52
8.1	50625.0	0.61	340.45	1.70	0.53
8.2	51250.0	0.61	349.03	1.75	0.53
8.3	51875.0	0.61	357.71	1.79	0.54
8.4	52500.0	0.61	366.50	1.83	0.55
8.5	53125.0	0.61	375.40·	1.88	0.55
8.6	53750.0	0.61	384.41	1.92	0.56
8.7	54375.0	0.61	393.52	1.97	0.56
8.8	55000.0	0.61	402.74	2.01	0.57
8.9	55625.0	0.61	412.07	2.06	0.58
9.0	56250.0	0.61	421.50	2.11	0.58
9.1	56875.0	0.61	431.05	2.16	0.59
9.2	57500.0	0.61	440.69	2.20	0.60
9.3	58125.0	0.61	450.45	2.25	0.60
9.4	58750.0	0.61	460.31	2.30	0.61
9.5	59375.0	0.61	470.28	2.35	0.62
9.6	60000.0	0.61	480.36	2.40	0.62
9.7	60625.0	0.61	490.55	2.45	0.63
9.8	61250.0	0.61	500.84	2.50	0.64
9.9	61875.0	0.61	511.24	2.56	0.64
10.0	62500.0	0.61	521.75	2.61	0.65
10.1	63125.0	0.61	532.36	2.66	0.66
10.2	63750.0	0.61	543.08	2.72	0.66
10.3	64375.0	0.61	553.91	2.77	0.67
10.4	65000.0	0.61	564.84	2.82	0.68
10.5	65625.0	0.61	575.89	2.88	0.68
10.6	66250.0	0.61	587.04	2.94	0.69
10.7	66875.0	0.61	598.29	2.99	0.69
10.8	67500.0	0.61	609.66	3.05	0.70
10.9	68125.0	0.61	621.13	3.11	0.71
11.0	68750.0	0.61	632.71	3.16	0.71
11.1	69375.0	0.61	644.39	3.22	0.72
11.2	70000.0	0.61	656.19	3.28	0.73
11.3	70625.0	0.61	668.09	3.34	0.73
11.4	71250.0	0.61	680.10	3.40	0.74
11.5	71875.0	0.61	692.21	3.46	0.75
11.6	72500.0	0.61	704.43	3.52	0.75

Table B4 : Velocity data for tunnel D

Ave. Vel in pipe (m/s)	Reynold No (-)	Discharge Coeff (-)	Calculated Differential Press (Pa)	Manometer Differential Press (kPa)	Vel in tunnel m/s (1000x250)
2.0	12500.0	0.63	19.39	0.019	0.06
2.5	15625.0	0.63	30.78	0.031	0.08
3.0	18750.0	0.62	44.83	0.045	0.10
3.5	21875.0	0.62	61.53	0.062	0.11
4.0	25000.0	0.62	80.90	0.081	0.13
4.5	28125.0	0.62	102.93	0.103	0.15
5.0	31250.0	0.62	127.64	0.128	0.16
5.5	34375.0	0.61	155.01	0.155	0.18
6.0	37500.0	0.61	185.05	0.185	0.19
6.5	40625.0	0.61	217.77	0.218	0.21
7.0	43750.0	0.61	253.16	0.253	0.23
7.5	46875.0	0.61	291.23	0.291	0.24
8.0	50000.0	0.61	331.98	0.332	0.26
8.5	53125.0	0.61	375.40	0.375	0.28
9.0	56250.0	0.61	421.50	0.422	0.29
9.5	59375.0	0.61	470.28	0.470	0.31
10.0	62500.0	0.61	521.75	0.522	0.32
10.5	65625.0	0.61	575.89	0.576	0.34
11.0	68750.0	0.61	632.71	0.633	0.36
11.5	71875.0	0.61	692.21	0.692	0.37
12.0	75000.0	0.61	754.40	0.754	0.39
12.5	78125.0	0.61	819.26	0.819	0.41
13.0	81250.0	0.61	886.81	0.887	0.42
13.5	84375.0	0.61	957.05	0.957	0.44
14.0	87500.0	0.61	1029.96	1.030	0.45
14.5	90625.0	0.61	1105.56	1.106	0.47
15.0	93750.0	0.61	1183.84	1.184	0.49
15.5	96875.0	0.61	1264.81	1.265	0.50
16.0	100000.0	0.61	1348.46	1.348	0.52
16.5	103125.0	0.61	1434.80	1.435	0.54
17.0	106250.0	0.61	1523.82	1.524	0.55
17.5	109375.0	0.61	1615.52	1.616	0.57
18.0	112500.0	0.61	1709.91	1.710	0.58
18.5	115625.0	0.61	1806.99	1.807	0.60
19.0	118750.0	0.61	1906.75	1.907	0.62
19.5	121875.0	0.61	2009.20	2.009	0.63
20.0	125000.0	0.61	2114.33	2.114	0.65
20.5	128125.0	0.61	2222.15	2.222	0.67
21.0	131250.0	0.61	2332.65	2.333	0.68
21.5	134375.0	0.60	2445.85	2.446	0.70
22.0	137500.0	0.60	2561.72	2.562	0.71
22.5	140625.0	0.60	2680.29	2.680	0.73
23.0	143750.0	0.60	2801.54	2.802	0.75
23.5	146875.0	0.60	2925.48	2.925	0.76
24.0	150000.0	0.60	3052.10	3.052	0.78
24.5	153125.0	0.60	3181.42	3.181	0.80
30.0	187500.0	0.60	4781.23	4.781	0.97

Table B5 : Velocity data for tunnel E

Ave. Vel in pipe (m/s)	Reynold No (-)	Discharge Coeff (-)	Calculated Differential Press (Pa)	Manometer Differential Press (kPa)	Vel in tunnel m/s(274 x 244)
0.4	2500.0	0.71	0.62	0.01	0.06
0.5	3125.0	0.69	1.01	0.02	0.07
0.6	3750.0	0.68	1.51	0.03	0.09
0.7	4375.0	0.67	2.11	0.04	0.10
0.8	5000.0	0.66	2.81	0.06	0.11
0.9	5625.0	0.66	3.61	0.07	0.13
1.0	6250.0	0.65	4.52	0.09	0.14
1.1	6875.0	0.65	5.54	0.11	0.16
1.2	7500.0	0.65	6.66	0.13	0.17
1.3	8125.0	0.64	7.88	0.16	0.19
1.4	8750.0	0.64	9.21	0.18	0.20
1.5	9375.0	0.64	10.64	0.21	0.21
1.6	10000.0	0.64	12.18	0.24	0.23
1.7	10625.0	0.64	13.82	0.28	0.24
1.8	11250.0	0.63	15.57	0.31	0.26
1.9	11875.0	0.63	17.43	0.35	0.27
2.0	12500.0	0.63	19.39	0.39	0.29
2.1	13125.0	0.63	21.45	0.43	0.30
2.2	13750.0	0.63	23.63	0.47	0.31
2.3	14375.0	0.63	25.91	0.52	0.33
2.4	15000.0	0.63	28.29	0.57	0.34
2.5	15625.0	0.63	30.78	0.62	0.36
2.6	16250.0	0.63	33.38	0.67	0.37
2.7	16875.0	0.63	36.08	0.72	0.39
2.8	17500.0	0.62	38.89	0.78	0.40
2.9	18125.0	0.62	41.81	0.84	0.41
3.0	18750.0	0.62	44.83	0.90	0.43
3.1	19375.0	0.62	47.96	0.96	0.44
3.2	20000.0	0.62	51.19	1.02	0.46
3.3	20625.0	0.62	54.53	1.09	0.47
3.4	21250.0	0.62	57.98	1.16	0.48
3.5	21875.0	0.62	61.53	1.23	0.50
3.6	22500.0	0.62	65.19	1.30	0.51
3.7	23125.0	0.62	68.96	1.38	0.53
3.8	23750.0	0.62	72.83	1.46	0.54
3.9	24375.0	0.62	76.81	1.54	0.56
4.0	25000.0	0.62	80.90	1.62	0.57
4.1	25625.0	0.62	85.09	1.70	0.58
4.2	26250.0	0.62	89.39	1.79	0.60
4.3	26875.0	0.62	93.80	1.88	0.61
4.4	27500.0	0.62	98.31	1.97	0.63
4.5	28125.0	0.62	102.93	2.06	0.64
4.6	28750.0	0.62	107.66	2.15	0.66
4.7	29375.0	0.62	112.49	2.25	0.67
4.8	30000.0	0.62	117.43	2.35	0.68
4.9	30625.0	0.62	122.48	2.45	0.70
5.0	31250.0	0.62	127.64	2.55	0.71
5.1	31875.0	0.62	132.90	2.66	0.73
5.2	32500.0	0.62	138.26	2.77	0.74
5.3	33125.0	0.62	143.74	2.87	0.76
5.4	33750.0	0.61	149.32	2.99	0.77
5.5	34375.0	0.61	155.01	3.10	0.78
5.6	35000.0	0.61	160.80	3.22	0.80
5.7	35625.0	0.61	166.71	3.33	0.81
5.8	36250.0	0.61	172.71	3.45	0.83
5.9	36875.0	0.61	178.83	3.58	0.84
6.0	37500.0	0.61	185.05	3.70	0.86

Appendix C

Simple Qbasic Programming for Analysis and Arrangement the Temperature Data Obtained in the Experiment

```
DIM store(20, 40)
PRINT "input data directory name ";
INPUT stem$
' max number of tunnel heights downstream is 17
thmax = 17
FOR th = 1 TO 9
ntot = 31
FOR tc = 1 TO 9
PRINT th; " "; tc
OPEN "c:\tun1000\dataext\" + stem$ + "\" + CHR$(48 + th) + "h\tc_d" + CHR$(48 + tc) + ".asc" FOR INPUT AS #1
av = 0
FOR n = 1 TO ntot
INPUT #1, x
av = av + x
NEXT n
store(th, tc) = av / ntot
CLOSE
NEXT tc
FOR tc = 0 TO 9
OPEN "c:\tun1000\dataext\" + stem$ + "\" + CHR$(48 + th) + "h\tc_d1" + CHR$(48 + tc) + ".asc" FOR INPUT AS #1
av = 0
FOR n = 1 TO ntot
INPUT #1, x
av = av + x
NEXT n
store(th, tc + 10) = av / ntot
CLOSE
NEXT tc
FOR tc = 0 TO 4
```

```
OPEN "c:\tun1000\dataext\" + stem$ + "\" + CHR$(48 + th) + "h\tc_d2" + CHR$(48 + tc) + ".asc" FOR
INPUT AS #1
av = 0
FOR n = 1 TO ntot
INPUT #1, x
av = av + x
NEXT n
store(th, tc + 20) = av / ntot
CLOSE
NEXT tc
FOR tc = 1 TO 5
OPEN "c:\tun1000\dataext\" + stem$ + "\" + CHR$(48 + th) + "h\tc" + CHR$(48 + tc) + ".asc" FOR
INPUT AS #1
av = 0
FOR n = 1 TO ntot
INPUT #1, x
av = av + x
NEXT n
store(th, tc + 24) = av / ntot
CLOSE
NEXT tc
OPEN "c:\tun1000\dataext\" + stem$ + "\" + CHR$(48 + th) + "h\pressure.asc" FOR INPUT AS #1
av = 0
FOR n = 1 TO ntot
INPUT #1, x
av = av + x
NEXT n
store(th, 30) = av / ntot
CLOSE
NEXT th
FOR th = 0 TO 7
ntot = 31
FOR tc = 1 TO 9
PRINT th; " "; tc
OPEN "c:\tun1000\dataext\" + stem$ + "\1" + CHR$(48 + th) + "h\tc_d" + CHR$(48 + tc) + ".asc" FOR
INPUT AS #1
av = 0
FOR n = 1 TO ntot
INPUT #1, x
```

```
av = av + x
NEXT n
store(th + 10, tc) = av / ntot
CLOSE
NEXT tc
FOR tc = 0 TO 9
OPEN "c:\tun1000\dataext\" + stem$ + "\1" + CHR$(48 + th) + "h\tc_d1" + CHR$(48 + tc) + ".asc"
FOR INPUT AS #1
av = 0
FOR n = 1 TO ntot
INPUT #1, x
av = av + x
NEXT n
store(th + 10, tc + 10) = av / ntot
CLOSE
NEXT tc
FOR tc = 0 TO 4
OPEN "c:\tun1000\dataext\" + stem$ + "\1" + CHR$(48 + th) + "h\tc_d2" + CHR$(48 + tc) + ".asc"
FOR INPUT AS #1
av = 0
FOR n = 1 TO ntot
INPUT #1, x
av = av + x
NEXT n
store(th + 10, tc + 20) = av / ntot
CLOSE
NEXT tc
FOR tc = 1 TO 5
OPEN "c:\tun1000\dataext\" + stem$ + "\1" + CHR$(48 + th) + "h\tc" + CHR$(48 + tc) + ".asc" FOR
INPUT AS #1
av = 0
FOR n = 1 TO ntot
INPUT #1, x
av = av + x
NEXT n
store(th + 10, tc + 24) = av / ntot
CLOSE
NEXT tc
OPEN "c:\tun1000\dataext\" + stem$ + "\1" + CHR$(48 + th) + "h\pressure.asc" FOR INPUT AS #1
```

```
av = 0
FOR n = 1 TO ntot
INPUT #1, x
av = av + x
NEXT n
store(th + 10, 30) = av / ntot
CLOSE
NEXT th
OPEN "C:\tun1000\dataext\" + stem$ + "\data3.prn" FOR OUTPUT AS #1
FOR th = 1 TO thmax
PRINT #1, 25 * (th - 1); ","; 40;  ","; store(th, 1); ","; store(th, 9);  ","; store(th, 17)
PRINT #1, 25 * (th - 1); ","; 70;  ","; store(th, 2); ","; store(th, 10); ","; store(th, 18)
PRINT #1, 25 * (th - 1); ","; 100; ","; store(th, 3); ","; store(th, 11); ","; store(th, 19)
PRINT #1, 25 * (th - 1); ","; 130; ","; store(th, 4); ","; store(th, 12); ","; store(th, 20)
PRINT #1, 25 * (th - 1); ","; 160; ","; store(th, 5); ","; store(th, 13); ","; store(th, 21)
PRINT #1, 25 * (th - 1); ","; 190; ","; store(th, 6); ","; store(th, 14); ","; store(th, 22)
PRINT #1, 25 * (th - 1); ","; 220; ","; store(th, 7); ","; store(th, 15); ","; store(th, 23)
PRINT #1, 25 * (th - 1); ","; 240; ","; store(th, 8); ","; store(th, 16); ","; store(th, 24)


NEXT th


CLOSE
```

Appendix D

Coefficient of Polynomial for Physical Properties in Finite Rate Formulation

$$\text{Pr operty} = AX^2 + BX + C$$

Table D1 : Coefficient of polynomial

	A	B	C
Density			
C_3H_8	4×10^{-6}	- 0.0067	3.3996
O_2	3×10^{-6}	- 0.0046	2.3782
CO_2	4×10^{-6}	- 0.0064	3.2921
H_2O	1×10^{-6}	- 0.0022	1.2199
N_2	3×10^{-6}	- 0.0041	2.0808
Viscosity			
C_3H_8	-4×10^{-12}	3×10^{-8}	9×10^{-8}
O_2	-2×10^{-11}	6×10^{-8}	3×10^{-6}
CO_2	-2×10^{-11}	6×10^{-8}	- 6×10^{-6}
H_2O	3×10^{-12}	4×10^{-8}	- 1×10^{-6}
N_2	-2×10^{-11}	5×10^{-8} T	4×10^{-6}
Heat Capacity			
C_3H_8	-0.0021	5.9466	94.237
O_2	1×10^{-5}	0.2635	837.02
CO_2	-0.0005	1.2197	531.9
H_2O	0.0007	- 0.2293	1921.5
N_2	0.0002	- 0.0975	1045.1
Thermal Conductivity			
C_3H_8	5×10^{-8}	8×10^{-5}	- 0.0125
O_2	-1×10^{-8}	9×10^{-5}	0.0011
CO_2	-1×10^{-8}	9×10^{-5}	- 0.0093
H_2O	7×10^{-8}	3×10^{-5}	0.006
N_2	-1×10^{-8}	7×10^{-5}	0.0045

Appendix E

Temperature Data in the Downstream Region

Table E1: Temperature data in the downstream in tunnel B (Q = 3.0 kW, Uc = 0.48 m/s)

x	(40, 0)	(70, 0)	(100, 0)	(130, 0)	(160, 0)	(190, 0)	(220, 0)	(240, 0)
				(y,z)				
250	53.56	84.86	130.13	169.56	166.81	120.22	87.40	85.01
500	27.43	31.44	36.35	50.73	78.47	99.70	121.00	128.76
750	24.49	29.78	35.09	45.99	68.10	85.22	104.07	112.79
1000	23.68	29.24	34.49	43.60	59.21	74.13	88.55	94.40
1250	23.63	29.80	35.68	44.97	58.85	71.44	81.98	83.83
1500	23.50	29.67	35.42	44.04	57.28	68.56	76.84	77.25
1750	23.41	29.50	34.66	42.71	54.89	65.78	73.08	72.38
2000	22.82	28.70	33.80	41.39	53.31	64.73	71.10	70.59
2250	23.12	28.89	34.19	41.63	53.24	64.28	70.05	69.71
2500	22.88	28.68	34.01	41.41	52.54	63.30	68.94	68.83
2750	23.11	28.78	33.94	40.87	51.03	61.14	66.63	66.24
3000	23.12	28.44	33.17	39.81	49.45	59.67	65.09	64.82
3250	23.28	28.34	32.88	39.21	48.72	58.39	63.28	62.84
3500	23.23	27.99	32.23	38.34	47.50	57.09	61.97	61.75

x	(40, 55)	(70, 55)	(100, 55)	(130, 55)	(160, 55)	(190, 55)	(220, 55)	(240, 55)
				(y,z)				
250	80.82	27.40	169.80	153.64	108.93	84.94	70.54	82.07
500	28.71	25.45	64.21	76.99	94.75	107.64	125.02	129.39
750	27.18	24.73	54.30	63.78	78.36	91.83	108.50	112.50
1000	25.54	25.48	44.05	52.52	65.37	78.21	92.53	95.57
1250	23.87	25.86	38.97	47.28	58.83	72.31	84.19	84.46
1500	23.17	25.83	36.79	44.05	54.76	68.31	78.45	77.88
1750	23.06	26.06	35.63	42.83	53.29	65.95	74.20	72.96
2000	22.96	26.07	35.35	42.48	52.57	65.11	72.25	71.38
2250	23.34	26.27	35.90	43.07	52.88	64.89	71.04	70.54
2500	23.20	25.96	35.48	42.57	51.93	63.77	69.77	69.11
2750	23.63	26.23	35.20	41.71	50.25	61.52	67.54	66.76
3000	23.63	25.96	34.70	41.05	49.31	60.20	66.19	65.35
3250	23.72	26.15	34.25	40.35	48.24	58.88	64.37	63.23
3500	23.73	25.91	33.36	39.19	46.73	57.19	62.90	62.20

x	(40, 110)	(70, 110)	(100, 110)	(130, 110)	(160, 110)	(190, 110)	(220, 110)	(240, 110)
				(y,z)				
250	39.24	61.49	62.91	54.87	40.09	41.29	61.31	64.55
500	29.81	50.86	68.38	86.88	102.46	116.88	123.65	123.06
750	27.11	42.95	60.30	75.22	91.24	104.36	109.18	108.50
1000	25.23	36.64	48.73	62.33	75.92	89.89	93.98	91.86
1250	23.95	31.05	39.12	49.71	62.96	78.28	83.70	80.03
1500	22.94	28.44	35.16	44.46	57.56	72.30	77.42	74.11
1750	22.92	28.51	35.21	44.01	55.97	69.12	73.37	69.81
2000	23.37	29.14	35.81	44.51	55.52	67.64	71.40	69.00
2250	23.78	29.11	35.73	44.46	55.65	66.90	70.11	68.61
2500	23.48	28.34	34.63	43.51	54.65	65.53	68.49	67.00
2750	23.52	28.33	34.35	42.46	52.92	63.73	66.43	64.73
3000	23.57	27.81	33.47	41.23	51.23	62.37	65.46	64.24
3250	23.61	27.73	33.18	40.63	50.22	60.61	63.36	61.52
3500	23.50	27.36	32.40	39.08	48.05	58.60	62.00	60.51

Table E2: Temperature data in the downstream in tunnel B (Q = 3.0 kW, U = 0.25 m/s)

x	(40, 0)	(70, 0)	(100, 0)	(130, 0)	(160, 0)	(190, 0)	(220, 0)	(240, 0)
				(y,z)				
250	56.17	72.59	86.86	113.31	154.59	164.63	170.50	171.45
500	46.88	64.56	75.26	92.61	123.72	132.36	148.30	158.40
750	31.97	38.39	44.53	54.34	74.49	90.90	112.67	124.48
1000	26.42	29.56	34.31	44.62	65.55	84.59	100.10	103.96
1250	22.87	25.04	28.25	37.39	56.66	78.24	90.96	90.81
1500	21.81	24.14	26.92	36.34	54.48	73.29	83.59	83.09
1750	20.55	23.02	25.68	34.07	50.03	67.90	77.89	77.57
2000	19.99	23.10	26.06	34.60	49.16	66.05	74.38	73.88
2250	20.32	23.51	26.99	35.52	49.16	64.51	71.81	71.78
2500	20.63	23.91	27.74	35.93	48.52	63.18	69.79	69.66
2750	20.77	23.90	27.71	35.48	47.51	60.82	67.26	67.32
3000	20.86	23.91	27.59	35.18	46.17	58.39	64.66	64.88
3250	21.25	24.38	28.37	35.58	45.46	57.04	62.79	62.75
3500	21.04	23.99	27.65	34.29	43.37	54.42	60.24	60.34

x	(40, 55)	(70, 55)	(100, 55)	(130, 55)	(160, 55)	(190, 55)	(220, 55)	(240, 55)
				(y,z)				
250	72.50	27.52	132.48	140.63	154.72	163.93	167.02	171.84
500	55.05	27.12	106.68	112.45	124.23	128.37	146.58	158.17
750	34.74	25.49	54.14	62.60	79.71	93.85	115.15	123.52
1000	26.36	24.09	38.31	49.01	67.43	86.53	102.13	104.64
1250	22.11	22.60	29.87	39.57	57.34	78.82	92.62	92.17
1500	21.20	22.25	28.43	38.28	54.54	74.34	85.11	83.23
1750	20.52	21.81	27.08	35.54	49.94	69.33	79.47	78.37
2000	20.41	21.87	27.27	35.77	49.08	66.95	75.71	74.66
2250	20.75	22.33	28.48	36.87	49.00	65.23	72.81	72.17
2500	21.10	22.45	29.13	37.40	49.07	64.16	70.74	70.64
2750	21.26	22.28	28.92	37.00	47.85	61.91	68.29	67.80
3000	21.38	22.26	28.93	36.55	46.27	59.21	65.75	65.12
3250	21.82	22.79	29.70	36.86	45.68	57.90	63.57	62.65
3500	21.65	22.39	28.77	35.26	43.38	54.88	61.14	60.83

x	(40, 110)	(70, 110)	(100, 110)	(130, 110)	(160, 110)	(190, 110)	(220, 110)	(240, 110)
				(y,z)				
250	44.84	56.72	71.15	95.93	117.20	136.49	152.46	150.06
500	43.14	58.76	76.03	100.03	121.30	135.37	144.64	142.27
750	32.01	40.38	52.03	71.89	93.86	110.59	118.84	116.89
1000	25.82	30.12	38.13	54.82	75.96	95.74	103.72	101.31
1250	22.07	24.52	29.65	43.00	64.31	83.53	91.20	87.84
1500	21.31	23.70	29.51	41.87	60.62	78.18	83.10	79.43
1750	20.46	22.60	27.36	37.85	54.98	73.07	77.58	73.69
2000	20.30	23.01	28.20	38.28	53.10	69.87	74.75	73.21
2250	20.78	23.55	28.63	38.98	53.08	68.08	72.34	71.46
2500	20.85	23.73	28.81	39.00	52.56	66.64	69.79	68.37
2750	20.79	23.78	29.13	38.52	50.96	64.24	67.29	65.82
3000	20.81	23.84	29.28	37.80	49.37	61.59	64.54	63.00
3250	21.22	24.59	30.15	37.96	48.31	59.55	62.67	61.09
3500	21.16	24.02	28.93	36.09	45.68	56.42	60.41	59.19

Table E3: Temperature data in the downstream in tunnel B (Q = 7.50 kW, Uc = 0.56 m/s)

x	(40, 0)	(70, 0)	(100, 0)	(130, 0)	(160, 0)	(190, 0)	(220, 0)	(240, 0)
250	147.71	267.27	397.12	423.08	359.97	237.78	143.09	109.54
500	66.19	72.54	85.18	131.53	203.22	250.98	282.07	284.94
750	38.10	48.55	58.40	76.77	107.01	139.17	171.24	180.54
1000	30.18	35.56	41.08	52.44	70.20	89.73	107.01	110.40
1250	36.67	48.20	58.94	75.81	103.15	126.96	148.00	152.44
1500	35.71	47.36	57.63	73.35	98.06	121.09	140.35	142.44
1750	34.83	45.49	55.11	69.00	91.75	115.42	133.29	133.86
2000	32.82	43.00	51.95	65.03	87.15	111.42	129.12	131.30
2250	30.39	38.77	46.86	58.41	79.03	100.64	113.58	112.93
2500	34.11	43.06	52.14	64.77	84.96	106.09	121.27	122.25
2750	33.47	41.98	50.71	62.88	82.13	103.07	118.36	119.34
3000	23.23	26.95	31.05	36.65	47.97	60.13	66.77	64.80
3250	27.42	33.51	39.89	49.13	66.01	84.68	95.48	94.09
3500	28.48	35.05	42.00	51.89	68.91	88.16	99.98	99.53

x	(40, 55)	(70, 55)	(100, 55)	(130, 55)	(160, 55)	(190, 55)	(220, 55)	(240, 55)
250	232.66	384.72	425.20	354.59	248.36	175.99	101.73	99.62
500	67.33	116.80	165.67	202.35	246.47	263.81	280.92	280.19
750	46.27	58.52	74.11	91.35	117.01	144.79	175.07	180.49
1000	30.55	36.77	46.36	57.81	71.98	93.50	109.24	112.69
1250	36.43	46.50	61.64	77.32	99.65	127.34	152.15	153.33
1500	34.16	44.34	59.04	73.65	93.75	121.02	144.39	143.73
1750	33.73	43.17	56.86	70.79	90.87	115.72	136.74	134.90
2000	32.73	41.40	54.90	68.61	87.53	112.17	132.95	132.94
2250	30.61	37.50	49.87	61.60	78.37	102.07	115.72	114.94
2500	34.21	42.12	54.82	66.79	83.52	105.79	123.63	122.84
2750	33.73	41.36	52.85	64.88	81.42	103.55	120.40	120.11
3000	23.22	26.30	33.42	39.03	46.79	62.16	67.57	67.59
3250	27.61	32.74	43.03	51.90	65.34	86.25	97.92	96.47
3500	28.51	34.06	44.44	54.11	68.10	89.42	102.85	101.24

x	(40, 110)	(70, 110)	(100, 110)	(130, 110)	(160, 110)	(190, 110)	(220, 110)	(240, 110)
250	78.98	130.91	137.68	112.70	74.74	56.51	68.92	74.66
500	67.89	106.29	149.53	195.13	228.13	260.07	267.88	255.37
750	45.61	70.90	89.80	111.25	134.20	168.62	179.02	169.97
1000	30.58	40.87	51.09	63.66	78.72	107.99	115.51	103.71
1250	36.31	47.71	61.69	79.50	104.91	138.07	152.05	144.60
1500	34.28	44.87	57.18	74.63	98.88	131.20	143.54	134.58
1750	33.55	43.85	56.70	74.27	96.47	125.18	135.60	127.24
2000	33.21	42.64	54.82	72.25	93.51	120.57	131.90	128.15
2250	31.09	39.53	49.82	63.51	81.49	107.83	115.82	111.00
2500	35.01	43.49	53.95	68.01	87.58	111.92	122.54	118.81
2750	34.41	41.89	51.51	65.64	84.97	109.25	119.28	114.41
3000	23.00	27.63	32.63	39.24	47.39	66.30	69.98	64.03
3250	27.59	34.03	42.15	52.36	66.99	91.89	98.03	91.96
3500	28.74	35.26	43.72	54.30	69.99	94.59	102.48	98.19

Table E4: Temperature data in the downstream in tunnel B (Q = 7.50 kW, U = 0.31 m/s)

x	(40, 0)	(70, 0)	(100, 0)	(130, 0)	(160, 0)	(190, 0)	(220, 0)	(240, 0)
				(y,z)				
250	146.80	226.53	320.90	406.65	429.30	399.65	372.76	343.96
500	98.74	139.42	181.57	224.29	251.64	257.41	282.89	294.85
750	53.65	64.29	77.63	96.82	129.35	162.59	200.95	221.40
1000	39.12	45.70	54.79	75.85	116.07	150.53	176.13	180.53
1250	33.25	38.64	46.15	64.93	99.81	138.25	160.56	160.31
1500	30.41	35.25	41.62	57.52	88.61	127.40	150.54	149.48
1750	30.04	34.64	40.78	56.30	86.01	122.43	142.70	140.71
2000	30.17	35.01	41.36	56.77	83.99	116.67	135.09	134.09
2250	30.49	35.71	42.69	57.88	82.66	112.30	128.82	129.20
2500	30.73	35.72	42.44	56.91	81.42	109.77	125.35	125.45
2750	22.98	26.50	31.41	42.05	61.90	89.46	107.31	106.75
3000	24.02	27.99	33.37	44.62	64.97	91.10	106.96	106.92
3250	25.05	29.31	34.79	46.47	65.74	89.86	103.93	103.76
3500	25.44	29.41	34.70	45.96	64.24	86.89	100.23	100.31

x	(40, 55)	(70, 55)	(100, 55)	(130, 55)	(160, 55)	(190, 55)	(220, 55)	(240, 55)
				(y,z)				
250	197.46	339.10	425.14	415.23	376.55	367.73	335.15	320.65
500	124.51	193.76	225.68	229.99	241.28	245.43	278.59	286.48
750	57.45	76.39	90.49	106.04	135.46	165.12	205.66	219.46
1000	39.88	49.41	60.16	80.51	112.99	150.91	179.80	179.61
1250	32.76	38.80	48.30	68.66	100.51	137.34	163.58	161.65
1500	30.11	34.85	43.27	60.52	88.75	127.29	152.71	151.43
1750	29.80	34.35	42.94	59.86	85.12	121.90	144.21	141.24
2000	29.62	34.47	43.03	58.93	82.74	117.15	137.10	135.70
2250	30.19	35.29	44.61	60.64	83.27	113.91	131.09	130.86
2500	30.55	35.47	44.45	59.80	82.07	111.44	127.56	127.40
2750	23.23	26.73	33.61	44.60	63.30	92.77	108.50	107.57
3000	24.30	28.21	35.90	47.25	65.78	94.38	108.60	108.24
3250	25.30	29.47	37.33	49.11	66.48	93.00	105.60	104.42
3500	25.61	29.67	37.01	48.22	64.45	88.65	101.81	101.85

x	(40, 110)	(70, 110)	(100, 110)	(130, 110)	(160, 110)	(190, 110)	(220, 110)	(240, 110)
				(y,z)				
250	111.65	169.22	203.48	221.49	227.27	266.76	292.60	244.83
500	92.52	126.90	158.04	196.80	223.42	248.27	264.45	245.62
750	55.63	70.13	88.20	122.14	163.12	198.27	213.59	205.32
1000	39.91	47.66	61.00	88.21	128.39	168.47	179.41	164.15
1250	32.72	37.46	48.47	75.36	112.69	148.35	161.43	152.31
1500	30.54	34.54	43.46	65.28	99.88	136.89	150.59	143.78
1750	30.55	34.69	43.72	63.30	95.60	130.08	141.62	133.16
2000	30.20	34.62	43.81	62.04	92.07	125.35	135.39	128.82
2250	30.60	35.57	44.90	63.47	91.61	121.40	129.51	125.20
2500	30.67	35.46	44.52	62.57	89.44	118.66	127.16	123.29
2750	23.26	27.76	34.11	46.32	66.15	99.10	108.16	105.52
3000	24.46	29.34	36.42	49.04	69.21	100.80	107.96	104.82
3250	25.50	30.44	37.92	50.47	70.94	99.05	105.38	102.19
3500	25.95	30.54	37.67	49.77	67.67	93.44	101.38	98.90

Table E5: Temperature data in the downstream in tunnel B (Q = 15.0 kW, Uc = 0.60 m/s)

x	(y,z) (40, 0)	(70, 0)	(100, 0)	(130, 0)	(160, 0)	(190, 0)	(220, 0)	(240, 0)
250	503.04	577.99	592.19	533.59	428.95	326.89	212.07	152.66
500	83.87	96.27	120.18	179.33	265.81	336.08	367.59	360.82
750	62.43	77.09	101.20	132.46	190.96	261.25	327.96	348.26
1000	60.29	75.87	97.11	129.17	185.06	239.97	290.90	302.76
1250	41.14	52.64	62.34	81.18	109.31	141.04	162.79	165.39
1500	48.18	69.09	85.64	112.02	150.52	187.52	219.10	221.86
1750	35.43	45.54	51.84	65.15	89.92	118.16	140.38	139.61
2000	34.09	42.78	49.94	62.08	84.61	111.57	128.42	126.87
2250	38.36	49.50	59.93	75.63	101.74	130.39	148.26	148.64
2500	31.58	39.14	45.41	57.14	80.58	106.85	120.17	116.66
2750	37.52	49.67	60.66	78.87	109.51	141.84	161.69	157.99
3000	40.49	53.06	65.76	83.87	114.00	145.43	165.50	164.12
3250	41.02	54.03	66.50	83.88	113.13	143.66	163.10	162.12
3500	42.15	55.12	67.53	84.65	112.39	142.43	160.46	159.46

x	(y,z) (40, 55)	(70, 55)	(100, 55)	(130, 55)	(160, 55)	(190, 55)	(220, 55)	(240, 55)
250	325.43	82.14	485.12	420.53	314.89	245.43	150.12	126.98
500	94.98	47.84	223.14	287.80	330.80	368.07	366.69	351.45
750	93.69	56.10	145.28	174.02	221.52	273.70	329.17	341.30
1000	80.30	60.55	124.56	154.17	198.08	245.52	293.95	298.55
1250	38.47	44.63	63.28	80.68	101.75	143.60	165.99	169.79
1500	46.13	52.28	85.11	108.15	139.55	186.94	223.91	224.61
1750	32.25	38.72	54.98	69.58	89.80	126.00	142.43	143.50
2000	32.85	38.40	53.43	67.05	84.60	116.27	128.68	129.80
2250	38.52	43.26	63.48	79.03	99.36	132.18	148.20	149.23
2500	29.20	36.18	48.33	59.96	76.78	109.22	120.79	121.07
2750	37.14	44.50	65.19	81.97	106.84	145.43	163.71	160.43
3000	40.45	47.82	70.50	87.79	113.57	150.39	168.21	165.11
3250	41.45	48.40	70.95	88.48	113.50	148.17	166.12	162.21
3500	42.99	49.15	71.40	87.80	111.85	145.50	163.71	161.46

x	(y,z) (40, 110)	(70, 110)	(100, 110)	(130, 110)	(160, 110)	(190, 110)	(220, 110)	(240, 110)
250	134.11	208.53	193.03	169.89	113.02	95.65	106.66	94.31
500	95.60	175.41	217.51	266.47	283.58	330.69	343.64	297.19
750	90.82	149.53	190.57	226.67	261.70	307.96	324.65	305.07
1000	80.50	120.56	150.86	184.44	222.52	270.80	285.98	262.17
1250	38.41	52.95	63.89	80.44	108.34	162.94	173.89	157.93
1500	46.33	61.47	80.03	105.35	145.93	205.46	223.12	210.50
1750	34.23	47.36	59.99	77.44	98.75	144.37	149.15	134.37
2000	34.48	46.38	57.56	72.33	88.94	126.64	133.68	127.46
2250	38.68	51.68	64.12	81.44	102.64	139.10	149.15	145.36
2500	29.96	41.01	50.95	63.52	78.62	116.04	123.58	116.27
2750	38.33	51.68	65.91	83.62	109.47	152.53	161.81	156.45
3000	41.22	54.58	69.08	88.55	116.32	157.14	163.88	157.69
3250	41.91	54.55	68.96	89.04	117.61	156.92	162.12	155.24
3500	42.20	53.69	68.01	86.50	114.03	152.52	159.66	155.21

Table E6: Temperature data in the downstream in tunnel B (Q = 15.0 kW, U = 0.34 m/s)

x	(40, 0)	(70, 0)	(100, 0)	(130, 0)	(160, 0)	(190, 0)	(220, 0)	(240, 0)
250	216.90	329.89	349.76	368.99	381.77	431.16	477.99	387.65
500	173.97	238.61	276.84	325.16	369.77	425.33	450.65	383.86
750	45.84	57.90	78.08	114.49	168.38	240.21	261.77	248.40
1000	50.81	63.58	84.85	123.72	183.29	257.06	279.32	257.52
1250	46.52	56.99	77.62	113.66	167.95	231.87	252.03	233.67
1500	43.98	53.17	69.48	102.13	154.26	213.76	231.93	217.54
1750	35.95	43.50	55.22	77.09	115.84	175.13	193.96	180.65
2000	39.35	48.34	60.25	82.88	124.11	179.39	197.68	188.89
2250	24.11	30.19	37.62	51.10	75.02	127.50	141.06	133.11
2500	30.16	36.61	45.68	62.91	95.70	151.31	165.43	160.47
2750	32.31	38.46	48.38	67.08	97.93	150.90	163.65	160.14
3000	34.58	40.70	51.60	71.11	99.42	147.71	158.96	155.41
3250	34.50	41.38	52.42	71.42	98.73	141.74	154.34	150.25
3500	35.88	42.70	53.16	71.20	96.27	135.87	148.82	144.30

x	(40, 55)	(70, 55)	(100, 55)	(130, 55)	(160, 55)	(190, 55)	(220, 55)	(240, 55)
250	333.65	77.82	600.53	578.33	546.13	547.02	537.46	501.46
500	229.96	64.24	372.10	375.41	398.68	429.04	474.65	466.67
750	46.97	37.39	70.37	97.23	134.34	196.70	251.65	266.79
1000	52.18	44.68	81.61	113.18	160.60	226.91	280.42	284.37
1250	47.31	46.00	75.57	105.34	153.11	213.62	259.19	254.44
1500	44.13	45.63	70.13	96.86	140.20	198.64	238.75	232.21
1750	35.26	38.76	53.22	72.22	105.01	162.74	197.70	191.90
2000	38.54	41.91	58.28	78.44	112.77	169.55	203.57	198.82
2250	24.47	27.56	35.61	47.71	70.04	115.53	139.96	137.94
2500	29.60	32.55	44.37	60.36	88.72	139.39	168.80	165.35
2750	32.73	36.13	48.55	65.28	93.95	140.56	169.14	165.88
3000	34.07	37.38	50.51	68.23	95.90	138.68	163.81	160.94
3250	35.06	38.76	51.95	69.34	95.29	134.06	158.66	156.44
3500	35.52	39.12	52.06	68.69	92.54	127.84	152.60	151.90

x	(40, 110)	(70, 110)	(100, 110)	(130, 110)	(160, 110)	(190, 110)	(220, 110)	(240, 110)
250	216.90	329.89	349.76	368.99	381.77	431.16	477.99	387.65
500	173.97	238.61	276.84	325.16	369.77	425.33	450.65	383.86
750	45.84	57.90	78.08	114.49	168.38	240.21	261.77	248.40
1000	50.81	63.58	84.85	123.72	183.29	257.06	279.32	257.52
1250	46.52	56.99	77.62	113.66	167.95	231.87	252.03	233.67
1500	43.98	53.17	69.48	102.13	154.26	213.76	231.93	217.54
1750	35.95	43.50	55.22	77.09	115.84	175.13	193.96	180.65
2000	39.35	48.34	60.25	82.88	124.11	179.39	197.68	188.89
2250	24.11	30.19	37.62	51.10	75.02	127.50	141.06	133.11
2500	30.16	36.61	45.68	62.91	95.70	151.31	165.43	160.47
2750	32.31	38.46	48.38	67.08	97.93	150.90	163.65	160.14
3000	34.58	40.70	51.60	71.11	99.42	147.71	158.96	155.41
3250	34.50	41.38	52.42	71.42	98.73	141.74	154.34	150.25
3500	35.88	42.70	53.16	71.20	96.27	135.87	148.82	144.30

Table E7: Temperature data in the downstream in tunnel D (Q = 3.0 kW, Uc = 0.40 m/s)

x	(40, 0)	(70, 0)	(100, 0)	(130, 0)	(160, 0)	(190, 0)	(220, 0)	(240, 0)
				(y,z)				
250	60.073	79.365	104.388	147.015	179.699	166.190	156.785	146.035
500	38.310	45.148	54.563	61.794	69.675	78.877	96.676	105.437
750	25.213	25.581	25.958	26.137	27.906	34.337	52.856	62.860
1000	24.230	24.497	24.696	24.756	26.137	31.883	49.209	58.695
1250	23.524	23.733	23.822	23.902	25.014	30.223	43.939	51.840
1500	22.996	23.284	23.403	23.683	25.452	31.704	43.294	48.477
1750	22.689	23.115	23.413	24.626	29.169	37.668	46.041	48.584
2000	22.580	22.937	23.554	26.565	33.513	42.081	47.439	48.447
2250	22.450	22.937	24.091	29.139	37.797	44.477	47.684	48.016
2500	22.361	22.828	23.892	28.950	37.319	44.056	46.853	47.253
2750	22.381	22.530	22.977	24.587	30.620	39.743	45.084	45.895
3000	22.530	22.470	22.669	23.643	27.559	36.117	43.450	44.546
3250	22.440	22.411	22.639	23.165	25.829	33.940	42.491	43.714
3500	22.351	22.182	22.341	22.778	25.263	33.563	41.456	42.179

x	(40, 250)	(70, 250)	(100, 250)	(130, 250)	(160, 250)	(190, 250)	(220, 250)	(240, 250)
				(y,z)				
250	33.085	35.163	31.724	32.956	33.334	36.146	101.705	117.745
500	28.344	30.441	27.758	28.662	32.072	48.525	94.676	104.640
750	23.184	23.554	23.294	26.565	33.582	46.511	65.538	71.393
1000	22.659	22.798	22.748	25.987	33.214	43.832	58.812	63.609
1250	22.192	22.252	22.728	25.631	31.158	38.870	50.217	54.206
1500	22.043	22.113	22.868	25.630	30.998	38.851	47.322	49.503
1750	22.063	22.311	22.927	25.283	30.421	38.930	47.449	48.535
2000	21.944	22.192	22.758	24.636	29.167	37.916	47.567	48.506
2250	21.944	22.242	23.006	25.004	29.337	38.433	46.363	46.804
2500	21.834	22.291	23.273	25.482	30.351	40.028	45.396	45.387
2750	21.785	22.113	22.907	25.223	30.431	40.057	44.741	44.761
3000	21.755	22.083	22.798	24.864	29.925	38.890	43.840	43.889
3250	21.765	22.033	22.758	24.785	29.278	37.458	43.284	43.274
3500	21.735	21.824	22.550	23.991	27.548	34.327	41.808	42.091

x	(40, 480)	(70, 480)	(100, 480)	(130, 480)	(160, 480)	(190, 480)	(220, 480)	(240, 480)
				(y,z)				
250	30.88	25.90	26.26	27.08	28.70	32.07	47.10	62.48
500	29.82	24.87	25.11	25.74	29.57	45.16	70.27	77.62
750	26.85	21.98	22.73	25.62	33.81	58.37	70.06	68.67
1000	26.16	21.39	22.84	26.26	36.62	58.56	66.01	63.33
1250	25.54	21.05	22.54	26.22	37.04	55.19	59.67	56.71
1500	25.30	20.82	22.23	25.44	33.82	49.45	54.06	52.98
1750	25.25	20.68	21.94	24.73	30.69	42.81	50.35	50.73
2000	25.26	20.53	21.43	23.61	27.82	37.46	47.35	49.48
2250	25.26	20.54	21.35	23.32	26.92	34.89	44.59	46.96
2500	25.22	20.66	21.80	23.62	27.10	35.22	43.06	44.35
2750	25.15	20.78	21.98	24.04	28.09	37.89	42.75	42.30
3000	25.14	20.90	22.52	25.25	30.25	39.27	42.13	41.48
3250	25.24	21.31	23.27	26.96	33.02	40.18	41.72	40.68
3500	25.16	21.11	22.98	26.16	32.49	39.73	40.88	39.89

Table E8: Temperature data in the downstream in tunnel D (Q = 3.0 kW, U = 0.18 m/s)

x	(40, 0)	(70, 0)	(100, 0)	(y,z) (130, 0)	(160, 0)	(190, 0)	(220, 0)	(240, 0)
250	39.74	40.39	41.26	41.15	48.52	78.54	143.19	182.71
500	33.65	34.77	35.46	34.56	37.77	52.08	93.27	125.04
750	27.77	28.51	28.94	28.62	29.46	32.70	52.66	79.18
1000	25.35	25.92	26.30	26.37	27.00	30.76	47.97	64.17
1250	24.11	24.62	24.91	25.22	26.20	35.53	49.59	55.59
1500	23.79	24.24	24.74	25.07	26.19	37.79	49.59	52.68
1750	23.60	24.07	24.50	24.80	25.90	40.30	48.66	49.87
2000	23.54	23.86	24.21	24.79	26.61	42.99	48.04	48.29
2250	23.41	23.67	24.11	24.56	27.09	41.86	46.55	46.63
2500	23.48	23.63	24.07	24.83	28.79	38.73	44.25	45.41
2750	23.54	23.63	24.00	25.36	30.50	37.27	41.78	43.23
3000	23.57	23.60	23.95	25.61	30.64	36.50	40.65	41.77
3250	23.48	23.62	24.01	25.61	30.05	35.66	39.54	40.25
3500	23.42	23.51	23.76	25.02	28.80	34.08	38.22	38.73

x	(40, 55)	(70, 55)	(100, 55)	(y,z) (130, 55)	(160, 55)	(190, 55)	(220, 55)	(240, 55)
250	33.36	35.10	31.79	34.42	37.58	42.59	95.39	115.51
500	30.24	31.79	29.53	31.18	34.16	38.74	79.76	91.06
750	26.38	27.15	26.33	27.30	29.36	35.62	66.12	73.15
1000	24.42	24.92	24.93	25.65	26.78	35.44	59.96	62.02
1250	23.53	23.98	24.22	24.63	25.31	31.30	54.80	56.02
1500	23.25	23.79	24.13	24.59	25.44	33.39	51.13	52.41
1750	23.26	23.77	24.13	24.74	26.25	38.27	49.16	49.31
2000	23.19	23.69	24.16	24.75	27.19	38.60	46.75	47.05
2250	23.22	23.63	24.16	25.08	28.71	37.02	45.16	45.99
2500	23.33	23.61	24.02	24.98	28.46	35.92	43.98	44.64
2750	23.40	23.58	23.99	25.10	28.61	36.42	42.75	43.01
3000	23.37	23.60	24.13	25.52	28.79	36.40	41.54	41.77
3250	23.39	23.62	24.35	26.24	29.25	35.54	40.25	40.39
3500	23.30	23.55	24.17	25.92	28.86	34.45	39.06	39.12

x	(40, 480)	(70, 480)	(100, 480)	(y,z) (130, 480)	(160, 480)	(190, 480)	(220, 480)	(240, 480)
250	33.55	28.49	29.07	30.67	35.90	71.61	87.79	88.70
500	31.62	26.76	27.24	28.58	34.16	66.75	78.58	79.09
750	29.65	24.89	25.07	26.01	31.05	59.42	69.48	69.22
1000	28.00	23.41	23.60	24.21	28.19	52.63	61.31	59.12
1250	27.80	23.38	23.67	24.21	26.96	44.08	55.04	53.86
1500	27.50	23.15	23.51	24.20	26.76	39.27	50.44	50.98
1750	26.65	22.43	23.24	24.57	27.50	38.21	46.44	46.76
2000	26.74	22.76	23.79	25.09	28.16	39.11	44.13	43.98
2250	27.75	23.86	24.78	25.95	29.30	40.33	44.04	43.52
2500	27.86	23.87	24.71	25.77	29.20	39.78	42.81	42.36
2750	26.91	22.82	23.63	24.53	27.79	37.64	40.26	39.61
3000	27.86	23.79	24.56	25.50	29.05	38.25	40.15	39.75
3250	27.90	23.76	24.48	25.74	30.49	38.06	39.57	38.74
3500	27.78	23.54	24.18	25.15	28.97	37.12	38.73	37.92

Table E8: Temperature data in the downstream in tunnel D (Q = 3.0 kW, U = 0.18 m/s)

x	(y,z) (40, 0)	(70, 0)	(100, 0)	(130, 0)	(160, 0)	(190, 0)	(220, 0)	(240, 0)
250	39.74	40.39	41.26	41.15	48.52	78.54	143.19	182.71
500	33.65	34.77	35.46	34.56	37.77	52.08	93.27	125.04
750	27.77	28.51	28.94	28.62	29.46	32.70	52.66	79.18
1000	25.35	25.92	26.30	26.37	27.00	30.76	47.97	64.17
1250	24.11	24.62	24.91	25.22	26.20	35.53	49.59	55.59
1500	23.79	24.24	24.74	25.07	26.19	37.79	49.59	52.68
1750	23.60	24.07	24.50	24.80	25.90	· 40.30	48.66	49.87
2000	23.54	23.86	24.21	24.79	26.61	42.99	48.04	48.29
2250	23.41	23.67	24.11	24.56	27.09	41.86	46.55	46.63
2500	23.48	23.63	24.07	24.83	28.79	38.73	44.25	45.41
2750	23.54	23.63	24.00	25.36	30.50	37.27	41.78	43.23
3000	23.57	23.60	23.95	25.61	30.64	36.50	40.65	41.77
3250	23.48	23.62	24.01	25.61	30.05	35.66	39.54	40.25
3500	23.42	23.51	23.76	25.02	28.80	34.08	38.22	38.73

x	(y,z) (40, 55)	(70, 55)	(100, 55)	(130, 55)	(160, 55)	(190, 55)	(220, 55)	(240, 55)
250	33.36	35.10	31.79	34.42	37.58	42.59	95.39	115.51
500	30.24	31.79	29.53	31.18	34.16	38.74	79.76	91.06
750	26.38	27.15	26.33	27.30	29.36	35.62	66.12	73.15
1000	24.42	24.92	24.93	25.65	26.78	35.44	59.96	62.02
1250	23.53	23.98	24.22	24.63	25.31	31.30	54.80	56.02
1500	23.25	23.79	24.13	24.59	25.44 .	33.39	51.13	52.41
1750	23.26	23.77	24.13	24.74	26.25	38.27	49.16	49.31
2000	23.19	23.69	24.16	24.75	·27.19	38.60	46.75	47.05
2250	23.22	23.63	24.16	25.08	28.71	37.02	45.16	45.99
2500	23.33	23.61	24.02	24.98	28.46	35.92	43.98	44.64
2750	23.40	23.58	23.99	25.10	28.61	36.42	42.75	43.01
3000	23.37	23.60	24.13	25.52	28.79	36.40	41.54	41.77
3250	23.39	23.62	24.35	·26.24	29.25	35.54	40.25	40.39
3500	23.30	23.55	24.17	25.92	28.86	34.45	39.06	39.12

x	(y,z) (40, 480)	(70, 480)	(100, 480)	(130, 480)	(160, 480)	(190, 480)	(220, 480)	(240, 480)
250	33.55	28.49	29.07	30.67	35.90	71.61	87.79	88.70
500	31.62	26.76	27.24	28.58	34.16	66.75	78.58	79.09
750	29.65	24.89	25.07	26.01	31.05	59.42	69.48	69.22
1000	28.00	23.41	23.60	24.21	28.19	52.63	61.31	59.12
1250	27.80	23.38	23.67	24.21	26.96	44.08	55.04	53.86
1500	27.50	23.15	23.51	24.20	26.76	39.27	50.44	50.98
1750	26.65	22.43	23.24	24.57	27.50	38.21	46.44	46.76
2000	26.74	22.76	23.79	25.09	28.16	39.11	44.13	43.98
2250	27.75	23.86	24.78	25.95	29.30	40.33	44.04	43.52
2500	27.86	23.87 ·	24.71	25.77	29.20	39.78	42.81	42.36
2750	26.91	22.82	23.63	24.53	27.79	37.64	40.26	39.61
3000	27.86	23.79	24.56	25.50	29.05	38.25	40.15	39.75
3250	27.90	23.76	24.48	25.74	30.49	38.06	39.57	38.74
3500	27.78	23.54	24.18	25.15	28.97	37.12	38.73	37.92

Table E9: Temperature data in the downstream in tunnel D (Q = 7.50 kW, Uc = 0.50 m/s)

x	(40, 0)	(70, 0)	(100, 0)	(130, 0)	(160, 0)	(190, 0)	(220, 0)	(240, 0)
250	124.43	201.98	285.20	343.63	363.96	321.46	284.35	261.38
500	90.79	153.47	190.97	202.06	204.20	195.90	204.96	211.94
750	34.53	38.55	41.46	40.03	43.66	55.18	85.96	109.12
1000	30.79	32.79	33.71	32.90	35.03	45.55	75.16	96.88
1250	28.35	29.60	29.86	29.50	31.41	39.94	62.25	79.52
1500	27.10	28.29	28.43	28.50	30.90	41.86	60.93	72.18
1750	26.30	27.43	27.64	28.57	34.36	50.67	65.77	72.54
2000	25.78	26.77	27.34	31.56	42.94	.59.93	68.83	71.50
2250	25.17	26.25	27.49	35.67	50.76	63.77	68.67	69.58
2500	24.65	25.48	26.67	33.01	47.70	61.78	66.38	66.92
2750	24.63	25.15	26.14	29.93	41.56	57.35	64.53	65.79
3000	24.62	24.96	25.34	26.79	33.00	47.74	60.70	63.45
3250	24.44	24.78	24.99	25.83	29.48	42.24	58.26	61.42
3500	24.19	24.50	24.78	25.31	28.78	42.53	57.30	59.80

x	(40, 250)	(70, 250)	(100, 250)	(130, 250)	(160, 250)	(190, 250)	(220, 250)	(240, 250)
250	51.35	55.57	48.64	51.22	51.96	69.17	161.69	186.42
500	47.01	52.64	44.98	48.13	54.22	84.52	164.41	182.76
750	30.08	32.01	28.90	34.42	48.74	76.95	116.21	127.13
1000	27.61	28.47	26.81	32.28	44.30	66.82	95.96	104.60
1250	.26.01	26.21	25.99	30.95	41.09	57.05	77.78	84.24
1500	25.02	25.18	25.81	30.14	38.30	53.44	72.06	76.37
1750	24.84	24.92	25.18	28.70	36.60	52.37	72.06	75.09
2000	24.64	24.77	24.86	27.54	34.24	49.28	70.87	74.54
2250	24.24	24.44	24.65	27.71	34.51	49.72	68.37	71.02
2500	23.82	24.05	24.63	28.26	36.21	54.06	65.50	65.99
2750	23.72	24.13	24.85	28.71	37.27	53.44	64.28	64.96
3000	23.58	23.92	24.77	28.38	36.23	51.76	62.51	62.92
3250	23.47	23.71	24.51	27.48	34.43	47.76	61.18	61.61
3500	23.44	23.64	24.33	26.93	33.19	46.01	59.43	59.85

x	(40, 480)	(70, 480)	(100, 480)	(130, 480)	(160, 480)	(190, 480)	(220, 480)	(240, 480)
250	40.90	35.41	35.80	36.32	37.99	50.61	86.46	106.78
500	40.21	34.69	35.22	35.54	39.39	62.95	105.00	116.40
750	33.82	28.70	29.42	33.21	45.94	91.95	121.43	120.01
1000	31.64	26.58	27.60	32.38	49.99	95.25	111.09	107.39
1250	29.72	25.09	26.81	32.75	50.37	86.53	96.58	93.04
1500	28.60	23.98	26.01	31.52	45.61	75.35	87.05	86.56
1750	28.29	23.49	25.06	29.63	39.66	63.30	80.38	82.94
2000	28.09	23.14	24.40	27.67	34.46	50.95	72.31	79.63
2250	27.87	22.97	24.36	26.94	32.62	46.07	65.69	73.42
2500	27.62	22.87	24.40	27.26	32.75	46.30	61.99	65.49
2750	27.66	23.17	24.90	27.98	33.88	49.08	61.46	63.33
3000	27.59	23.52	25.87	30.23	38.63	54.67	61.97	61.51
3250	27.49	23.62	26.42	32.20	43.54	57.94	61.83	61.00
3500	27.41	23.55	26.42	32.19	43.63	56.53	59.81	58.97

Table E10: Temperature data in the downstream in tunnel D (Q =7.50 kW, U = 0.28 m/s)

x	(40, 0)	(70, 0)	(100, 0)	(130, 0)	(160, 0)	(190, 0)	(220, 0)	(240, 0)
250	78.01	85.59	95.19	110.03	156.67	222.81	310.80	325.81
500	64.97	74.99	83.90	93.62	123.97	160.52	215.81	242.45
750	40.25	43.69	46.31	46.16	51.64	60.98	94.08	119.42
1000	34.58	36.67	38.12	37.58	40.10	46.60	74.75	99.86
1250	30.55	31.81	32.44	32.81	34.98	48.87	71.84	82.75
1500	31.01	32.22	32.92	33.47	36.85	55.23	74.43	81.28
1750	29.51	30.67	31.28	31.91	35.86	56.64	72.82	74.38
2000	28.94	29.93	30.61	30.93	33.56	56.71	71.44	73.33
2250	29.40	30.08	30.74	31.21	35.25	59.60	71.32	70.81
2500	27.65	28.28	28.80	29.39	33.90	56.82	66.31	67.33
2750	27.63	28.20	28.52	29.32	35.76	54.09	64.05	63.90
3000	27.46	27.95	28.33	29.41	37.25	51.12	60.36	62.42
3250	28.25	28.60	29.08	30.49	39.36	50.69	58.79	60.47
3500	27.85	28.30	28.70	29.77	37.09	48.57	57.17	58.47

x	(40, 250)	(70, 250)	(100, 250)	(130, 250)	(160, 250)	(190, 250)	(220, 250)	(240, 250)
250	55.23	59.51	51.16	59.85	69.59	94.12	201.42	227.31
500	50.86	54.85	47.00	54.23	63.81	82.15	161.94	179.10
750	36.80	37.95	35.06	39.33	46.02	58.24	101.54	112.37
1000	32.37	33.06	31.49	34.05	38.11	53.01	91.56	98.65
1250	28.67	29.16	28.60	29.77	31.41	40.08	77.39	81.22
1500	29.42	29.85	29.49	30.54	32.07	43.51	76.85	79.41
1750	27.98	28.61	28.48	29.56	32.24	50.02	73.48	73.09
2000	27.47	28.30	28.25	29.53	33.29	51.86	70.68	71.41
2250	28.28	28.77	28.87	30.51	36.42	51.72	68.72	68.57
2500	26.89	27.32	27.52	29.10	35.15	48.56	63.58	64.32
2750	26.84	27.25	27.33	28.83	34.93	50.10	62.41	61.89
3000	26.76	27.08	27.19	28.60	34.37	49.56	60.68	61.11
3250	27.64	27.82	28.07	30.17	36.38	50.21	59.54	59.82
3500	27.48	27.67	27.99	30.33	36.28	47.38	57.72	58.47

x	(40, 480)	(70, 480)	(100, 480)	(130, 480)	(160, 480)	(190, 480)	(220, 480)	(240, 480)
250	46.89	40.41	41.57	46.15	59.60	123.55	151.90	150.97
500	45.54	39.40	40.19	44.68	58.23	119.49	140.95	142.10
750	38.82	33.19	34.08	37.56	51.18	96.89	109.20	108.32
1000	35.57	30.35	30.95	33.44	44.92	85.78	99.47	94.53
1250	32.07	27.29	27.78	29.08	33.63	57.38	81.16	82.90
1500	31.67	26.95	27.61	28.93	33.35	54.86	76.82	79.87
1750	31.29	26.72	27.59	29.24	34.27	54.47	71.78	74.14
2000	31.05	26.60	27.72	30.04	36.78	57.45	68.67	69.88
2250	30.77	26.34	27.57	29.94	36.56	57.16	65.90	65.97
2500	30.54	26.24	27.60	29.76	35.82	55.52	61.33	60.70
2750	30.53	26.20	27.60	29.67	36.11	54.91	60.31	59.65
3000	30.57	26.37	27.69	29.55	35.92	53.39	58.21	57.88
3250	30.56	26.47	27.80	29.73	36.44	53.16	56.36	55.38
3500	30.48	26.39	27.46	29.03	34.95	52.00	55.46	54.18

Table E10: Temperature data in the downstream in tunnel D (Q =7.50 kW, U = 0.28 m/s)

x	(y,z) (40, 0)	(70, 0)	(100, 0)	(130, 0)	(160, 0)	(190, 0)	(220, 0)	(240, 0)
250	78.01	85.59	95.19	110.03	156.67	222.81	310.80	325.81
500	64.97	74.99	83.90	93.62	123.97	160.52	215.81	242.45
750	40.25	43.69	46.31	46.16	51.64	60.98	94.08	119.42
1000	34.58	36.67	38.12	37.58	40.10	46.60	74.75	99.86
1250	30.55	31.81	32.44	32.81	34.98	48.87	71.84	82.75
1500	31.01	32.22	32.92	33.47	36.85	55.23	74.43	81.28
1750	29.51	30.67	31.28	31.91	35.86	56.64	72.82	74.38
2000	28.94	29.93	30.61	30.93	33.56	56.71	71.44	73.33
2250	29.40	30.08	30.74	31.21	35.25	59.60	71.32	70.81
2500	27.65	28.28	28.80	29.39	33.90	56.82	66.31	67.33
2750	27.63	28.20	28.52	29.32	35.76	54.09	64.05	63.90
3000	27.46	27.95	28.33	29.41	37.25	51.12	60.36	62.42
3250	28.25	28.60	29.08	30.49	39.36	50.69	58.79	60.47
3500	27.85	28.30	28.70	29.77	37.09	48.57	57.17	58.47

x	(y,z) (40, 250)	(70, 250)	(100, 250)	(130, 250)	(160, 250)	(190, 250)	(220, 250)	(240, 250)
250	55.23	59.51	51.16	59.85	69.59	94.12	201.42	227.31
500	50.86	54.85	47.00	54.23	63.81	82.15	161.94	179.10
750	36.80	37.95	35.06	39.33	46.02	58.24	101.54	112.37
1000	32.37	33.06	31.49	34.05	38.11	53.01	91.56	98.65
1250	28.67	29.16	28.60	29.77	31.41	40.08	77.39	81.22
1500	29.42	29.85	29.49	30.54	32.07	43.51	76.85	79.41
1750	27.98	28.61	28.48	29.56	32.24	50.02	73.48	73.09
2000	27.47	28.30	28.25	29.53	33.29	51.86	70.68	71.41
2250	28.28	28.77	28.87	30.51	36.42	51.72	68.72	68.57
2500	26.89	27.32	27.52	29.10	35.15	48.56	63.58	64.32
2750	26.84	27.25	27.33	28.83	34.93	50.10	62.41	61.89
3000	26.76	27.08	27.19	28.60	34.37	49.56	60.68	61.11
3250	27.64	27.82	28.07	30.17	36.38	50.21	59.54	59.82
3500	27.48	27.67	27.99	30.33	36.28	47.38	57.72	58.47

x	(y,z) (40, 480)	(70, 480)	(100, 480)	(130, 480)	(160, 480)	(190, 480)	(220, 480)	(240, 480)
250	46.89	40.41	41.57	46.15	59.60	123.55	151.90	150.97
500	45.54	39.40	40.19	44.68	58.23	119.49	140.95	142.10
750	38.82	33.19	34.08	37.56	51.18	96.89	109.20	108.32
1000	35.57	30.35	30.95	33.44	44.92	85.78	99.47	94.53
1250	32.07	27.29	27.78	29.08	33.63	57.38	81.16	82.90
1500	31.67	26.95	27.61	28.93	33.35	54.86	76.82	79.87
1750	31.29	26.72	27.59	29.24	34.27	54.47	71.78	74.14
2000	31.05	26.60	27.72	30.04	36.78	57.45	68.67	69.88
2250	30.77	26.34	27.57	29.94	36.56	57.16	65.90	65.97
2500	30.54	26.24	27.60	29.76	35.82	55.52	61.33	60.70
2750	30.53	26.20	27.60	29.67	36.11	54.91	60.31	59.65
3000	30.57	26.37	27.69	29.55	35.92	53.39	58.21	57.88
3250	30.56	26.47	27.80	29.73	36.44	53.16	56.36	55.38
3500	30.48	26.39	27.46	29.03	34.95	52.00	55.46	54.18

Table E11: Temperature data in the downstream in tunnel D (Q = 15.0 kW, Uc = 0.59 m/s)

x	(y,z) (40, 0)	(70, 0)	(100, 0)	(130, 0)	(160, 0)	(190, 0)	(220, 0)	(240, 0)
250	562.20	650.68	685.00	638.52	539.14	439.65	361.93	325.32
500	199.41	264.89	291.35	277.59	316.36	327.16	356.51	359.34
750	55.27	64.51	74.60	73.37	102.96	127.72	181.93	218.50
1000	40.11	43.37	46.93	45.82	57.08	73.03	127.32	164.16
1250	33.24	35.30	37.08	37.09	43.36	57.85	98.56	128.83
1500	30.69	32.39	33.47	33.81	40.27	58.91	92.52	114.74
1750	29.10	30.30	31.15	33.87	47.17	73.77	97.48	108.63
2000	28.12	29.51	31.05	40.15	59.82	85.78	100.97	105.71
2250	27.21	28.61	31.25	43.85	70.18	92.06	99.70	101.17
2500	27.07	28.08	30.18	39.62	63.90	86.75	96.44	98.72
2750	26.96	27.63	28.69	31.97	47.02	71.39	90.38	95.15
3000	26.73	27.24	27.87	29.27	37.74	59.21	84.07	91.35
3250	26.34	26.72	27.26	28.28	35.02	55.44	81.55	88.40
3500	27.13	27.57	28.11	29.31	37.09	61.69	83.22	86.50

x	(y,z) (40, 250)	(70, 250)	(100, 250)	(130, 250)	(160, 250)	(190, 250)	(220, 250)	(240, 250)
250	84.41	86.32	77.53	79.26	79.71	87.14	135.55	159.94
500	76.91	88.17	74.28	82.13	95.81	159.07	273.80	300.44
750	47.61	54.94	46.97	62.77	92.18	138.89	207.29	226.94
1000	36.30	39.53	37.43	51.46	76.11	103.13	149.37	165.96
1250	30.51	32.26	34.05	47.84	64.46	79.60	112.02	124.36
1500	28.14	29.32	32.32	41.85	54.88	72.48	99.90	108.31
1750	27.06	27.67	29.69	36.54	49.13	72.34	99.92	104.53
2000	26.83	27.34	28.67	34.93	46.98	72.20	97.46	100.61
2250	26.16	26.78	27.85	33.43	45.53	73.63	94.47	95.62
2500	25.90	26.57	27.48	33.05	45.96	74.29	94.24	95.00
2750	25.54	26.30	27.68	33.37	46.30	72.37	91.90	92.66
3000	25.43	26.21	27.65	32.79	44.95	68.84	88.75	89.95
3250	25.38	25.92	27.26	32.23	43.11	64.30	86.50	87.65
3500	26.24	26.77	28.22	32.91	43.53	63.11	84.98	85.71

x	(y,z) (40, 480)	(70, 480)	(100, 480)	(130, 480)	(160, 480)	(190, 480)	(220, 480)	(240, 480)
250	50.65	43.76	45.02	46.09	44.80	45.23	67.13	94.96
500	55.60	48.63	50.41	51.42	55.13	94.46	163.48	180.05
750	48.03	41.34	43.09	48.19	65.48	143.81	195.85	192.89
1000	40.85	34.60	36.72	44.54	73.93	145.26	169.27	163.26
1250	34.85	29.99	34.34	44.38	74.49	128.93	141.12	136.31
1500	31.80	27.18	31.53	41.53	66.43	111.89	126.78	125.39
1750	30.45	25.50	29.06	36.34	51.45	84.13	110.22	114.65
2000	30.08	25.06	28.28	34.29	45.52	69.90	97.51	106.91
2250	29.59	25.03	28.05	33.35	42.56	62.51	86.95	96.17
2500	29.44	25.11	28.53	33.88	43.57	66.61	88.07	92.63
2750	29.43	25.95	30.24	37.13	49.73	75.50	88.44	88.34
3000	29.56	26.63	31.78	40.63	54.84	77.83	86.46	86.02
3250	29.57	26.87	32.79	42.89	58.94	79.57	85.14	83.07
3500	29.23	26.10	30.71	38.57	52.56	76.70	83.21	82.05

Table E12: Temperature data in the downstream in tunnel D (Q =15.0 kW, U = 0.33 m/s)

x	(40, 0)	(70, 0)	(100, 0)	(130, 0)	(160, 0)	(190, 0)	(220, 0)	(240, 0)
				(y,z)				
250	198.53	233.62	284.45	368.96	479.52	517.94	555.49	550.15
500	123.71	147.86	172.65	198.60	248.71	288.10	354.95	386.79
750	67.46	73.49	79.17	78.72	93.01	113.15	174.05	214.88
1000	49.11	52.38	54.48	53.59	59.65	72.36	122.18	161.18
1250	40.76	43.22	44.29	44.68	49.31	64.40	105.36	132.56
1500	38.16	40.59	41.88	42.99	52.13	77.30	106.96	121.66
1750	37.71	39.74	41.07	42.11	52.05	85.78	110.27	118.10
2000	35.68	37.18	38.13	38.72	44.62	79.69	104.71	109.44
2250	35.91	37.17	37.98	38.54	43.99	82.26	103.29	106.19
2500	34.43	35.29	36.15	36.77	42.79	82.84	99.94	101.57
2750	33.72	34.73	35.31	36.17	44.29	77.05	94.25	96.84
3000	33.02	34.03	34.66	36.66	48.40	72.52	88.66	92.25
3250	32.57	33.35	33.98	36.51	51.26	70.69	84.72	88.21
3500	32.87	33.63	34.16	35.68	47.50	67.08	80.62	83.39

x	(40, 250)	(70, 250)	(100, 250)	(130, 250)	(160, 250)	(190, 250)	(220, 250)	(240, 250)
				(y,z)				
250	107.16	118.65	102.60	122.57	145.39	202.76	393.69	418.30
500	89.40	100.91	84.82	100.81	124.86	167.03	283.89	312.39
750	60.29	64.73	56.28	65.55	81.62	98.98	168.70	194.69
1000	46.05	47.42	43.48	48.84	58.53	80.37	137.29	148.64
1250	38.54	39.39	37.48	40.10	44.71	63.78	127.37	132.68
1500	36.01	37.16	36.07	38.21	41.43	58.61	117.45	122.03
1750	35.73	36.87	36.19	38.46	42.14	71.16	112.80	114.60
2000	33.56	34.83	34.37	37.28	44.75	75.13	105.87	106.72
2250	34.02	34.93	34.69	37.78	47.38	72.17	100.66	102.25
2500	32.66	33.41	33.24	36.27	46.00	68.29	94.78	96.48
2750	32.32	32.95	32.71	35.41	43.98	69.06	91.63	92.31
3000	31.98	32.57	32.46	34.90	43.94	69.70	88.59	88.55
3250	31.53	32.05	32.09	35.07	44.82	69.03	85.74	85.92
3500	32.24	32.74	32.84	35.69	45.18	64.93	82.03	83.04

x	(40, 480)	(70, 480)	(100, 480)	(130, 480)	(160, 480)	(190, 480)	(220, 480)	(240, 480)
				(y,z)				
250	73.03	63.47	65.61	73.34	92.62	194.22	242.36	237.95
500	70.39	62.02	63.69	71.43	94.66	195.88	232.33	232.42
750	57.71	50.36	51.25	58.50	87.51	164.55	185.36	184.46
1000	46.99	41.03	42.40	48.21	72.94	137.61	156.14	149.21
1250	40.72	35.27	36.59	40.59	52.95	98.83	136.47	137.71
1500	38.14	33.20	34.73	38.41	46.96	81.74	118.09	123.74
1750	37.07	32.47	34.30	37.84	46.11	77.66	108.93	114.02
2000	36.46	31.97	34.01	37.75	48.69	84.98	104.20	105.28
2250	36.01	31.60	33.74	37.78	48.65	85.20	99.51	99.67
2500	35.67	31.44	33.59	37.39	47.39	81.23	94.74	94.06
2750	35.47	31.27	33.43	36.89	46.65	77.98	89.66	88.63
3000	35.32	31.25	33.49	36.79	46.96	76.44	86.08	85.84
3250	34.99	30.93	33.12	36.23	46.51	76.61	82.88	81.21
3500	34.69	30.78	32.54	34.97	42.46	71.27	79.28	77.81